NASA Reference Publication 1025

Handbook on Astronaut Crew Motion Disturbances for Control System Design

M. Conlon Kullas

MAY 1979

NASA

NASA Reference Publication 1025

Handbook on Astronaut Crew Motion Disturbances for Control System Design

M. Conlon Kullas
Martin Marietta Aerospace
Denver, Colorado

National Aeronautics
and Space Administration

Scientific and Technical
Information Office

1979

PREFACE

The purpose of this handbook is to present information on astronaut crew motion disturbances so that a spacecraft control system designer can account for their effects. The reader is cautioned that guidelines only are presented; consequently, the document is not a definitive step-by-step design procedure covering all control system designs. Rather, the guidelines give information through which a designer can assess crew motion effects on a new control system without being distracted by the details of actuator or control law selection.

CONTENTS

SYMBOLS

a	acceleration, m/sec^2
$f(t)$	function of time
$f(\omega)$	function of frequency
F_X, F_Y, F_Z	local force at FMU, N
$G(j\omega)$	system transfer function
$H(j\omega)$	frequency response function
H_X, H_Y	modal displacement at location of disturbance force, m/m
I	vehicle inertia, $kg\text{-}m^2$
K_A	actuator gain, N-m/V
K_D	displacement gyro gain, V/rad
K_R	rate gyro gain, V/rad/sec
m	mass, kg
m_{eq}	generalized modal mass, kg
M_C	control torque, N-m
M_D	vehicle disturbance torque, N-m
$M_{D_X}, M_{D_Y}, M_{D_Z}$	disturbance moments about Skylab center of mass
M_E	effective torque, N-m
M_T	total torque, N-m
M_X, M_Y, M_Z	local moment at FMU
M_{ZV}	total Z-axis vehicle moment, N-m
P	probability
q	generalized bending coordinate
Q	generalized bending force

R_X, R_Y, R_Z	moment arm in x,y,z coordinate system, m
s	Laplace variable (S in appendix A)
t	time, sec
V_D	sensed vehicle attitude, V
V_R	sensed vehicle rate, V
x,y,z	distance along axes
X,Y,Z	coordinate axis system at an FMU
ζ	modal damping
θ	total vehicle attitude, rad
θ_C	attitude command, V
θ_E	attitude error, V
θ_F	attitude feedback, V
θ_{FB}	flexible-body attitude, rad
θ_{RB}	rigid-body attitude, rad
σ	standard deviation
σ_A	slope at actuator, rad/m
σ_{DG}	slope at displacement gyro, rad/m
σ_Z	slope at disturbance moment application, rad/m
τ	filter gain
ϕ, θ, ψ	Euler angles
Φ	power spectral density (PSD)
ω	modal frequency
ω_F, ζ_F	filter parameters tabulated in appendix A
ω_Z	angular rate about the Z-axis (fig. 6-6)

Subscripts:

1,2	with respect to FMU 1 or FMU 2

Abbreviations:

ATM	Apollo telescope mount
CMG	control moment gyro
DT	digital time increment
EDS	experiment data system
EVA	extravehicular activity
FMU	force measuring unit
JSC	Lyndon B. Johnson Space Center
LIMS	limb motion sensing system
MMU	manned maneuvering unit
OWS	orbital workshop
PSD	power spectral density
RHC	rho hand controller (console operation)
rms	root mean square
RN	random number generator output
SAL	scientific air lock
THC	theta hand controller (console operation)

PART I

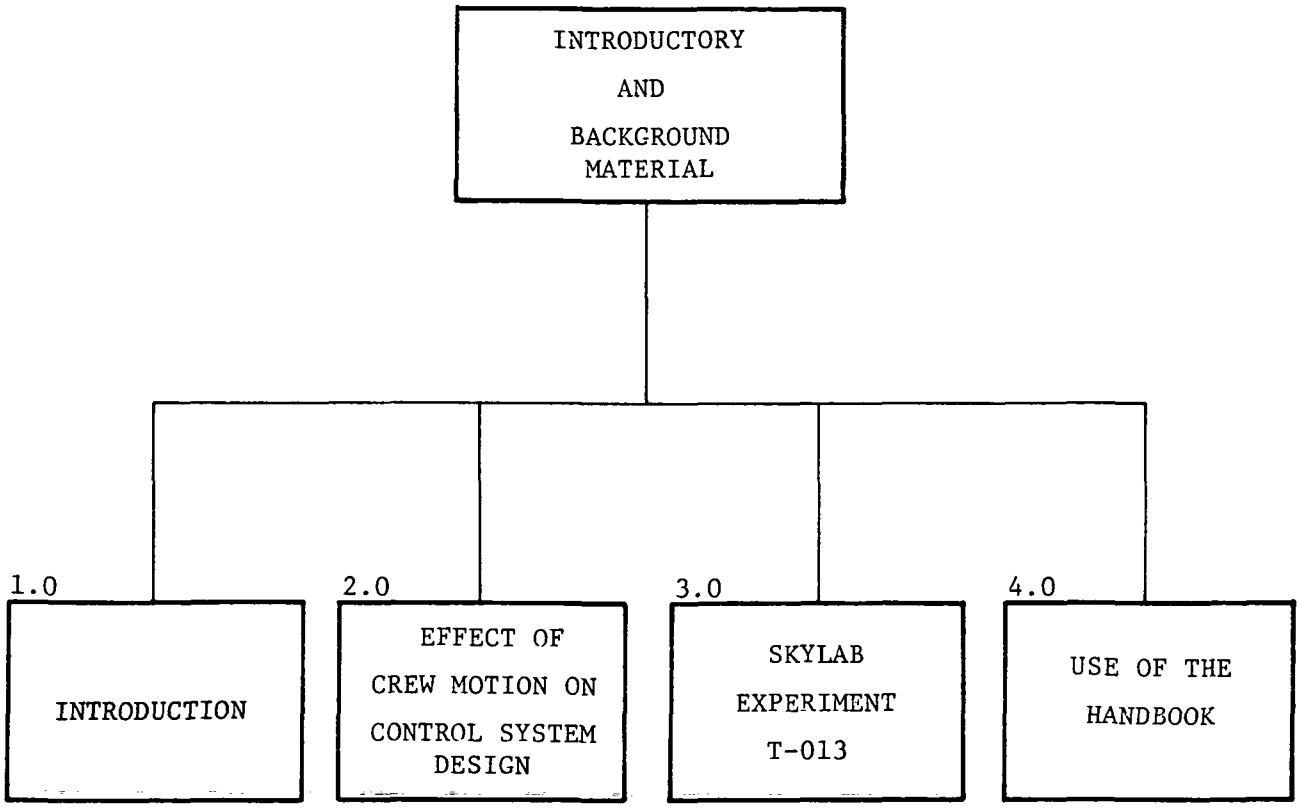
INTRODUCTORY
AND
BACKGROUND
MATERIAL
1.0
INTRODUCTION
2.0
EFFECT OF
CREW MOTION ON
CONTROL SYSTEM
DESIGN
3.0
SKYLAB
EXPERIMENT
T-013
4.0
USE OF THE
HANDBOOK

1.0 INTRODUCTION

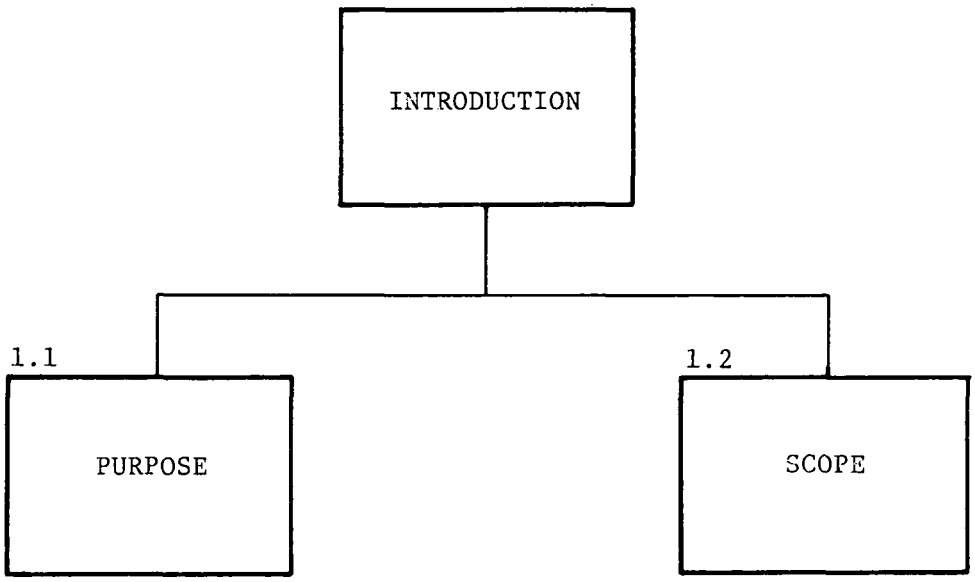

PAGE 2 INTENTIONALLY BLANK

1.0 INTRODUCTION

Skylab experiment T-013 (crew/vehicle disturbances) was conducted in August 1973, aboard the second manned Skylab mission. Its objective was to characterize and assess the effects of astronaut crew motion disturbances on a manned spacecraft. Through successful performance of experiment T-013, considerable crew motion data have been obtained and analyzed. When combined with preflight simulation and analytical experience, the Skylab data form a base for more effective design of control systems for manned spacecraft of the future.

1.1 Purpose

The major objective of this handbook is to provide a control system designer with techniques to model crew motion disturbances and guidelines to integrate crew motion effects into the control system design process. The second objective is to summarize results of the analyses of Skylab experiment T-013.

1.2 Scope

The handbook is composed of two major parts whose common purpose is to aid the control system designer in evaluating the effects of crew motion.

Part I, chapters 1.0 to 4.0, contains introductory material to familiarize the reader with the general control system design problem, the contribution of crew motion to that problem, the background of the Skylab experiment developed to characterize crew motion, and the role of the handbook in analyzing the effect of crew motion upon the design process.

Chapters 5.0 and 6.0 of part II deal with modeling representations of crew motion disturbances. An explanation of modeling is carried out in chapter 5.0 by introducing pertinent modeling techniques of varying complexity, by developing these models for typical nominal and worst case crew activities, and by applying them to the control system design problem from preliminary design to detailed simulation. Skylab characteristics were used for verification, and an example of future model usage was obtained using space shuttle characteristics.

The final chapter of part II, chapter 7.0, summarizes the results presented in the handbook and continues the discussion of how to attack future problems by identifying methods of developing data for new activities. Earth-based simulation techniques are presented. Experiment T-013 preflight data are compared with actual recorded data to establish a basis for future study.

Two appendixes contain further details to support the crew motion models. Presented in appendix A are the analyses of all T-013 activities; appendix B documents the particular models in the manner of a user's guide.

Since the nature of a handbook is to aid and instruct, attempts have been made throughout to identify to the reader the type and location of information available in the document. An outline of the entire handbook given in figure 1-1 provides visibility of the document's content. In addition, chapters are headed by an outline of their contents and a simple diagram identifying the location of related topics.

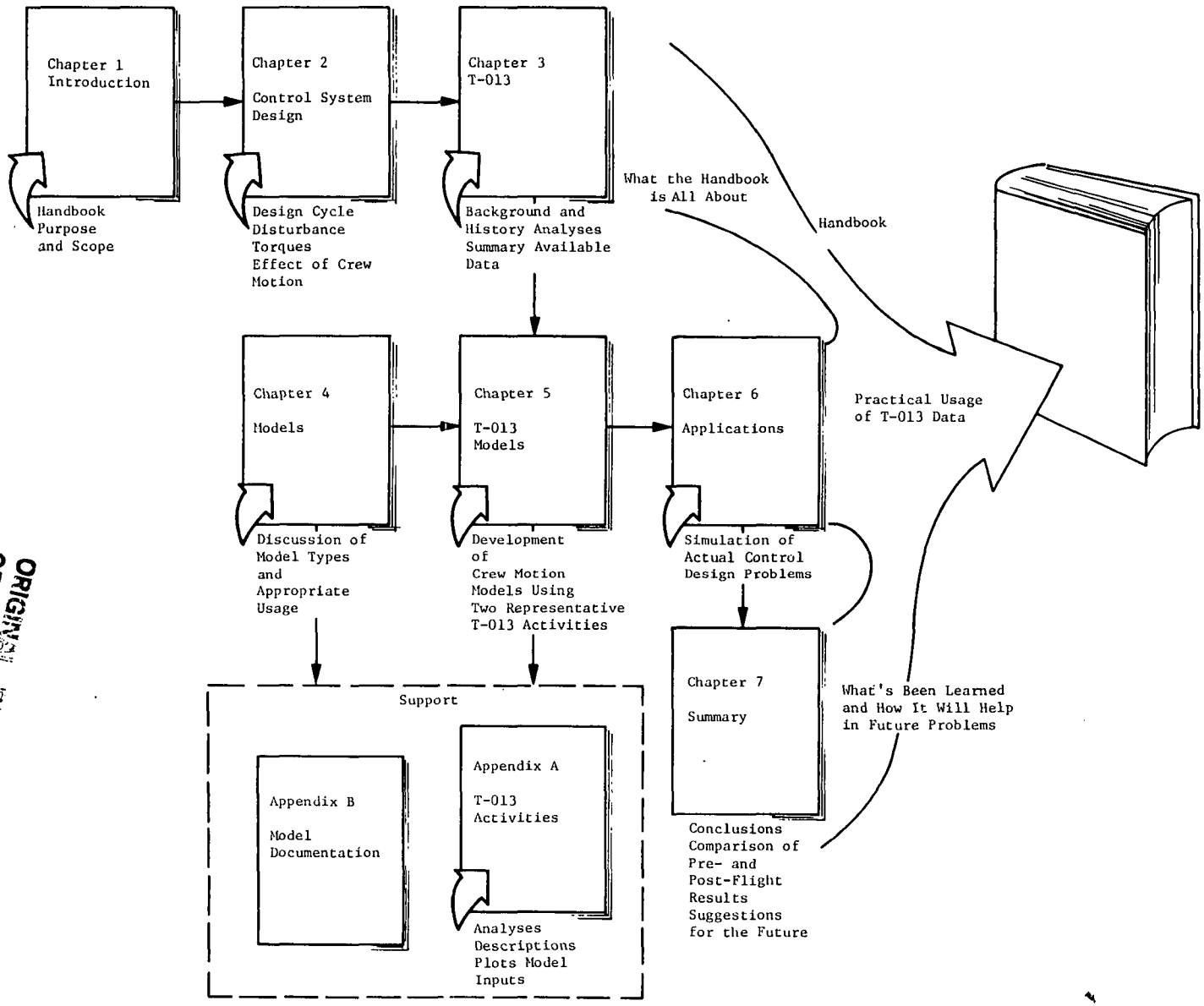

Figure 1-1.- Flow of the handbook.

2.0 EFFECT OF CREW MOTION ON CONTROL SYSTEM DESIGN

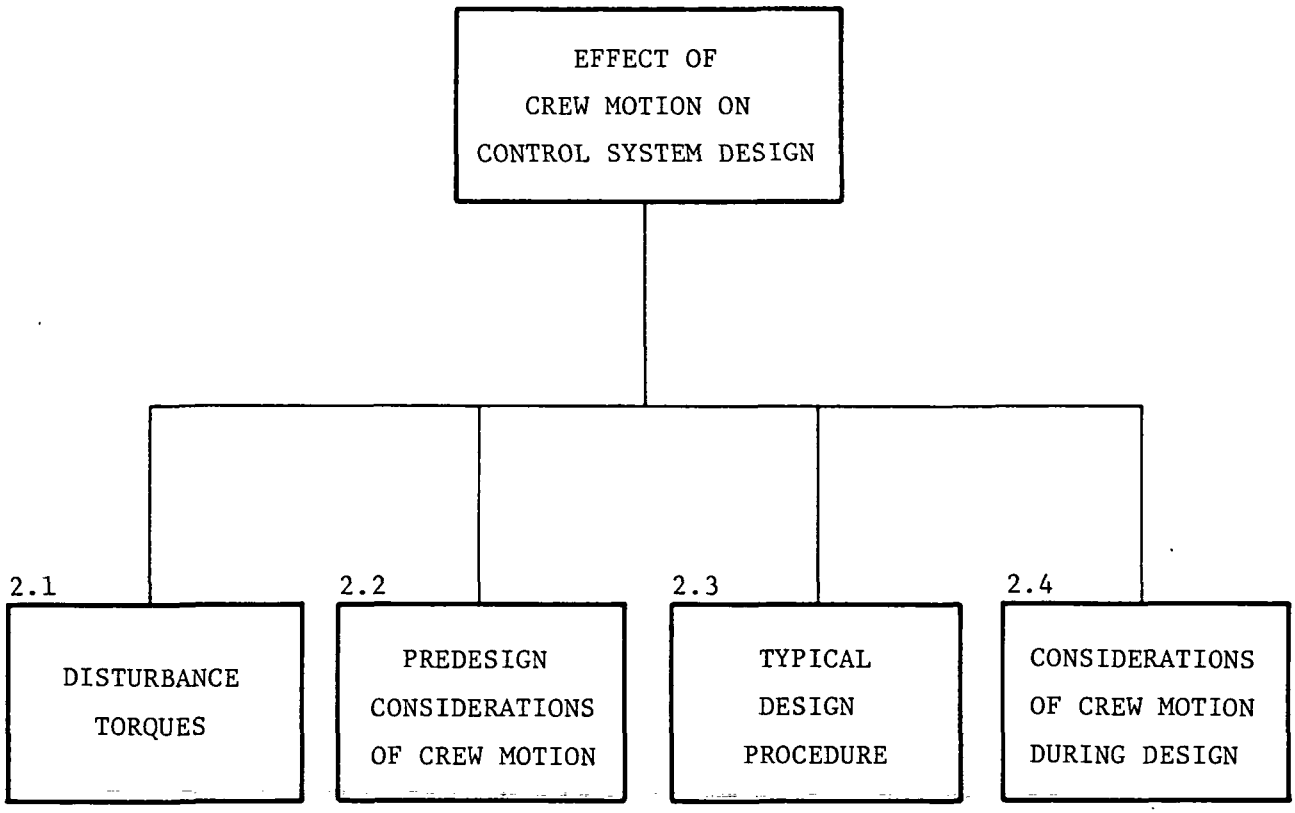

2.0 EFFECT OF CREW MOTION ON CONTROL SYSTEM DESIGN

Understanding vehicle disturbances caused by crew activity in a zero-gravity environment is essential for defining both the control system and the allowable crew motions during portions of the mission where pointing accuracies and/or stability are the governing requirements. Structural flexibility of the spacecraft can be excited by crew movements, and interaction with the control system can occur. All of these factors must be considered, and the control system bandwidth, dead zone, and control authority must be carefully selected to meet objectives of the mission and the design.

2.1 Disturbance Torques

Many types of manned and unmanned space vehicles or satellites have been shown to be operationally feasible; however, many unsolved problems remain for the increasingly sophisticated and complex configurations of the future. In many cases, only the actual flight will establish whether a severe problem exists or whether, indeed, there is any cause for concern at all. Some concern remains about the nature and effect of disturbance torques external to the control system. The time profile and magnitude of these disturbances are important, particularly when the disturbances are cyclic. Given a torque caused by a forceful crew motion, the control system reacts to overcome resulting attitude and rate errors. The control system's time constant and the time between movements determine whether the system may or may not have recovered from the initial disturbance, as shown in figure 2-1. This figure illustrates the system's responses to a one-pulse and a two-pulse disturbance for time constants of 1.0 and 10.0 sec. The response seen in figure 2-1(c) shows less excursion than that in figure 2-1(b), but the much longer time needed to stabilize indicates system searching, or continual oscillation.

In theory, if the passband of the control system is so large that the control system either does not initially react to a disturbance or reacts sluggishly (i.e., a time constant large in relation to the time between torques), the system does not control the disturbance although the vehicle still reacts, thereby affecting pointing accuracies. Also, a disturbance such as a gravity gradient torque, which is cyclic for orbiting vehicles that maintain a constant inertial attitude, requires a cyclic type of control and expenditure of energy. Again, time profiles of disturbances, in light of mission requirements and the control system design, affect the expenditure of energy.

Of the many torques (solar pressure, magnetic effects, gravity gradient, momentum of onboard equipment, vehicle center-of-gravity shift, etc.) that a vehicle may encounter, the one addressed in this handbook is that caused by crew motion. This torque includes disturbances caused when an astronaut performs maintenance or other activities external to an unmanned vehicle as well as the obvious disturbances caused by a crew residing onboard the vehicle.

Crew motion disturbances are divided into two general categories: restrained crew activities and translational (or unrestrained) activities. The first is defined as those actions in which the astronaut is prevented from gross translational movement of his center of mass either by position (sitting at a console) or by restraining devices (e.g., harnesses or foot restraints).

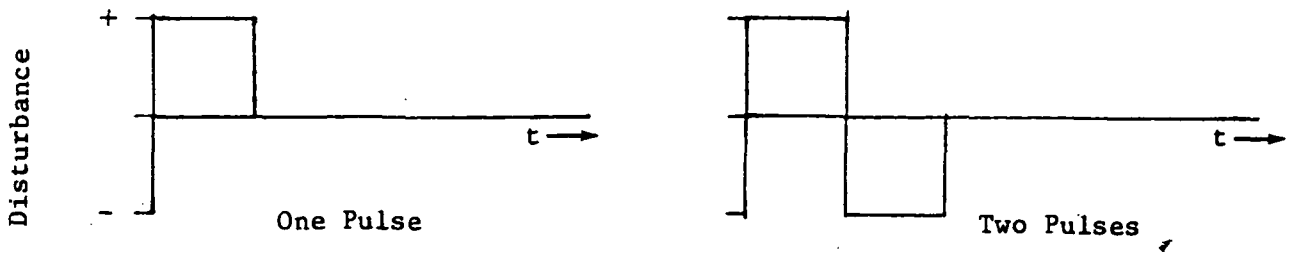

(a) Input.

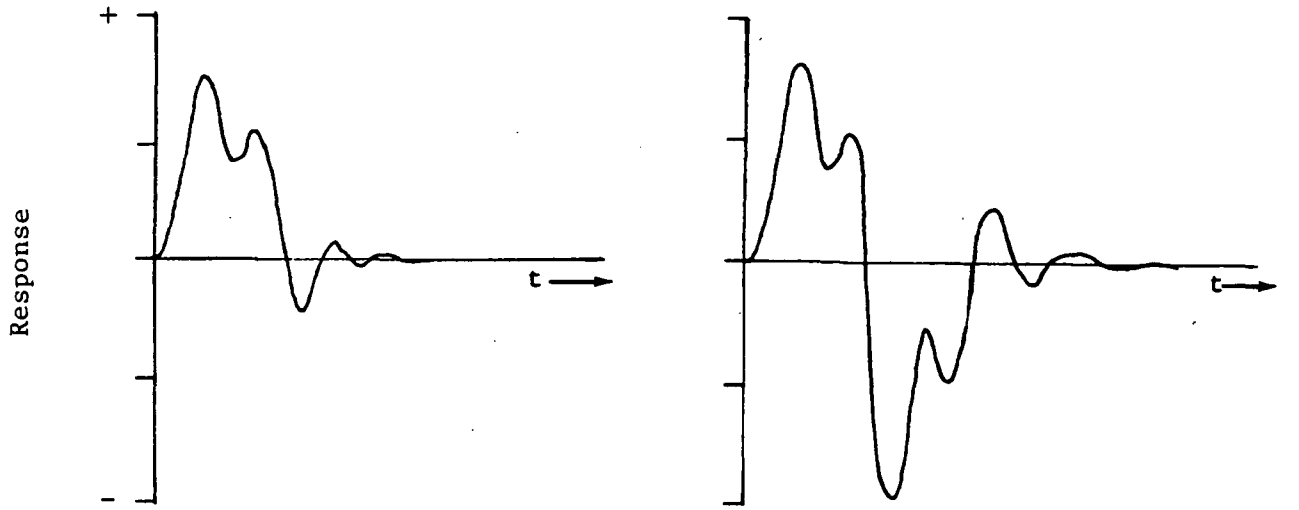

(b) Small time constant.

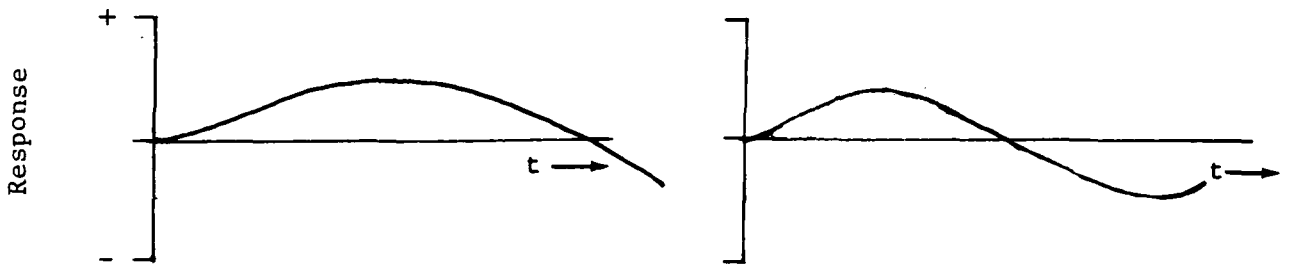

(c) Large time constant.

Figure 2-1.- Comparison of control system responses to one- and two-pulse disturbances.

Translational activities are those which do allow the astronaut's center of mass to move several meters or more.

2.2 Predesign Considerations of Crew Motion

Before one actually designs a control system, he must determine whether crew motion is truly a valid design consideration. The particular mission requirements usually decide the issue because the pointing accuracy considered in terms of the type or range of crew actions involved may well dictate whether the predominant frequency content of the disturbances are within or outside the control system bandwidth. Crew motions generally represent the largest single disturbance force and torque for any manned spacecraft, and their frequency contents are orders of magnitude higher than those of such disturbances as gravity gradient or aerodynamic moments. However, forceful crew motions are not frequent occurrences. Even a low-level activity like console operations, a nominal action anticipated by any manned mission, is expected to occupy only 10 percent of the crew's time. In contrast to this is gravity gradient. The effect of this disturbance torque may be of the same order as that of console operations, but for certain missions with constant, inertial attitude, gravity gradient is a recurring disturbance and thus may cause a greater design problem than the higher level, but infrequent, crew motions.

The implication here is that the designer must consider all possible disturbances in light of the mission requirements to determine whether crew motion can cause a disturbance torque that must be handled by the control system or whether it is better to restrict activities during certain portions of a mission requiring fine pointing. The data in appendix A will be useful in this decision. Appendix A describes a set of crew motions and contains tabulations of both the maximum and the average (1σ) forces and moments for these activities. Similarly, the designer might attempt a preliminary simulation of his worst case crew disturbance, using a first-order model, to determine whether crew motion is indeed a problem.

If the designer determines that crew motion is a disturbance to be designed for, the control system engineer then enters a design cycle to assess the impact of such disturbances on the performance expectations of his design for a new manned vehicle configuration. The following section presents control system design guidelines for the consideration of crew motion disturbance effects.

2.3 Typical Design Procedure

Figure 2-2 is a basic diagram (simplified) of a typical control system. It is included to identify the elements that must be considered in the design of the system. Vehicle characteristics and system performance are generally dictated through envelope constraints and performance requirements, but sensors, actuators, and controller characteristics are derived requirements that evolve to satisfy the mission and system requirements when the vehicle is subjected to internal and external forces.

Mission requirements and corresponding performance requirements not only form the primary starting point in design definition, but also become the fundamental criteria against which the results of the synthesis process must be

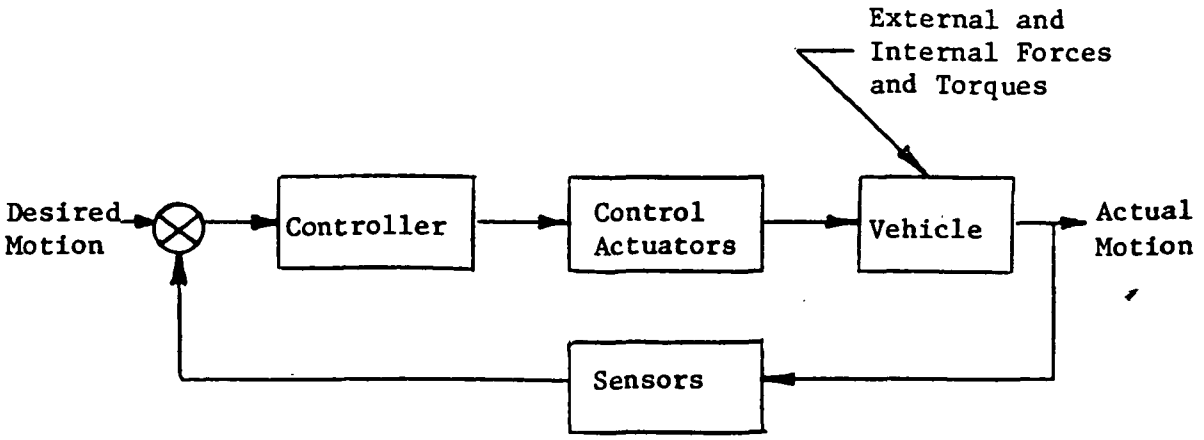

Figure 2-2.- Basic control system diagram.

compared to evaluate the suitability and performance anticipated from the hardware and software design. Figure 2-3 shows the mission (1) and system requirements (2) as one of the two sets of input to the design cycle.

The internal and external disturbance forces (3) are fundamental inputs to the general sizing of system elements. The magnitude of its forces can make crew motion one of the most significant disturbances. As such, its characteristics must be determined either from tabulated data or from modeling techniques to define what peak and nominal force and moment levels as well as frequency content can be expected. This must be taken into account to satisfy the dynamic behavior requirements of the system.

Figure 2-3 portrays the top-level activities involved in the design cycle. Sizing (4) is the design step where some elements are initially defined and impractical considerations are quickly eliminated. A typical control authority of the actuators establishes a derived requirement on actuator size and type. This step requires a physical description (5) of the vehicle to define, for instance, the torque levels needed to satisfy requirements.

The next block in the diagram (6) represents the second step in the selection of control system elements where detailed configuration tradeoffs are performed. Candidate configurations are assembled using the information that characterizes types of sensors, actuators, controllers, and processors. Both hardware and software characteristics are considered. An optimization process takes place at this time where different combinations of subsystems or components are studied to establish the system configuration that best satisfies the imposed requirements with minimum complexity.

By this stage in the design process, the characteristics of all the elements identified in figure 2-2 have been estimated, and the parameters describing these elements have been assigned initial numerical values. A set of candidate configurations has been selected also, with some sort of inherent ranking to suggest choices nearer to "optimum." The next step is to conduct simulations of each to obtain a better understanding of system behavior.

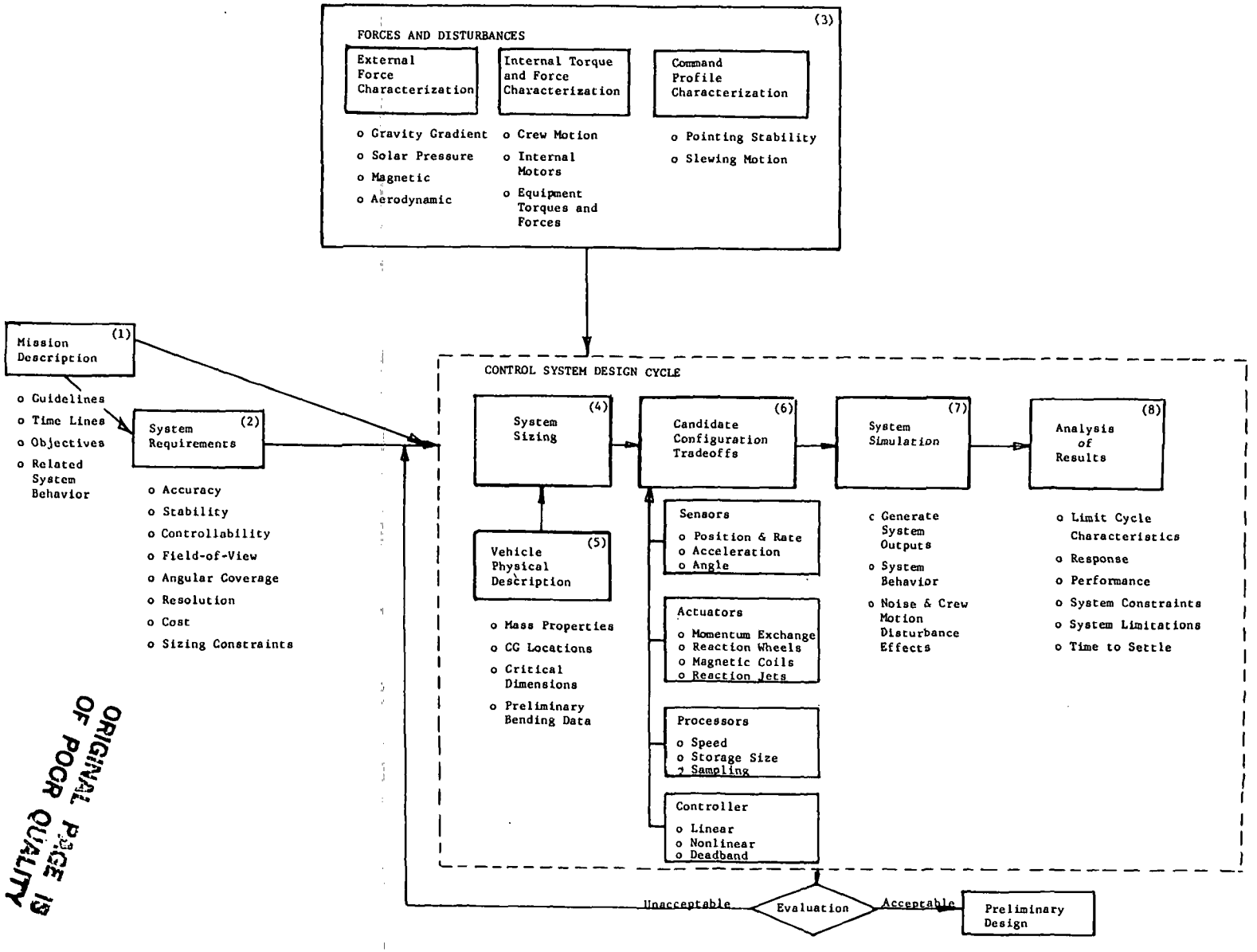

Figure 2-3.- Control system design cycle.

The detailed simulations (7) which now occur are performed to evaluate the forces and moments imposed by the requirements or estimated to be part of the anticipated disturbances. The various techniques for modeling crew motion are now incorporated in the design scheme. Either time histories themselves, or a way of modeling them, can be used as a front end driver to control system simulation programs to produce a range of parametric variations, general system behavior, and noise upon the system.

The interpretation or analysis of the simulation results (8) involves studies of the various recorded outputs (8) which may themselves be force and moment data, statistics or PSD, depending upon the performance requirements being evaluated. Alternative combinations may be examined to determine the best overall performance. Results are quantified in terms of hardware and system limitations.

This last analytic step concludes one iteration of the design cycle. The final step in the design process is an evaluation that takes a broader outlook in deciding whether the "optimum" configuration satisfies all considerations. The factors that must be taken into account now are not only the mission requirements described previously, but also the feasibility given the broader problems of state-of-the-art technology and new development, use of energy and consumption levels, and cost-risk relationships.

2.4 Considerations of Crew Motion During Design

The portion of the tradeoff studies pertinent to this handbook begins with the decisions of whether a linear or nonlinear control system is required, and if the predominant frequency content of the disturbances due to crew motion should be within or outside the control system bandwidth. Unfortunately, there is no simple formula to determine these answers. They generally depend on mission and pointing requirements, as demonstrated by Skylab. The Skylab linear control moment gyro (CMG) control system was designed to control gravity gradient torques. The predominant frequencies due to crew motion occurred outside the bandwidth of the linear CMG control system. Low-pass filtering was relied on (to a certain extent) to decouple crew motions from the CMG control system. However, the crew motion frequencies are within the bandwidth of the high-response Skylab Apollo telescope mount (ATM) vernier pointing control system. In this case, the ATM control system reacted to or "controlled" the crew motion disturbances to maintain high pointing accuracy of the instruments.

Another illustration of the dependence of design on mission requirements is the manned maneuvering unit (MMU) that was test flown in Skylab and is being developed further for space shuttle extravehicular activity (EVA). In this example, the control system was nonlinear with a dead band to "desensitize" the control system to astronaut limb motions. This technique is required to minimize use of the limited propellant supply.

These are just two examples of actual control systems that had to deal with crew motions, yet they display different ends of a wide range of problems. The values of MMU mass properties are several orders of magnitude less than those of Skylab and the mission and pointing requirements are vastly different.

3.0 SKYLAB EXPERIMENT T-013

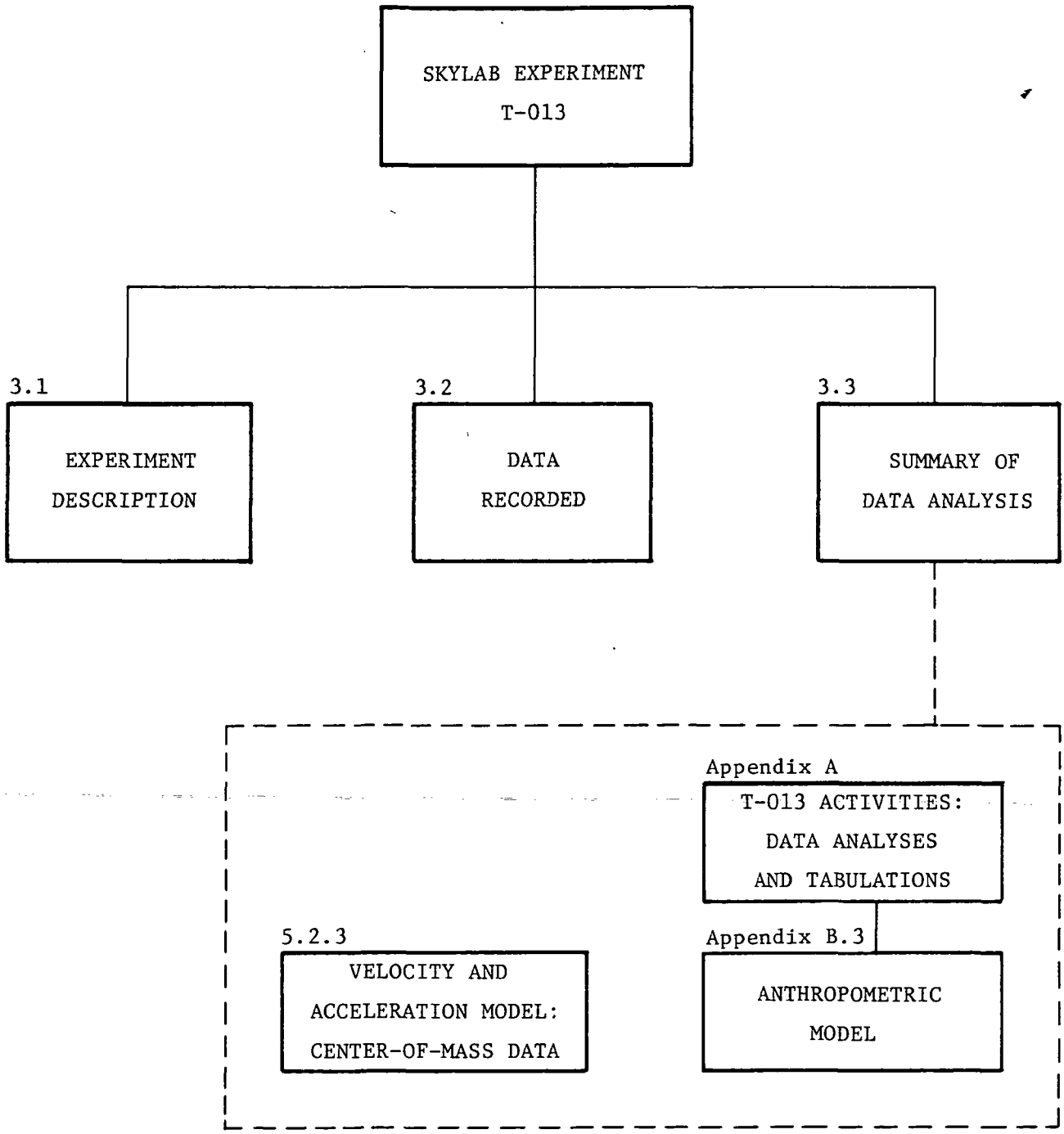

3.0 SKYLAB EXPERIMENT T-013

Experiment T-013 was conducted on the second manned Skylab mission to determine the characteristics and effects of crew motion disturbance. Its purpose was to correlate data from histories of specified astronaut body motions, the disturbance forces and torques produced by these motions, and the resultant spacecraft control system response to the disturbances. Primary application of the disturbance data was intended for the sizing and design of future manned spacecraft control and stabilization systems. Reference 1 discusses the development of T-013.

3.1 Experiment Description

The experiment required an astronaut to perform various partial and total body motions in the forward or dome area of the Skylab Orbital Workshop (OWS). A photograph of the T-013 operations area is given in figure 3-1. The force measuring units (FMU's) depicted in the photograph were the devices used to record force and moment profiles. One FMU consisted of a flat plate and six load cells arranged to sense the forces applied to the plate. Figure 3-2 pictures the load cell array diagram. Since the sense plate is relatively stiff, any force applied to it is sensed by all load cells. For most of the experiment exercises, the astronaut was strapped to foot restraints attached to FMU 1. The second unit was used for the soaring activity only.

The activities performed for the experiment consisted of normal or typical exercises such as breathing, coughing, simple arm and leg movements, and worst case exercises such as soaring and wall push-offs. The area depicted in figure 3-1 is repeated schematically in figure 3-3 to indicate the paths of one or two astronauts during the soaring activity.

3.2 Data Recorded

Three sets of data were recorded by T-013 to measure crew disturbance. The following discussion summarizes them briefly. A detailed history, including descriptions of hardware, data reduction, and preliminary analysis, is available in reference 2. Appendix E of this reference document also includes information on a digital magnetic tape containing the reduced T-013 telemetry data and gives details describing how to read the data.[1]

---

[1] Inquiries concerning availability of these data should be addressed to:

National Space Sciences Data Center
National Aeronautics and Space Administration
Goddard Space Flight Center
Code 601
Greenbelt, MD 20771

Reference: NSSDC ID 73-027A-42A

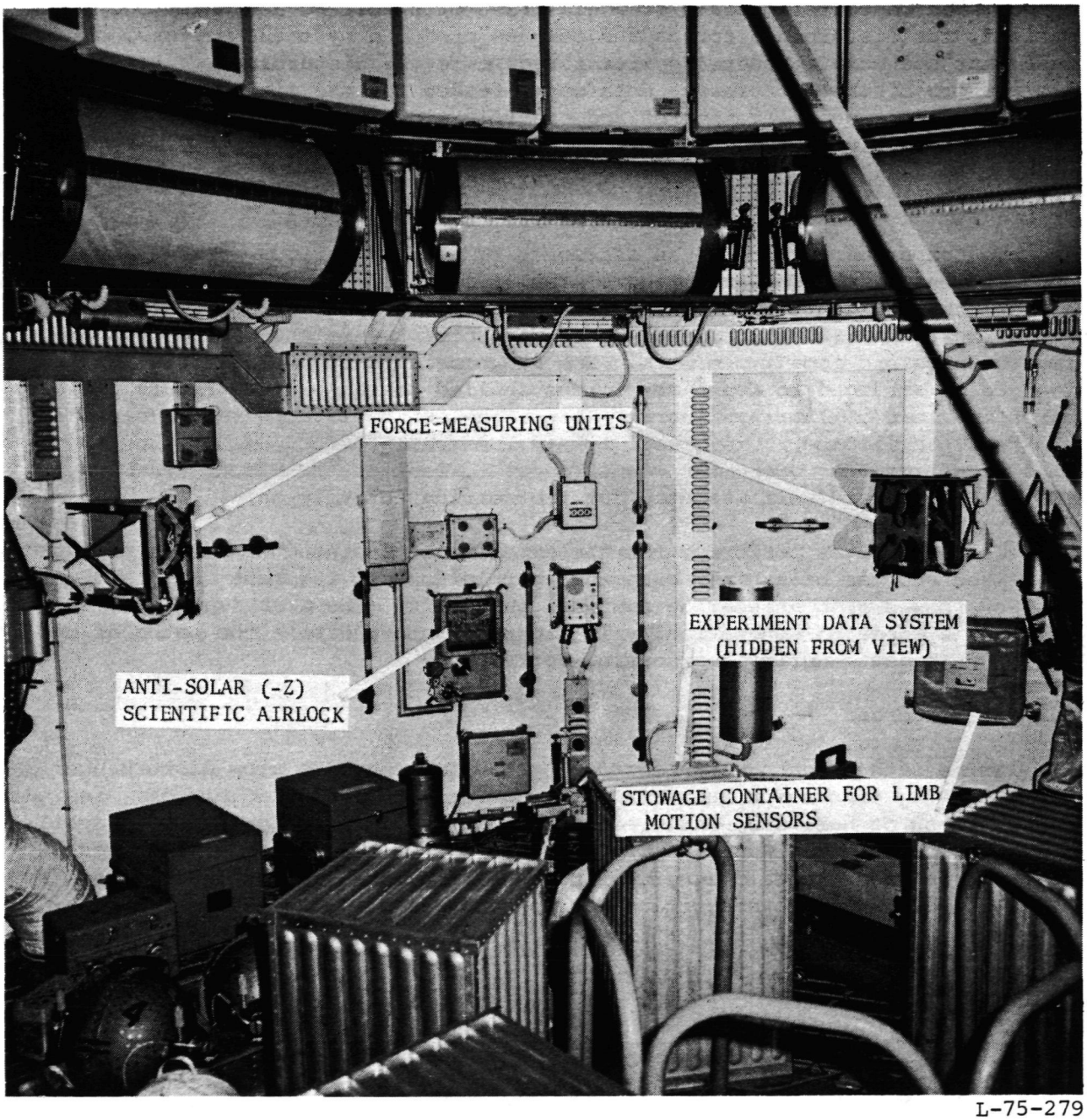

L-75-279

Figure 3-1.- Photograph of T-013 operations area in OWS (from ref. 2).

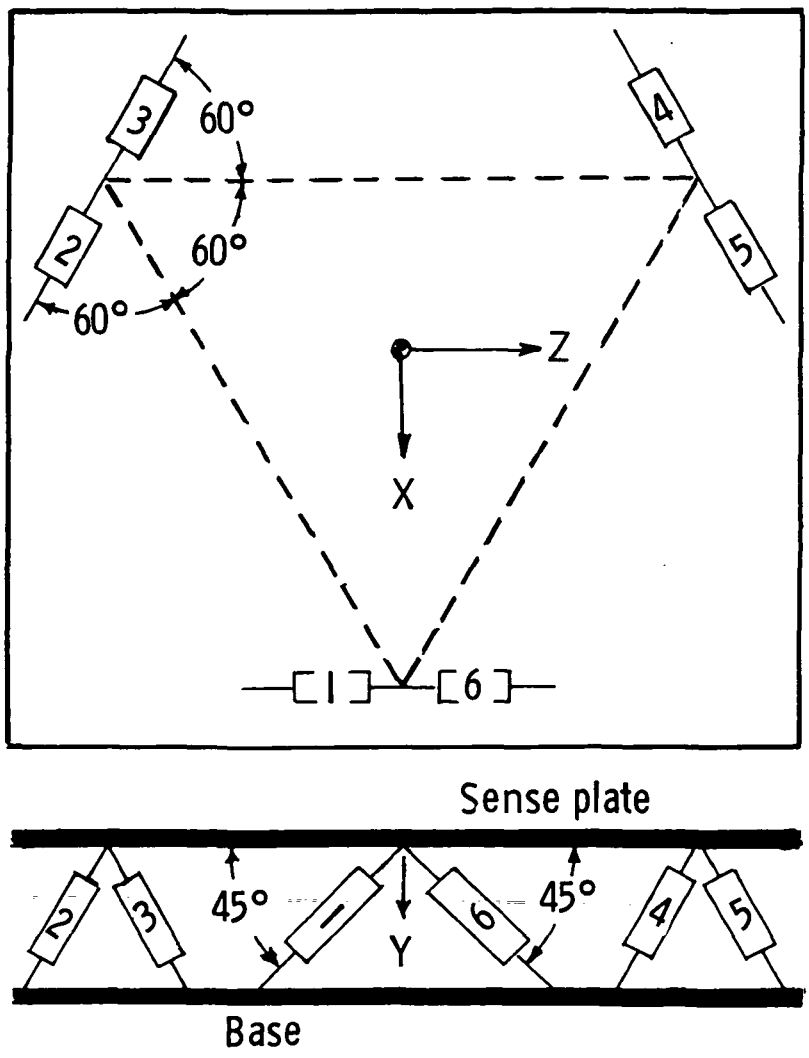

Figure 3-2.- Load cell array diagram (from ref. 2).

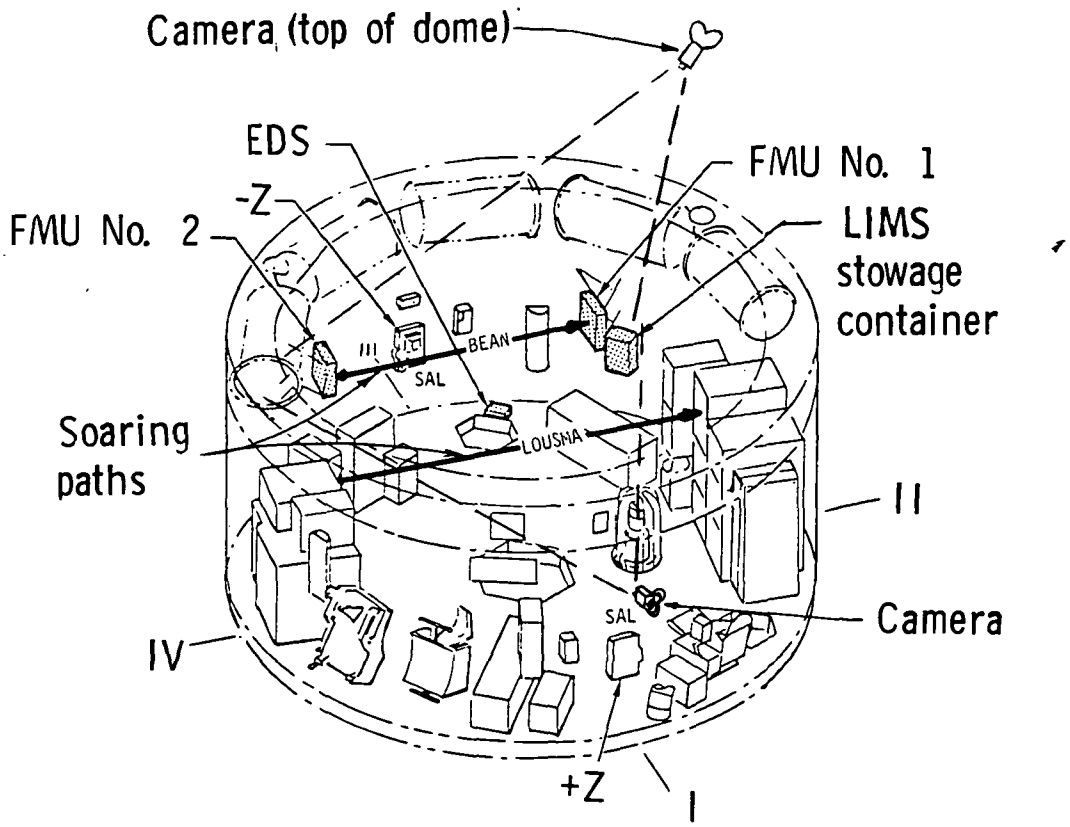

Figure 3-3.- T-013 operations area of OWS (from ref. 2).

The forces and moments sensed at an FMU are functions of the load cell measurements and were derived by the set of equations given in reference 2, pages 16 and 17. The coordinate system for the recordings relative to the FMU's and the astronaut's position is given in figure 3-4, showing the orientation of each FMU as installed in the OWS and the conversion to the analysis coordinate system. The insert is a top view of the primary subject as he is strapped onto FMU 1.

Astronaut movements were recorded on motion-picture film for selected exercises and reduced to x-, y-, and z-coordinates of center-of-mass motion for the soaring activities. This information was collected for use in developing velocity and acceleration data for wall push-off, soaring, and subsequent impact.

The third set of data required knowledge of the time orientation of the subject's limbs with respect to his torso during the performance of the exercises. To obtain this information, a limb motion sensing system (LIMS) was developed for T-013. The LIMS measured limb movements as Euler angles (roll, pitch, and yaw sequence) at the subject's shoulders and hips. A diagram of the hardware is shown in figure 3-5. Figure 3-6 is a photograph of the LIMS as worn by the subject astronaut. The targets identified were used in the motion-picture data reduction effort.

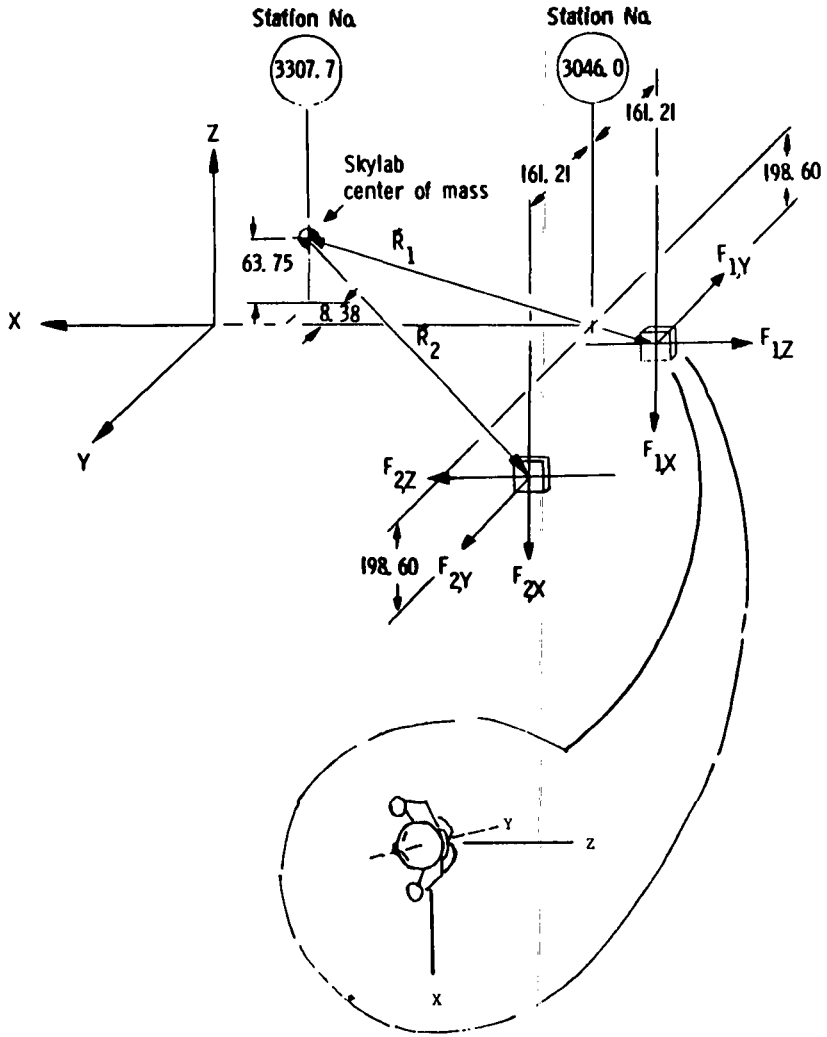

Figure 3-4.- FMU locations in OWS (adapted from ref. 2). All dimensions are in centimeters.

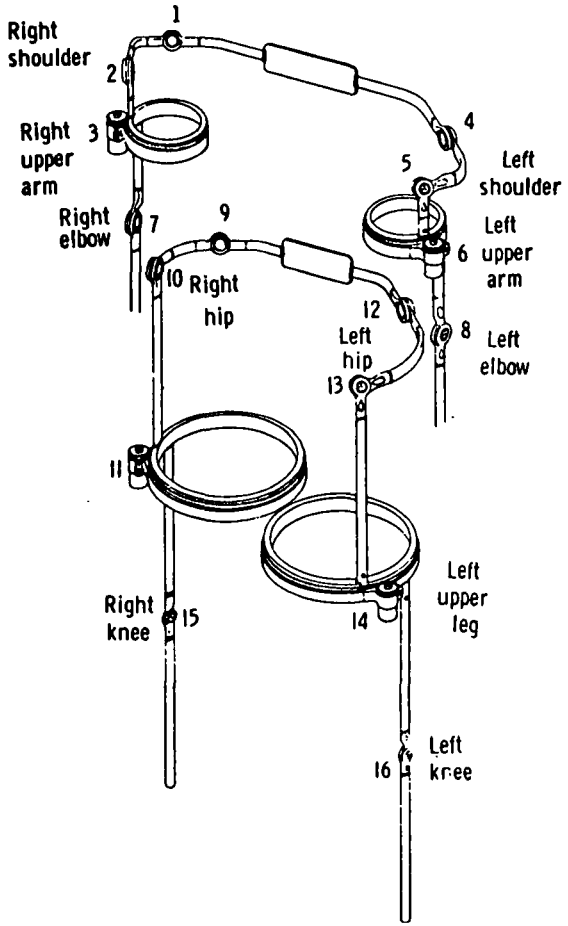

Figure 3-5.- Limb motion sensor (LIMS) exoskeleton showing potentiometer identification (from ref. 2).

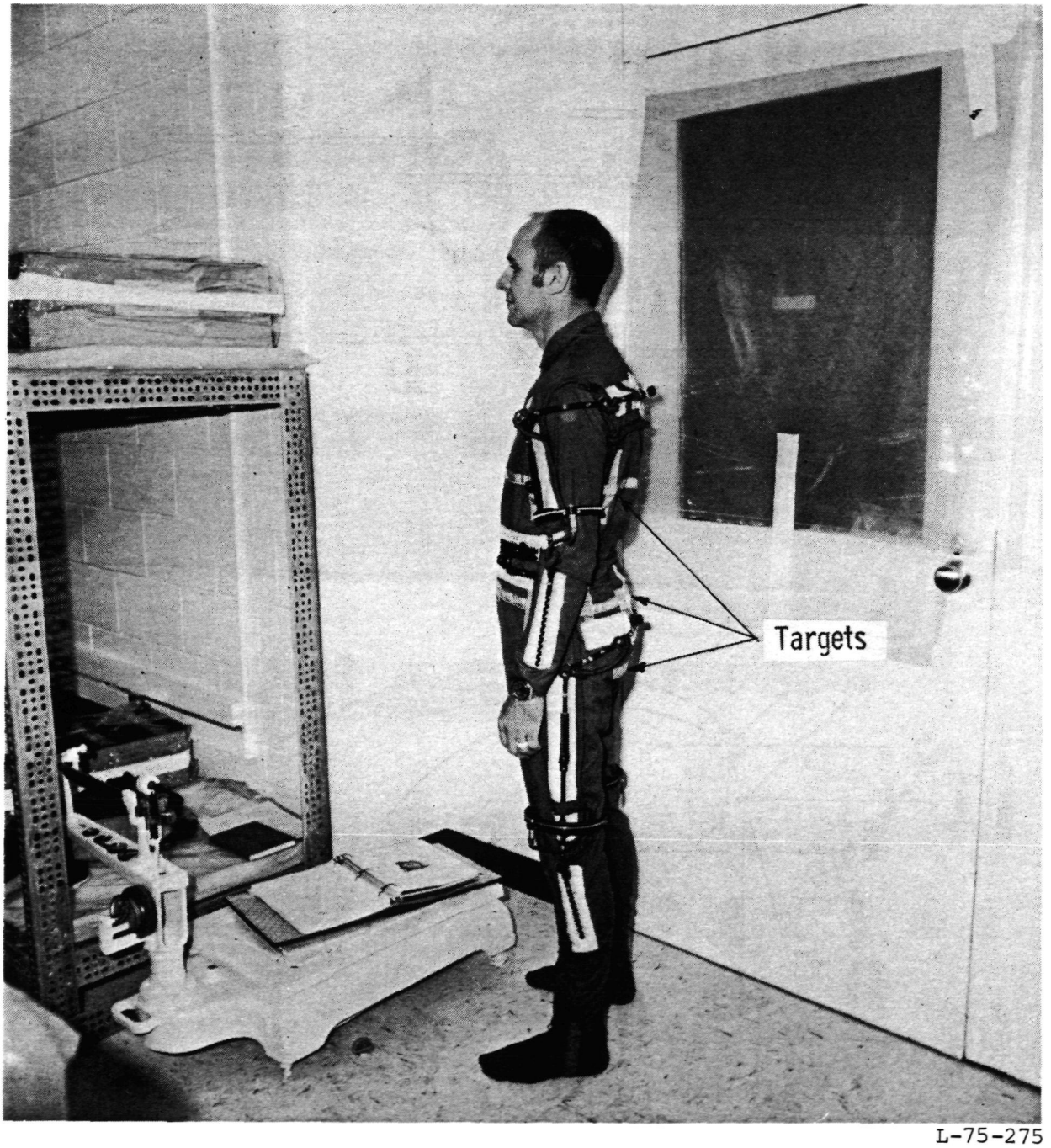

L-75-275

Figure 3-6.- LIMS as worn by subject.

3.3 Summary of Data Analysis

For the purposes of this handbook, the T-013 crew motion forces and moments have been analyzed for statistical characteristics and frequency content. The types of tabulations and graphical representations available are

(1) Time histories

(2) Maximum level

(3) Range

(4) Standard deviation

(5) Power spectral density (PSD)

(6) Peak power

(7) Frequency of peak power

(8) Root mean square (rms) of PSD

These data, with pertinent descriptions and discussions, are available for each category of the T-013 activities. This information is contained in appendix A together with a detailed explanation of the nature of the data. The following chapter indicates the use of the data in control system design.

A discussion of the center-of-mass data is given in section 5.2.3. Similarly, the LIMS data are addressed in appendix B, section 3. Although these two sets of information were part of the overall T-013 experiment, they have not found immediate use for the present purposes of this handbook and are included only for information.

4.0 USE OF THE HANDBOOK

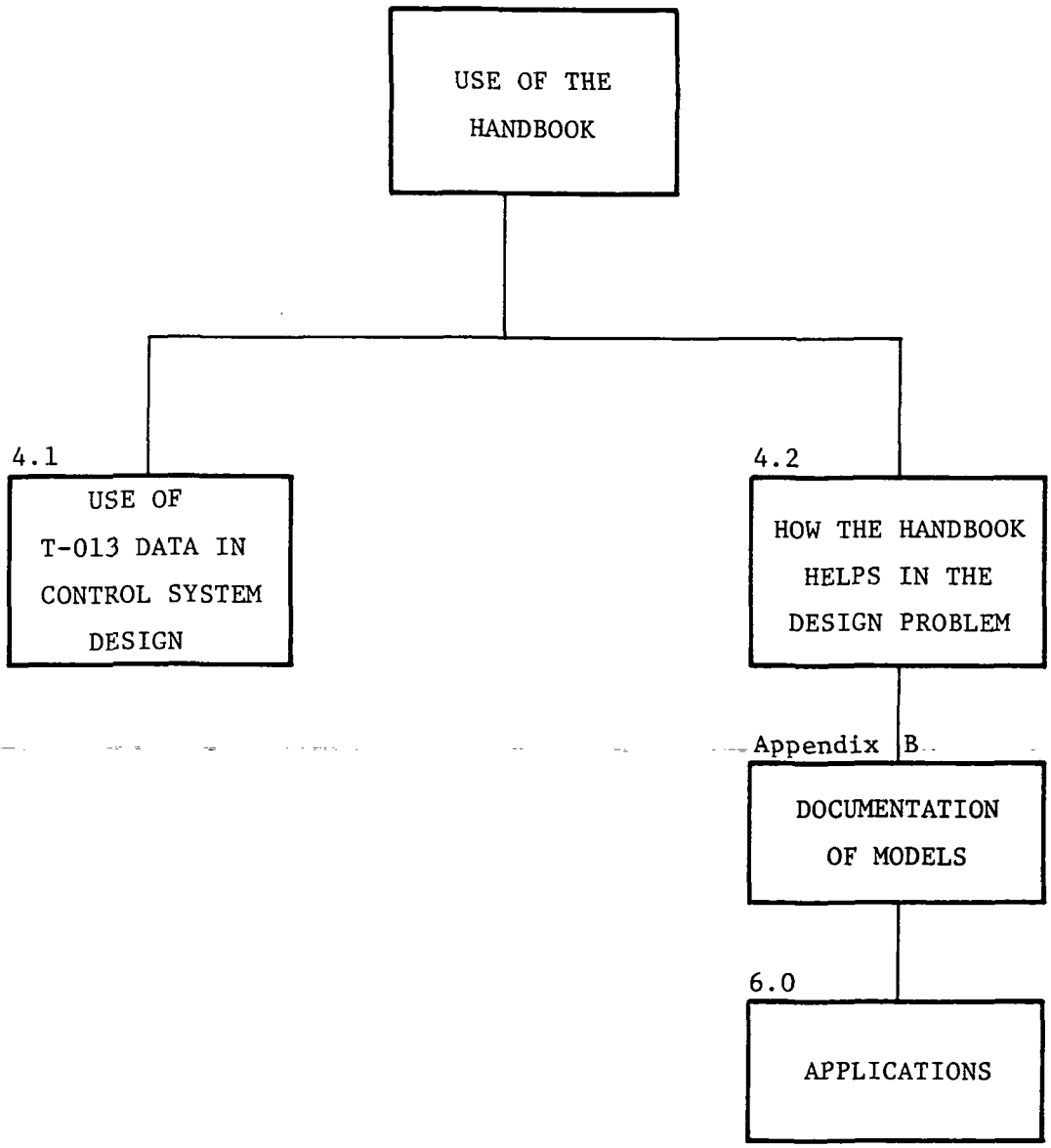

4.0 USE OF THE HANDBOOK

The most important function of this handbook is to serve as a guide for incorporating crew motion effects into the control system design process. The preceding chapters introduced the subject and pertinent background to provide the user with an understanding of both the typical procedure followed and the significance of crew motion to that procedure. This chapter details specific uses of crew disturbance data in control system design and identifies locations of the needed data and sample applications within the handbook.

4.1 Use of T-013 Data in Control System Design

This discussion refers to the forces and disturbances block of the design cycle depicted in figure 2-3.

Assessment of the effect of crew motion disturbances on a new manned vehicle requires that configurations involve estimates of mass properties and vehicle geometry, including the location of the crew activities within the configuration. This requirement is necessary because the T-013 data described in this handbook are local disturbances about the FMU and do not include Skylab moment arms. Reference 2 gives the appropriate conversion equations for the Skylab vehicle. For the new design, the analyst must define anticipated vehicle disturbance moments by applying the modeled disturbance of the crew activities at the crew locations, considering the appropriate moment arms.

Figure 4-1 highlights the development of the T-013 data and delineates the role that crew motion plays in the preliminary design cycle as applied to the design of a new manned space vehicle control system.

Initially the absolute maximum range and standard deviation of the crew motion force and moment time histories are used in system sizing. The magnitudes of the crew motion disturbances, in conjunction with the vehicle mass properties, help determine the moment magnitudes that must be generated by candidate actuators.

Second, the power spectral densities (PSD's) find utility in designing controllers for candidate configurations. At this stage of the design process, a linear system is assumed. If y denotes the vehicle motion in response to crew motion disturbance x, the output PSD can be related to the crew motion PSD by

$$\Phi_y(\omega) = |H(j\omega)|^2 \cdot \Phi_x(\omega)$$

where $H(j\omega)$ is the frequency response function of the total control system. In addition to providing adequate stability margins, the controller must also be designed so that system response to both external and internal disturbances (such as crew motion) is satisfactory. Altering controller parameters can modify $H(j\omega)$ to produce required changes in the output $\Phi_y(\omega)$. The process

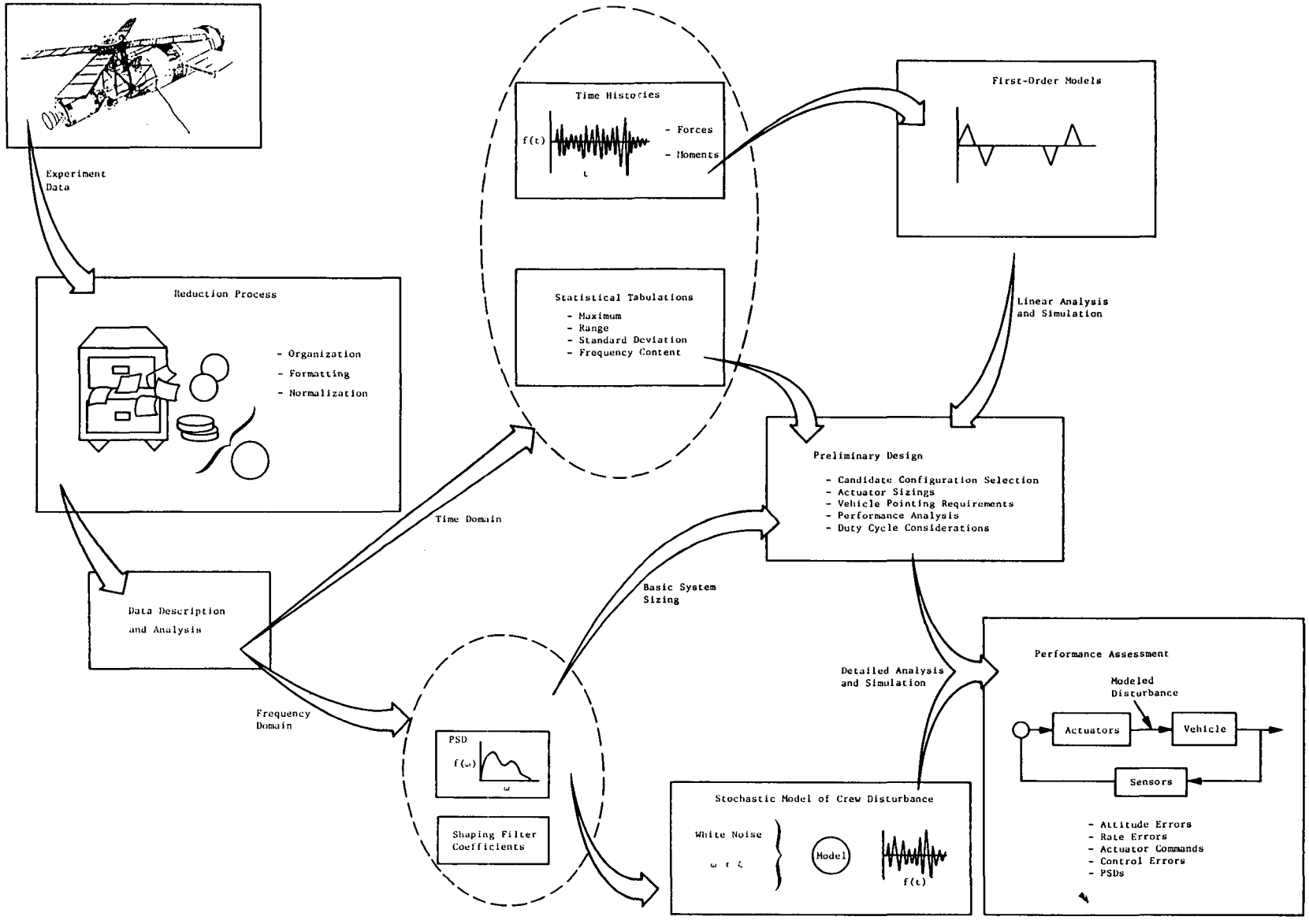

Figure 4-1.- Use of T-013 data.

for doing this is by no means simple and often involves trial and error. One objective of the design process is to minimize the variance of the system response to disturbance inputs. The variance $\left(\text{or } (\text{rms})^2\right)$ is given by the integral of the output PSD.

Finally, the crew motion time histories and the related models can be used in a total nonlinear system simulation. This stage of the design process is necessary to verify the linear control system design that was developed in the preceding stage.

4.2 How the Handbook Helps in the Design Problem

Aside from characterizing the types of crew motion, the most useful product of gathering and studying the T-013 data is the development of models to simulate crew motion disturbance. Chapters 5.0 and 6.0 of part II address this modeling problem by identifying various techniques, by developing specific models for two different crew motions, and finally, by applying the models to actual control system problems. This last subject, the models' application, probably makes up the most useful portion of the handbook since it is designed to be a practical guide for incorporating the effects of crew motion into actual problems.

PART II

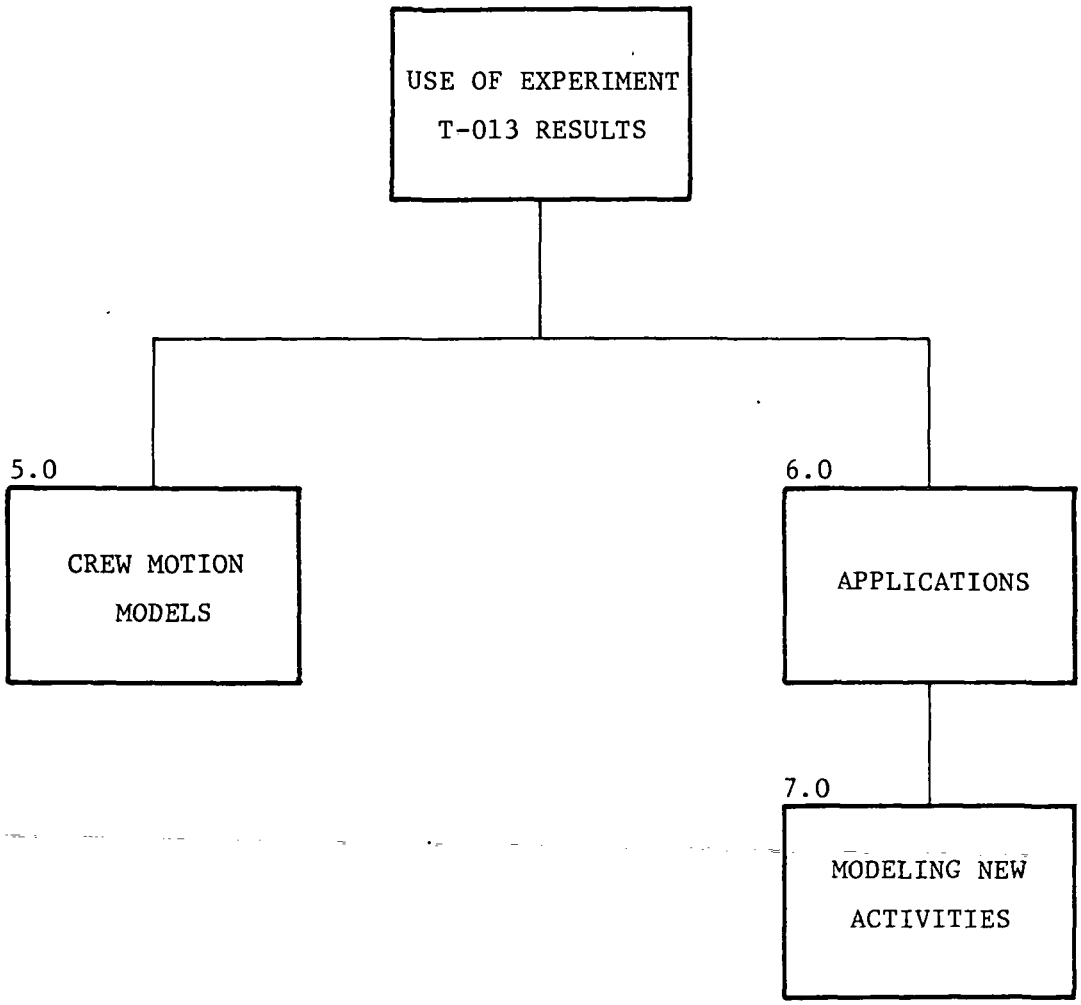

5.0 CREW MOTION MODELS

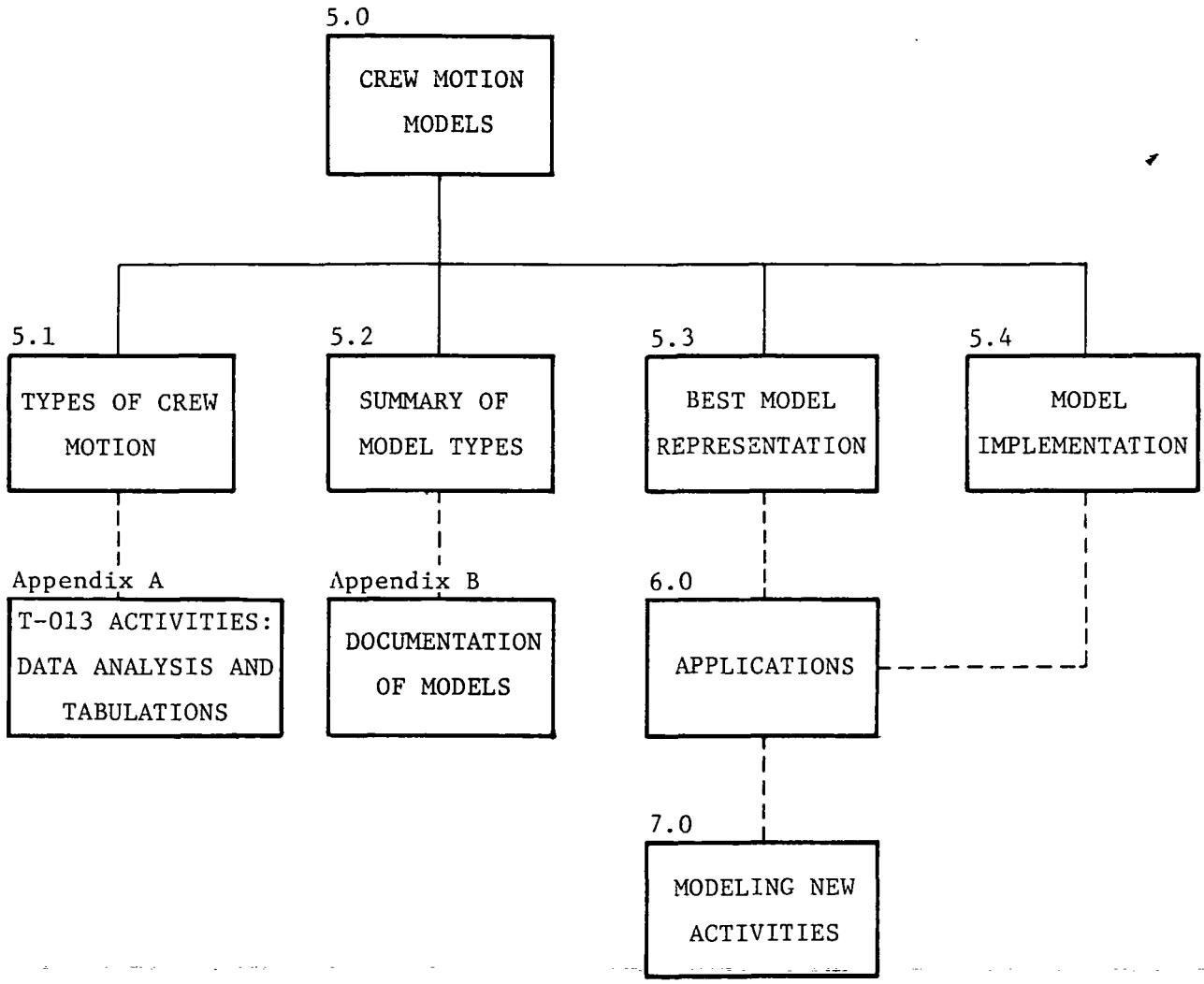

5.0 CREW MOTION MODELS

This chapter discusses the modeling of crew motion disturbances. The summaries of crew motion types and modeling techniques in sections 5.1 and 5.2 and the resolution of a best model representation in 5.3 serve as an important introduction to the applications by considering the problem of selecting the appropriate model for a particular activity, thus establishing some important guidelines.

5.1 Types of Crew Motion

For modeling purposes, crew motion disturbances are divided into two categories, random (stochastic) movements and deterministic actions. Stochastic activities are repetitive actions which are reasonably independent of the personality of the individual performing them. Of the activities designed for T-013, only console operations appear to be stochastic in nature, but personal hygienic functions and food preparation actions (ref. 3) might also be considered random movements. A deterministic action, on the other hand, exhibits a definate energy content at periodic intervals (such as a wall push-off) or is characterized by an individual's interpretation of how to perform an exercise (intentional and controlled body motions). For example, arm flapping forces largely depend on the enthusiasm the subject may put into the activity, and the frequency content varies depending upon how fast he performs.

The pattern of an activity's force profile is often helpful in determining its nature. Deterministic actions show up on time histories as triangularly shaped pulses which (1) are quite large in magnitude or (2) form a distinctive pattern. A case in point is the T-013 respiration activity. At first thought, breathing, coughing, and sneezing would seem to be as random in nature as console operations. But in actual fact, the time histories (fig. A-5) show that the astronaut's distinct simulations of "five breaths" or "six sneezes" during T-013 are distinctive, identifiable pulses whose magnitudes appear to increase proportionally with the subject's enthusiasm.

It may not always be the action itself but the manner in which it was executed or recorded that determines its "nature." The manner in which an activity is performed may be instrumental in defining whether the action is stochastic or deterministic. If, for instance, the respiration exercises mentioned above had not been segregated by type but rather had been mixed and randomly repeated, then the general category of respiration exercises could be considered stochastic, since the individual actions (breathing, etc.) would not be identifiable in the composite motion. Similarly, if different subjects perform an action which seems to be deterministic often enough, then the final composite could be analyzed stochastically.

The two T-013 activities selected for sample applications are console operations and one-man forcefully soaring. Not only do the actions themselves represent two different levels of forces and torques, but of all the T-013 exercises, they perhaps form the best representations for two distinctly different modeling techniques.

5.2 Summary of Model Types

This section introduces some of the possible types of crew motion models. More details, including listings and sample input cases, where pertinent, are available in appendix B.

5.2.1 Anthropometric model

Initial studies of crew motion disturbances considered crew members as point masses and investigated the effects on a spacecraft of translating one or more of these masses from one point to another within the spacecraft. Following these earlier simulations, consideration of man as a dynamic system was begun. Development of an anthropometric model of the human body was carried out, using earlier U.S. Air Force anthropometric studies. This anthropometric model was extended to include the dynamics of body-segment motions. The resultant analytic model may be used to compute crew disturbance forces and torques in a spacecraft for specified astronaut motions. A computer program that incorporates this model with a simulated control system can be used to define the resultant spacecraft rate and attitude errors to aid the designer in selecting control torque levels and response times needed to compensate for the crew motion torques.

Although the time-dependent orientation of the astronaut's limbs with respect to his torso was measured as part of experiment T-013 for all the activities, the anthropometric model was not exercised for the purposes of the handbook. This resulted because the existing computer program of the model is large, and resolution of executional difficulties exceeded the scope of current effort. Section 3 of appendix B describes the model and input data further and gives references for those who wish to pursue the matter. (See appendixes A and B of ref. 1.)

5.2.2 First-order models

For the purposes of this discussion, first-order models are those procedures that are easy to implement, require only general characterization of the disturbance, produce preliminary results, and/or indicate whether more detailed analysis is necessary. Some activities, generally deterministic ones, lend themselves more to a first-order representation than to other more sophisticated and complex techniques.

First-order models are particularly useful at the beginning of a design study when detailed information is unavailable. In fact, resources required to analyze properly a wealth of data are generally unavailable at a preliminary stage (when it may even be questionable whether crew motions have any significant impact on a particular mission).

The particular type of first-order model developed for the applications in the next chapter is a time function that identifies the large magnitude spikes of a deterministic action and sets any disturbances to zero that represent noise or insignificant activities.

5.2.3 Velocity and acceleration model: center-of-mass data

The velocity and acceleration model is a special type of first-order model for soaring exercises based on the relation F = ma. It was postulated that the center-of-mass data, reduced from experiment T-013 motion-picture film, would form the basis of development for such a model. However, in reality, the process of taking first and second derivatives of position data proved to be highly untrustworthy and misleading. The computational method used to derive acceleration tended to exaggerate small but sudden movements, and the points of importance, such as push-off and landing, were lost among the large values of the second derivatives of noise. The outcome was that instead of verifying the velocity and acceleration results, the experimental force data had to be used to make sense out of the accelerations.

It is thus concluded that if a designer wishes to use an accurate velocity and acceleration model, he should use the force profiles of T-013 telemetry data, deriving acceleration from dividing force by the mass of the primary T-013 subject (69.4 kg). Using force profiles might be useful when determining the effect of a different astronaut.

5.2.4 Stochastic model

The stochastic model studied for use in simulating types of random crew disturbances is developed by shaping the constant frequency spectrum of a wideband noise. "White" noise theoretically contains all frequency components, and its power spectrum is consequently a straight (horizontal) line in the frequency domain. For modeling purposes, a constant PSD wideband noise is generated as an input to a shaping filter to acquire the frequency characteristics of a particular crew motion. Input to the model consists of three shaping parameters: τ (gain), ω (frequency), and ζ (damping). The output represents a disturbance in the time domain whose profile should "resemble" that of recorded data for the same activity, insofar as magnitudes of peak and average forces or torques should approximate anticipated or expected values. For T-013 activities, these values are given in statistical tabulations in appendix A.

The model is limited because the results of a stochastic process look "regular," i.e., values large in magnitude but infrequent in occurrence are averaged, and the chief characteristics in the time domain of a deterministic action are lost. The model and its results are verified if: (1) the total energy of original data approaches that of modeled data; (2) rms's of resulting PSD's are approximately equal; and (3) if the computed vehicle response to both disturbances is the same. It is not sufficient to meet conditions (1) and/or (2). The third criterion, that of effecting the same type of vehicle response, must also be met. Therefore, the importance of magnitudes of the output disturbance is stressed.

5.3 Best Model Representation

It is difficult to recommend a general best model because of the many problems involved, and it is virtually impossible to do so without including a few qualifying stipulations.

The T-013 activities have been characterized (as presented in appendix A) in sufficient detail to allow a confident choice of the best method for modeling a particular T-013 disturbance. One problem arises when new activities for which there are no simulations occur and, therefore, no time profiles, no idea of pattern, maximum level, frequency content, etc. This subject is addressed further in section 7.2, which presents some suggestions for obtaining required information. A second difficulty is mentioned in section 5.1: Is the activity random or deterministic? A third complication may arise from the mission requirements and the degree of accuracy and refinement required of the modeling technique.

When the type of activities involved in a particular mission is ignored, the stochastic model is clearly a good analytic tool for analyzing extreme pointing accuracies. Less stringent requirements mean that the coarser results of a first-order model are generally sufficient.

Appendix A identifies the filter parameters needed to input the T-013 exercises into the stochastic model. By definition, the results of such a simulation produce a disturbance with the same frequency content as that of the original data. But this technique may not indicate the disturbance profile magnitude for deterministic actions adequately because the magnitudes of peak and average forces and torques may be distorted to between 2/3 and 1/2 of those values actually obtained during the experiment.

Activities that are not found among the T-013 types may dictate the "best" model by virtue of the quantity and quality of the data available to characterize the movements. Usually, unless a detailed simulation has been performed, a first-order representation best suits the purpose. If a time profile is well identified, the designer desiring to use the stochastic model can determine the frequency content and subsequently derive filter parameters.

The most significant criterion to be considered in selecting a good representation of crew motion, however, should be the model's purpose. The principal function of a model is to evoke accurate responses in a control system simulation. The overall conclusion seems to be that deterministic actions are best represented by force and moment profiles in the time domain. Thus, the easier, more straightforward, and often more accurate way to model the effect of crew motion is to use a first-order model such as the one described in section 5.2.1 and documented in appendix B, section 1. A first-order model needs only a sketch of the principal impulses plotted against a time line in order to initiate a control system simulation. The greater detail and depth of analysis available with the stochastic model is not generally required and often not worth the trouble involved in studying the problem thoroughly or setting up the solution. The most typical stochastic action is console operation, which is fully characterized in this handbook (section A.2.1). The required information is available to execute its stochastic representation.

Thus, if an activity is truly random or if the frequency content is needed, the stochastic model is the analyst's best tool. For most other cases, the first-order model is easier and faster to implement and often effects more dependable responses.

5.4 Model Implementation

For the following demonstration of model implementation, two T-013 activities were selected: soaring (one man forcefully) and console operations. Not only do the actions themselves represent two different levels of forces and torques, but of all the T-013 exercises, the soaring and console operations best represent the different modeling techniques, stochastic and deterministic. These two modeled activities are used in a planar control system design presented in a subsequent applications chapter.

5.4.1 Soaring

Four cases of soaring were performed for the T-013 exercise to demonstrate differences when normal is compared to forceful and one man is compared to two men. One man soaring forcefully between FMU's (refer to fig. 3-3) was selected for application purposes as more interesting and representative.

The deterministic first-order model for soaring is a time function consisting of triangular pulses to represent the subject's push-off from one FMU (or wall) and the subsequent landing on the opposite one. The astronaut performing this activity had a mass of 69.4 kg and achieved a velocity of 2.16 m/sec. Since he pushed off with his feet and landed with his hands, the astronaut's body length and reach had to be taken into account when time to soar was determined. Thus, the distance traveled was on the order of 2.1 m rather than the 3.2 m between FMU's. This defines a pulse of 1.0-sec duration for the model with a peak value at its midpoint determined from the data in appendix A to be 300 N. A total time of 10.0 sec between the end of impact and the start of next push-off was allowed for the astronaut's movements in turning around. Any forces applied during this time are defined as noise and are ignored for the present purposes. Figure 5-1 presents a schematic of this model.

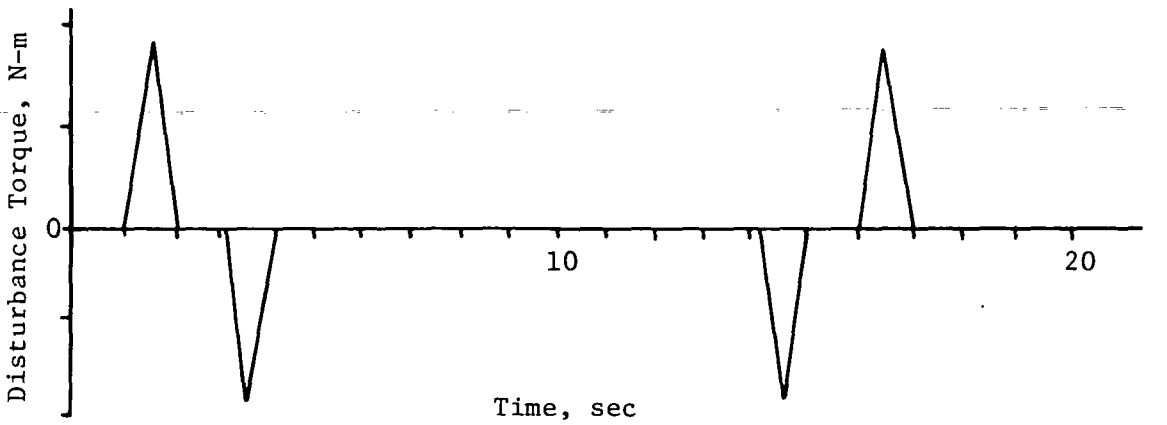

Figure 5-1.- First-order model.

Disturbances developed in this manner compose the deterministic, first-order model which is implemented by means of a table lookup with linear interpolation between the set of table data points. This model is detailed in appendix B for the interested reader.

5.4.2 Console operations

Among the T-013 activities, console operations make up a good set of random activities. As such, they are suitably represented by the stochastic model which was first introduced in section 5.2.4 and is documented in appendix B.2.

To illustrate the model implementation of a stochastic process, the Z-axis component of force F_Z for console operations is detailed. The corresponding PSD is presented in figure 5-2. The solid curve represents the analyzed flight data while the dashed one indicates the output of a second-order shaping filter as discussed in section 5.2.4.

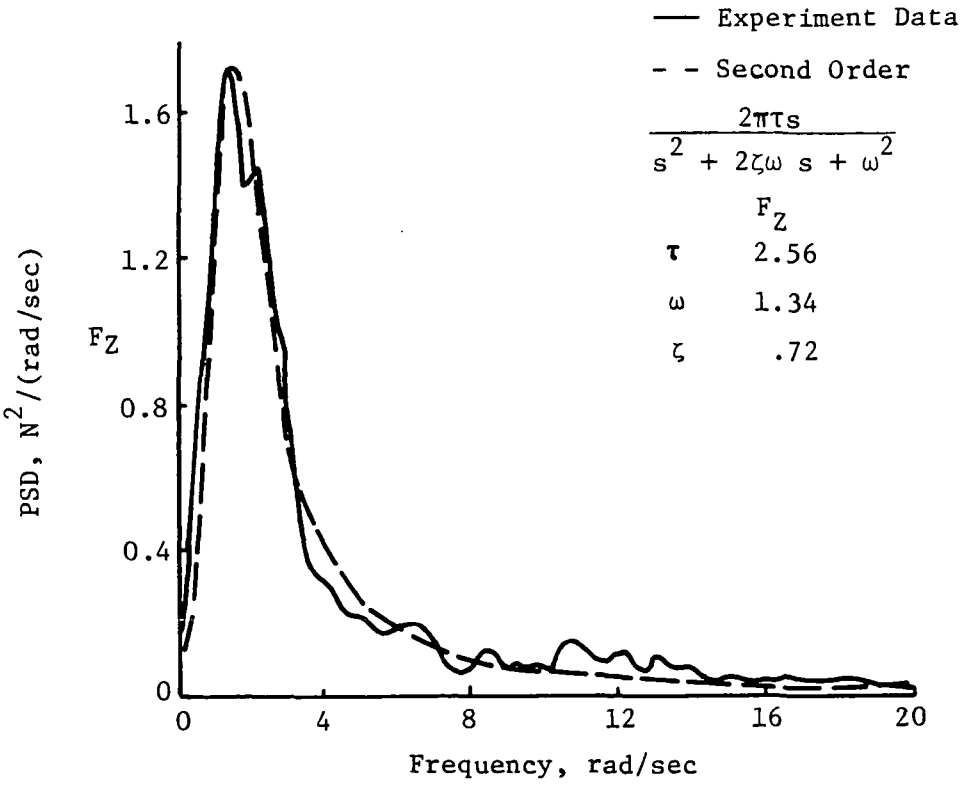

Figure 5-2.- PSD of F_Z of console operations.

If a noise generator (characterized with a PSD of $\Phi_N(\omega)$) is input to a linear system whose transfer function is $G_S(s)$, then the linear system output is defined in terms of its PSD as

$$\Phi_S(\omega) = \Phi_N(\omega) \left| G_S(j\omega) \right|^2$$

Conceptually, the implementation of this stochastic process is quite straightforward. It is discussed in terms of an all-digital simulation application for the purposes of this document.

Given the frequency characteristics of a specific shaping filter, figure 5-2 for example, the objective of the model implementation is to generate a random signal whose PSD is constant (unity) for frequencies covering the dominant characteristics of the shaping filter. The final linear system output of such a model exhibits amplitude characteristics approaching that of a Gaussian distribution. Most digital computer facilities have software packages through which random number generators are easily accessible. Their amplitude distributions are typically either Gaussian or uniform; either can be used in an application pertaining to a stochastic crew motion model.

Inherent in a digital simulation is the digital time (DT), the increment between simulation computations. An impulse sampling function of time can be represented as shown in figure 5-3.

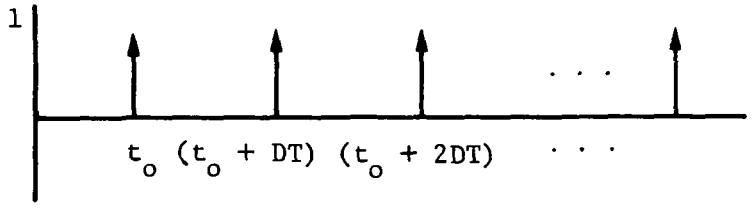

Figure 5-3.- Impulse sampling function.

At each increment DT, the random number generator output is integrated and a new one obtained. The typical time function thus produced is shown in figure 5-4. At each sample point, the next number in the random sequence updates the previous number and is constant until the next sample time DT.

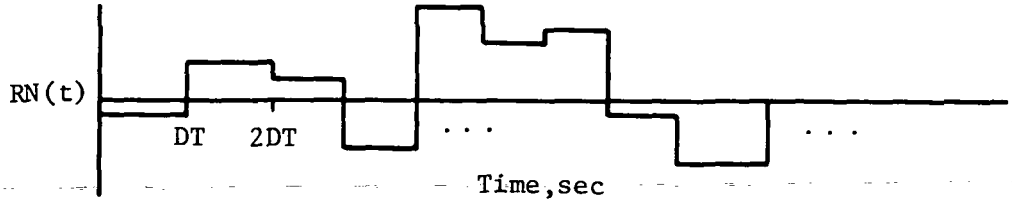

Figure 5-4.- Random number generator output.

Therefore, DT functions as a simulation input parameter and must be "compatible" with the highest frequency of the simulation dynamics or signals. A detailed discussion of digital simulation is beyond the scope of this handbook; the reader is encouraged to review a basic sample data dissertation if he is to perform such simulations.

The amplitude distribution of the output signal shown in figure 5-4, as stated previously, is either Gaussian or uniform. For the present purposes, it is assumed to be uniform with zero mean. The associated probability distribution is shown in figure 5-5.

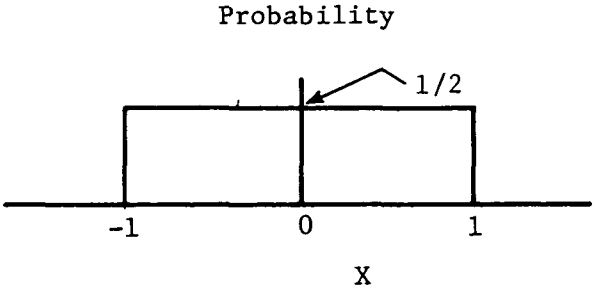

$$\sigma^2 = \int_{-\infty}^{\infty} x^2 P(x)\, dx$$

$$\sigma^2 = 1/3$$

Figure 5-5.- Uniform distribution.

Each adjacent number obtained is statistically independent of the previous one. The autocorrelation function of the time function given in figure 5-4 can be described as in figure 5-6 (refs. 4 and 5).

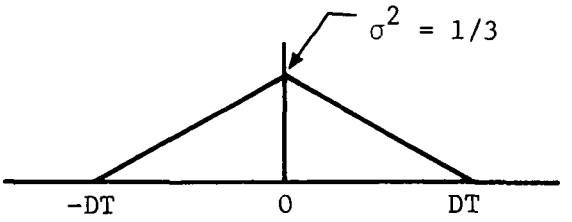

Figure 5-6.- Autocorrelation function.

The corresponding PSD is then

$$\Phi_{RN}(\omega) = DT \cdot \sigma^2 \frac{\sin^2\left(\frac{\omega DT}{2}\right)}{\left(\frac{\omega DT}{2}\right)^2}$$

To obtain a "low" frequency PSD that is unity, the generator output is simply scaled by $\left(\frac{1}{\sigma^2} DT\right)^{1/2}$. This scaled output is now the input to the shaping filters.

Finally, because the PSD shape follows a $\frac{\sin X}{X}$ curve, the analyst can compute a required DT to have a flat output PSD (within 5 percent) out to a frequency ω_o, where ω_o is beyond the frequency characteristic of the shaping filter.

6.0 APPLICATIONS

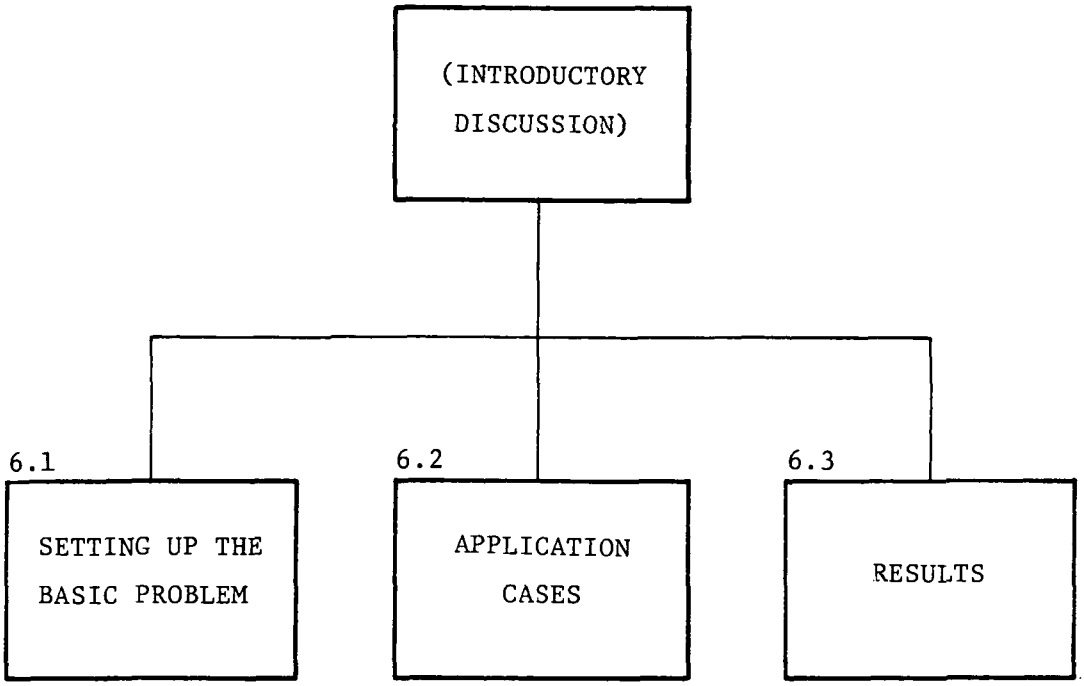

6.0 APPLICATIONS

Space vehicle control system designs and performance analyses typically deal with perturbations of the vehicle caused by disturbances from varied sources. Chapter 2.0 provided an overview of the control system design process which might be outlined as follows:

(1) Compilation of mission and performance requirements

(2) Selection of coordinate systems

(3) Gathering of vehicle basic data

(4) Preliminary control system gain determination

(5) Selection of actuator(s) based on mission requirements

(6) Flexible-body considerations

(7) Development of control system/vehicle simulation

(8) Selection of disturbance model

(9) Control system performance analysis

The need to select a reasonable coordinate system is not always readily apparent. In practice, the actual selection depends not only on the configuration of the vehicle under consideration but also its mission. Consider, for example, a vehicle that has a principal axis about which the moment of inertia is smaller than that of either of the other two principal axes. Also assume that a reference frame has been selected that is aligned with the local vertical, i.e., the vehicle maintains a constant attitude relative to the orbit. In this case, gravity gradient torque tends to align the "minimum" principal axis with the gravity gradient vector. Since the gravity gradient as seen by the vehicle does not have a constant angular velocity in inertial space as the vehicle moves in its orbit, control torques must be applied for the vehicle to have the necessary angular acceleration to keep up with the accelerating reference.

In the case of a manned vehicle, the equations of motion include time-varying moments of inertia due to the crew motion. In this situation, the selection of a reference coordinate system should minimize the effect of crew motion on the moment of inertia.

The selection of a proper actuator or controller is primarily a function of the mission requirement, i.e., (1) type of energy constraints; (2) maneuver (slewing) requirements; (3) space or location constraints; (4) restrictions on mass expulsion; and (5) attitude or pointing requirements. Currently, three general classes of actuators or controllers are in vogue: (1) mass expulsion devices (hot or cold gas thrusters); (2) momentum management or exchange devices (flywheels and gyrotorquers, which include control moment gyros); and (3) magnetic devices such as magnetometers.

For a preliminary analysis, basic data will probably be scarce. In many cases exact data, sensors, or actuators may not be available because the final selection on model type will generally not have been made. Therefore, the designer must rely on experience and/or past designs to obtain estimates of these data. Preliminary mass properties must, however, be available.

The choice of control system bandwidth and gains, in the presence of disturbance torques, presents a problem to the designer. With the representation of the crew motion disturbances as presented in this document, the problem becomes analytical when crew motion is the primary disturbance.

6.1 Setting up the Basic Problem

For the following applications, a planar representation of the vehicle and the control system is chosen. The selected controller is a rate plus position feedback that uses gyros as sensors. Displacement and rate units are mounted at the same point. The actuator is assumed to be ideal and sizing requirements will be discussed. A functional block diagram of the system is presented in figure 6-1. One mode of flexible-body considerations is shown, but the loop was not used in the actual applications where the modal gains were set to zero for rigid body.

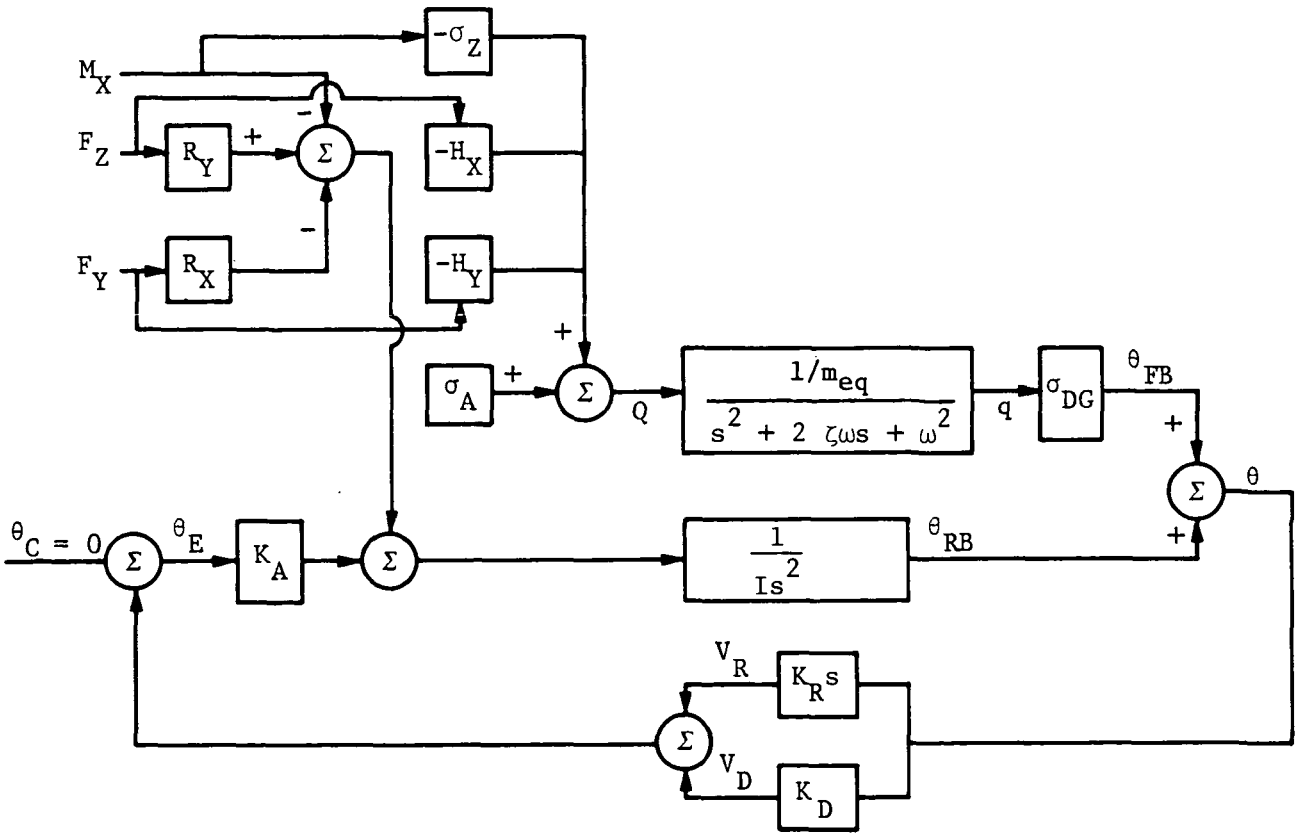

Figure 6-1.- Control system functional block diagram.

The impact of crew motion at this point in the design process is accounted for primarily in the following discussions of bandwidth selection, actuator sizing, and flexibility considerations.

6.1.1 Preliminary gain determination

The block diagram of figure 6-1 is reduced to its rigid-body equivalent in figure 6-2.

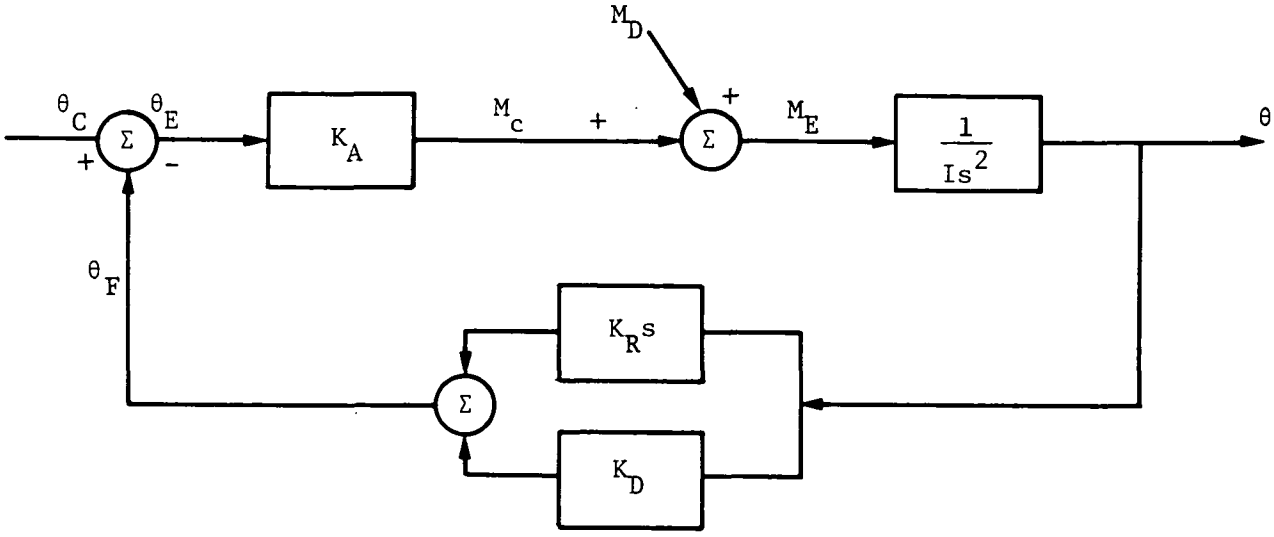

Figure 6-2.- Rigid-body block diagram.

The closed-loop transfer function relating vehicle attitude to a disturbance torque forcing function is given by

$$\frac{\theta}{M_D} = \frac{1/I}{s^2 + \frac{K_A K_R}{I} s + \frac{K_A K_D}{I}} \tag{6.1}$$

If the system characteristic desired is assumed to be 0.7 damped with a frequency of 0.1 Hz (0.628 rad/sec), the system has a characteristic equation that is merely the denominator of equation (6.1):

$$s^2 + 2\zeta\omega s + \omega^2 \tag{6.2}$$

When like terms are equated,

$$\frac{K_A K_R}{I} = 2\zeta\omega \tag{6.3}$$

and

$$\frac{K_A K_D}{I} = \omega^2 \tag{6.4}$$

The estimate of the vehicle inertia I allows the designer to determine the preliminary vehicle attitude and rate gains through equations (6.3) and (6.4), respectively, to satisfy his desired characteristics.

$$K_A K_R = 2\zeta\omega I = 2(0.7)(0.628)I = 0.88I \tag{6.5}$$

$$K_A K_D = \omega^2 I = (0.628)^2 I = 0.394I \tag{6.6}$$

Equations (6.5) and (6.6) apply to a characteristic equation that is 0.7 damped at a frequency of 0.628 rad/sec.

6.1.2 Crew motion effects on control system bandwidth selection

Given a vehicle disturbance caused by a crew motion activity, the control system may react, providing that the bandwidth of the system is compatible with the disturbance frequency. If the disturbance frequency is large in comparison to the control system bandwidth, the resulting attitudes and rates depend on the magnitude of the disturbance and the structural characteristics of the system. This technique can be used to make an initial assessment of the impact of crew motion disturbances on the pointing performance of a vehicle whose structural characteristics have been estimated.

Rewriting equation (6.1) gives

$$\frac{\theta(s)}{M_D} = \frac{\frac{1}{K_A K_D}}{\frac{I}{K_A K_D} s^2 + \frac{K_R}{K_D} s + 1} \tag{6.7}$$

Given equation (6.7) and the characteristics of the vehicle disturbance torque (M_D, reflecting pertinent moment arms for the new vehicle configuration), the control system designer is now in a position to estimate the resulting performance of the conceptual design.

Case 1: Constant Disturbance Torque

If the disturbance is a step function where $M_D(s) = \frac{M_D}{s}$ and if the final value theorem is used, the steady-state attitude is given by

$$\theta(t) = \frac{M_D}{K_A K_D} \tag{6.8}$$

This equation indicates that the vehicle assumes an attitude error equal to the magnitude of the step disturbance scaled as a function of the sensor gains. Static error may affect pointing accuracy. The magnitude of the error is a function of the magnitude of the disturbance (i.e., crew motion) and the total amplitude gain of the control system.

Case 2: Cyclic Disturbance Torque

If the disturbance torque is cyclic with a given frequency, different results are obtained. Again, the attitude response is inversely proportional to $K_A K_D$ when the disturbance frequency is significantly less than the control system bandwidth. However, if the disturbance frequency equals the bandwidth frequency, the vehicle response lags the disturbance by $\pi/2$ rad and its amplitude is further modified by the system damping. If the disturbance frequency is much greater than the bandwidth frequency, the system response lags the disturbance by π rad and its amplitude is inversely proportional to the vehicle inertia and the square of the disturbance frequency. This latter case is indicative of open-loop excitation with minimal feedback through the sensors, controllers, and actuators.

Case 3: Stochastic Disturbance

For a disturbance that is stochastic in nature (such as console operations), the stochastic model described in section 5.2.4, modified by the appropriate moment arms, can be used to predict expected performance in the following manner.

The output of a linear system forced with a stochastic disturbance $\left[\Phi_{IN}(\omega)\right]$ is given by

$$\Phi_{OUT}(\omega) = \phi_{IN}(\omega) \left|G_S(j\omega)\right|^2 \tag{6.9}$$

where $G_S(j\omega)$ is given through equation (6.7) for the control design being evaluated. The standard deviation of the resulting output is easily evaluated through use of standard tables, such as those given on page 339 of reference 4.

The designer can now establish the anticipated control system bandwidth required to satisfy mission and performance requirements. Because the bandwidth and performance expectations are functions of vehicle inertia and gains, the tradeoff is easily performed.

6.1.3 Actuator sizing (rigid body)

The actuator output torque M_c, defined in figure 6-2, is the variable of interest in defining actuator sizing requirements. The actuator sizing as affected by crew motion disturbances is discussed here although mission requirements generally dictate maneuver, coordinate, and similar requirements that affect actuator sizing. These latter aspects of sizing are standard considerations for control system design.

The transfer function relating the vehicle disturbance torque M_D to the actuator output torque M_C (see fig. 6-2) can be given by

$$\frac{M_C(s)}{M_D} = \frac{-\left(\frac{K_R}{K_D}s + 1\right)}{\frac{I}{K_A K_D}s^2 + \frac{K_R}{K_D}s + 1} \tag{6.10}$$

Substitution of equations (6.3) and (6.4) into equation (6.10) leads to

$$\frac{M_C(s)}{M_D} = \frac{-\frac{2\zeta s}{\omega} - 1}{\frac{s^2}{\omega^2} + \frac{2\zeta s}{\omega} + 1} \tag{6.11}$$

Upon completion of the analysis in the previous section, the control system designer has established the preliminary bandwidth requirements to accommodate the effects of crew motion disturbances on the pointing performance of his design. The designer can now define the actuator sizing required to accommodate these effects. This is accomplished through evaluation of equation (6.10) for the disturbance M_D. Typical examples follow.

Case 1: Constant and Low-Frequency Cyclic Disturbances

For the class of disturbances whose frequency is lower than the system bandwidth, the control torque required is equal in magnitude to the disturbance torque.

Case 2: Stochastic Disturbance Torque

For this case, the control torque requirements can be established through use of the standard tables referenced in section 6.1.2.

The designer now has estimates of each class of disturbance torque requirements resulting from crew motion. Knowing estimates of crew motion activities from mission requirements, he can define the final actuator size needed to accommodate the anticipated rigid-body crew motion disturbances.

6.1.4 Flexible-body considerations

Crew motion disturbances excite the flexible-body characteristics through the modal characteristics of the vehicle at the location of the crew activity. Figure 6-1, at the beginning of this chapter, gives the block diagram representation. This crew motion excitation does not affect the control loop stability, although it affects pointing stability performance and actuator sizing. Modal characteristics to this level of detail are not available until later in the design cycle.

The analyst can perform parametric studies, using the diagram of figure 6-1, to evaluate a derived requirement of σ_Z, H_X, H_Y, ζ, and ω for flexible considerations when crew motions are involved. Conceptually this is straightforward; however, control loop stability must be considered as the modal frequency approaches the rigid-body gain and phase margin frequencies.

One example of flexible-body considerations is given on pages 22 to 24 of reference 2. In that example (which used a model of the Skylab spacecraft) flexible-body angular rates were found to add from 3 to 6 percent to the rigid-body rates in the presence of a simulated crew motion disturbance. In this case, flexibility contributions were relatively small; other spacecraft models, different crew locations, or another type of disturbance would be expected to produce different results. It should be noted that while vehicle flexibility can be a major factor in considering crew motion effects, a full treatment of flexibility effects is beyond the scope of this handbook. The reader is cautioned and advised to keep vehicle flexibility characteristics in mind throughout the control system design cycle; he should include these characteristics at appropriate points as they become better defined.

6.1.5 Simulation development for performance predictions

To evaluate performance predictions, the designer must establish simulations for analysis. Different types of simulations are easily generated to handle various analysis efforts. Certain considerations usually require a "time" simulation. The time simulation considered for the following applications is an all-digital, time-response simulation containing a packaged program available to users through the Martin Marietta Computer Center. This program is called MIMIC; listings of sample input cases are presented in appendix B.

6.2 Application Cases

Implementation of selected applications of the techniques and developments discussed in the previous sections are now presented to aid the designer in completing a design cycle.

Two of the T-013 disturbances, console operations and soaring, have been chosen for the applications because they represent typical and worst case effects. They also illustrate best use of the two modeling techniques discussed in chapter 5.0. Two vehicles are considered, first to validate the results against previously analyzed and documented Skylab studies, and second to extend the applications to the space shuttle mission.

The applications were performed by using the appropriate disturbance model (chosen for the different activities) as a front end driver to a Martin Marietta control system response program, MIMIC (see section 6.1.5 and appendix B). The output produced by the MIMIC program, presented in the remainder of this chapter, gives vehicle rates and attitudes resulting from the modeled disturbances.

The T-013 moments presented in this handbook are local moments about the FMU and thus do not include Skylab moment arms. For Skylab, equations to convert local forces and moments to vehicle coordinates are given in reference 2.

They were obtained from the particular vehicle geometry and astronaut position relative to vehicle center of mass, and they must be derived for future vehicles.

From figure 3-4, the Skylab vehicle moment for the Z-coordinate can be determined by

$$M_{ZV} = R_Y F_Z - R_X F_Y - M_X \qquad (6.12)$$

where M_X is the local FMU moment, F_Y and F_Z are local FMU forces, and R_X and R_Y are moment arms (Skylab coordinates).

The M_{ZV} moment was chosen for this discussion because, for the Skylab vehicle, M_{ZV} generally represented the largest vehicle torque. This moment M_{ZV} is primarily a function of F_Y, usually the largest force for Skylab, and R_X, the largest moment arm for Skylab.

Table 6-1 identifies the cases that were exercised to apply the T-013 data and models.

TABLE 6-1.- APPLICATION CASES

Activity	Basis of comparison for -		Rigid-body simulation
	Disturbance	Vehicle response	
Soaring	T-013 profiles Reference 2 Figure 6-3	Reference 2 Figures 6-4, 6-5	Skylab Improved first-order model Figure 6-6
Console operations	T-013 profiles Reference 2		Skylab Stochastic model Figures 6-8, 6-9, 6-10 Space shuttle Figures 6-11, 6-12, 6-13
"Satellite maintenance" (Soaring and console operations)			Hypothetical satellite First-order and stochastic models Figures 6-14, 6-15, 6-16

6.2.1 Soaring

Reference 2 documents a detailed simulation of the forceful soaring disturbance to the Skylab vehicle. The results are presented in figures 6-3, 6-4, and 6-5. Figure 6-3 shows the actual vehicle disturbance torques as derived from T-013 data; figures 6-4 and 6-5 show the simulated vehicle rate and attitude, respectively, in response to the disturbance.

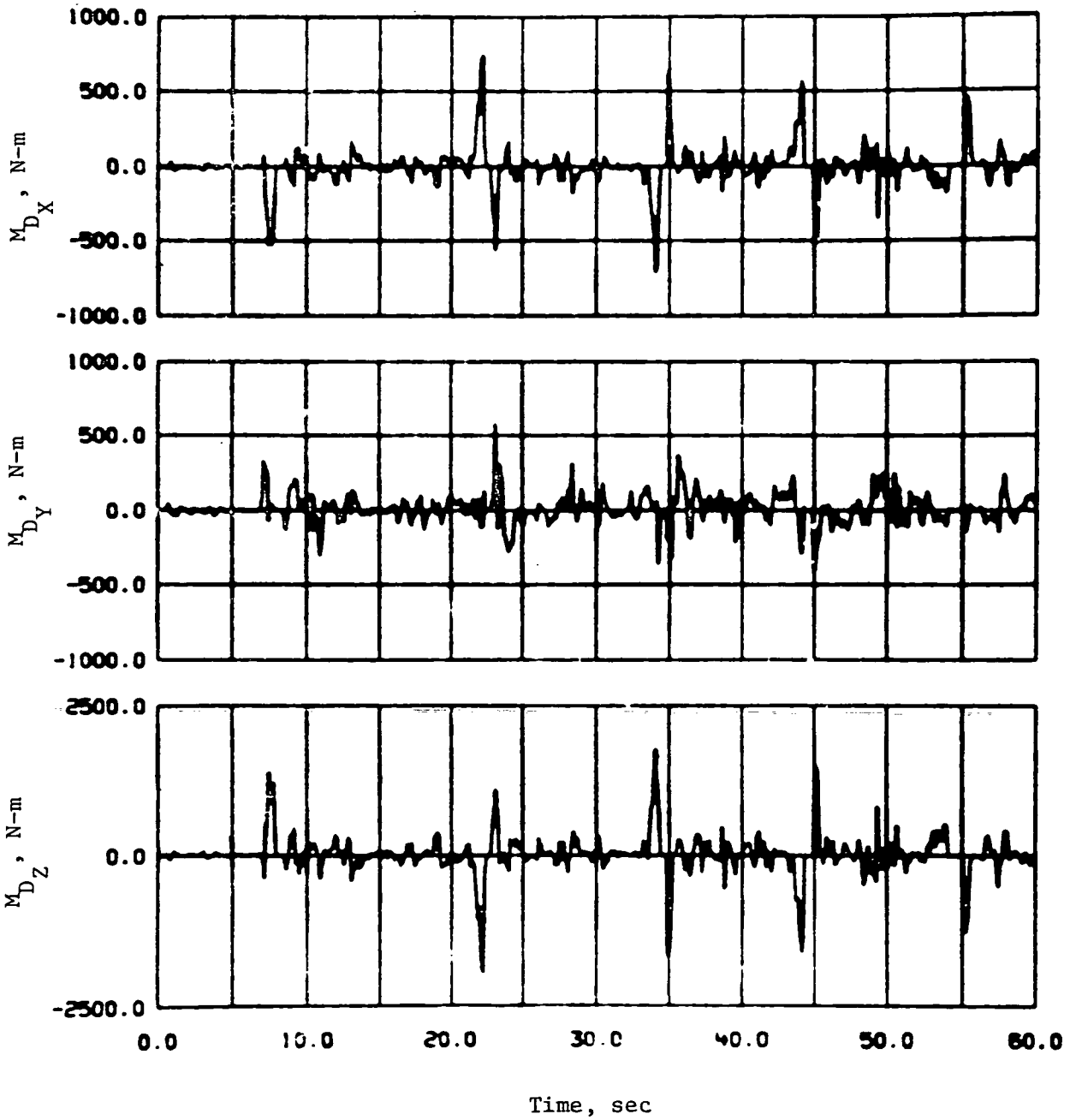

Figure 6-3.- Disturbance moment about Skylab center of mass.

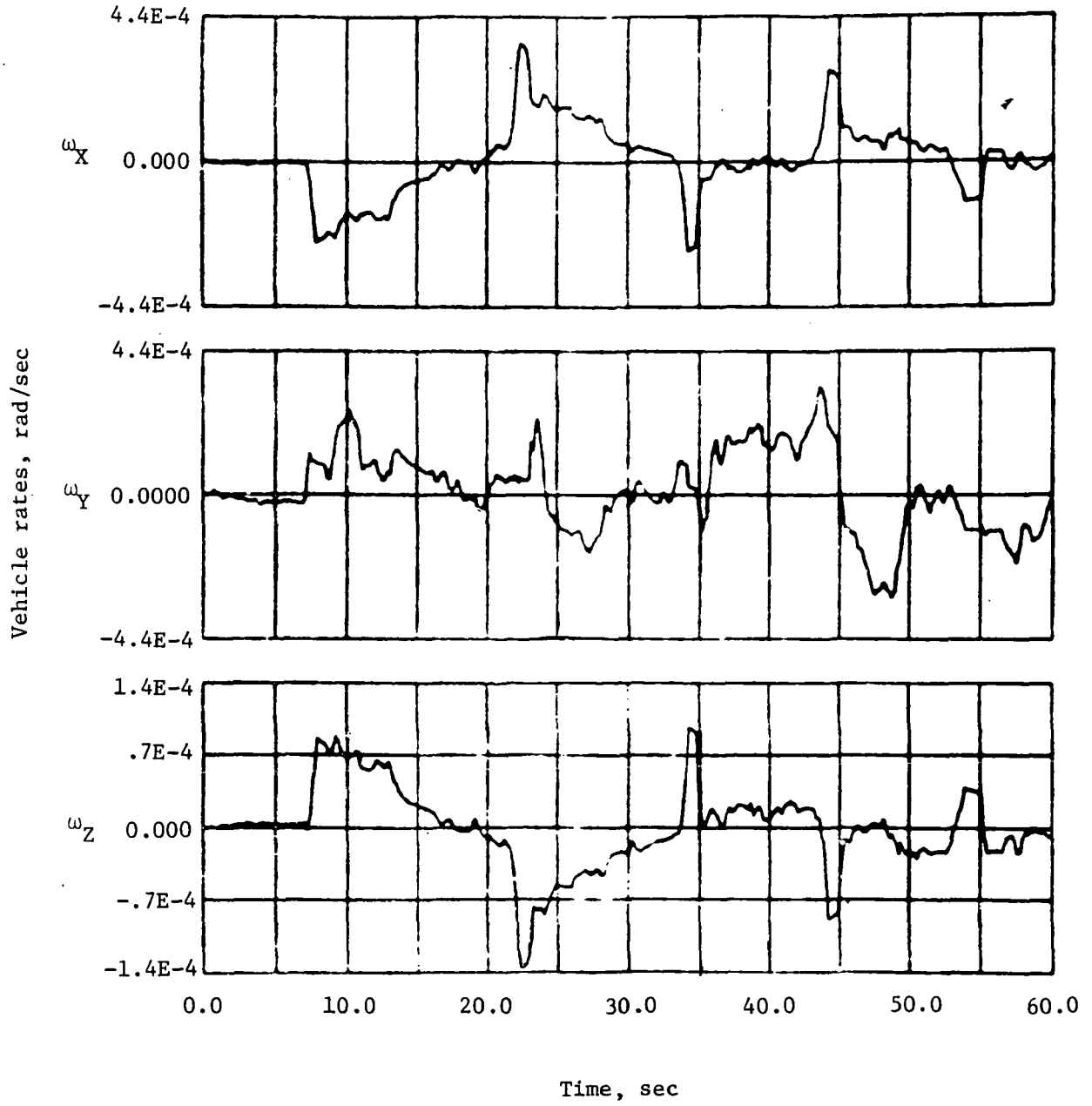

Figure 6-4.- Skylab vehicle rates, detailed simulation.

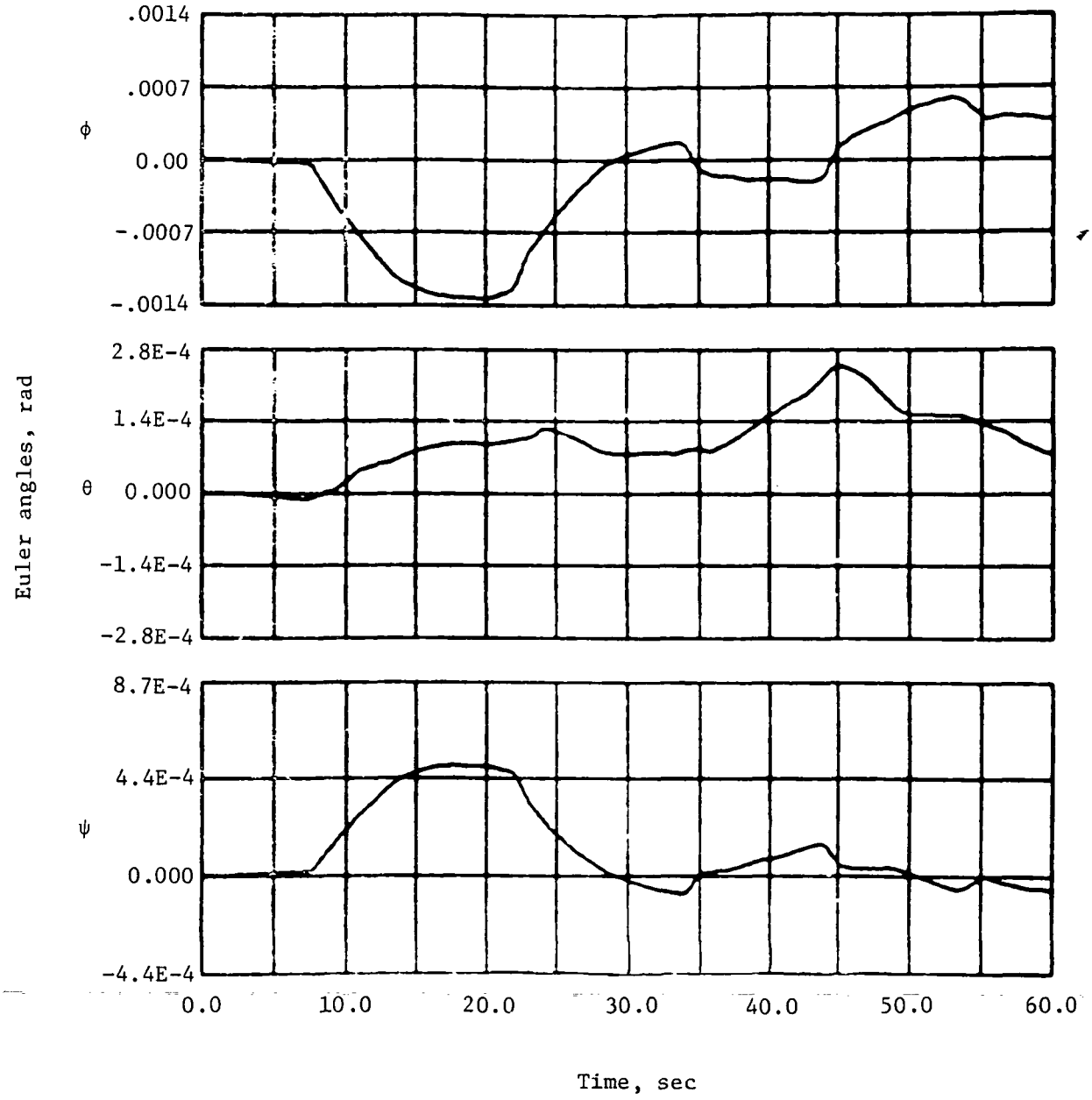

Figure 6-5.- Skylab vehicle attitude, detailed simulation.

Section 5.2.2 describes the development of the deterministic first-order model that is most suitably used for soaring. For the following applications, an improved first-order model was developed from a typical impact profile of recorded T-013 data. This model is considered "improved" because the single midpoint value was replaced by force and moment values selected at every tenth of a second.

The final disturbance torque was generated using equation (6.12) and the improved first-order model. This disturbance is shown in figure 6-6 with the corresponding vehicle rates and attitudes.

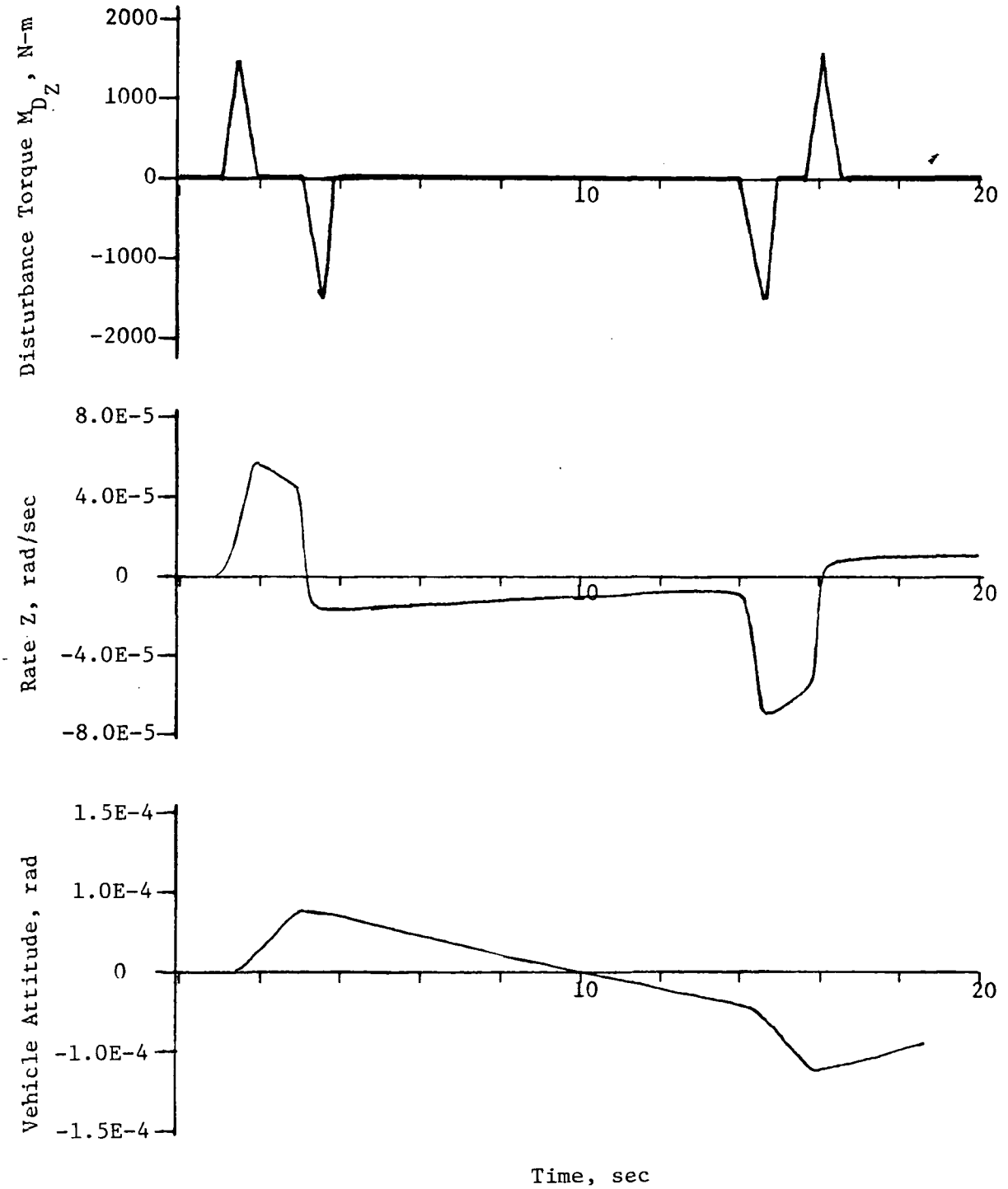

Figure 6-6.- Improved first-order model soaring disturbance and Skylab response.

The detailed simulation is shown in reference 2 to have closely matched the actual Skylab vehicle rates as measured by the onboard system. The first-order model indicates that similar trends are observed in vehicle responses.

The initial Skylab vehicle rates and attitude histories presented in figures 6-4 and 6-5 show system initial condition effects at $t = 7.5$ sec. The reader should consider the Z-axis torques and responses from 32 sec to almost 48 sec in figures 6-3, 6-4, and 6-5 when comparing them with first-order model responses so that similar initial conditions prevail.

6.2.2 Console operations (Skylab)

As stated previously, of the T-013 activities, console operations make up a good set of random or stochastic actions. As such, they are suitably represented by the stochastic model first introduced in section 5.2.4 and documented in appendix B.2. The implementation is as given in section 5.4.2. The moment arm consideration of section 6.2 and figure 6-7 describes the model's implementation of the vehicle disturbance torque; the output of the K_0 block produces a unity spectral density covering a frequency range that exceeds the model characteristics (as discussed in section 5.4.2). The filter parameters used in the console operations applications can be found in appendix A and figures A-3 and A-4.

A function of time can be adequately represented by the passage of constant PSD noise through a linear filter. The power spectrum of the output of such a system can be represented by

$$\Phi(\omega) = \Phi(0)G(j\omega)^2 \tag{6.13}$$

where $\Phi(0)$ is the dc or gain of the filter at zero frequency. The gain can be readily calculated for a given power spectrum amplitude and frequency $\Phi(\omega)$. For the model used, this becomes

$$\Phi(0) = \frac{\Phi(\omega_o)}{\dfrac{\left(\dfrac{\omega_o}{\omega_1}\right)^2 + 1}{\left[1 - \left(\dfrac{\omega_o}{\omega_F}\right)^2\right]^2 + \left(\dfrac{2\zeta_F\omega_o}{\omega_F}\right)^2}} \tag{6.14}$$

where ω_F and ζ_F are filter parameters tabulated in appendix A, ω_o is the frequency at maximum PSD, ω_1 is the model parameter, and $\Phi(\omega_o)$ is the maximum PSD value. In the time domain, this gain is $\left[\Phi(0)\right]^{1/2}$.

Figure 6-8 shows the modeled disturbance torque applied to the Skylab vehicle simulation. The amplitudes closely approximate those in reference 2. The vehicle rate shown in figure 6-9 and vehicle attitude shown in figure 6-10 are 2.4×10^{-6} rad/sec and 2.2×10^{-6} rad, respectively. This rate and attitude are considerably smaller than normal pointing accuracy requirements.

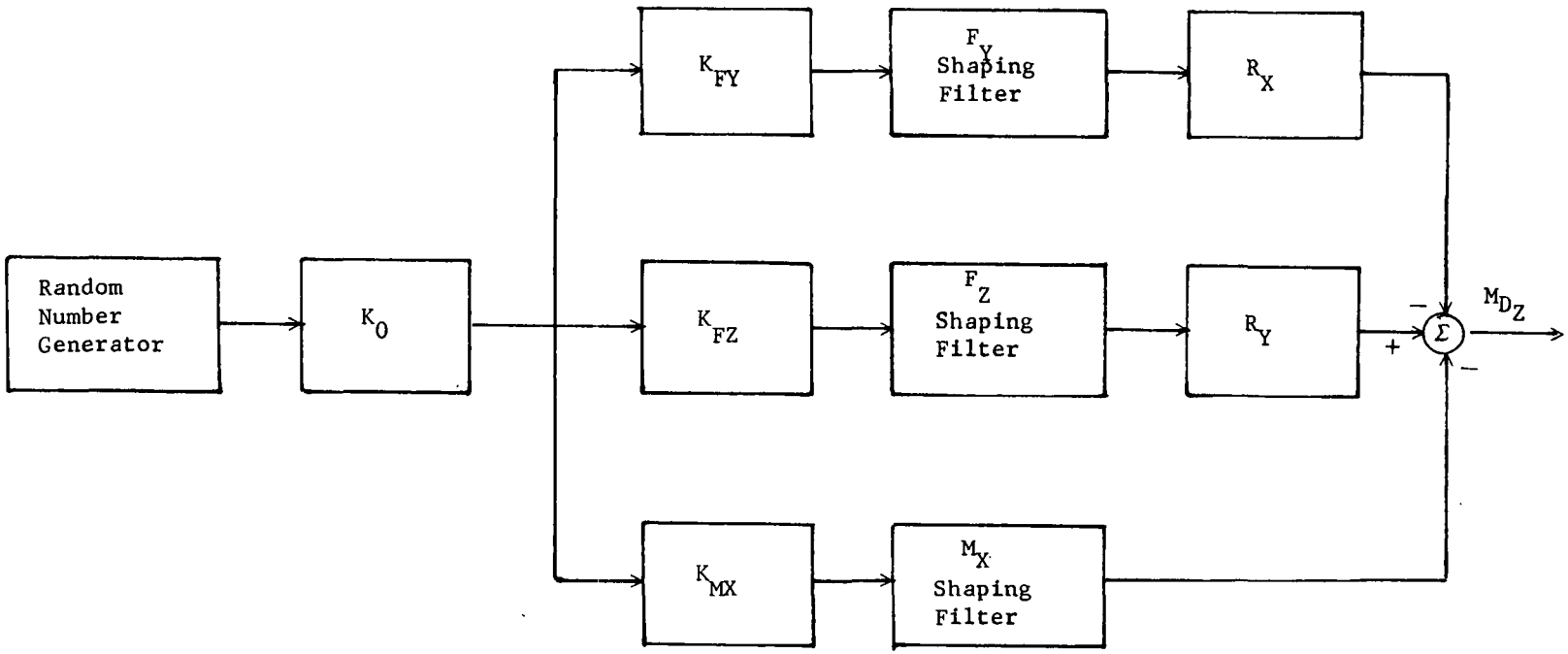

Where:

		Uniform Distribution		Normal Distribution
Random Number	K_0 =	$\left[\frac{1}{\sigma^2 \Delta t}\right]^{\frac{1}{2}}$	or	$\left[\frac{1}{\Delta t}\right]^{\frac{1}{2}}$
Gains K_{FY}, K_{FZ}, K_{MX}	=	$\left[\Phi(0)\right]^{\frac{1}{2}}$	or	$\left[\Phi(0)\right]^{\frac{1}{2}}$

Figure 6-7.- Disturbance torque generator.

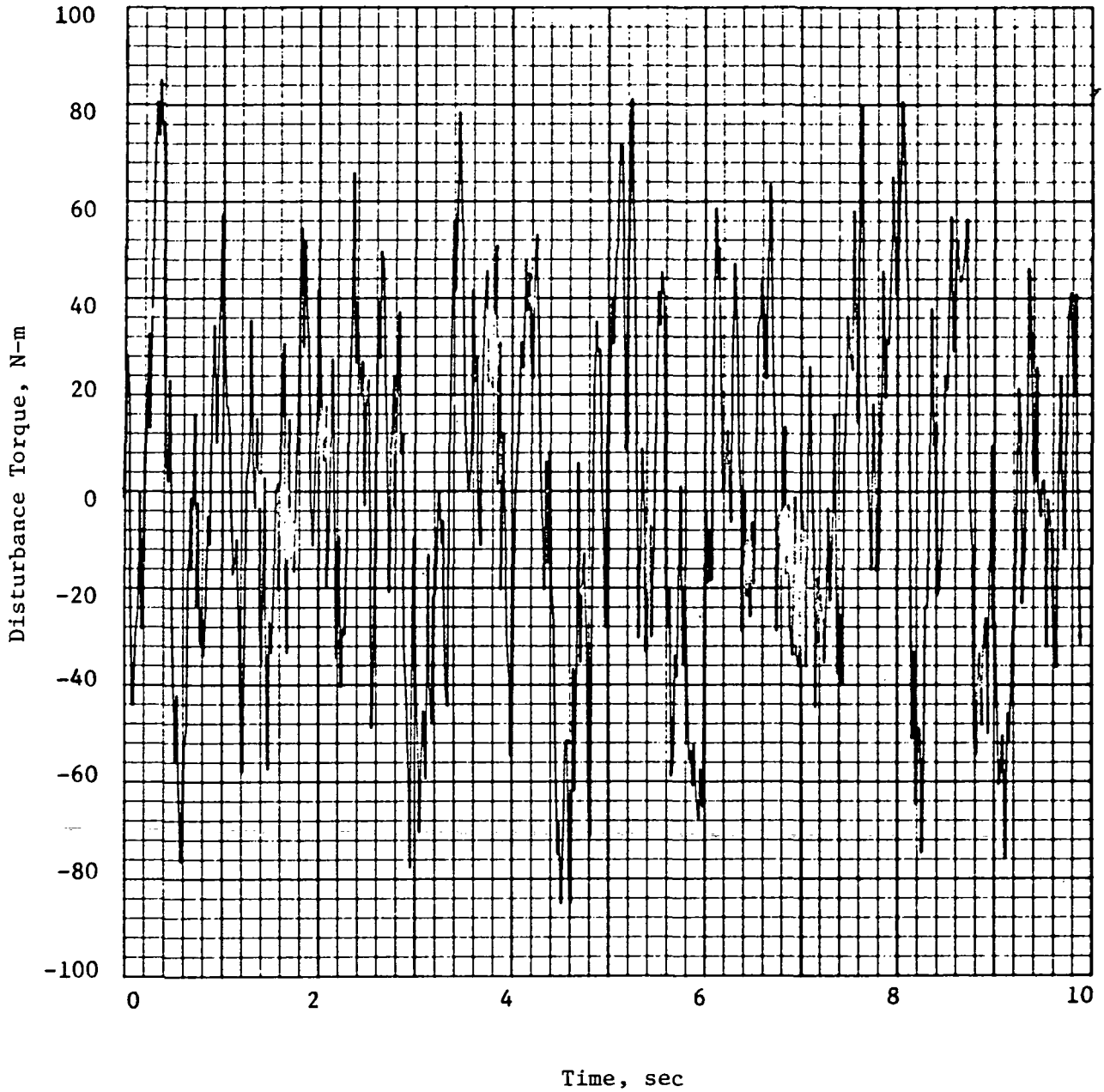

Figure 6-8.- Console operation disturbance torque.

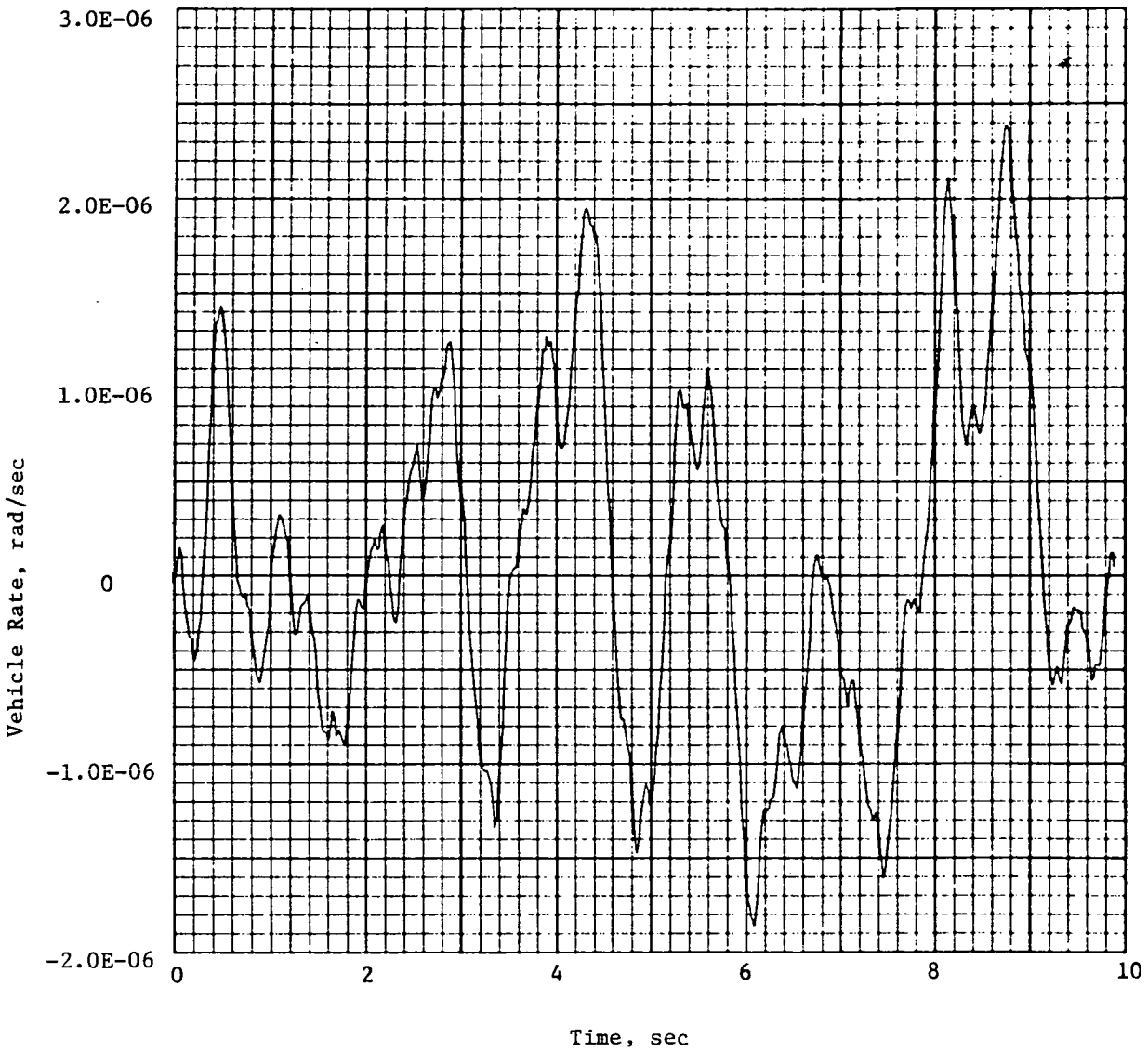

Figure 6-9.- Console operation, Skylab rate response.

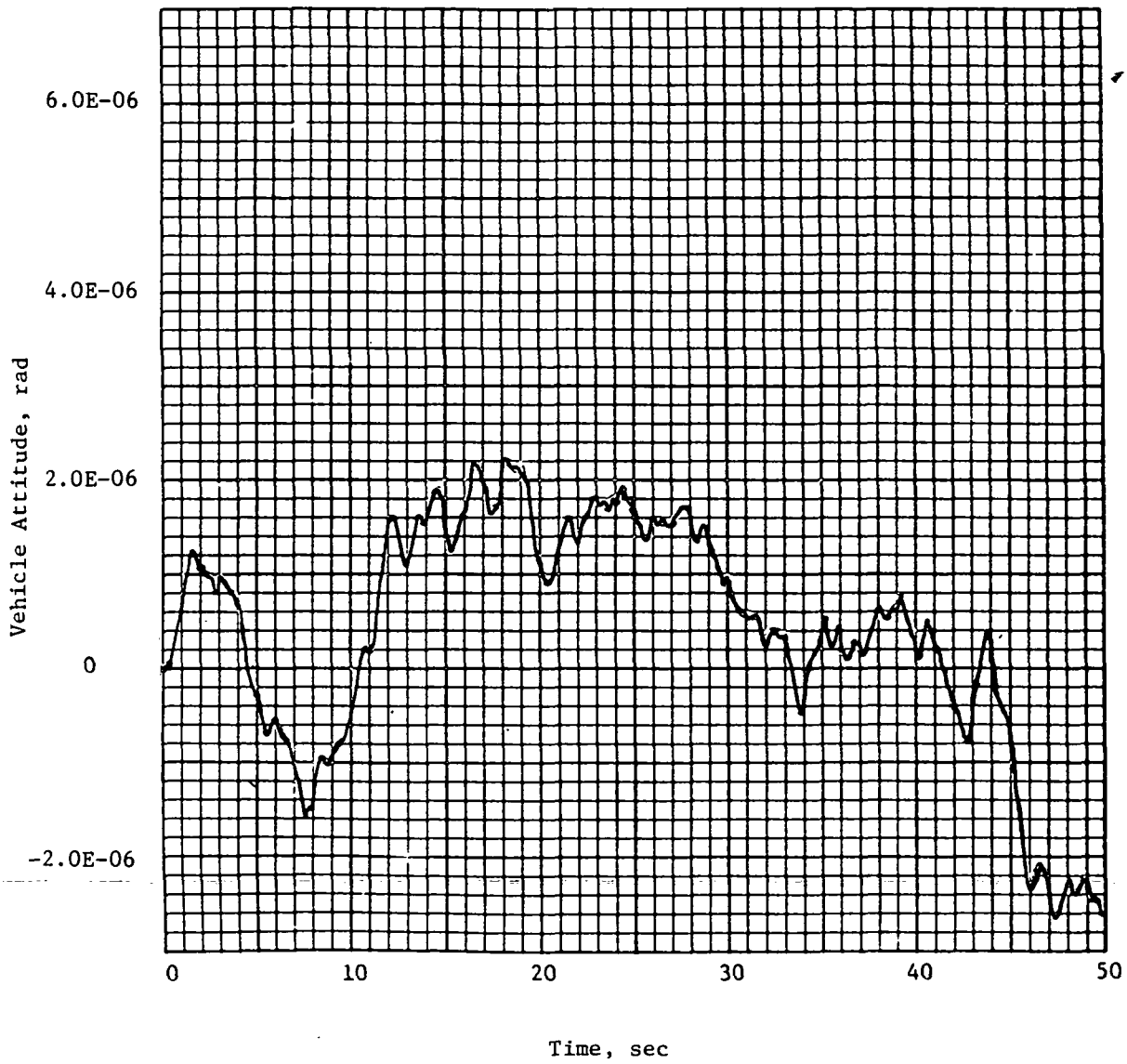

Figure 6-10.- Console operation, Skylab attitude response.

6.2.3 Console operations (space shuttle)

The mechanization of console operations disturbance torques for the space shuttle is straightforward. The same equations and simulation used for Skylab were adapted for the space shuttle by choosing different gains and moment arms as dictated by space shuttle inertia and the assumed astronaut position (facing aft in the cockpit, looking into the cargo bay).

As expected, the vehicle rate of figure 6-11 and the vehicle attitude of figure 6-12 (resulting from the disturbance shown in fig. 6-13) are much lower than those in the Skylab simulation. This difference is primarily due to the larger inertia, but is slightly offset by the larger moment arm.

6.2.4 Sequential crew motion activities

One practical application of some of the T-013 actions to different but similar problems is given in the simulation of the following scenario.

An astronaut performs an EVA from the space shuttle to do minor external maintenance on a satellite. The satellite is in the 200 $kg\text{-}m^2$ inertia class. For modeling purposes, we can assume that at $t = 0$ sec the astronaut lands against the satellite; from $t = 1$ sec to $t = 10$ sec, he performs external repairs in movements similar to console operations; at $t = 10$ sec, he pushes off to return to the space shuttle.

Figure 6-14 shows the resulting disturbance which is simply the stochastically modeled console operations in between the two large pulses of the wall push-off time function. Figures 6-15 and 6-16 present the responses for this hypothetical application.

6.3 Results

As stated previously, the documented and detailed simulations of reference 2 substantiate the results of the first-order soaring model; similarly, the stochastically modeled disturbances are confirmed by the actual time histories of the recorded data. Thus, for their pertinent activities, the models are considered to be reliable methods of generating a disturbance which in turn drives a control system simulation and produces a reliable response.

This chapter has demonstrated specific uses of both deterministic and stochastic models and has also developed an example which demonstrates improvisation, using a combination of models. This last case also applies existing data to a problem that is not composed of actual T-013 activities. Actions that are assumed to be of the same nature and force levels are substituted, thus enabling the analyst to size the problem in at least a preliminary sense inexpensively and easily.

Further concepts and suggestions for applying the T-013 models and data are presented in chapter 7.0.

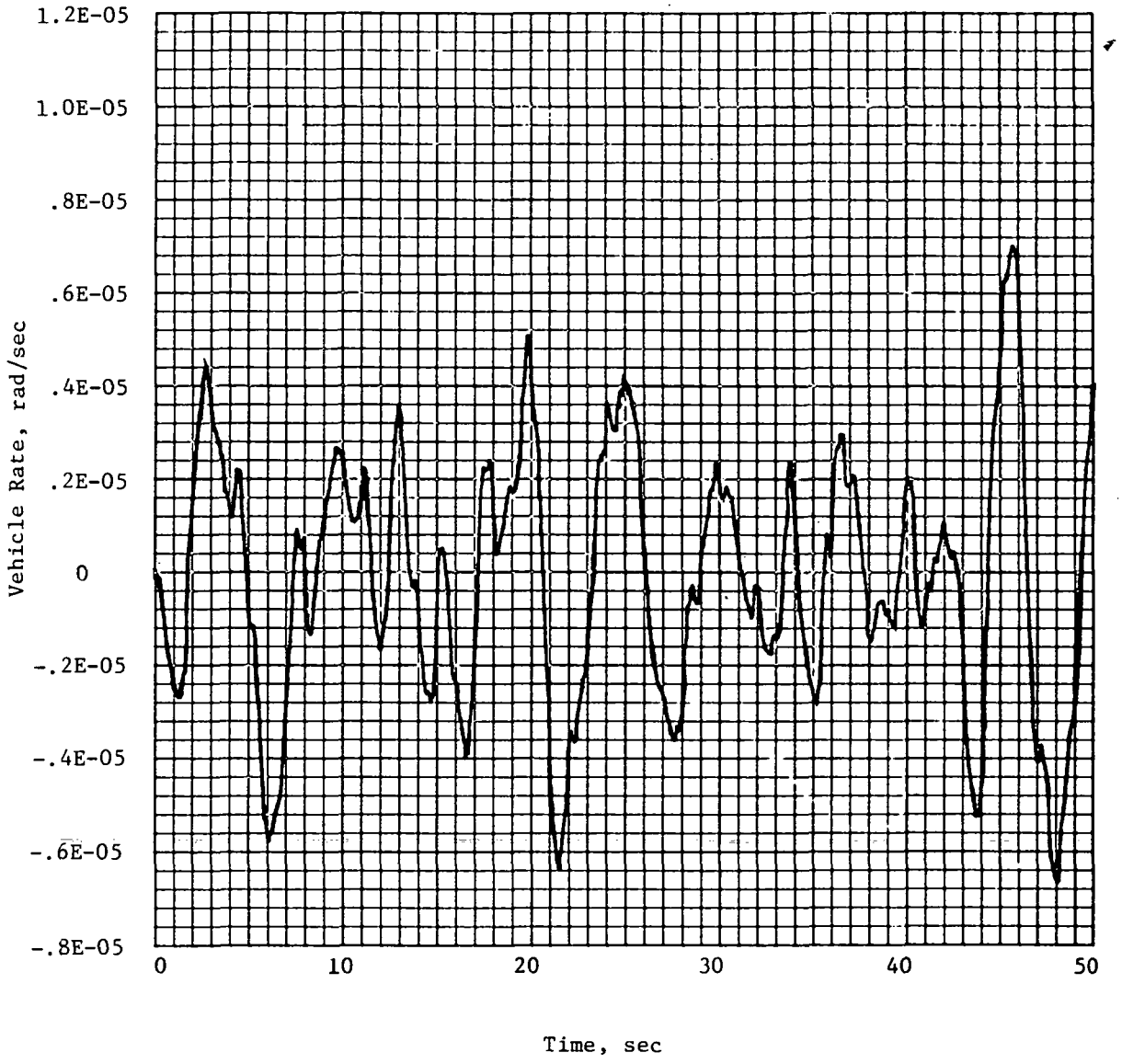

Figure 6-11.- Console operation, vehicle rate response, space shuttle.

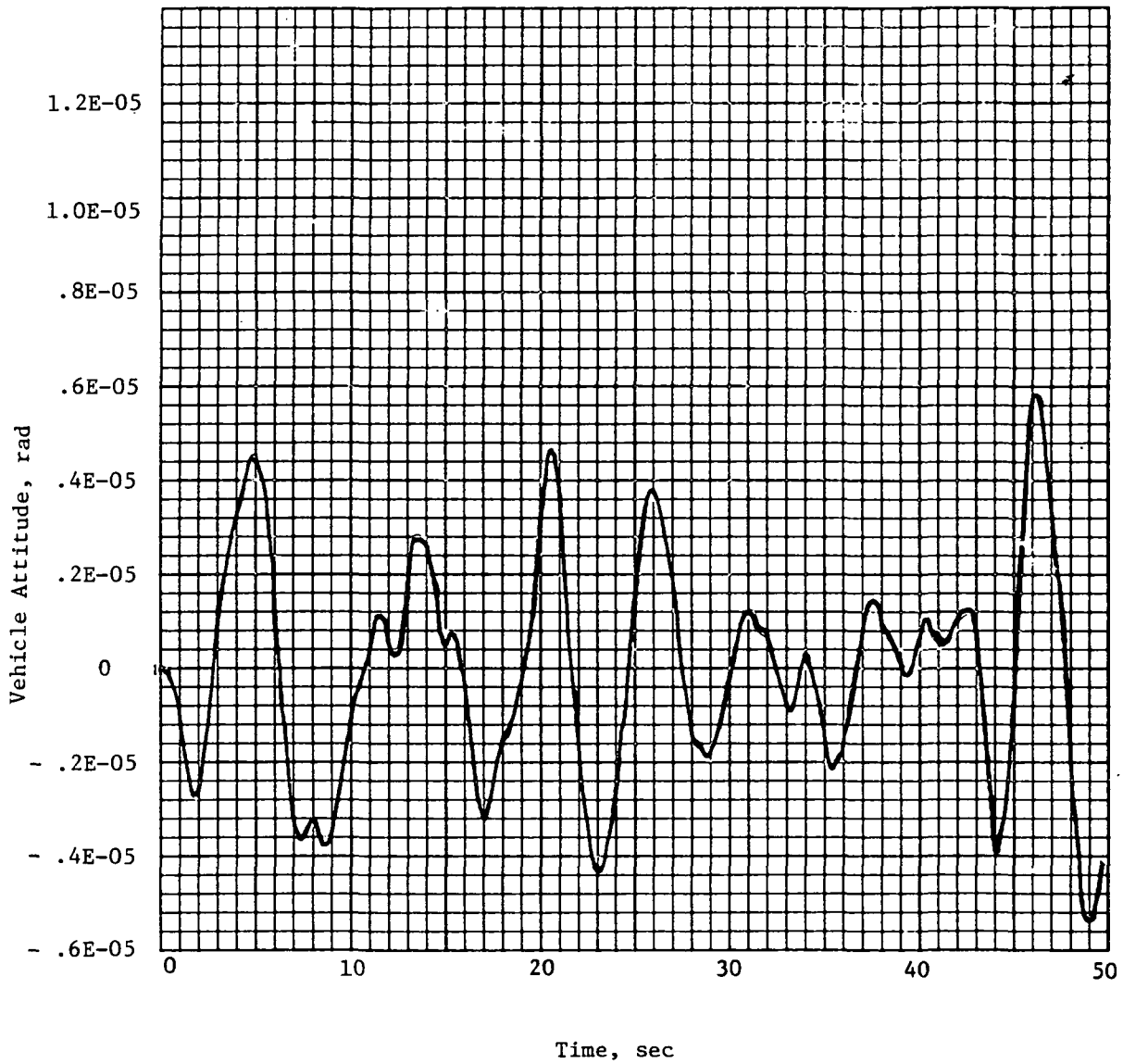

Figure 6-12.- Console operations, vehicle attitude response, space shuttle.

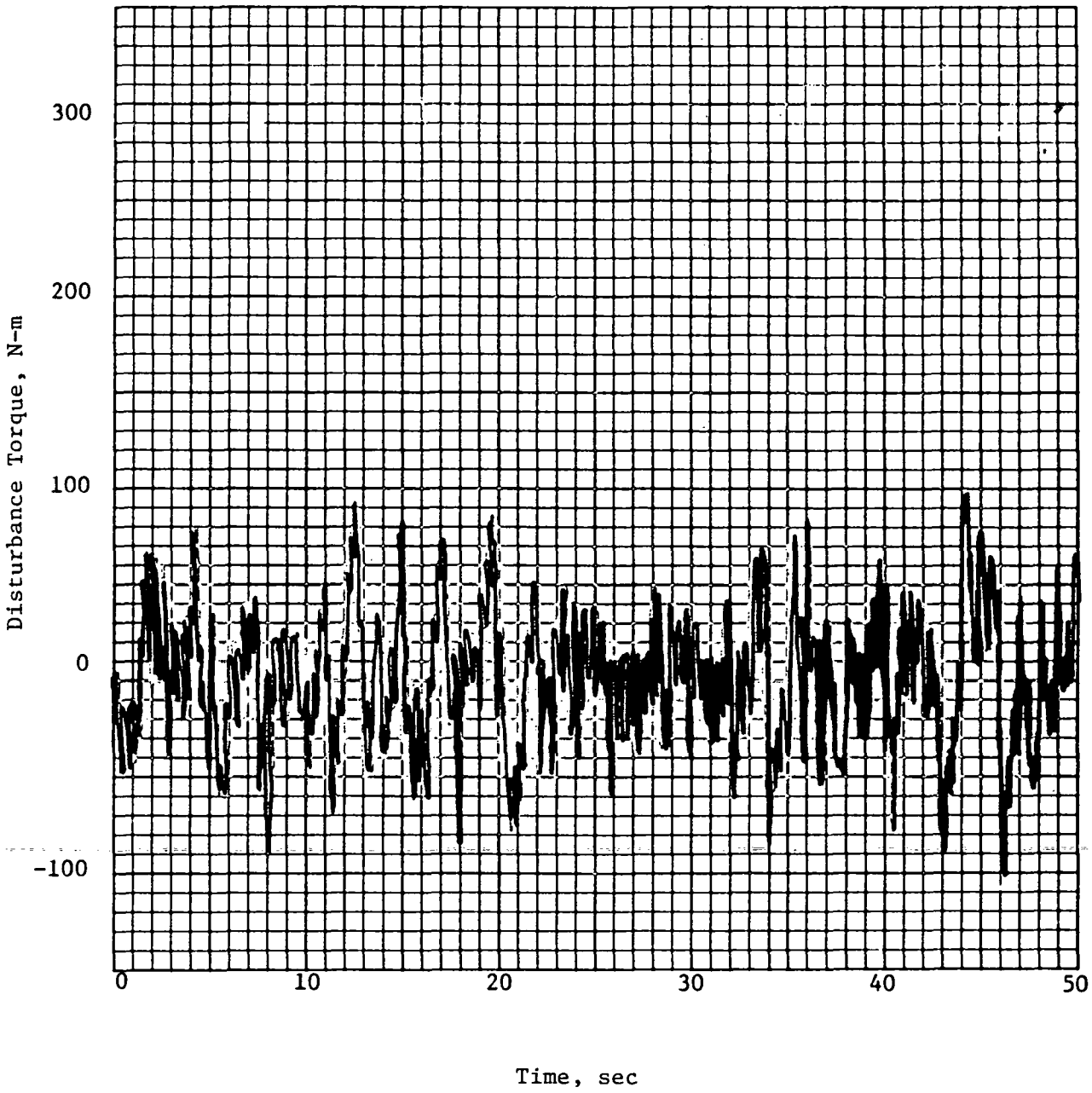

Figure 6-13.- Console operations disturbance.

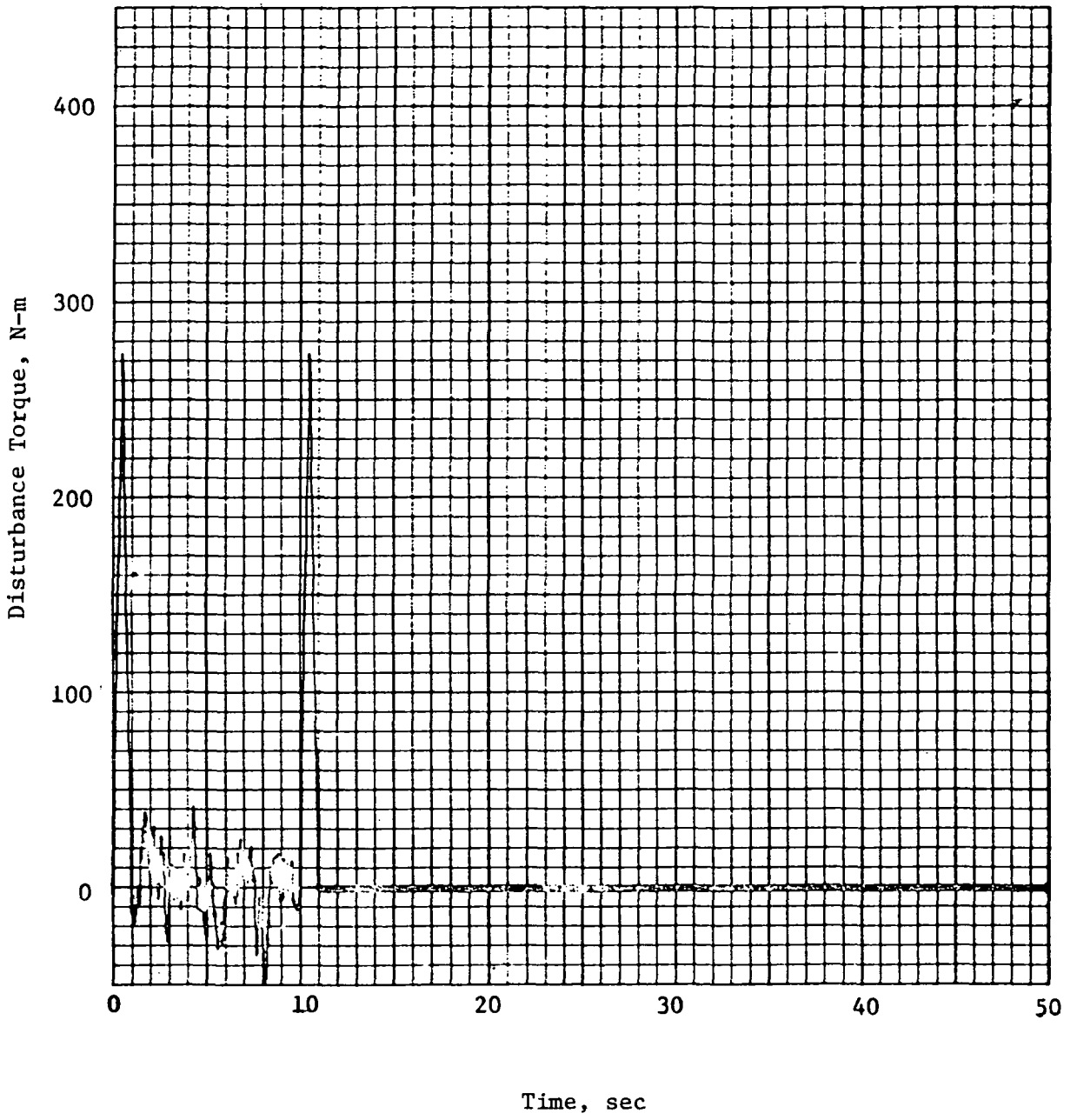

Figure 6-14.- Hypothetical application, sequential disturbance.

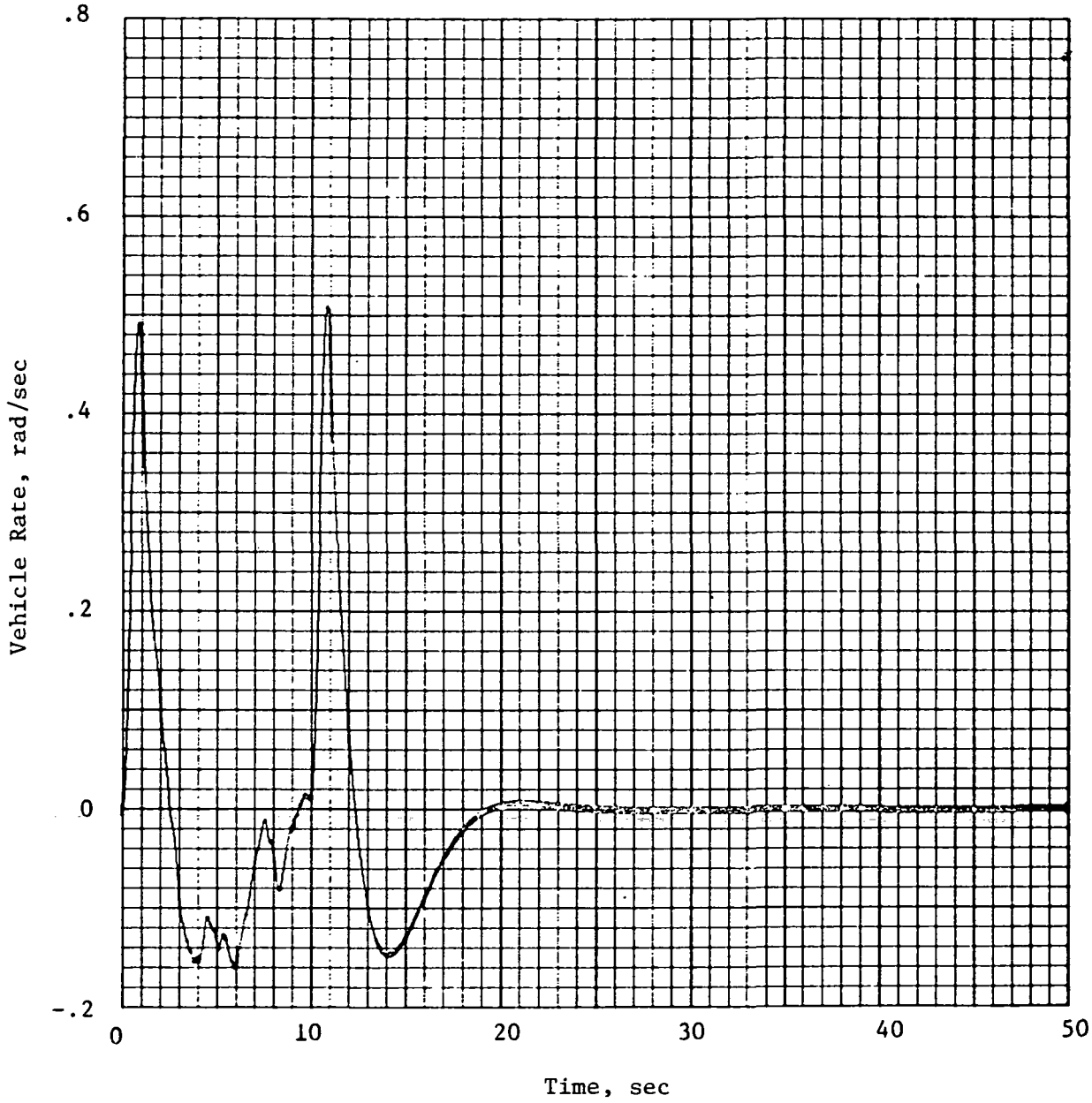

Figure 6-15.- Hypothetical application, vehicle rate response.

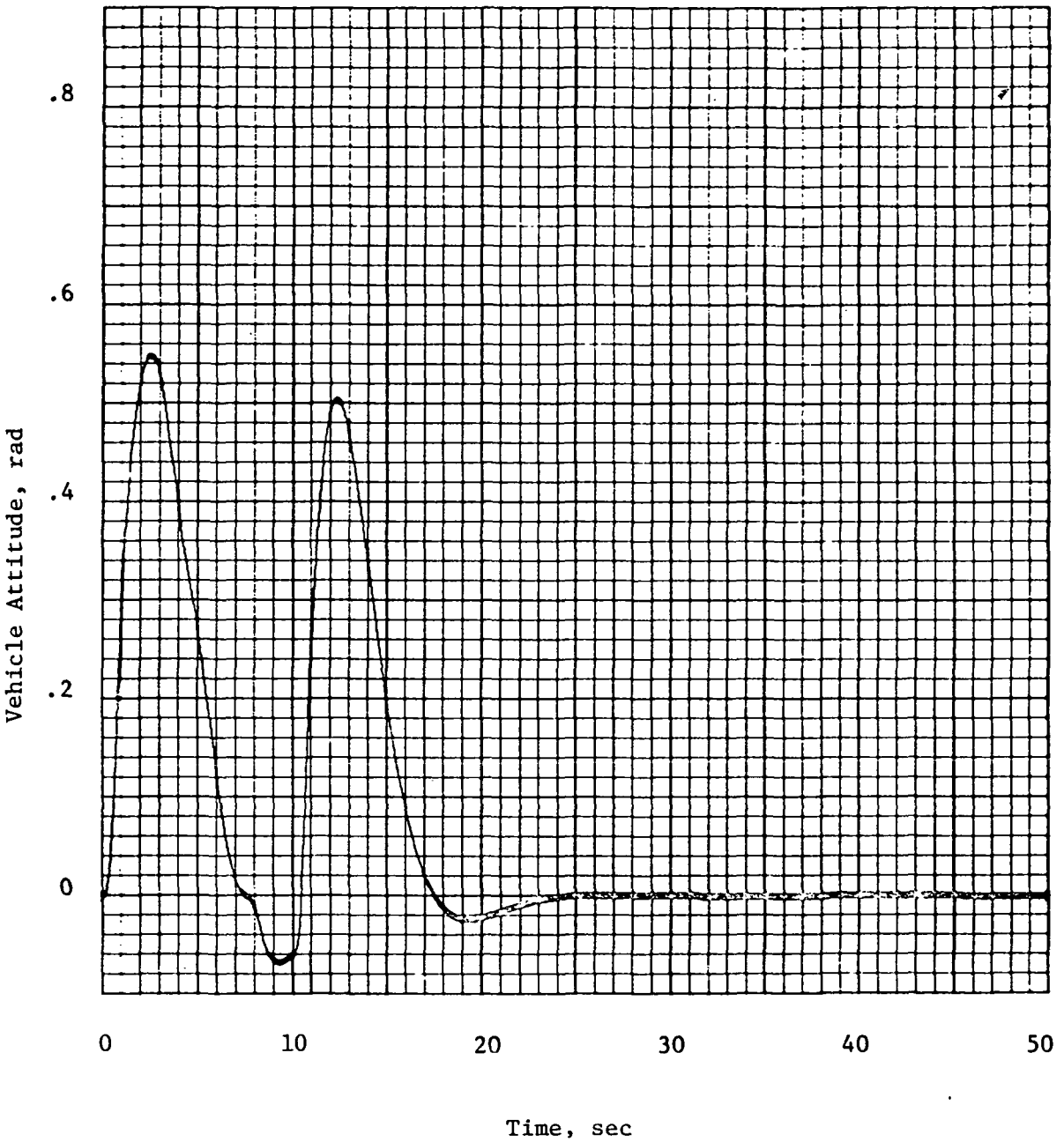

Figure 6-16.- Hypothetical application, vehicle attitude response.

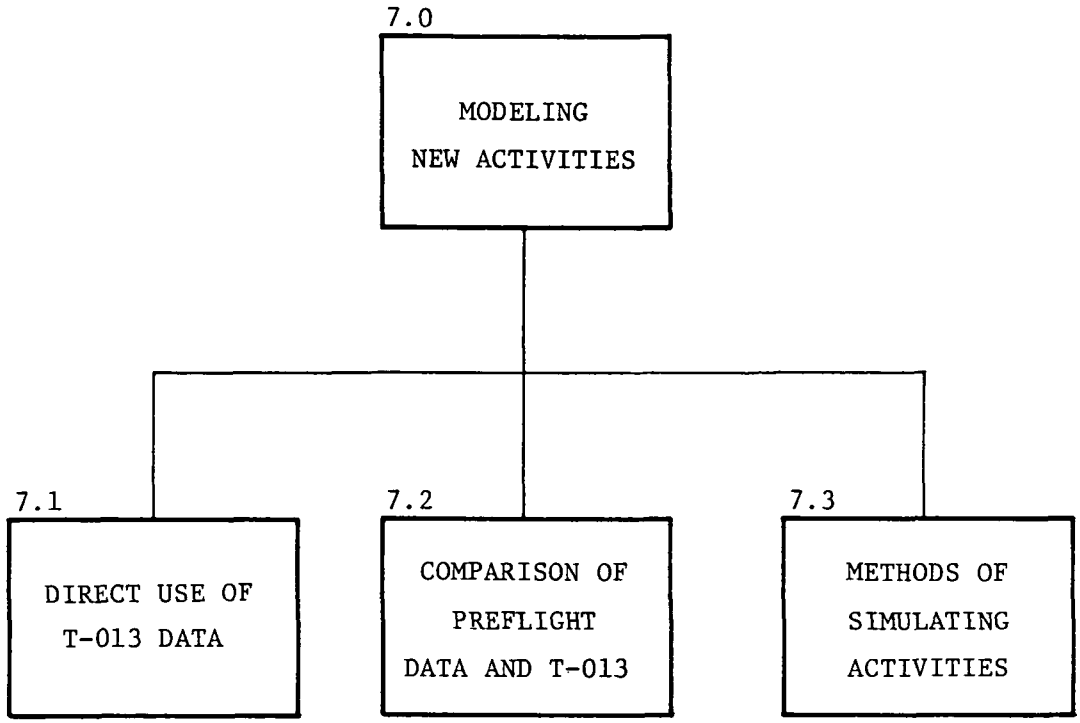
7.0
MODELING
NEW ACTIVITIES
7.1
DIRECT USE OF
T-013 DATA
7.2
COMPARISON OF
PREFLIGHT
DATA AND T-013
7.3
METHODS OF
SIMULATING
ACTIVITIES

7.0 MODELING NEW ACTIVITIES

Skylab experiment T-013 evaluated only a limited number of possible crew activities. These activities are extensively characterized in appendix A. Two have been modeled in detail in chapter 6.0, "Applications." These two, console operations and one-man forcefully soaring, were chosen because they best represent a key set of movements and a worst case.

The question that now arises is how future activities should be handled and, more specifically, how they should be modeled. This chapter suggests ideas and guidelines both to extend T-013 material for use in preliminary analyses and to identify methods of simulating future activities for more detailed design. In all cases, characterization of disturbances depends upon the vehicle in question and the different moment arms which result.

7.1 Direct Use of the T-013 Data for Future Activities

The applications of the two T-013 models given in chapter 6.0 represent low and high force levels. These activities and models were selected for this use not only because of their range but also because, of all crew motions, these two activities are the primary design drivers. Console operations are necessary during many portions of a manned mission while soaring (wall push-off) represents a worst case. These have been chosen to represent the types of motion that cause the designer the most concern: they bound the problem; in addition, all other movements fall within this described range.

7.1.1 Effects of more than one astronaut

Comparisons of one- and two-man activities for the purpose of understanding the effect of several astronauts cannot be based upon the T-013 force and moment data. Of all these activities, only the soaring had one- and two-man parts, but the manner in which the second subject participated in the exercise did not involve contact with either FMU. Reference 2 notes that vehicle rates increased from 0.02 deg/sec to between 0.03 and 0.04 deg/sec during soaring, indicating "that the secondary subject was providing disturbance inputs comparable with those of the primary subject."

The same conclusion cannot be derived from the force and moment data. The secondary subject soared across a different path, a longer one than that covered by the primary astronaut, and consequently, he did not push from or land on an FMU.

The only accurate way to derive this information, then, is to model it. Modeling can be implemented for astronauts performing different T-013 activities, using the appropriate moment arm for each subject according to his location in the vehicle, by simply summing the disturbances deterministically or statistically.

7.1.2 Sequential T-013 activities

Several actions performed by the same astronaut, occurring in a sequence, can be modeled in the same fashion as the final example of chapter 6.0. The

different T-013 models of the separate disturbances, incorporating the same moment arm if nontranslational, are simply input sequentially to the control system simulation.

7.1.3 Activities similar to T-013

For informative purposes, figure 7-1 is included to show the relative level of each T-013 action. Maximum and average (1σ) forces are displayed in order to identify approximate ranges of intermediate motions. A crude first-order model could be generated, if necessary, by identifying the activity on the figure that most closely approximates the new exercise in question and then deriving a time function in the manner of the soaring model. (See appendix A for descriptions of the activities in fig. 7-1.)

7.2 Comparison of Preflight Simulation Data and Experiment T-013 Data

References 3 and 6 describe activity simulations which were accomplished by using a load cell array similar to that in T-013. In brief, most of the restrained motions were performed on mockups for console activities or hygiene functions and were measured on a load cell array system. A motion simulator was used in conjunction with additional mockups to study translational activities where the subject's center of mass could move several feet or more (ref. 6). The load cell forces and moments, equal and opposite to those felt by the astronaut, were used in calculating the anticipated response that the astronaut would have in a zero-gravity environment relative to the spacecraft.

A careful and detailed comparison of these ground-based simulations with corresponding T-013 flight activities (deep breathing, console operations, coughing and sneezing) indicates excellent correlation. Therefore, for the purposes of expanding the data base of characterized crew motions, the results displayed in references 3 and 6 are applicable. The frequency content of some of these activities is similarly presented. These actions, motions necessary to personal hygiene and meal preparation, are considered stochastic and thus are aptly represented by a stochastic model. For reference purposes and convenience, these activities are listed in table 7-1 along with their filter parameters which are necessary inputs to the stochastic model. The good correlation recommends this method of simulating low to midlevel activities as a valid and reliable way to obtain detailed force and moment data.

Earth-based simulations of translational movements were also performed, but the results, particularly when wall push-offs were used, indicate a poor correlation with T-013. The in-orbit force levels exceeded the simulated levels by a factor of 2. Analysis of film data revealed that the primary reason for the disagreement is the increased velocity produced by the astronaut in a zero-gravity environment. The conclusion, based upon these observations and studies, is that it is difficult to simulate realistic forces associated with translational activities. Since the forceful soaring truly is a worst case translational activity, the T-013 soaring data should be used in a bounding sense.

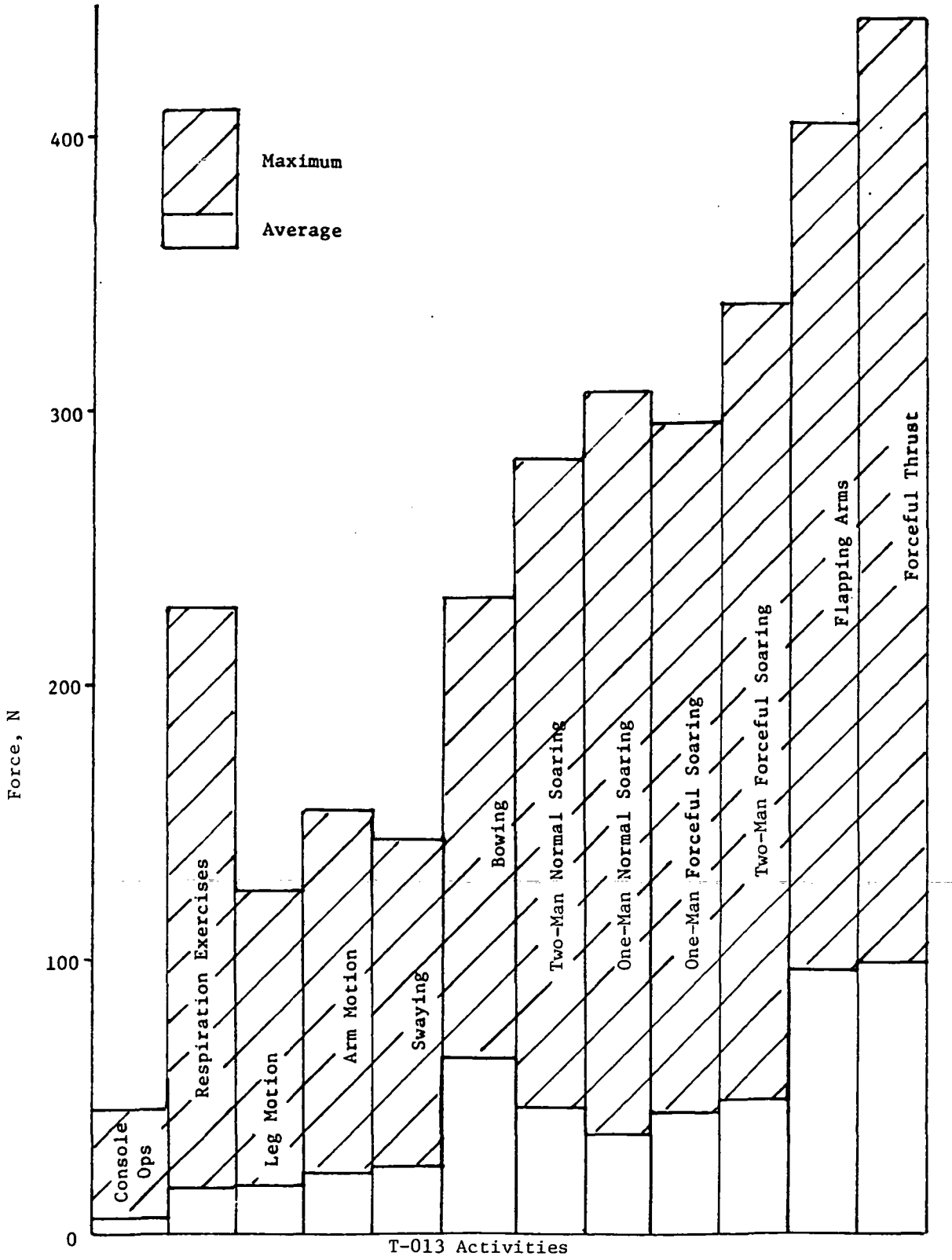

Figure 7-1.- Force levels of T-013 activities.

TABLE 7-1.- STOCHASTIC ACTIVITIES (NON T-013)

AND THEIR FILTER PARAMETERS

Activity	F_X for -			F_Y for -			F_Z for -		
	τ	ω	ζ	τ	ω	ζ	τ	ω	ζ
Hand wash	3.93	4.65	1.05	736.51	4.81	0.29	5.96	6.64	1.14
Meal preparation	3.90	4.69	.67	2483.27	6.27	.98	4.08	7.57	.78
Shaving	4.58	5.10	.88	3.91	11.35	4.6	7.89	10.94	1.74
Shower preparation	6.79	3.31	.65	7.27	3.91	.68	15.63	5.38	.33
Shower	4.38	3.79	5.6	0.00	2.67	1.00	22.52	5.14	.45
Secure shower	4.99	4.06	.52	277.74	4.35	.24	17197.88	2.42	.38

Activity	M_X for -			M_Y for -			M_Z for -		
	τ	ω	ζ	τ	ω	ζ	τ	ω	ζ
Hand wash	12.86	7.12	0.75	9.49	4.29	0.66	4.44	7.83	0.61
Meal preparation	4824.44	5.84	.92	11.92	4.18	.70	3.84	6.40	.59
Shaving	6126.40	2.91	1.00	11.63	4.81	.76	3.90	6.54	.71
Shower preparation	12.00	4.53	.56	20.13	2.91	.60	4.42	4.37	.61
Shower	4527.27	1.61	1.00	12.54	3.52	.54	4.27	3.90	.52
Secure shower	4710.99	2.38	1.00	15.20	3.20	.62	4.98	3.81	.47

7.3 Methods of Simulating Activities

Different types of man-in-the-loop simulations are given in table 7-2. The table shows that an FMU system or the three-degree-of-freedom air bearing simulator are the best candidates for an Earth-based simulation. As long as limb motions are made in the horizontal plane, the effects of gravity should be minimized, i.e., motions in zero gravity are approximated. The FMU system is superior to the air bearing method because it measures the effects of gravity on limb motions made in the vertical plane.

TABLE 7-2.- METHODS OF SIMULATING ACTIVITIES

Simulation method	Advantages	Disadvantages
Three-degree-of-freedom air bearing simulator at JSC	Provides good approximation to zero-gravity limb motion effects in two translational and one rotational degrees of freedom (the horizontal plane). Low cost because air bearing floor and other hardware already exist at JSC.	Additional instrumentation of current JSC simulator configurations may be required. Computer program must be written to reduce data from instrumentation system. Torque and forces from air and instrumentation wires are negligible except for all but smallest limb motions. Cannot measure effect of limb motions in the vertical plane in the direction of gravity. Thus, comparison of the effect with and without gravity on simulator limb motions is not possible.
FMU	Engineering design and computer program to reduce instrumentation already developed. Can measure effect of similar limb motions in both the vertical and horizontal plane and thus obtain comparisons with and without gravity.	Presence of gravity can affect manner in which motions are performed.
Single-degree-of-freedom air bearing simulator	Provides good zero-gravity approximation in one degree of freedom. Relatively inexpensive since single axis air bearing installations currently exist.	Complex instrumentation is required to separate forces and moments due to limb motions unless the test subject is positioned on the bearing in a certain way. This positioning is probably incompatible with the moment capability of the bearing.
Underwater neutral buoyancy	Approximates actual zero gravity for unsuited subject.	Drag excessive for all but slowest motions. Breathing equipment restrictive. May be more expensive than previous methods. Instrumentation complex due to presence of water.
Servo-drive simulation	Can be tied together directly with computer simulation of spacecraft dynamics.	Must counteract gravity in many motions. Mounting harnesses too restrictive. Relatively expensive.
Cable suspension	Relatively low cost.	Degrees of freedom limited. Pendulum effects present. Support apparatus restrictive.
Zero-gravity aircraft	Actual zero-gravity environment.	Short run times. Unnatural positive-gravity forces interspersed between zero-gravity runs. Expensive.

APPENDIX A

EXPERIMENT T-013 ACTIVITIES: DATA ANALYSES AND TABULATIONS

APPENDIX A

EXPERIMENT T-013 ACTIVITIES: DATA ANALYSES AND TABULATIONS

A.1 Introduction

The T-013 data analyzed in this appendix are force and moment information obtained from the Force Measuring Unit 1 (FMU 1). An FMU comprised a sense plate, a base plate, an array of six load cells, load cell caging devices, a calibration check mechanism, and signal conditioning electronics. Although two FMU's were intended to record data for portions of the experiment, the failure of two of the six load cells on the Force Measuring Unit 2 (FMU 2) precluded obtaining meaningful data from that FMU. Previous efforts to correct the data were unsuccessful; therefore information from FMU 2 is not included here. Since half of the soaring activities was measured on FMU 1, this loss of data was not considered detrimental to the analysis.

A.1.1 Experiment T-013 activities

The various actions required for the T-013 experiment fall into two main categories: normal and forceful. The normal activities form a baseline of typical actions performed by a crew during any manned mission. These motions include simple arm and leg movements and breathing and coughing exercises. Limb motions consist of single- and double-pendulum arm and leg movements and body bending at the waist. These body motions were meant to corroborate activities performed in earlier ground simulations.

Of the T-013 activities analyzed, only the console operations indicate a random or stochastic process. The console operations are composed of a sequence of individual events related to the activities performed at a console. It is assumed that such events are performed indefinitely and that the net activity is time-stationary.

Respiration exercises (sneezing, coughing, deep breathing) are dependent actions, relying upon such factors as rapidity of action, individuality in sneezing, or stress in coughing or deep breathing. The normal body exercises separated typical body motions into single, identifiable movements, yet, by definition, these actions and their corresponding forces and moments depend on the size and flair of the subject performing them.

The second principal category of T-013 activities, forceful, was designed to provide worst case crew motion disturbances. Examples of these are one- and two-man soaring activities where the primary and secondary subjects used the paths indicated previously in figure 3-3, and vigorous one-man exercise motions performed with the subject restrained to FMU 1. As with the majority of the normal exercises, these worst case activities depend inherently upon the size and characteristics of the performing subject. With the single exception of the two-man soaring exercise, however, all activities were performed by the single primary subject. In this manner, all of the T-013 data establish a baseline, and the force and moment levels measured during the experiment indicate the relative impact or effect of each of the seven main activities.

A.1.2 Activity organization

Names and organization of the specific T-013 actions are given in table A-1. Start and end times are given in two different forms so that anyone interested in further use of the recorded data may have easy access to either the data tape that uses the first form or to the previous, more extensively displayed, time histories found in reference 2 which generally use the second form. The time intervals also indicate the duration of each activity.

The underlined categories represent the level at which the results are presented in the handbook. The analysis was intended to present sufficient detail, yet allow enough data to be studied together to develop better results and more reliable trends.

A.1.3 Time histories

Previous documentation (ref. 2) displayed one continuous sequential time history for the entire T-013 experiment, all on the same scale so that different activities could be directly compared. It is not the intention to duplicate prior work, yet some visual representation of force and moment data is necessary to give the analyst a perspective or basis to aid in the interpretation of the following analyses. Selected segments of time histories are given together with a description of the activities which attempt, where possible, to identify spikes, patterns, and time between specific actions.

Note that since the time histories presented are only a portion of the total activity profile, they may not contain the maximum value. Therefore, there may not always be an obvious correspondence between the given profiles and statistical tabulations.

A.1.4 Statistical analysis

Statistics is concerned with scientifically collecting, organizing, summarizing, and analyzing data to aid in drawing valid conclusions and making reasonable decisions. The important statistical results for crew motion data are maximum levels, ranges, standard deviations, and frequency content. These factors are important in assigning pertinent design specifications and requirements for control system bandwidth, control authority, sensor/actuator deadbands, and overall control system performance.

The maximum level is defined to be the largest absolute value of the set of activity data, either force or moment. Range is calculated as the difference between the maximum positive value and the minimum negative value. Standard deviation is defined as the square root of the difference between the mean of the squares and the square of the mean. Frequency content identifies the energy concentration.

Statistical tabulations are given to provide the designer with a means of determining peak expected values for activities extended in time. Typical force levels are represented by standard deviation while extreme levels are bounded by range and maximum values that often reflect numbers as high as 10σ or 12σ.

APPENDIX A

TABLE A-1.- T-013 ACTIVITIES

Activity	Time from beginning of year 1973, sec		Time from beginning of experiment, sec	
	Start	End	Start	End
Console operations	1975 7375	1975 7540	3155	3320
Respiration exercises:				
Deep breathing	1975 6396	1975 6416	2176	2196
5 coughs	6427	6465	2207	2245
5 sneezes	6465	6485	2245	2265
Coughs, sneezes	8152	8210	3932	3990
Normal body exercises:				
Arm motion				
Wave right arm (1)	1975 6526	1975 6532	2306	2332
Wave right arm (2)	6602	6610	2382	2390
Wave left arm (1)	6575	6584	2355	2364
Wave left arm (2)	6650	6660	2430	2440
Wave both arms	6624	6634	2404	2414
Arm movements	8207	8297	3987	4077
Leg motion				
Swing right leg	1975 6715	1975 6725	2495	2505
Bend right knee	6753	6767	2533	2547
Leg lifts	8315	8372	4095	4152
Bowing motion				
Bowing (1)	1975 6676	1975 6715	2456	2495
Bowing (2)	8297	8315	4077	4095
Gross body exercises:				
Arm flapping				
Flapping (1)	1975 4812	1975 4862	592	642
Flapping (2)	7590	7640	3370	3420
Crouch				
Crouch and straighten	1975 7645	1975 7660	3425	3440
Crouch and push-off	4881	4893	661	673
Swaying	1975 6020	1975 6200	1800	1980
Soaring:				
One man normal				
One man (1)	1975 7195	1975 7222	2975	3002
One man (2)	8370	8392	4150	4172
Normal (3)	5035	5140	815	920
One man forceful				
Forceful (1)	1975 4990	1975 5035	770	815
Push-offs (worst case) (2)	7695	7751	3475	3531
Two men normal	7832	7890	3612	3670
Two men forceful				
Forceful (1)	1975 5225	1975 5375	1005	1155
Forceful (2)	5470	5520	1250	1300
Forceful (3)	5667	5700	1447	1480

APPENDIX A

The statistical tabulations are the only data presented that consider the total as well as individual value of the x-, y-, and z-components. It is obvious from glancing at the tabulations that total value does not differ significantly from that of the dominant component (usually y) for each activity. This reinforces the conclusion that the analysis of the total force or moment is generally repetitious. Totals have been included for statistical evaluation because the computations are relatively trivial as compared with those required for power spectral density.

A.1.5 Power spectral density analysis

Power spectral density (PSD) is a measure of the power or energy density contained in an activity or signal. It is commonly computed as the Fourier transform of the autocorrelation function of the activity plotted against time. The area under the PSD curve provides useful information because it equals the variance of an activity with a zero mean. Thus, the square root of this integral should equal the standard deviation as computed from the time function. This can be used as a partial measurement of the validity of the PSD.

The control system designer has a particular interest in PSD because it identifies the amount of energy or power in the disturbance at various frequencies. This information is useful in selecting a controller to meet the mission requirements and pointing accuracies. If high pointing requirements were involved, a designer might consider a controller having response characteristics that would follow the disturbance with minimum lag. If the pointing requirements were less severe, some degradation in controller response would be acceptable. Also, realizing that the vehicle "sees" the disturbance and perhaps excites a structural mode, the designer must determine to what extent his sensors, rate gyros, etc., will respond.

The initial step in determining PSD's was to decide how to structure the time function for input. Longer time segments give better resolution of the data, but more time segments averaged together produce smoother PSD results. The averaging technique was selected for computation, and table A-2 shows the length and number of segments per activity. The computer model used to evaluate the PSD's performs the discrete Fourier transform of the averaged time segments of an activity, then computes the squared magnitude of the transform. The results are then smoothed using a weighted averaging technique called Hanning to reduce leakage and soften irregularities that cloud the actual distribution.

Thus, averaging both input (time segments) and output (PSD data) represents two attempts to provide smooth PSD curves. The smoothing process is important to evaluate the results reasonably, and it establishes a method of producing data that can be modeled more efficiently and easily. However, it also explains why the rms of the PSD data may only approximate rather than equal the standard deviations of the time function.

The PSD data are displayed graphically in section A.2. Like the time histories and statistical data, the plots are grouped according to activity. Magnitude of the PSD is given in $N^2/(rad/sec)$ for force and $N^2\text{-}m^2/(rad/sec)$ for moment plotted against frequency in rad/sec.

APPENDIX A

TABLE A-2.- T-013 ACTIVITY SEGMENTS FOR PSD

Activity	Length of time segments, sec	Number of time segments
Console operations	35	5
Respiration exercises . . .	35	4
Normal body exercises:		
Arm motion	10	11
Leg motion	10	5
Bowing	10	2
Gross body exercises:		
Flapping arms	10	6
Crouch and push-off . . .	35	2
Swaying	30	6
One-man soaring:		
Normal	10	8
Forceful	10	6
Two-man soaring:		
Normal	10	10
Forceful	10	11

In addition to the plots, each activity section contains a table that indicates how the force and moment data were segmented for input to the PSD calculations and a table summarizing maximum PSD levels and corresponding frequencies. Referencing this latter set of tables is an important step in making the user aware of the difference in scales before the PSD plots are visually compared for the three components. The first figure in section A.5.1.4 is a vivid example of a case where the analyst must note that the F_Y plot is by far the more significant representation even though visually the plot looks smaller than that for F_X.

A.2 Simulated Console Operations

A.2.1 Activity description

This exercise consisted of the subject performing motions typically associated with a console operation, such as the flipping of switches, hand-controller inputs, and keyboard entries.

APPENDIX A

The following description is taken from the Skylab experiments checklist detailing the crew tasks.

(1) Attach self to FMU 1 feet restraints.

(2) Tell mission science pilot (SPT) not to perform any gross motions during the experiment.

(3) Read the following simulated actions to the primary experiment subject (SUB) for him to perform. Allow a 3- to 5-sec pause between each item.

(a) Right hand - flipping switches
(b) Right hand - rotating selector switches (chest, height)
(c) Right hand - flipping switches
(d) Left hand - THC operations
(e) Right hand - flipping switches
(f) Left hand - keyboard entry
(g) Right hand - RHC attitude nulling sequence
(h) Right hand - RHC yaw inputs
(i) Left hand - keyboard entry
(j) Right hand - RHC yaw inputs
(k) Left hand - keyboard entry
(l) Right hand - RHC pitch inputs
(m) Left hand - keyboard entry
(n) Right hand - flipping switches (reach up)

A.2.2 Time histories

Figures A-1 and A-2 are selected time profiles of force and moment, respectively. Table A-3 correlates specific console operation motions with the two profiles. Time is given in seconds from the reference times.

TABLE A-3.- DESCRIPTION OF CONSOLE OPERATIONS PROFILE

Time, sec	Action
0 to 15	Right-hand flip switches (A)
15 to 25	Right-hand rotating selector switches (B)
25 to 35	Right-hand flip switches (C)
35 to 45	Left-hand THC operations (D)
45 to END	Right-hand flip switches (E)

APPENDIX A

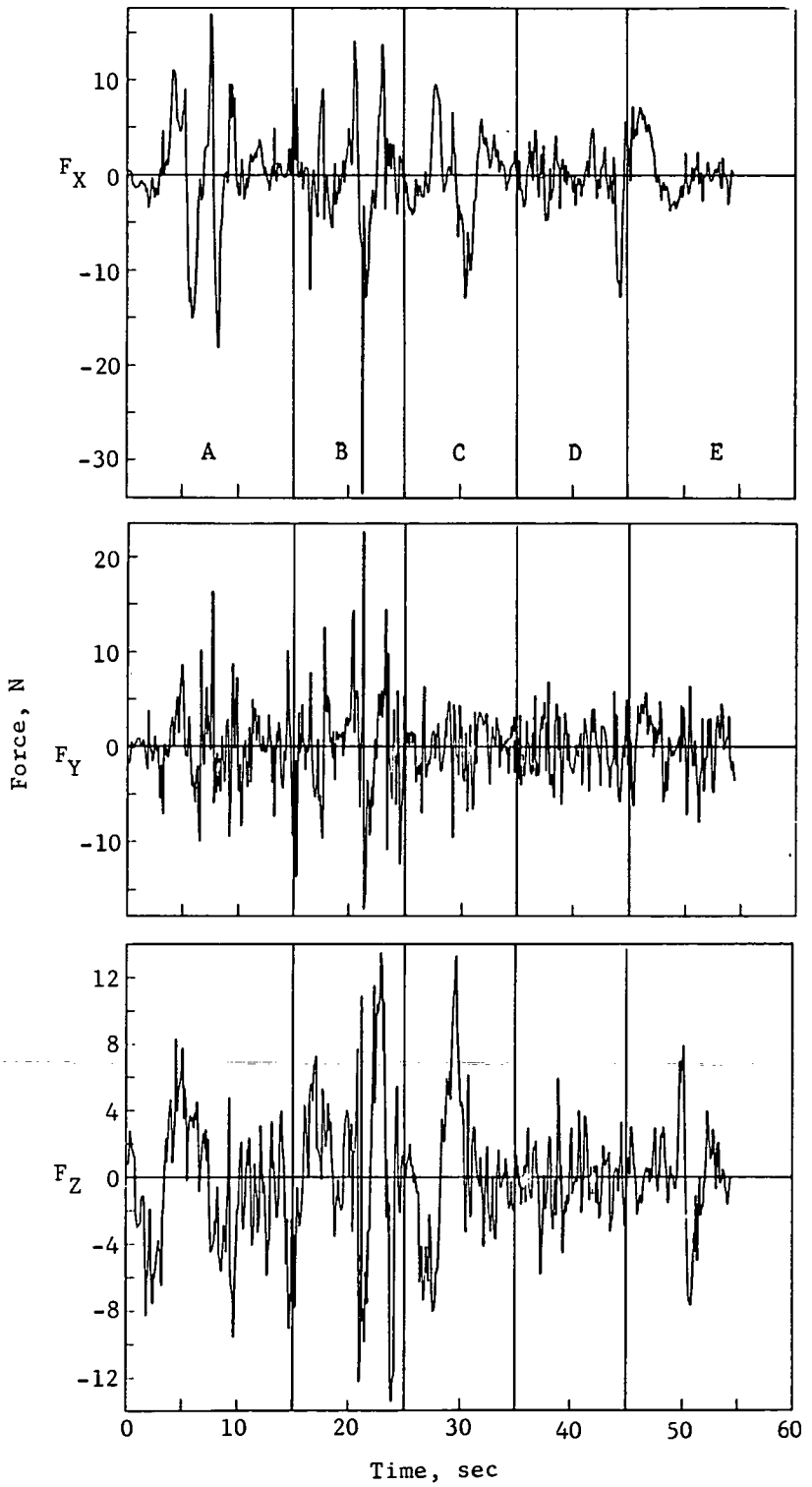

Figure A-1.- Force profile of console operations.

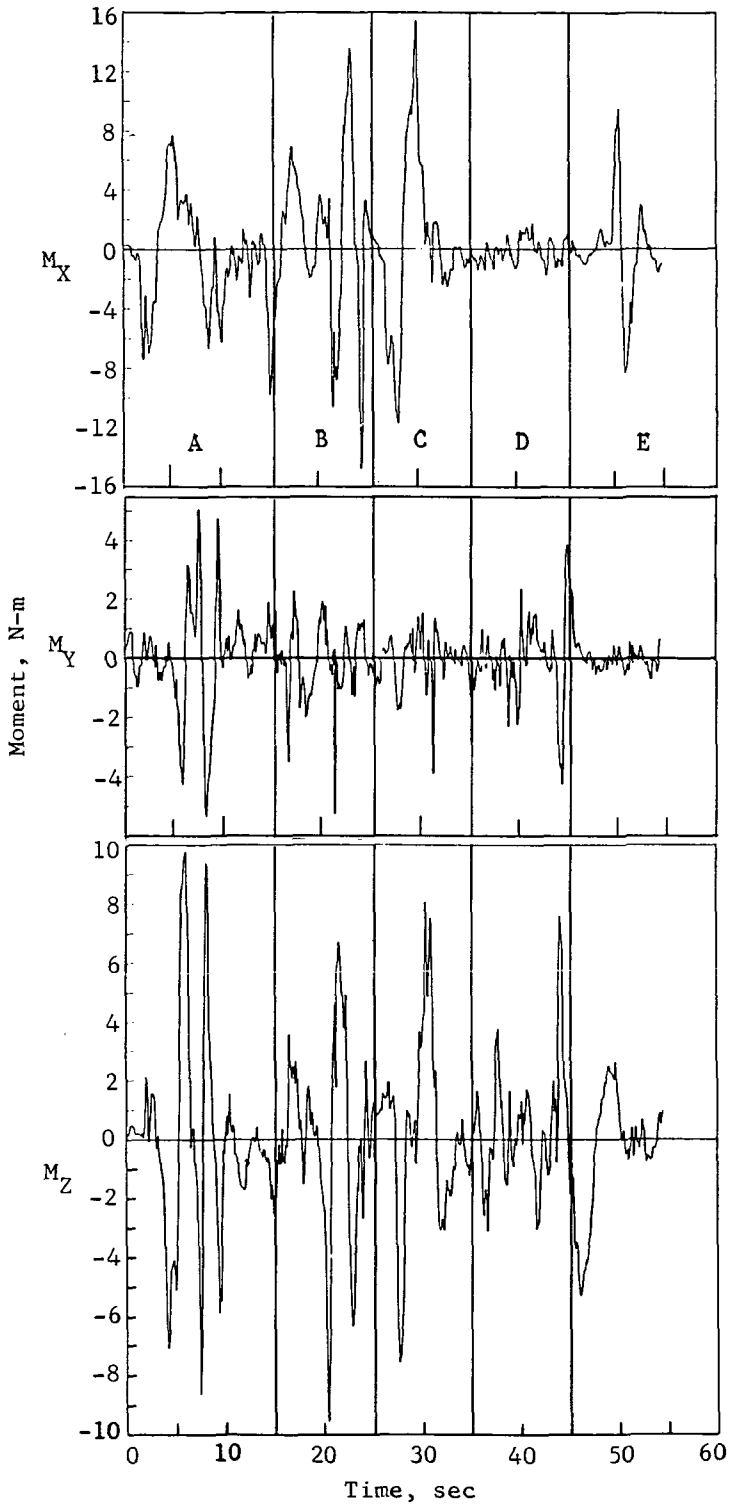

Reference time:
19757375., 3155.

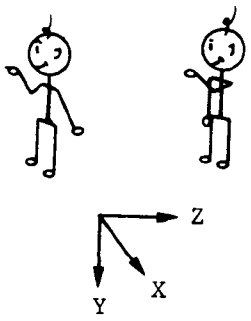

Figure A-2.- Moment profile of console operations.

APPENDIX A

A.2.3 Statistical data

Table A-4 summarizes the pertinent console operations statistics.

TABLE A-4.- CONSOLE OPERATIONS STATISTICS

Statistical results for -	Force, N				Moment, N-m			
	F_X	F_Y	F_Z	F_T	M_X	M_Y	M_Z	M_T
Range	57.36	57.41	26.97	75.77	30.19	12.13	24.37	31.06
Maximum level	33.55	32.29	13.50	41.95	15.35	7.06	13.58	16.10
Standard deviation	3.93	4.13	3.28	6.57	3.40	.99	2.30	4.22

The maximum force level in the x or lateral direction occurred during exercise (b) where the subject's right hand rotated selector switches at chest height. A single spike accounts for this maximum value. The operation which causes the next highest force level for the x-component is I (not shown), left-hand keyboard entries. All other activities approximate the time histories displayed in figure A-1. The maximum values of F_Y and F_Z occur during exercise (a). While this force level is characterized by only one spike for F_Y, the forward direction F_Z contains several spikes during this exercise which are close to the maximum. In both cases, exercise (b) causes the next highest level of force. The same trends are found for moment.

According to table A-4, the total force range, maximum, and standard deviation are about one-third greater than those of the largest component. Also, F_X and F_Y values (lateral and upward/downward motions) are close to each other in all three cases. The implication is that, for console operations, no one component is dominant. At least two out of the three have a significant effect upon the total value. This observation is reinforced by the time histories. This conclusion is not as obvious for moment since there is a closer approximation of M_T to M_X even though M_Z and M_X are not far apart in value.

A.2.4 Frequency content

Figures A-3 and A-4, respectively, show the PSD of force and moment for console operations. The solid line represents the PSD computed from actual data while the broken lines represent a theoretical PSD derived from a set of filter parameters. For all cases but F_Y, the theoretical PSD is estimated by a first-order equation. The finer broken line in the F_Y plot represents a fourth-order equation which is seen to produce a better visual approximation than the second-order equation. In all cases except F_Y again, power is obviously highly concentrated in lower frequencies, quickly dropping at mid and high frequencies. The F_Y plot, on the other hand, shows that while much power is still found at low frequency, a significant level is maintained at least through 16 rad/sec and is only starting to decrease at 20 rad/sec. This

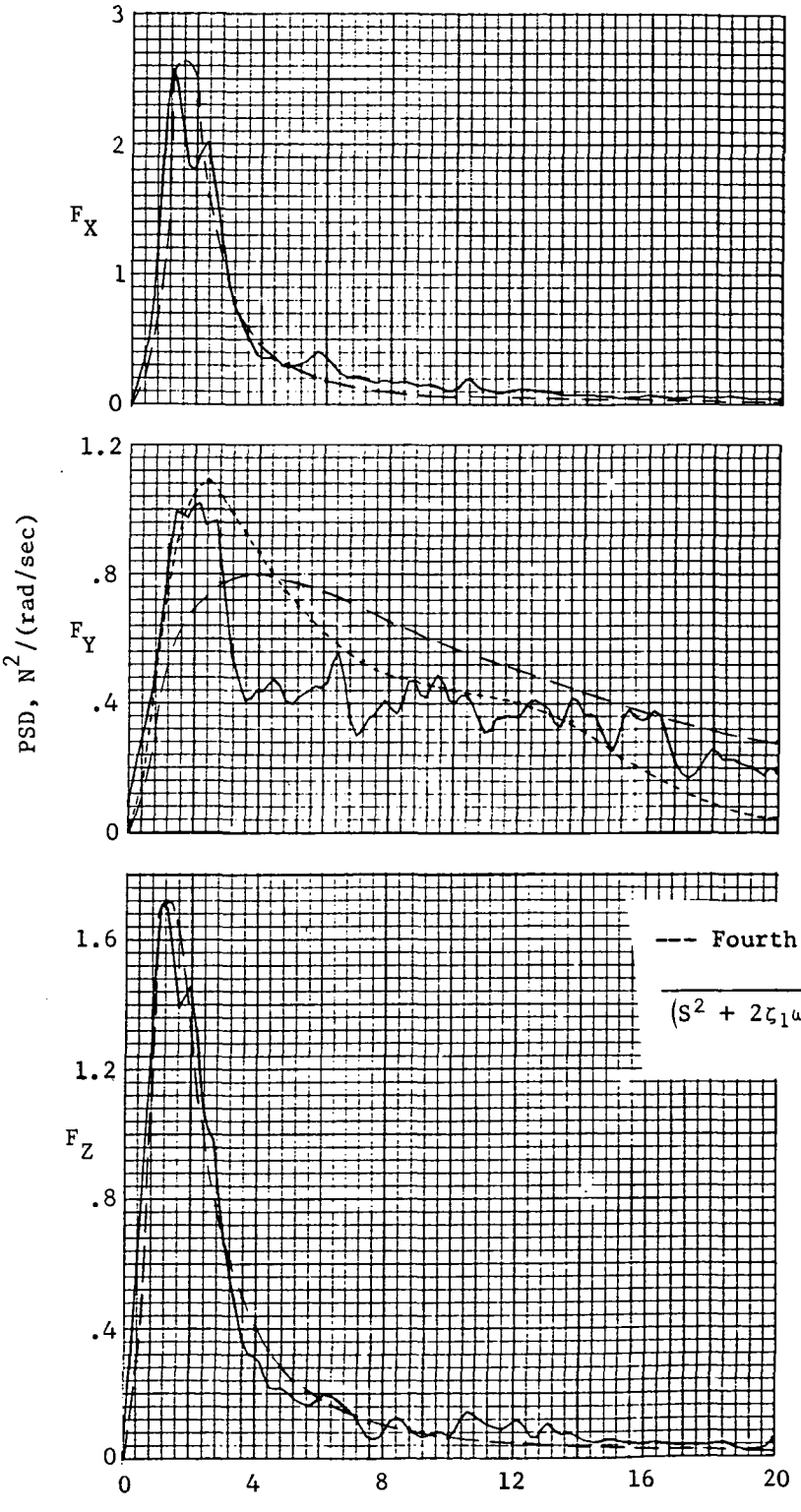

—— Experiment Data

– – Second Order

$$\frac{\tau S}{S^2 + 2\zeta\omega\, S + \omega^2}$$

	F_X	F_Y	F_Z
τ	2.46	12.29	2.56
ω	1.67	3.80	1.34
ζ	.45	1.81	.72

--- Fourth Order

$$\frac{\tau S}{(S^2 + 2\zeta_1\omega_1\, S + \omega_1^2)(S^2 + 2\zeta_2\omega_2\, S + \omega_2^2)}$$

	F_Y
τ	10.40
ω_1	2.25
ω_2	14.68
ζ_1	1.06
ζ_2	.31

Figure A-3.- PSD of force of console operations.

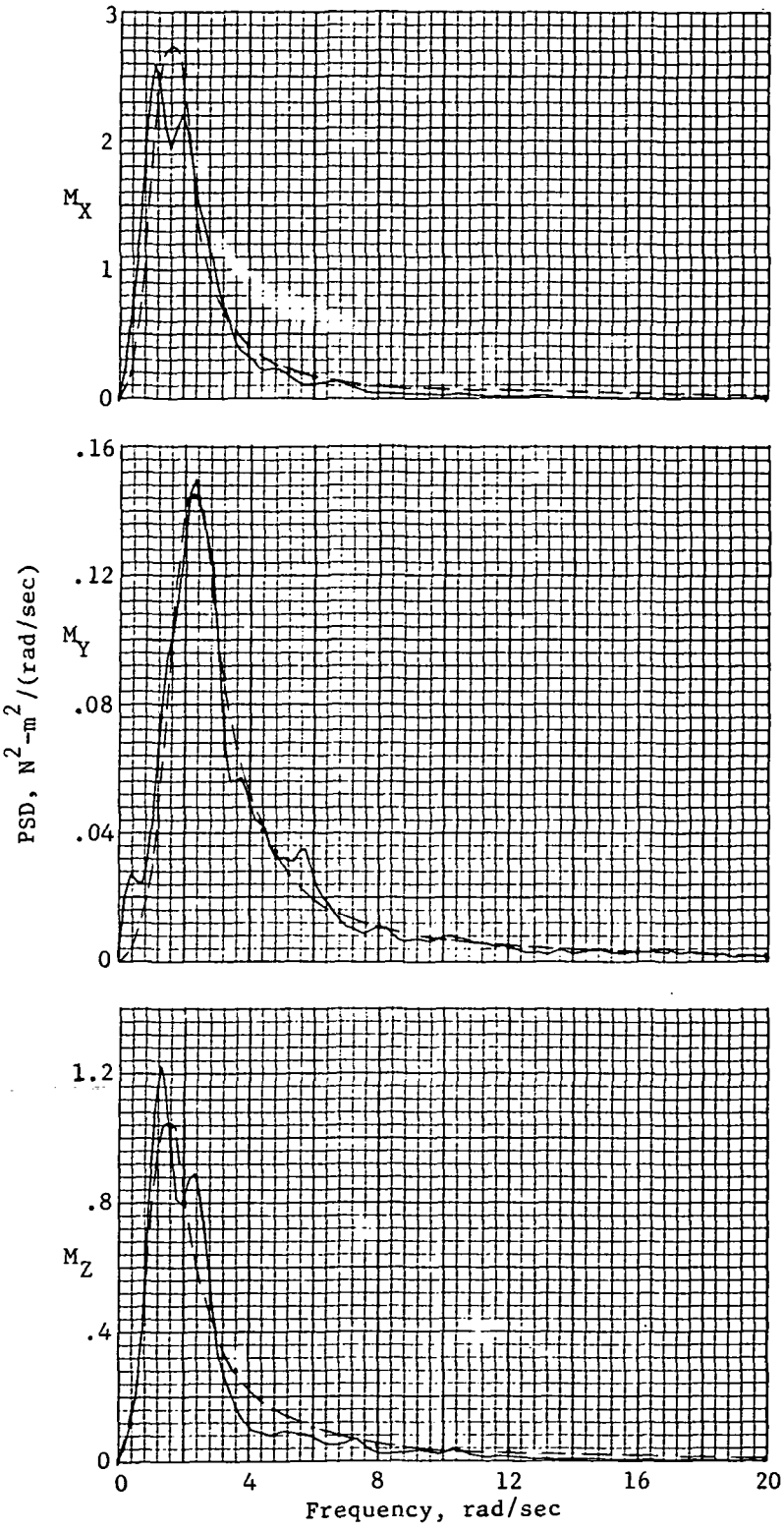

— Experiment Data

– – Second Order

$$\frac{\tau S}{S^2 + 2\zeta\omega\, S + \omega^2}$$

	M_X	M_Y	M_Z
τ	2.38	.78	1.88
ω	1.48	2.20	1.47
ζ	.48	.46	.62

Figure A-4.- PSD of moment of console operations.

observation is substantiated by studying the force profile of F_Y and comparing it to those of F_X and F_Z. F_Y is a "denser" plot than either of the other two.

Table A-5 summarizes the numeric quantities associated with the frequency content of console operations.

TABLE A-5.- CONSOLE OPERATIONS FREQUENCY CHARACTERISTICS

Force	Maximum PSD, $N^2/(rad/sec)$	Frequency at maximum, rad/sec	rms, N
X	2.5	1.2	3.8
Y	1.0	2.0	4.1
Z	1.7	1.0	3.3

Moment	Maximum PSD, $N^2-m^2/(rad/sec)$	Frequency at maximum, rad/sec	rms, N-m
X	2.6	1.0	3.5
Y	.15	2.0	1.0
Z	1.2	1.2	2.3

A.3 Respiration Exercises

A.3.1 Description

The subject was instructed to breathe deeply, cough, and simulate sneezing The time histories indicate eight breaths, five coughs, and six sneezes.

A.3.2 Time histories

Figures A-5 and A-6 depict force and moment profiles for the three basic types of respiration exercises, breathing, coughing, and sneezing. The scale of F_Y shows the force in the y-direction to be almost an order of magnitude larger than F_X and F_Z. The pattern of the different respirations is clearly indicated in the plot of F_Y.

A.3.3 Statistical data

Table A-6 summarizes force and moment statistics for one level of detail, i.e., at the coughing, sneezing, and breathing level. The quantity F_Y is obviously the dominant component in force.

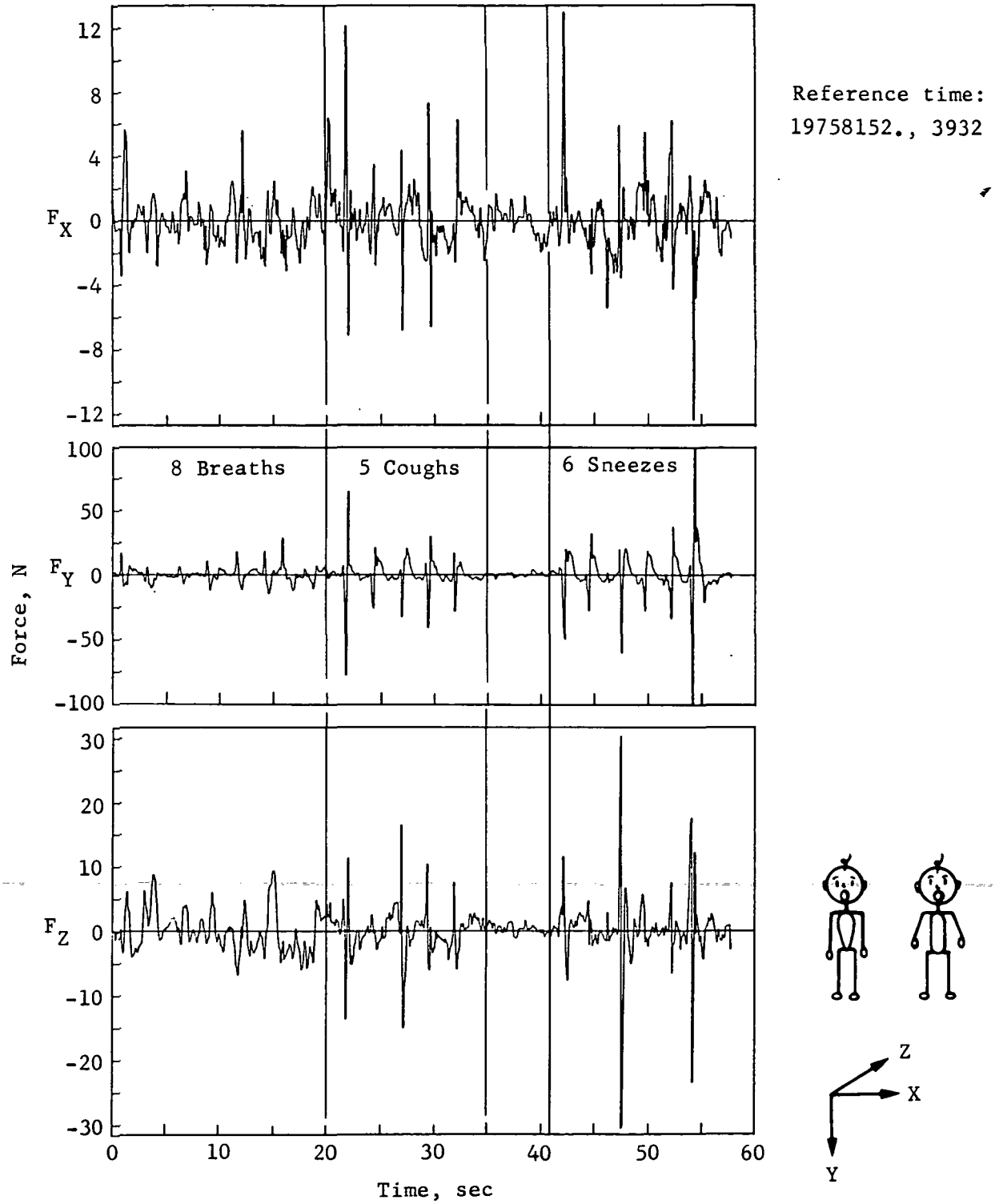

Figure A-5.- Force profile of respiration exercises.

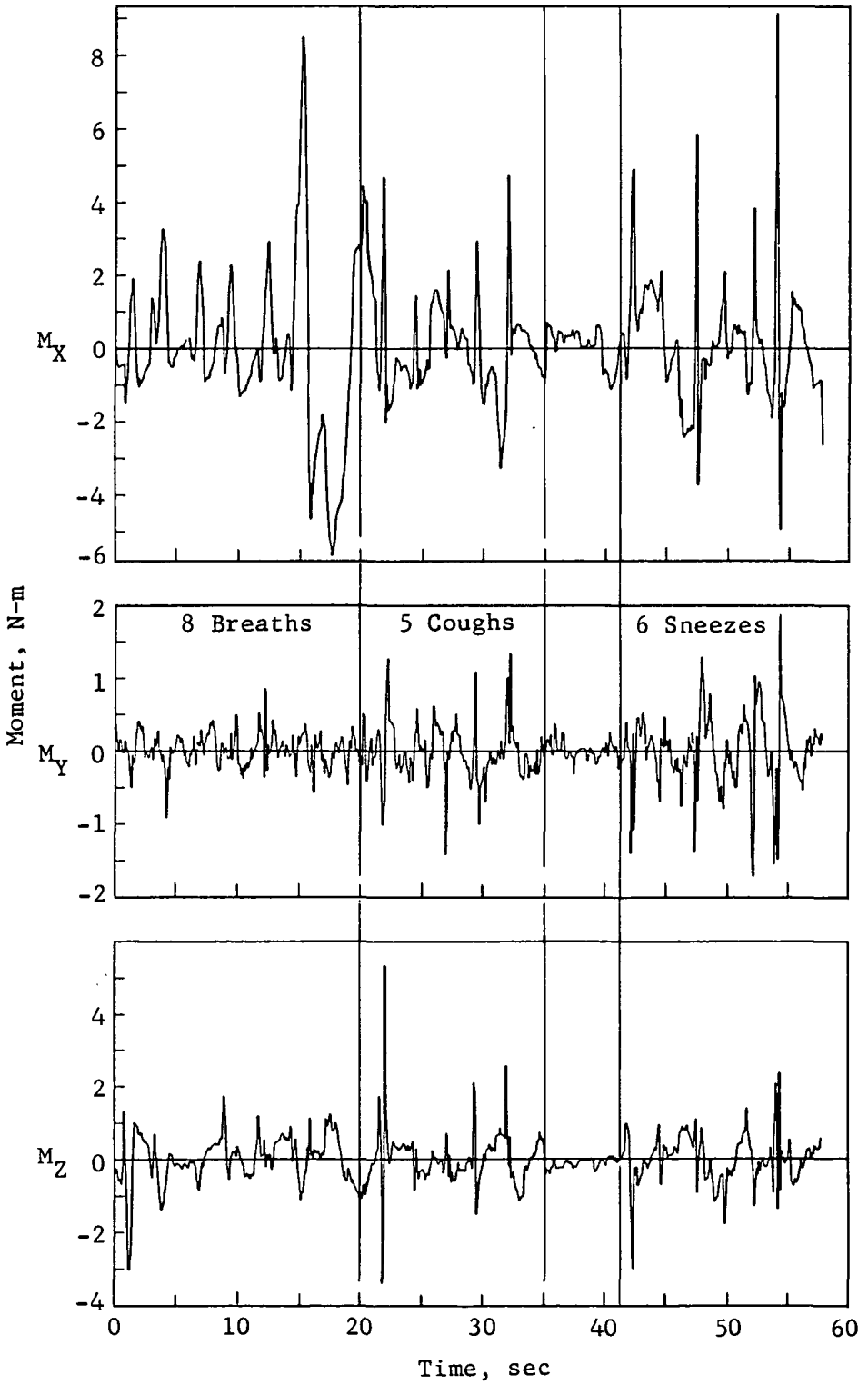

Figure A-6.- Moment profile of respiration exercises.

TABLE A-6.- RESPIRATION EXERCISES STATISTICS

Activity	Force, N				Moment, N-m			
	F_X	F_Y	F_Z	F_T	M_X	M_Y	M_Z	M_T
Range, maximum - minimum								
5 Coughs	23.61	163.74	63.54	167.03	7.81	4.41	4.96	8.03
5 Sneezes	27.20	325.39	68.94	330.09	13.21	4.94	13.56	23.50
Coughs, sneezes . . .	25.45	199.54	60.98	203.03	14.82	3.60	8.71	17.92
Deep breathing . . .	94.07	161.09	70.39	179.27	23.28	17.26	33.74	37.15
Maximum level								
5 Coughs	15.56	96.40	37.60	97.08	4.06	2.57	2.67	4.08
5 Sneezes	19.03	212.69	34.56	216.29	8.48	2.61	9.97	13.01
Coughs, sneezes . . .	13.02	100.65	30.69	103.38	9.15	1.88	5.32	9.38
Deep breathing . . .	56.63	92.41	39.83	109.12	12.68	10.74	18.63	19.22
Standard deviation								
5 Coughs	1.86	10.66	3.82	11.48	1.49	0.41	0.62	1.67
5 Sneezes	3.18	29.02	5.51	29.71	2.13	.49	1.52	2.66
Coughs, sneezes . . .	1.88	11.60	4.09	12.44	1.78	.37	.68	1.94
Deep breathing . . .	9.80	21.51	10.69	25.94	4.54	2.34	4.13	6.56

A.3.4 Frequency content

Figures A-7 and A-8 display force and moment frequency content. The plots of PSD of moment data are smooth and regular, and they demonstrate that power is primarily concentrated at lower frequencies, gradually reduced at mid frequencies and virtually gone at high frequencies. The plots for PSD of force, however, are quite different. Only F_X is even approximately regular or typical in the fact that power predominates in one portion of the frequency range. Both F_Y and F_Z PSD plots show large fluctuations; both also show a significant retention of power through the high frequencies.

The higher order filter (short-dashed line) provides the better approximation for F_X but does not appear to be especially advantageous for F_Y.

Table A-7 summarizes the PSD quantities for this activity.

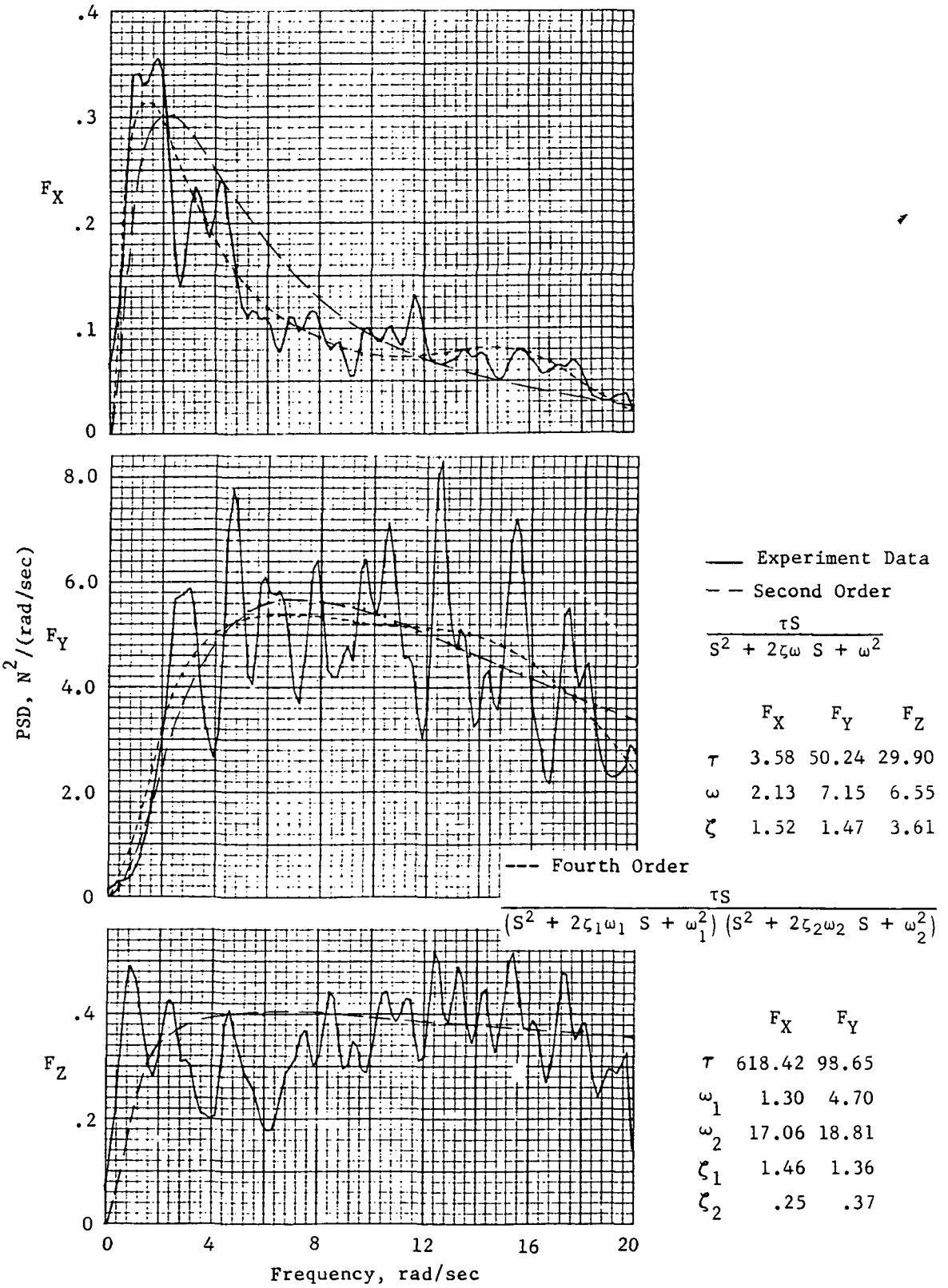

	F_X	F_Y	F_Z
τ	3.58	50.24	29.90
ω	2.13	7.15	6.55
ζ	1.52	1.47	3.61

	F_X	F_Y
τ	618.42	98.65
ω_1	1.30	4.70
ω_2	17.06	18.81
ζ_1	1.46	1.36
ζ_2	.25	.37

Figure A-7.- PSD of force of respiration exercises.

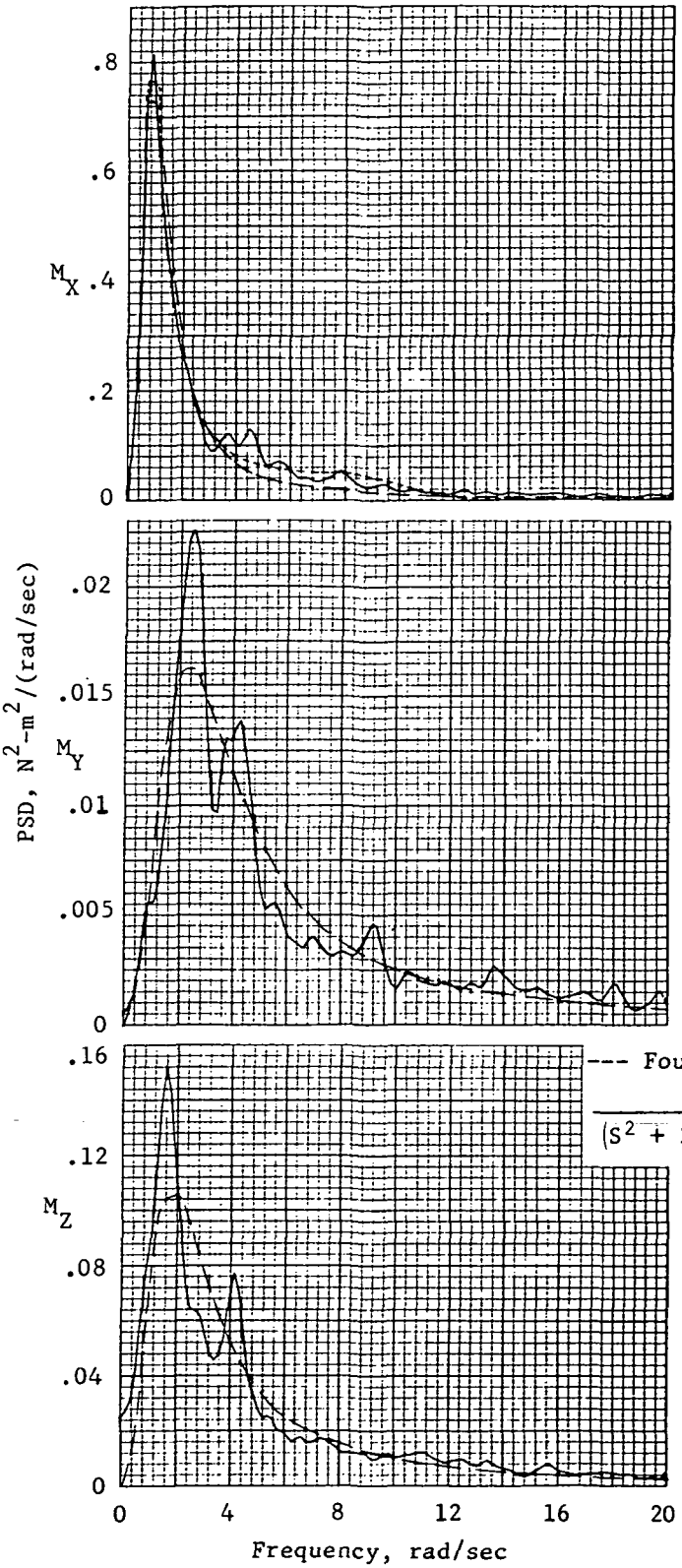

—— Experiment Data

– – Second Order

$$\frac{\tau S}{S^2 + 2\zeta\omega\, S + \omega^2}$$

	M_X	M_Y	M_Z
τ	1.03	.52	1.01
ω	.93	2.34	1.84
ζ	.63	.87	.84

--- Fourth Order

$$\frac{\tau S}{(S^2 + 2\zeta_1\omega_1\, S + \omega_1^2)(S^2 + 2\zeta_2\omega_2\, S + \omega_2^2)}$$

	M_X
τ	81.32
ω_1	.89
ω_2	9.27
ζ_1	.60
ζ_2	.27

Figure A-8.- PSD of moment of respiration exercises.

APPENDIX A

TABLE A-7.- RESPIRATION EXERCISES FREQUENCY CHARACTERISTICS

Force	Maximum PSD, $N^2/(rad/sec)$	Frequency at maximum, rad/sec	rms, N
X	0.35	2.0	2.2
Y	8.0	5 and 12	13.2
Z	.5	1, 12, 15.5	3.7

Moment	Maximum PSD, $N^2\text{-}m^2/(rad/sec)$	Frequency at maximum, rad/sec	rms, N-m
X	0.8	1.0	1.8
Y	.02	2.5	.4
Z	.15	1.7	1.0

A.4 Normal Body Exercises

Two sets of body exercises were performed as part of T-013. The set described below as "normal" was composed of arm, leg, and bowing motions which were intended to be done in a nonstrenuous, i.e., "normal" fashion.

A.4.1 Arm motion

A.4.1.1 Activity description

The following commands are taken from the Skylab experiments checklist detailing the crew tasks.

Arm exercises:

Perform each of the following three times as shown:

(a) With right arm straight and rigid at side, raise it out 90° from side and return.

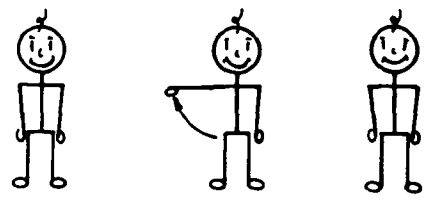

(b) With right arm straight and rigid at side, raise it in front of body 90° and return.

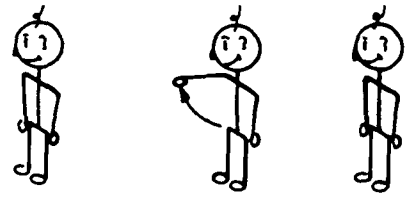

(c) In one continuous movement, raise left arm out 90° from side and move hand toward shoulder through an angle of 150°. Return arm to side while straightening.

(d) With right arm straight and rigid at side, raise arm 90° in front of body. Move it through 90° to right side, and return to side.

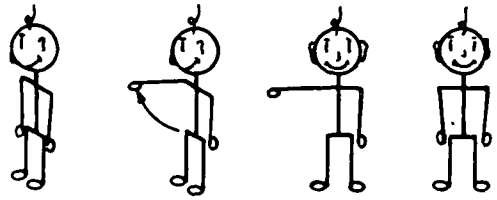

(e) With both arms straight and rigid at side, raise them simultaneously straight out 90° from each side. Move them through 90° to front of body, then lower both arms to side simultaneously.

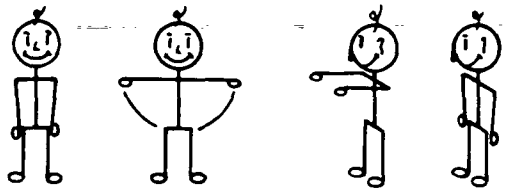

(f) In one continuous movement, raise left arm in front of body 90° and move hand toward shoulder through an angle of 150°. Return arm to side while straightening.

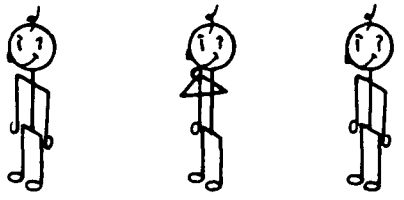

A.4.1.2 Time histories

Figures A-9 and A-10 show representative T-013 activities 9a to 9f for force and moment profiles. The movements cause large, distinguishable spikes in all three directions primarily in the force profile, but also to some extent in the moment profiles.

A.4.1.3 Statistics

Table A-8 summarizes statistical data for arm motion.

TABLE A-8.- ARM MOTION STATISTICS

Activity	Force, N				Moment, N-m			
	F_X	F_Y	F_Z	F_T	M_X	M_Y	M_Z	M_T
Range, maximum - minimum								
Wave right arm . . .	33.33	164.55	55.67	171.11	6.23	18.22	11.90	19.07
Wave left arm . . .	34.74	123.57	43.10	131.01	4.66	7.75	10.70	12.09
Arm movements . . .	35.89	140.77	62.42	150.65	18.34	10.96	13.07	21.69
Both arms	18.01	270.31	99.69	280.64	9.97	4.15	6.37	11.35
Maximum level								
Wave right arm . . .	20.65	93.71	39.47	101.69	3.19	10.50	8.40	10.83
Wave left arm . . .	18.13	78.65	26.86	83.21	2.39	4.81	6.08	6.73
Arm movements . . .	25.81	82.13	32.19	84.27	11.12	7.30	8.31	11.20
Both arms	10.60	149.30	53.48	157.01	5.08	2.57	3.54	6.24
Standard deviation								
Wave right arm . . .	4.28	20.58	6.50	22.00	0.54	2.13	1.40	2.67
Wave left arm . . .	4.70	15.32	4.94	16.77	.84	.91	1.54	1.98
Arm movements . . .	4.25	16.18	6.39	17.91	2.09	1.14	1.42	2.77
Both arms	2.62	38.12	16.24	41.52	1.47	.57	1.11	1.92

One thing most apparent from studying this table is that of all arm motions, moving both arms causes noticeably greater forces in the y- and z-components (upward/downward and forward/backward directions) but the corresponding x or lateral direction is less affected. This trend is not true for moments, where both maximums and standard deviations are somewhat smaller for all three components than for the other single arm motions.

Another fact which is obvious from studying the statistics and plots of force is that the y-component is dominant. Some of the exercises try to establish motions which are clearly either forward or lateral (9a and 9b, for

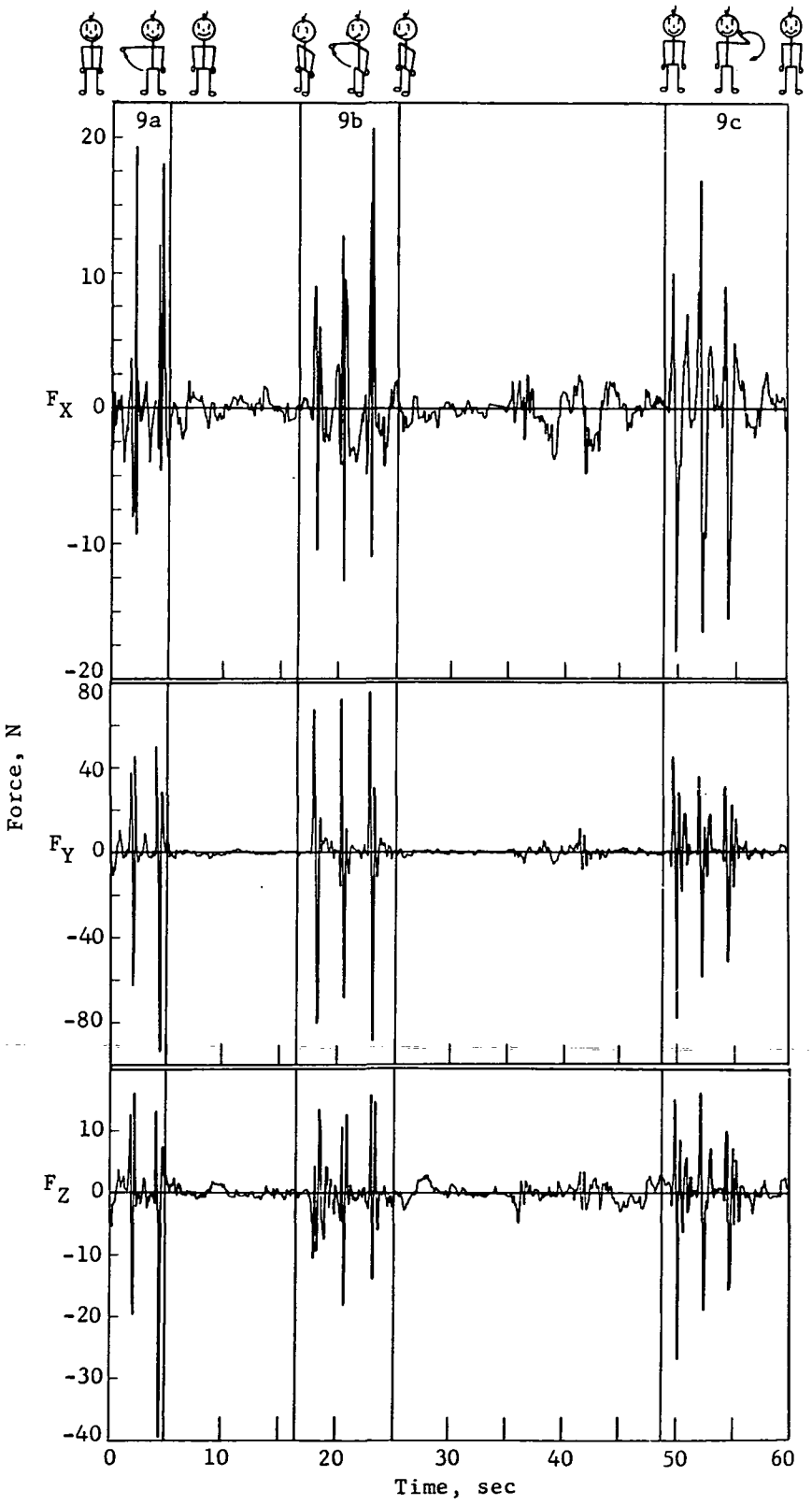

Reference time:
19756526., 2306

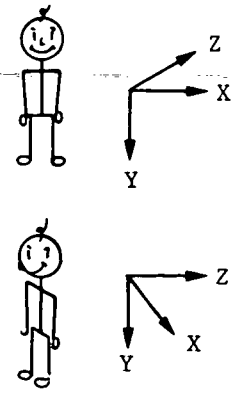

Figure A-9.- Force profile of arm motion.

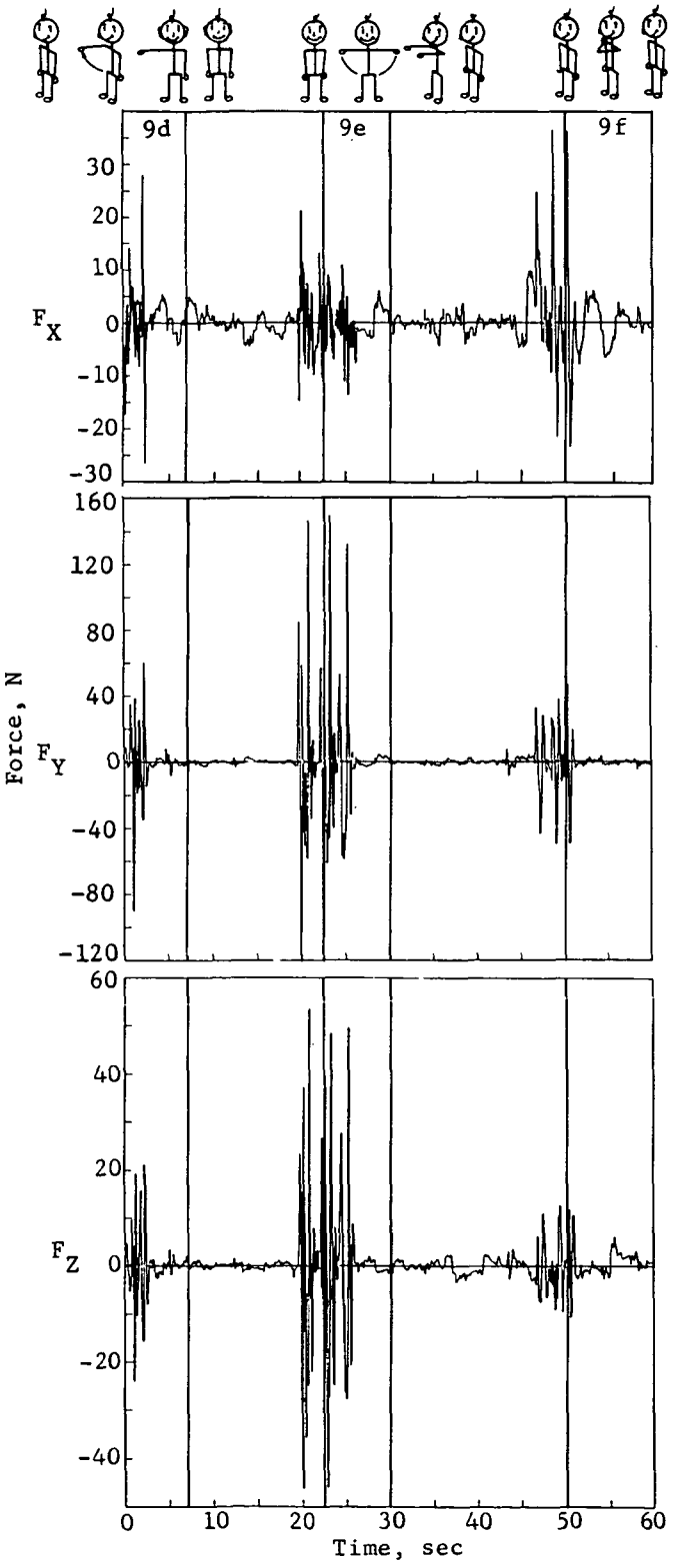

Reference time:
19756606., 2382.

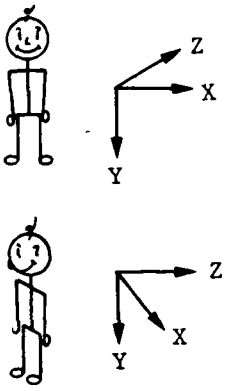

Figure A-9.- Concluded.

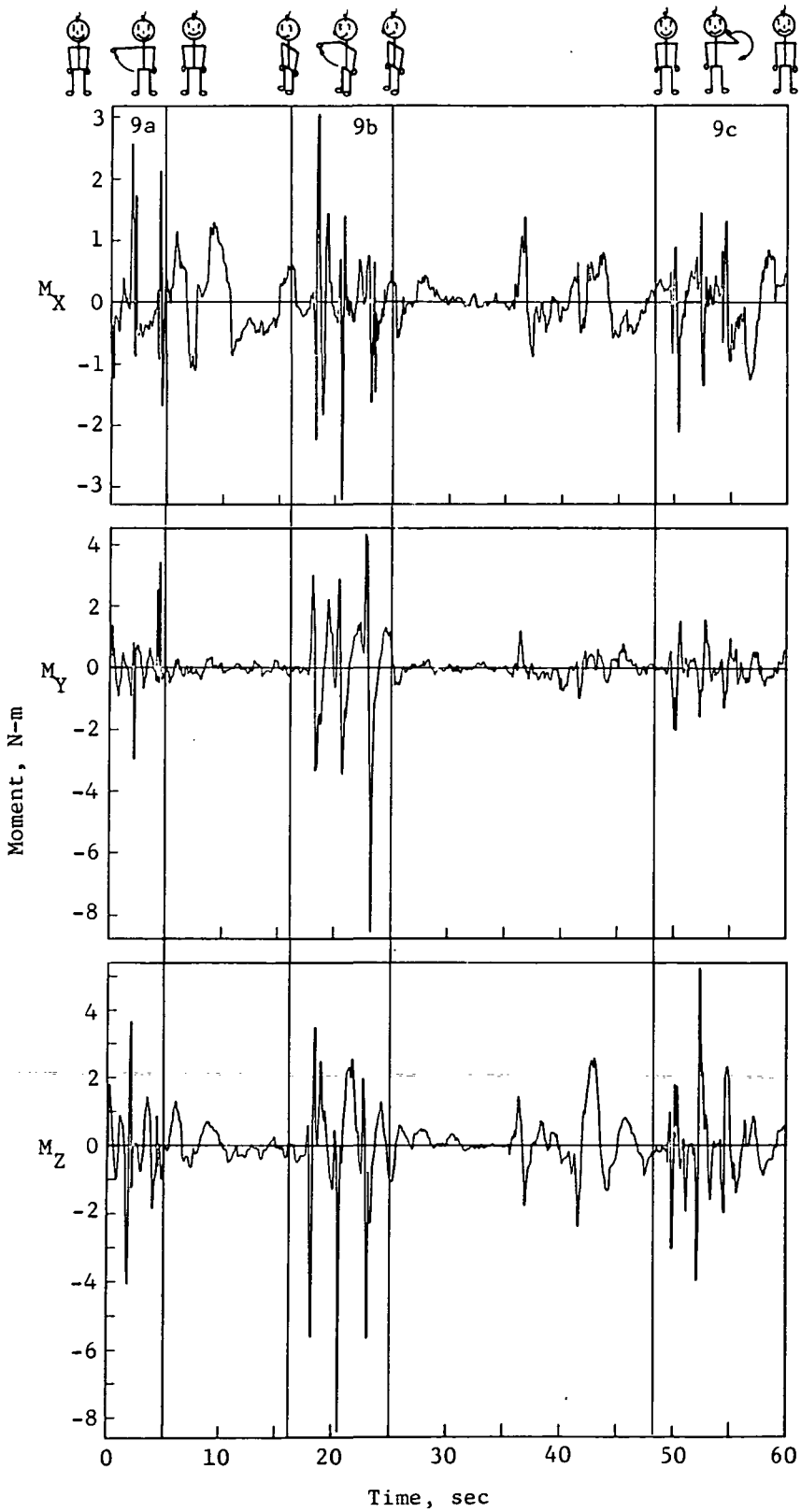

Reference time:
19756526., 2306.

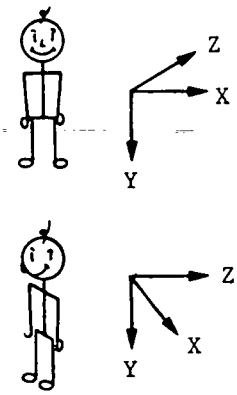

Figure A-10.- Moment profile of arm motion.

C-2

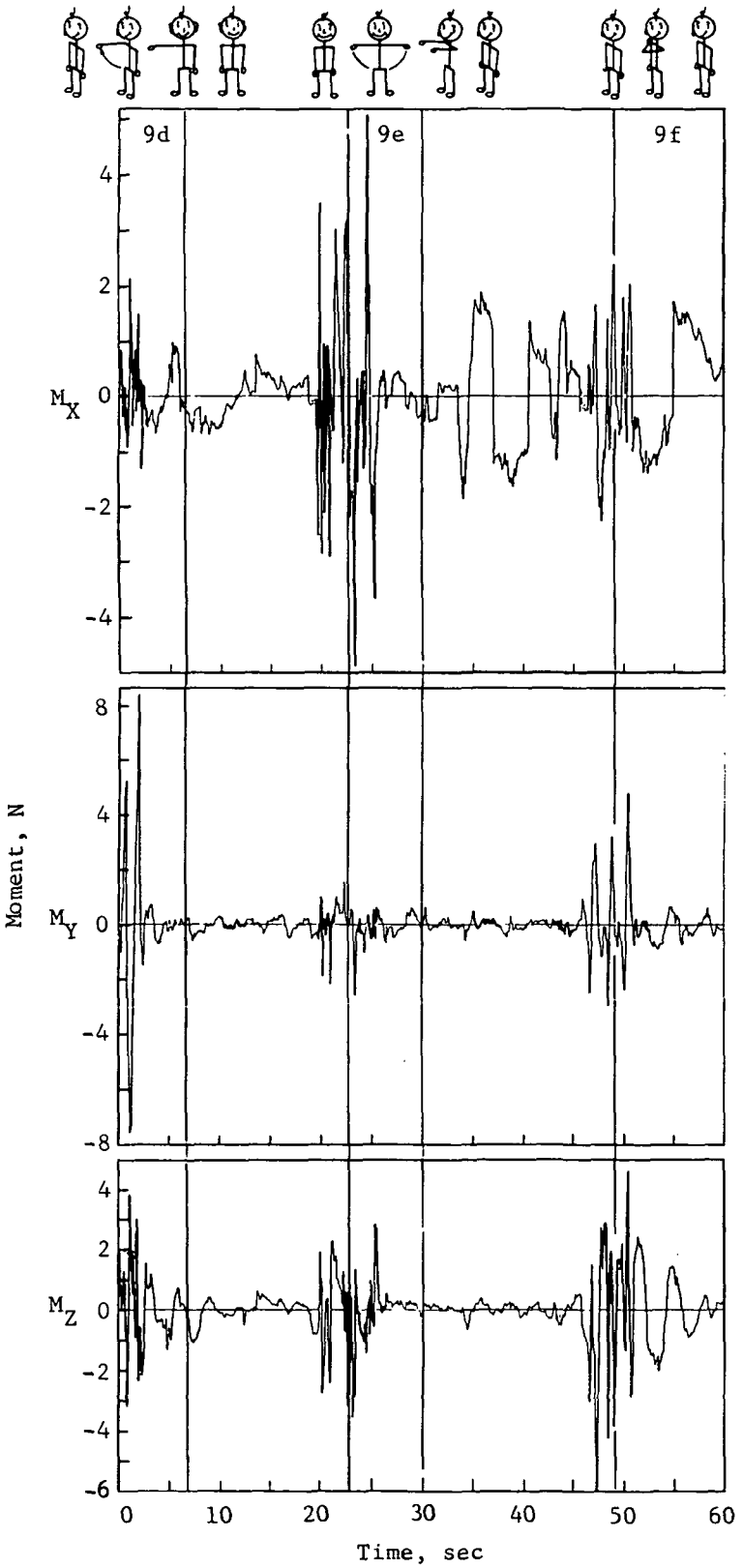

Reference time:
19756606., 2382.

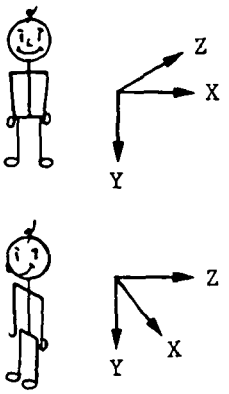

Figure A-10.- Concluded.

instance), but all six motions involve the upward/downward movement. And, no clear distinction between the x- and z-plots can be found for exercises which were meant to occur in only the xy-plane or only the yz-plane. Exercise 9a, for example, was an upward and lateral movement, yet the z-component during this time shows about as much force as during 9b which is meant to be an upward and forward motion. In the corresponding segment of the moment plot, higher moments occur for 9b than 9a in z-component, which could be expected, but the x also increases during this time, which is not expected. The only conclusion is that for all actions, the y-force is predominant but the moments are relatively even, and the value of M_T suggests that all three moment components contribute to the total.

A.4.1.4 Frequency content

Figures A-11 and A-12 present the PSD of force and moment for all arm motions. Only the lower order theoretical PSD computation (long-dashed line) is given for F_X, M_X, and M_Y. This simpler calculation approximates the peak power for F_Y better than the higher order (represented by the short-dashed line), but it does not describe the span of frequency as well. The same trend is true for F_Z and M_Z but the differences are smaller between the two calculations.

Table A-9 summarizes the PSD characteristics.

TABLE A-9.- ARM MOTION FREQUENCY CHARACTERISTICS

Force	Maximum PSD, $N^2/(rad/sec)$	Frequency at maximum, rad/sec	rms, N
X	0.6	2.5	4.2
Y	16.4	10.0	20.4
Z	2.6	10.0	7.7

Moment	Maximum PSD, $N^2\text{-}m^2/(rad/sec)$	Frequency at maximum, rad/sec	rms, N-m
X	0.29	1.0	1.6
Y	.19	4.4	1.4
Z	.11	2.0	1.4

A.4.2 Leg motion

A.4.2.1 Activity description

The three leg movements were designed to be straightforward and basic. All use the right leg to describe a single motion.

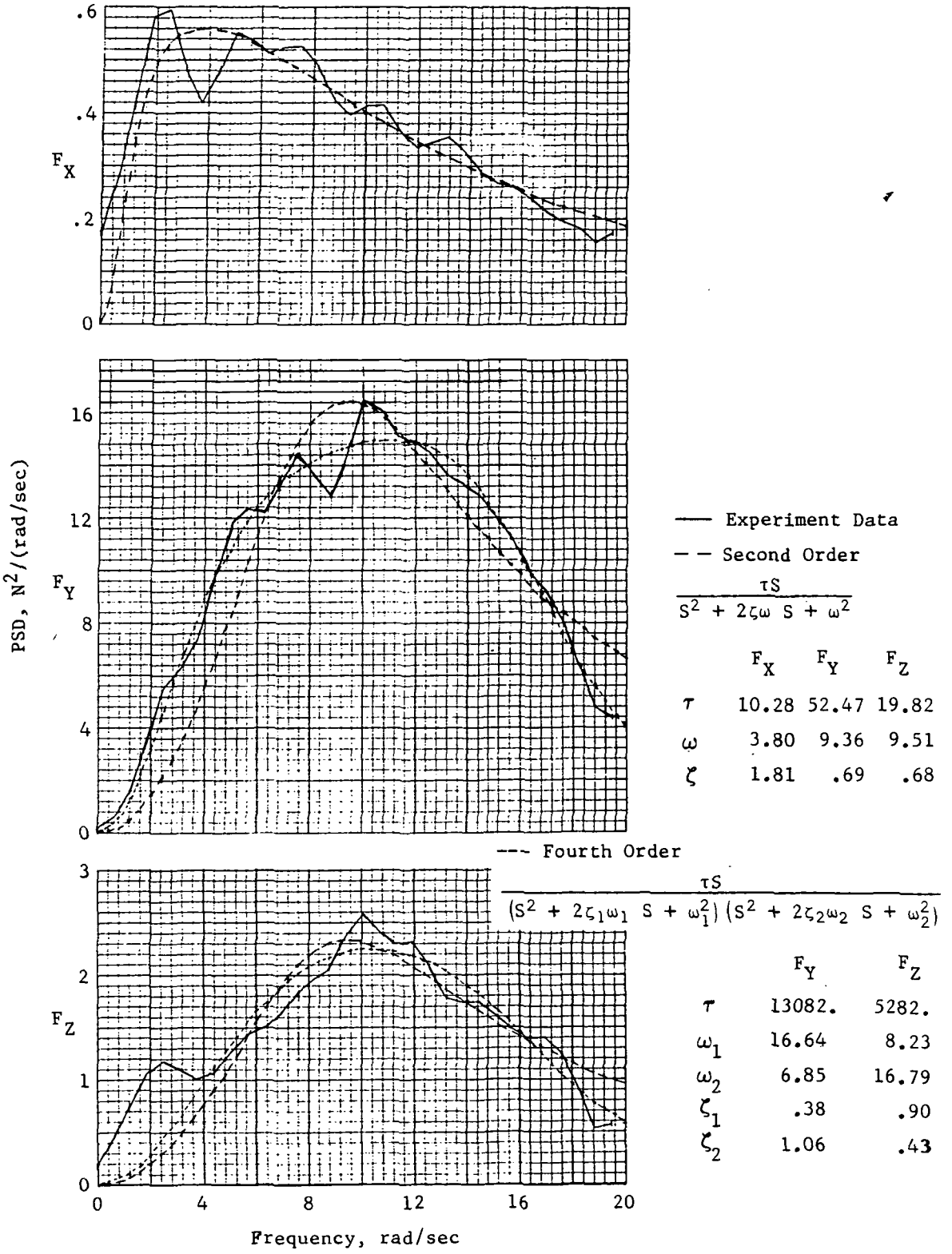

	F_X	F_Y	F_Z
τ	10.28	52.47	19.82
ω	3.80	9.36	9.51
ζ	1.81	.69	.68

	F_Y	F_Z
τ	13082.	5282.
ω_1	16.64	8.23
ω_2	6.85	16.79
ζ_1	.38	.90
ζ_2	1.06	.43

Figure A-11.- PSD of force of arm motion.

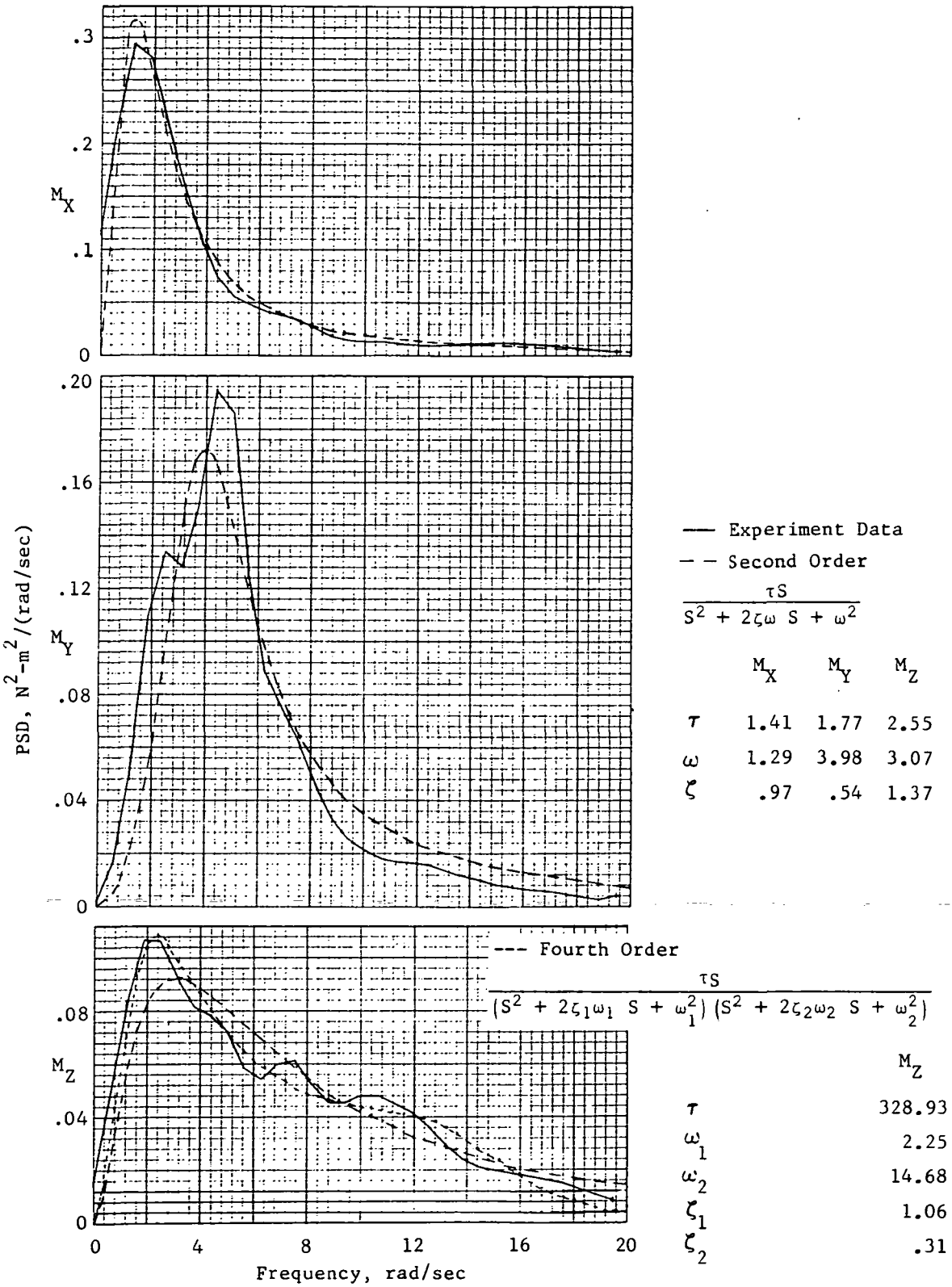

	M_X	M_Y	M_Z
τ	1.41	1.77	2.55
ω	1.29	3.98	3.07
ζ	.97	.54	1.37

	M_Z
τ	328.93
ω_1	2.25
ω_2	14.68
ζ_1	1.06
ζ_2	.31

Figure A-12.- PSD of moment of arm motion.

APPENDIX A

Leg exercises:

Perform each of the following three times as shown:

(a) With right leg straight and rigid, raise it out to side through an angle of 35° to 45° and return.

(b) With right leg straight and rigid, raise it in front of body through an angle of 35° to 45° and return.

(c) In one continuous movement, raise right knee upward in front of body through an angle of 45° while keeping lower leg vertical and return gently.

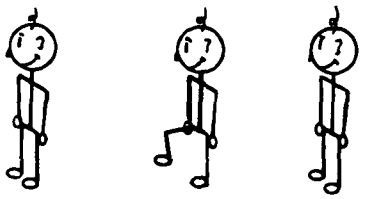

A.4.2.2 Time histories

Figures A-13 and A-14 are the force and moment profiles for leg motion. Table A-10 describes the action plotted. Time is given in seconds from the reference time indicated in both figures.

TABLE A-10.- DESCRIPTION OF LEG MOTION PROFILE

Time, sec	Action
0 to 7	Task 1, motion 12a, right leg out to side, three times
9 to 15	Task 1, motion 12b, right leg to front, three times
21 to 30	Task 1, motion 12c, right knee to front, three times
35 to 42	Bend and release feet
47	Place feet on FMU 1

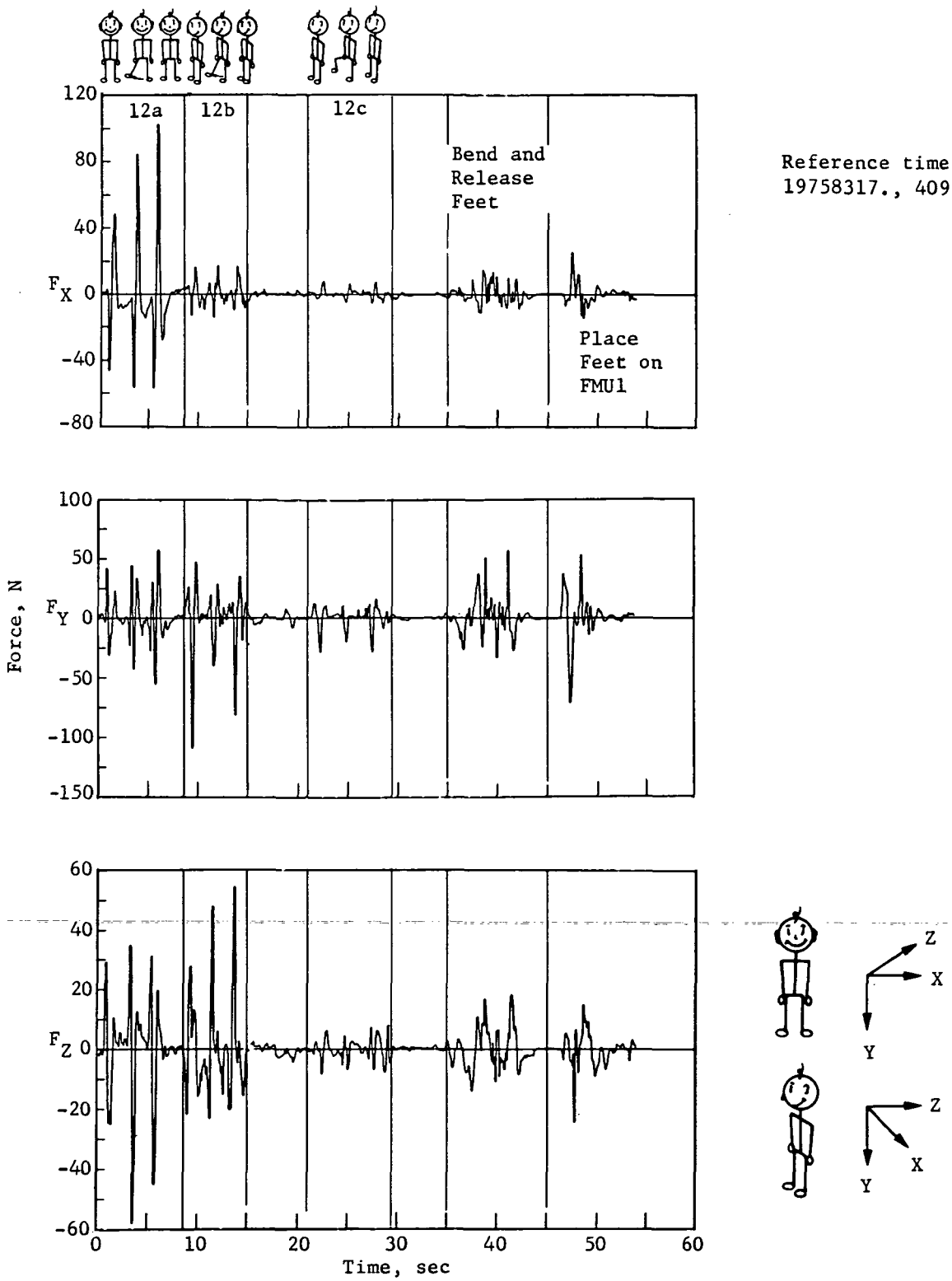

Figure A-13.- Force profile of leg motion.

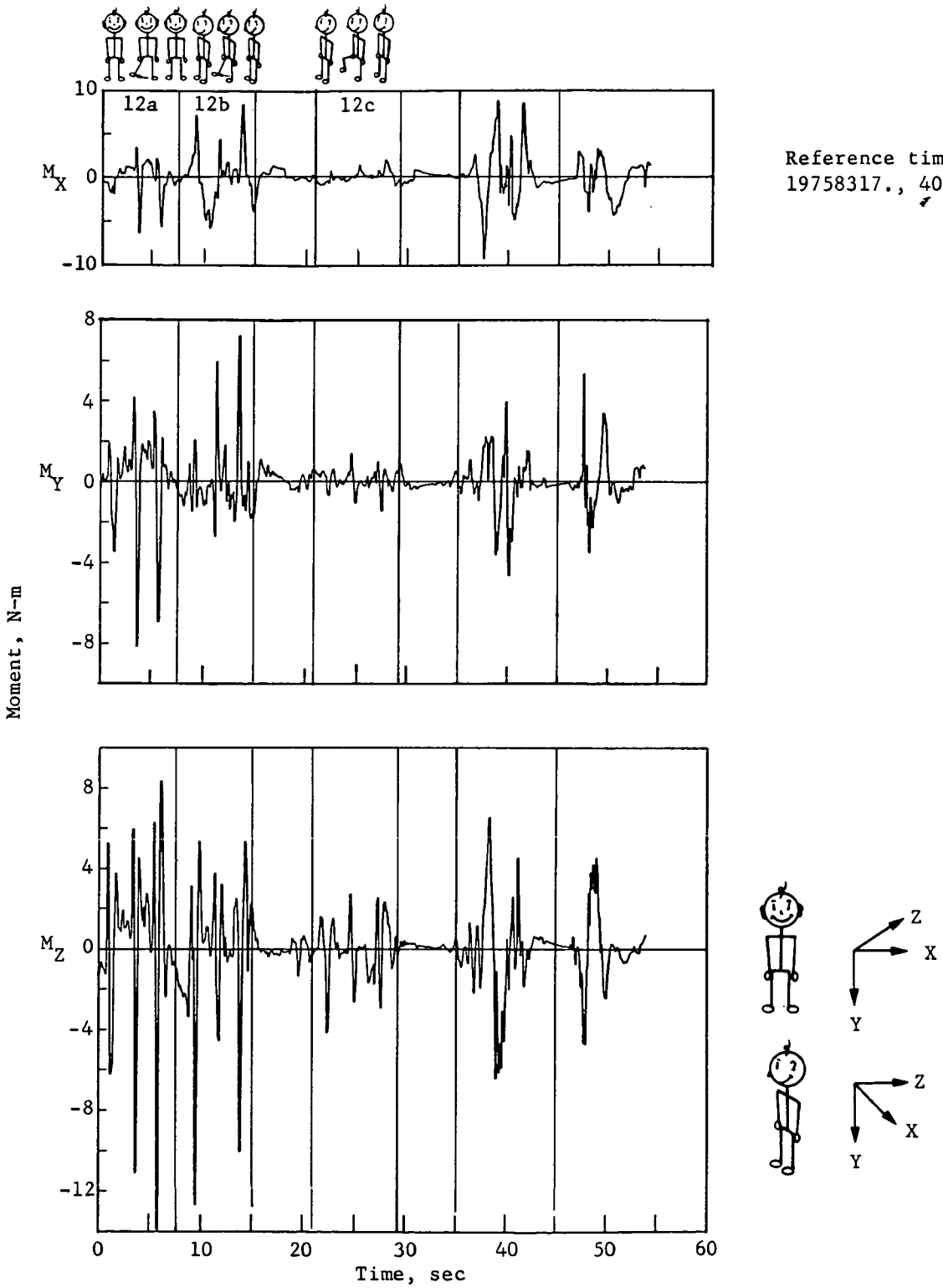

Reference time:
19758317., 4097.

Figure A-14.- Moment profile of leg motion.

A.4.2.3 Statistics

Table A-11 summarizes the statistical data gathered for leg motion.

TABLE A-11.- LEG MOTION STATISTICS

Activity	Force, N				Moment, N-m			
	F_X	F_Y	F_Z	F_T	M_X	M_Y	M_Z	M_T
Range, maximum - minimum								
Swing right leg . . .	139.98	124.83	97.90	187.09	12.06	12.02	23.02	27.78
Bend right knee . . .	25.45	76.83	23.79	82.50	3.93	3.35	11.35	12.20
Leg lifts	159.29	166.96	112.78	188.38	18.18	15.39	22.24	27.50
Maximum level								
Swing right leg . . .	91.92	71.50	58.92	125.54	6.56	7.91	15.07	18.05
Bend right knee . . .	17.08	51.99	12.69	55.43	2.71	2.08	7.75	8.39
Leg lifts	102.54	109.56	58.15	121.58	9.39	8.16	13.90	16.46
Standard deviation								
Swing right leg . . .	12.32	12.97	8.95	19.98	1.45	1.27	2.45	3.11
Bend right knee . . .	2.96	9.05	3.27	10.06	.62	.48	1.35	1.56
Leg lifts	10.75	14.71	8.85	20.25	2.02	1.29	2.19	3.25

It is apparent from the tabulation that there is no one predominant component for either force or moment. This is obvious since the motions performed are meant to occur in both the xy- and yz-planes and are not large movements in any one direction. From the time histories, exercise 12a seems to account for the maximum levels and the larger standard deviations; this exercise is identified in table A-11 as part of both "swing right leg" and "leg lifts."

A.4.2.4 Frequency content

Table A-12 summarizes leg motion frequency characteristics.

TABLE A-12.- LEG MOTION FREQUENCY CHARACTERISTICS

Force	Maximum PSD, $N^2/(rad/sec)$	Frequency at maximum, rad/sec	rms, N
X	20.0	5.8	15.2
Y	17.5	8.8	16.1
Z	8.0	5.8	10.7

Moment	Maximum PSD, $N^2-m^2/(rad/sec)$	Frequency at maximum, rad/sec	rms, N-m
X	0.53	2.5	2.1
Y	.15	3.2	1.5
Z	.47	8.8	2.8

Figures A-15 and A-16 display leg motion frequency content. The plots of PSD for F_X and F_Y are somewhat similar in that the peak values are relatively close and the shapes of both the actual PSD's and the theoretical computations are comparable between F_X and F_Y. The frequencies at which the maximums occur are different, but this difference is less when the theoretical PSD's (short-dashed lines) are considered.

All PSD plots, except M_X, indicate that the activity is composed of two and even three waveforms since there are two or three distinct peaks at different frequencies, separated by approximately 3 rad/sec. These peaks predominate even after an extensive smoothing process was performed.

For all cases except M_X, both higher and lower order filter parameters are given. In all cases, the lower order describes the peak better, but the higher order encompasses the range of frequencies more accurately and seems to give the better approximation.

A.4.3 Bowing

A.4.3.1 Activity description

This exercise, like the others in this section, consists of a simple movement. The official description instructed the subject to "bend upper body forward (bow) 0^o to 80^o at waist three times," then "remove right foot from restraint and stabilize."

A.4.3.2 Time histories

Figures A-17 and A-18 present the force and moment time histories of bowing. F_Y and M_X show a distinct pattern of the three motions.

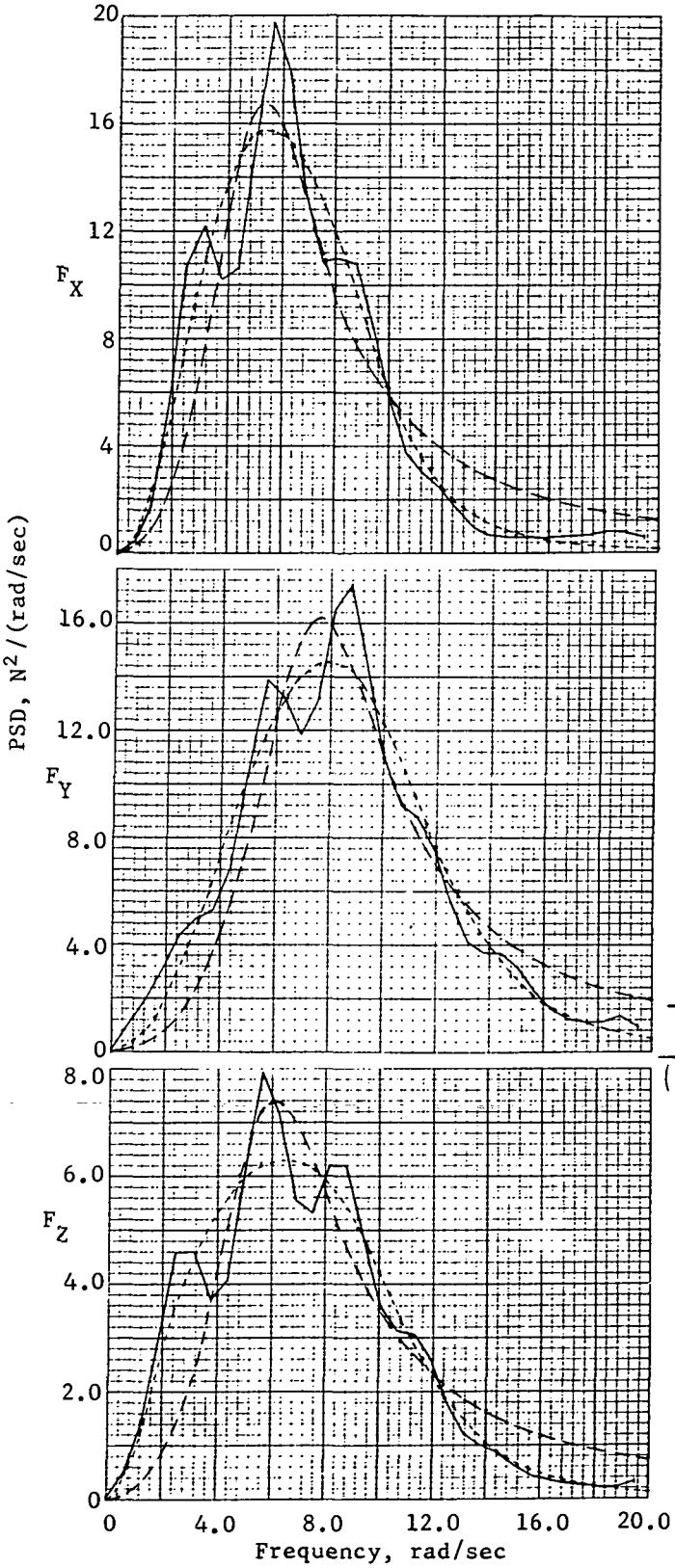

—— Experiment Data

– – Second Order

$$\frac{\tau S}{S^2 + 2\zeta\omega\, S + \omega^2}$$

	F_X	F_Y	F_Z
τ	21.47	25.28	16.34
ω	5.33	7.54	6.10
ζ	.49	.42	.49

--- Fourth Order

$$\frac{\tau S}{(S^2 + 2\zeta_1\omega_1\, S + \omega_1^2)(S^2 + 2\zeta_2\omega_2\, S + \omega_2^2)}$$

	F_X	F_Y	F_Z
τ	24.23	49.11	27.21
ω_1	4.67	7.02	4.87
ω_2	9.43	11.71	10.68
ζ_1	.85	.81	1.13
ζ_2	.46	.46	.47

Figure A-15.- PSD of force of leg motion.

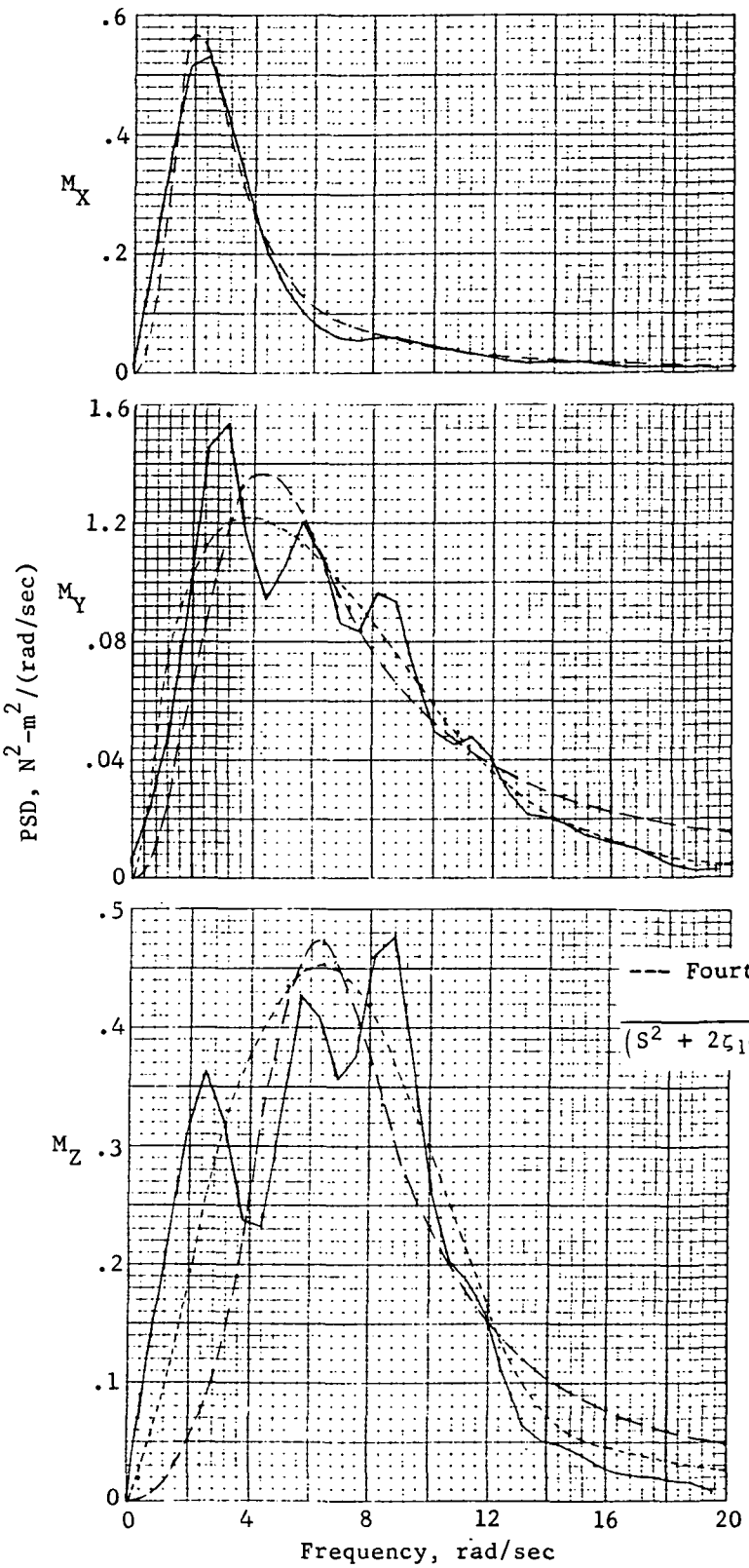

—— Experiment Data

– – Second Order

$$\frac{\tau S}{S^2 + 2\zeta\omega\ S + \omega^2}$$

	M_X	M_Y	M_Z
τ	2.01	2.41	4.15
ω	2.09	4.25	6.18
ζ	.64	.76	.49

--- Fourth Order

$$\frac{\tau S}{(S^2 + 2\zeta_1\omega_1\ S + \omega_1^2)(S^2 + 2\zeta_2\omega_2\ S + \omega_2^2)}$$

	M_Y	M_Z
τ	591.25	727.28
ω_1	3.75	4.87
ω_2	11.48	10.68
ζ_1	1.73	1.13
ζ_2	.67	.47

Figure A-16.- PSD of moment of leg motion.

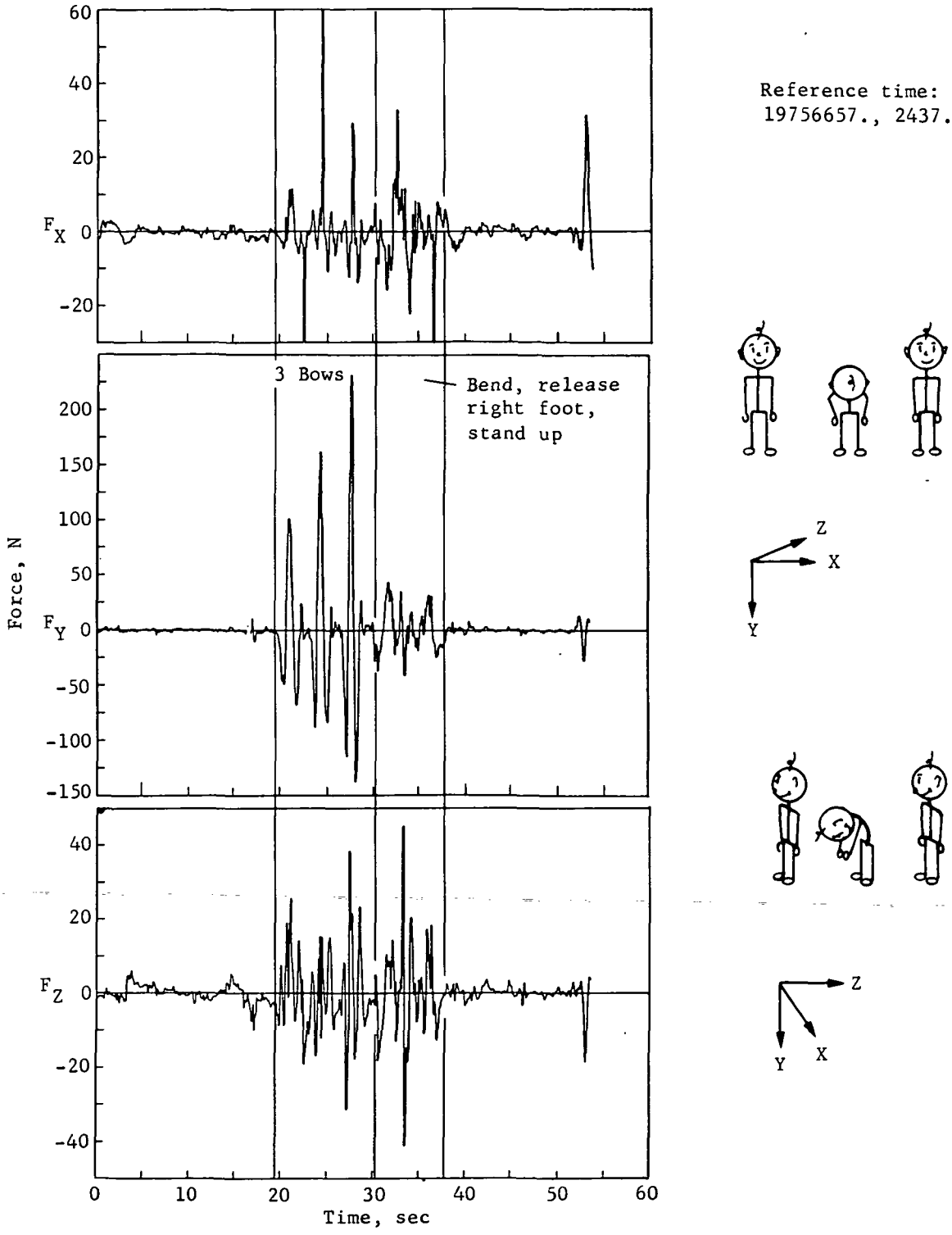

Figure A-17.- Force profile of bowing motion.

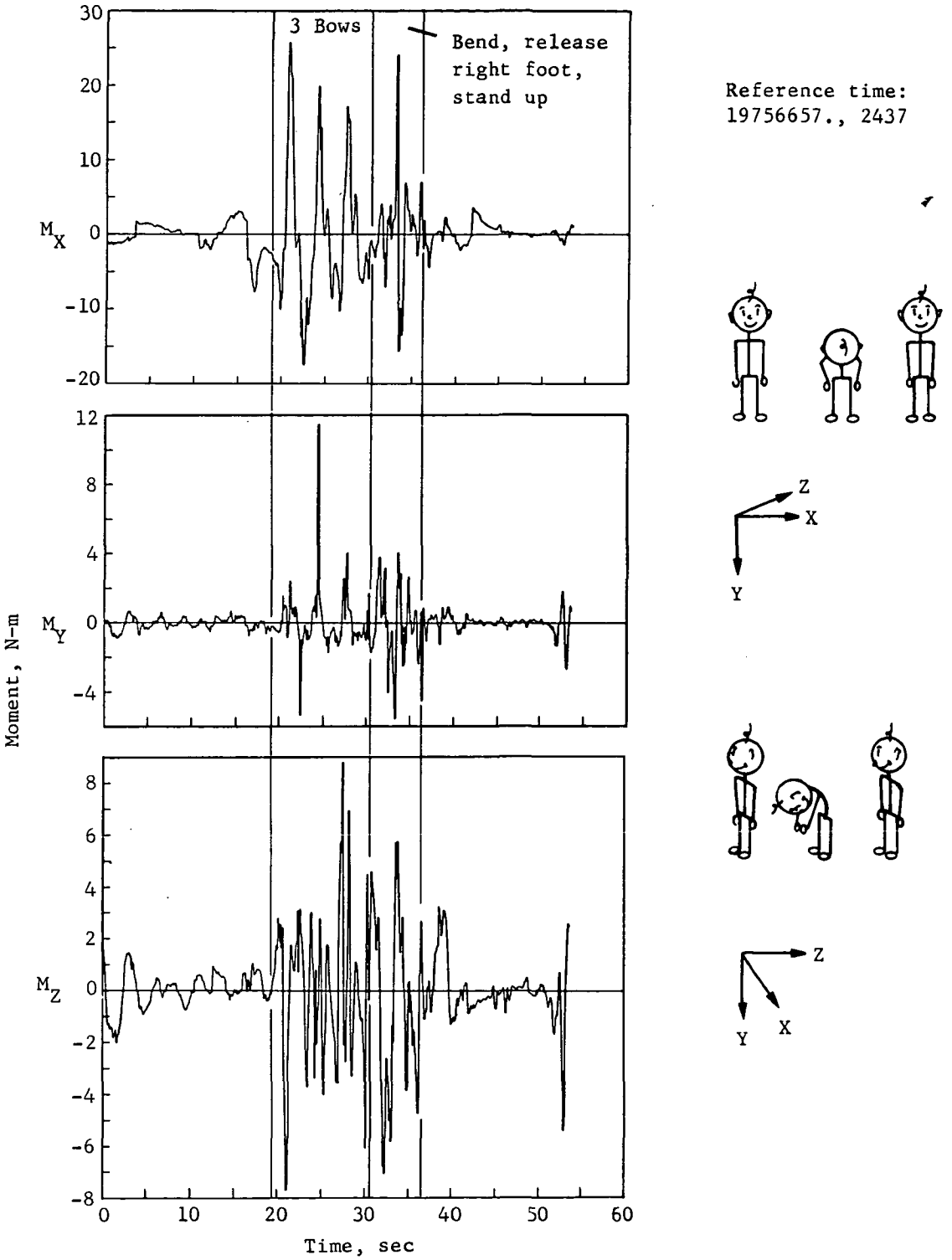

Figure A-18.- Moment profile of bowing motion.

A.4.3.3 Statistics

Table A-13 details statistical data gathered for two ((1) and (2)) separate performances of bowing motions.

TABLE A-13.- BOWING STATISTICS

Bowing	Force, N				Moment, N-m			
	F_X	F_Y	F_Z	F_T	M_X	M_Y	M_Z	M_T
Range, maximum - minimum								
(1)	90.36	368.84	70.14	373.16	43.36	16.85	16.49	52.03
(2)	99.13	336.28	71.42	338.74	23.85	15.90	14.41	27.69
Maximum level								
(1)	60.66	231.85	38.60	234.34	25.82	11.50	8.82	26.40
(2)	78.86	209.15	36.39	210.04	12.03	12.69	7.21	14.15
Standard deviation								
(1)	8.98	65.23	11.39	66.82	9.67	1.63	2.71	10.14
(2)	9.14	61.78	12.46	63.69	4.54	1.66	2.65	5.53

As is the case for most activities, the y-component is shown to be the dominant one for force. Moment, however, is more distributed among the three directions.

A.4.3.4 Frequency content

Figures A-19 and A-20 give the force and moment PSD's for bowing. The regularity and clear definition of the F_Y and M_X time histories are evident in the corresponding PSD's which reflect only one peak and are closely approximated by the theoretical representations given by the short-dashed lines. The other curves show two distinct peaks at frequencies which are 5 to 6 rad/sec apart. The possible exception to this observation is M_Y, but it is also on a much smaller scale than the other two moment plots.

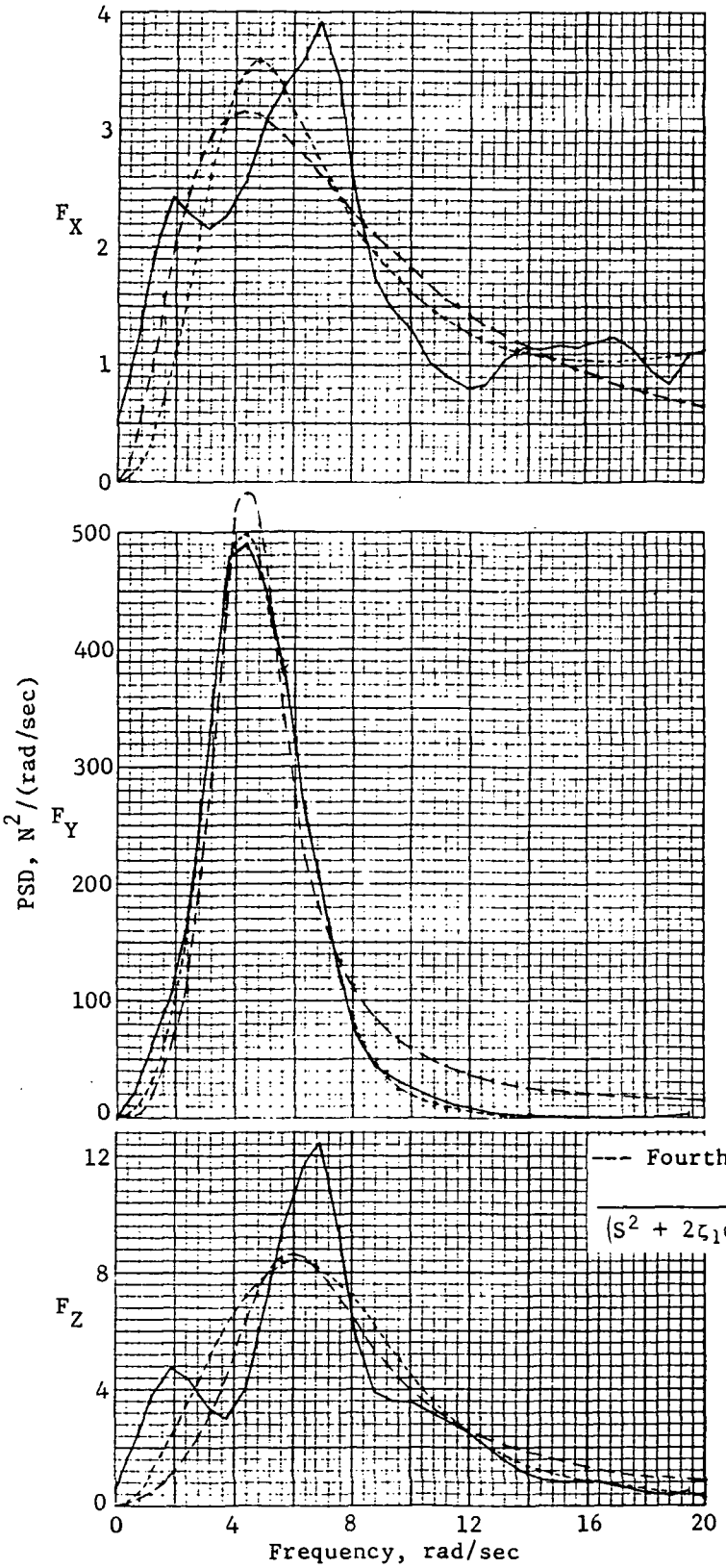

—— Experiment Data

– – Second Order

$$\frac{\tau S}{S^2 + 2\zeta\omega\, S + \omega^2}$$

	F_X	F_Y	F_Z
τ	17.23	67.32	17.96
ω	4.23	4.34	5.96
ζ	1.15	.33	.51

--- Fourth Order

$$\frac{\tau S}{(S^2 + 2\zeta_1\omega_1\, S + \omega_1^2)(S^2 + 2\zeta_2\omega_2\, S + \omega_2^2)}$$

	F_X	F_Y	F_Z
τ	8394.	3123.	7846.
ω_1	4.61	3.93	8.60
ω_2	27.54	6.86	10.70
ζ_1	.65	.47	.57
ζ_2	.15	.39	1.70

Figure A-19.- PSD of force of bowing motion.

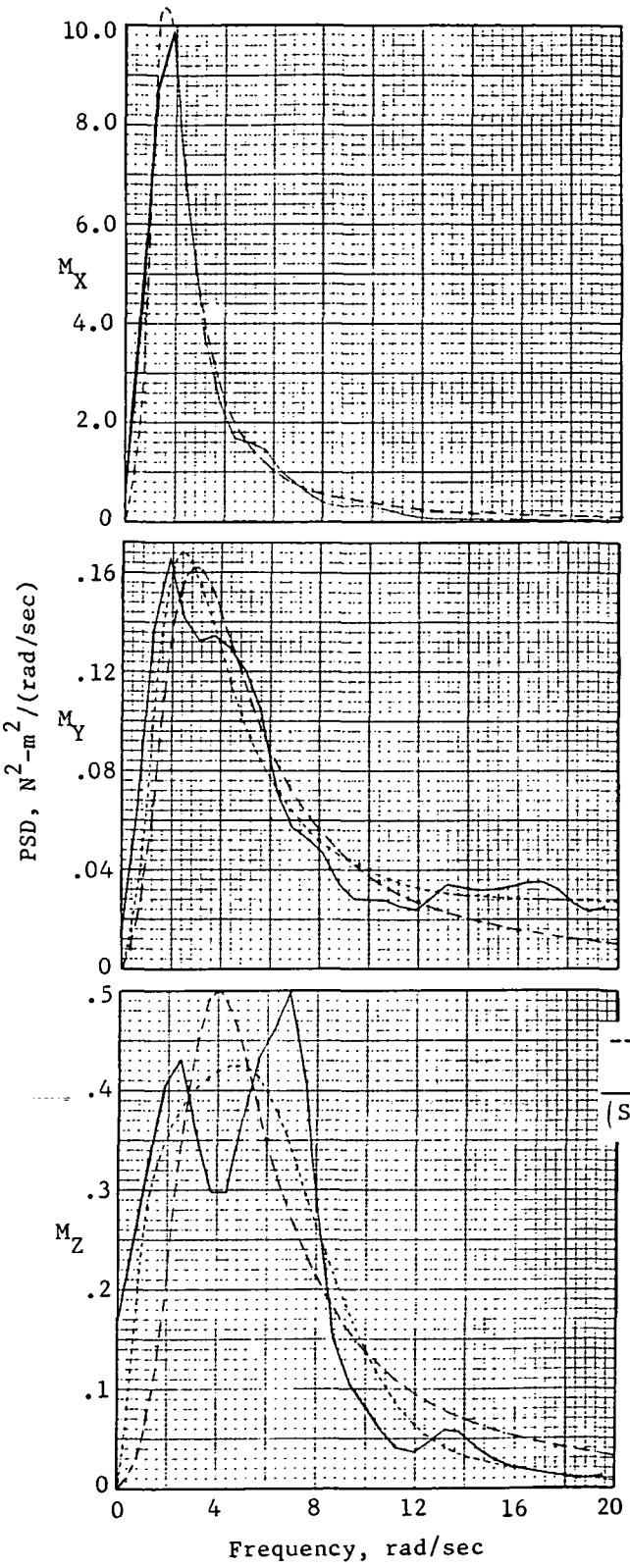

—— Experiment Data

– – Second Order

$$\frac{\tau S}{S^2 + 2\zeta\omega\, S + \omega^2}$$

	M_X	M_Y	M_Z
τ	6.06	2.03	3.68
ω	1.58	2.95	3.95
ζ	.59	.85	.66

--- Fourth Order

$$\frac{\tau S}{(S^2 + 2\zeta_1\omega_1\, S + \omega_1^2)(S^2 + 2\zeta_2\omega_2\, S + \omega_2^2)}$$

	M_Y	M_Z
τ	855.60	991.80
ω_1	2.40	4.46
ω_2	22.37	7.87
ζ_1	.88	2.94
ζ_2	.27	.57

Figure A-20.- PSD of moment of bowing motion.

Table A-14 summarizes pertinent PSD information.

TABLE A-14.- BOWING FREQUENCY CHARACTERISTICS

Force	Maximum PSD, $N^2/(rad/sec)$	Frequency at maximum, rad/sec	rms, N
X	3.8	7.0	8.3
Y	490.0	4.5	65.0
Z	12.4	7.0	11.9

Moment	Maximum PSD, $N^2-m^2/(rad/sec)$	Frequency at maximum, rad/sec	rms, N-m
X	10.00	2.0	7.5
Y	.16	2.0	1.5
Z	.5	7.0	2.7

A.4.4 Summary

All three actions, arm movements, leg movements, and bowing, were chosen because they are uncomplicated, nonforceful motions, descriptive of typical activities which commonly occur. The bowing motion is clearly the most "forceful" motion; this is obvious since more of the subject's mass, i.e., his torso, is involved in that movement. The others require the moving of limbs only. Moving both arms exerts the second highest level of force while moving one limb, either arm or leg, ranks third. The higher moments are not easy to correlate with actions because swinging a leg causes as much or more torque as bowing in most cases, for most coordinates.

Plots of frequency content show that in comparison to the other types of exercises arm movements tend to peak less sharply or distinctively, and they maintain a higher level of power at higher frequencies.

A further comparison of PSD plots shows many of the components of the normal body exercises to be composed of more than a single waveform. This tendency is present in arm movements but is more obvious for many of the leg movements and bowing components. One possible explanation is that these movements, while apparently uncomplicated, cause additional secondary body movements.

A composite of the appropriate tables already presented in this section, table A-15 shows all the data describing the three types of normal body exercises for comparison.

APPENDIX A

TABLE A-15.- SUMMARY OF NORMAL BODY EXERCISES DATA

Activity	Force, N				Moment, N-m			
	F_X	F_Y	F_Z	F_T	M_X	M_Y	M_Z	M_T
Range, maximum - minimum								
Arm motion:								
Wave right arm	33.33	164.55	55.67	171.11	6.23	18.22	11.90	19.07
Wave left arm	34.74	123.57	43.10	131.01	4.66	7.75	10.70	12.09
Arm movements	35.89	140.77	62.42	150.65	18.34	10.96	13.07	21.69
Both arms	18.01	270.31	99.69	280.64	9.97	4.15	6.37	11.35
Leg motion:								
Swing right leg	139.98	124.83	97.90	187.09	12.06	12.02	23.02	27.78
Bend right knee	25.45	76.83	23.79	82.50	3.93	3.35	11.35	12.20
Leg lifts	159.29	166.96	112.73	188.38	18.18	15.39	22.24	27.50
Bowing motion:								
(1)	90.36	368.84	70.14	373.16	43.36	16.85	16.49	52.03
(2)	99.13	336.28	71.42	338.74	23.85	15.90	14.41	27.69
Maximum level								
Arm motion:								
Wave right arm	20.65	93.71	39.47	101.69	3.19	10.50	8.40	10.83
Wave left arm	18.13	78.65	26.86	83.21	2.39	4.81	6.08	6.73
Arm movements	25.81	82.13	32.19	84.27	11.12	7.30	8.31	11.20
Both arms	10.60	149.30	53.48	157.01	5.08	2.57	3.54	6.24
Leg motion:								
Swing right leg	91.92	71.50	58.92	125.54	6.56	7.91	15.07	18.05
Bend right knee	17.08	51.99	12.69	55.43	2.71	2.08	7.75	8.39
Leg lifts	102.54	109.56	58.15	121.58	9.39	8.16	13.90	16.46
Bowing motion:								
(1)	60.66	231.85	38.60	234.34	25.82	11.50	8.82	26.40
(2)	78.86	209.15	36.39	210.04	12.03	12.69	7.21	14.15
Standard deviation								
Arm motion:								
Wave right arm	4.28	20.58	6.50	22.00	0.54	2.13	1.40	2.67
Wave left arm	4.70	15.32	4.94	16.77	.84	.91	1.54	1.98
Arm movements	4.25	16.18	6.39	17.91	2.09	1.14	1.42	2.77
Both arms	2.62	38.12	16.24	41.52	1.47	.57	1.11	1.92
Leg motion:								
Swing right leg	12.32	12.97	8.95	19.98	1.45	1.27	2.45	3.11
Bend right knee	2.96	9.05	3.27	10.06	.62	.48	1.35	1.56
Leg lifts	10.75	14.71	8.85	20.25	2.02	1.29	2.19	3.25
Bowing motion:								
(1)	8.98	65.23	11.39	66.82	9.67	1.63	2.71	10.14
(2)	9.14	61.78	12.46	63.69	4.54	1.66	2.65	5.53
Maximum PSD, $unit^2/(rad/sec)$								
Arm motion	0.6	16.4	2.6		0.29	0.19	0.11	
Leg motion	20.0	17.5	8.0		.53	.15	.47	
Bowing	3.8	490.0	12.4		10.0	.16	.50	
Frequency at maximum, rad/sec								
Arm motion	2.5	10.0	10.0		1.0	4.4	2.0	
Leg motion	5.8	8.8	5.8		2.5	3.2	8.8	
Bowing	7.0	4.5	7.0		2.0	2.0	7.0	

APPENDIX A

A.5 Gross Body Exercises

The movements chosen for this category were expected to have potentially large force and moment inputs to the ATM pointing control system. These are vigorous one-man exercise-type motions performed with the subject restrained to FMU 1.

A.5.1 Arm flapping

A.5.1.1 Activity description

The first of the two vigorous exercises is described as:

Rapidly move both arms up and down out from the side through an angle of 90^{o} like a bird flapping its wings for 10 to 20 sec.

Stabilize.

Repeat arm movements.

Stabilize.

A.5.1.2 Time histories

Figures A-21 and A-22 are force and moment profiles of arm flapping. The force plots of the y- and z-coordinates and the x-coordinate of moment show a very definite and regular pattern. The action is quickly stabilized, as shown in any of the plots.

A.5.1.3 Statistics

Table A-16 presents statistical data describing three repetitions of arm flapping.

Three separate entries of arm flappings are useful to compare the information, to see if there is any consistency, or to learn what the truer reading may be. The maximum of all three values is indeed a worst case value for the activity as performed, but it may not necessarily be realistic. Having more than one sample case per exercise, then, gives the analyst a truer idea of typical values.

Both the magnitude of the y-component and the close correlation with the total make it apparent that y is dominant for force. However, for the same reasons, x is the dominant moment component for two of the three segments.

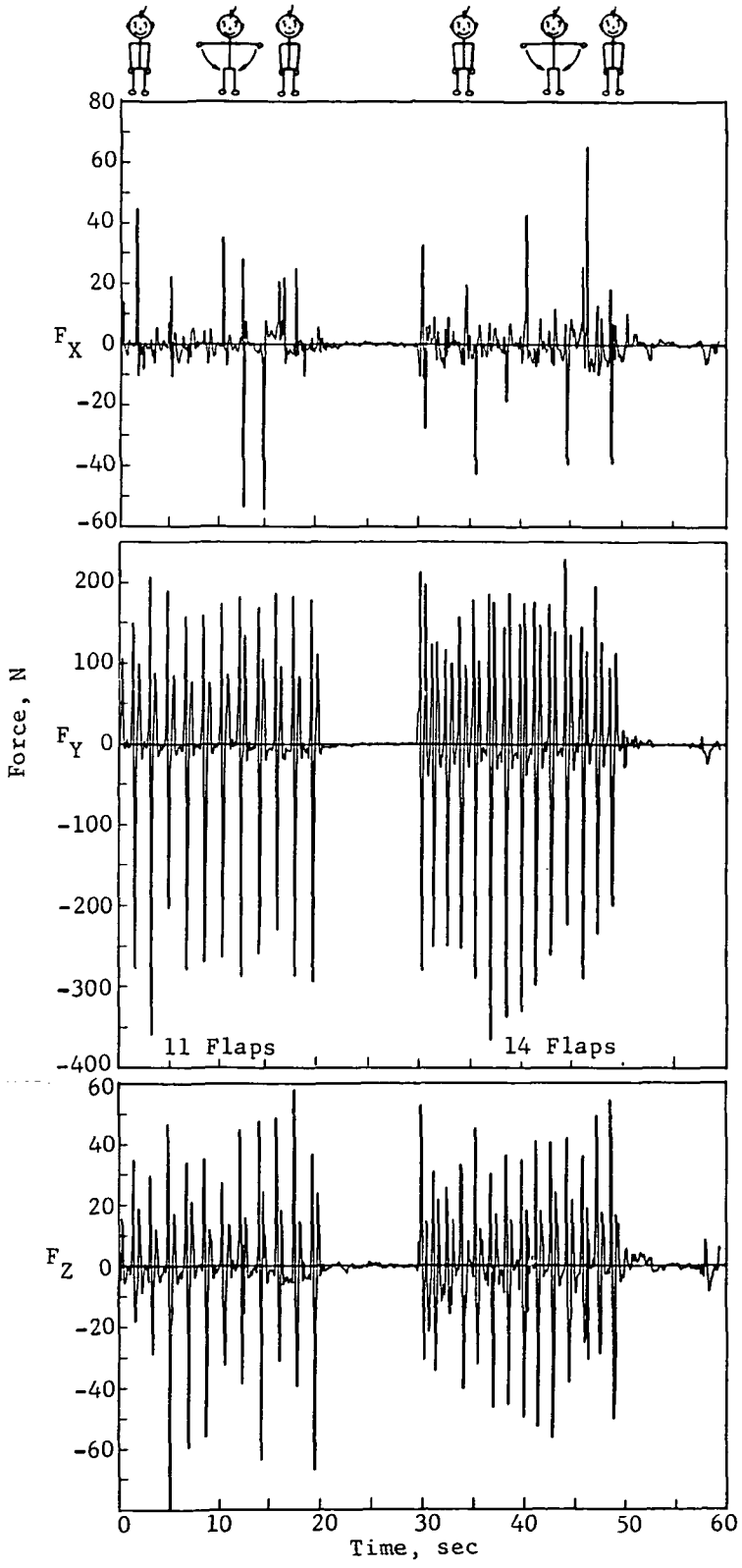

Reference time:
19754812., 592.

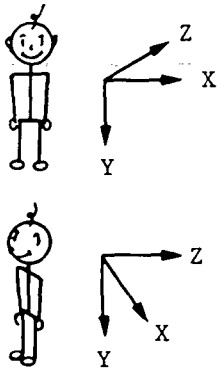

Figure A-21.- Force profile of arm flapping.

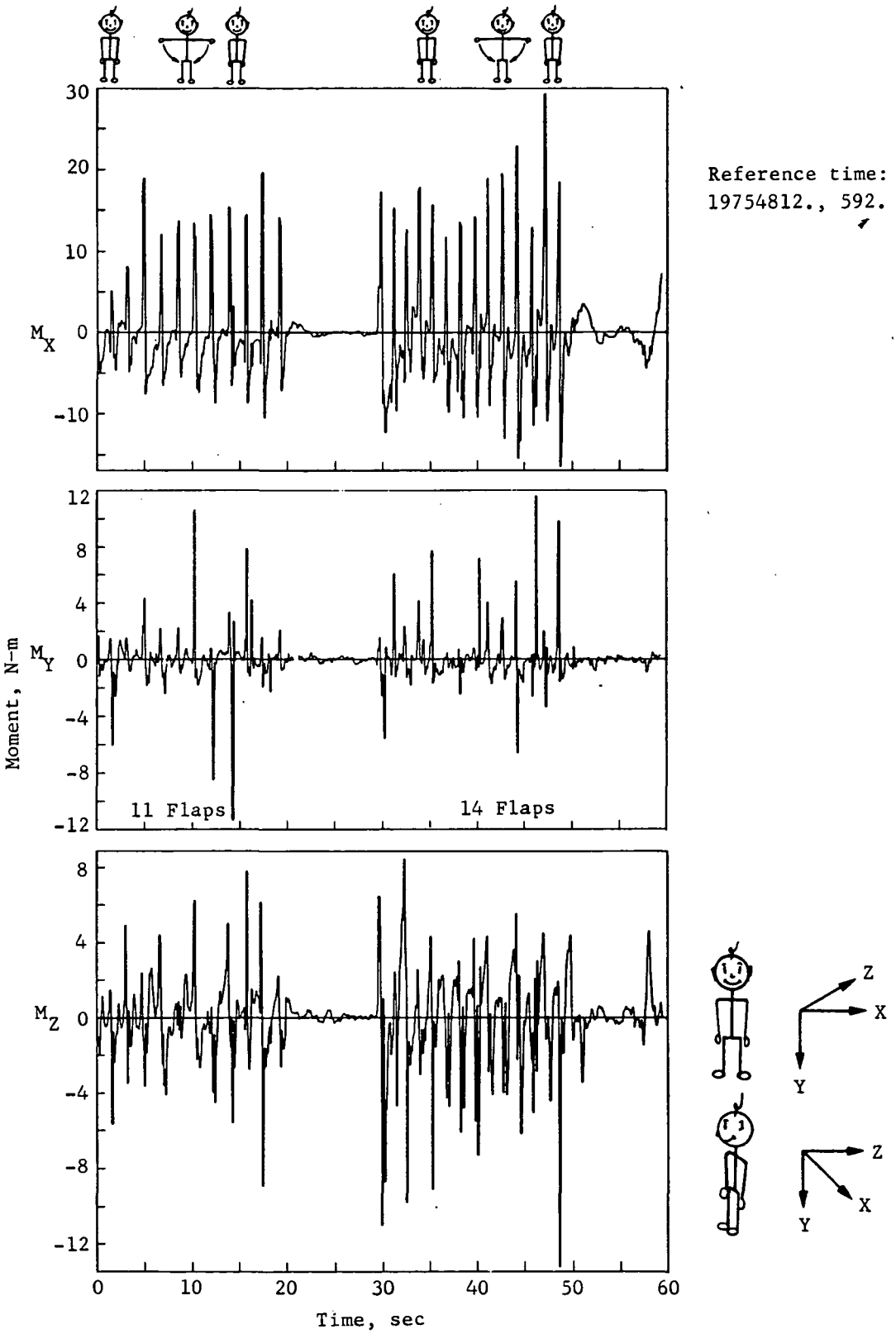

Figure A-22.- Moment profile of arm flapping.

APPENDIX A

TABLE A-16.- ARM FLAPPING STATISTICS

Arm flapping	Force, N				Moment, N-m			
	F_X	F_Y	F_Z	F_T	M_X	M_Y	M_Z	M_T
Range, maximum - minimum								
(1)	99.23	567.11	139.79	569.34	30.12	21.96	16.68	32.84
(2)	108.10	595.57	111.34	598.07	45.82	18.20	21.66	45.85
(3)	58.57	395.73	125.37	407.84	12.43	12.16	15.66	19.32
Maximum level								
(1)	54.43	360.04	81.81	360.13	19.60	11.42	8.91	19.70
(2)	65.43	366.31	56.74	366.32	29.34	11.53	13.24	29.37
(3)	39.43	256.36	87.87	264.69	7.10	7.32	8.36	10.52
Standard deviation								
(1)	7.97	88.28	16.81	90.22	5.08	1.66	1.88	5.66
(2)	9.39	104.51	18.77	106.60	7.42	1.83	2.87	8.17
(3)	7.52	85.05	26.20	89.30	2.81	1.73	2.84	4.36

A.5.1.4 Frequency content

A brief look at the frequency characteristics of arm flapping, given in table A-17, is necessary before viewing the plots given in figures A-23 and A-24 in order to put them in perspective with one another.

TABLE A-17.- ARM FLAPPING FREQUENCY CHARACTERISTICS

Force	Maximum PSD, $N^2/(rad/sec)$	Frequency at maximum, rad/sec	rms, N
X	1.3	5.0	6.3
Y	520.0	10.3	87.9
Z	32.0	10.3	18.7

Moment	Maximum PSD, $N^2-m^2/(rad/sec)$	Frequency at maximum, rad/sec	rms, N-m
X	1.7	8.0	5.2
Y	.07	5 and 11	1.4
Z	.34	4.2	2.4

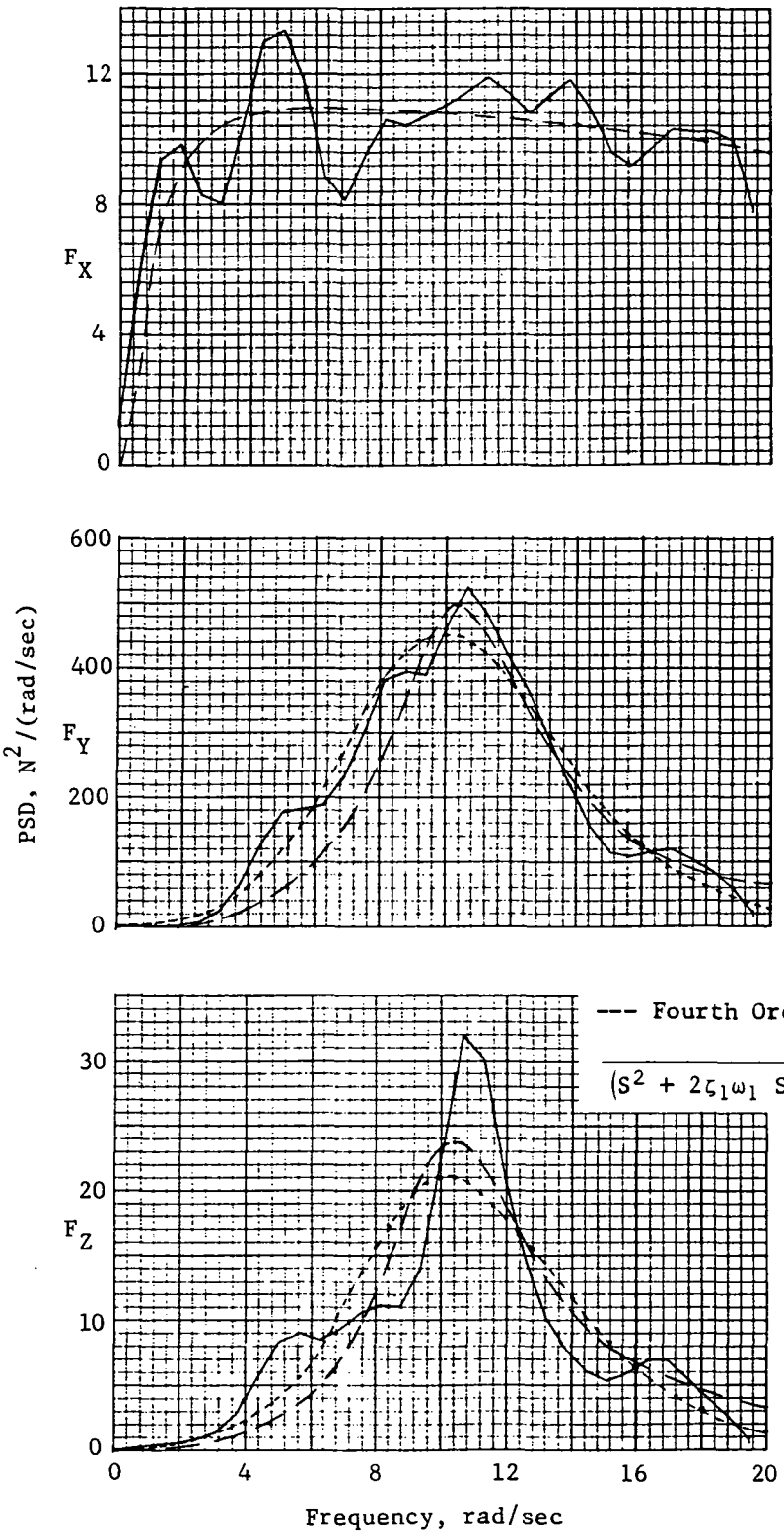

—— Experiment Data

– – Second Order

$$\frac{\tau S}{S^2 + 2\zeta\omega\, S + \omega^2}$$

	F_X	F_Y	F_Z
τ	49.58	128.10	28.06
ω	6.55	10.37	10.37
ζ	3.61	.28	.28

--- Fourth Order

$$\frac{\tau S}{(S^2 + 2\zeta_1\omega_1\, S + \omega_1^2)(S^2 + 2\zeta_2\omega_2\, S + \omega_2^2)}$$

	F_Y	F_Z
τ	290.64	63.56
ω_1	9.00	9.50
ω_2	14.51	14.70
ζ_1	.47	.44
ζ_2	.40	.39

Figure A-23.- PSD of force of arm flapping.

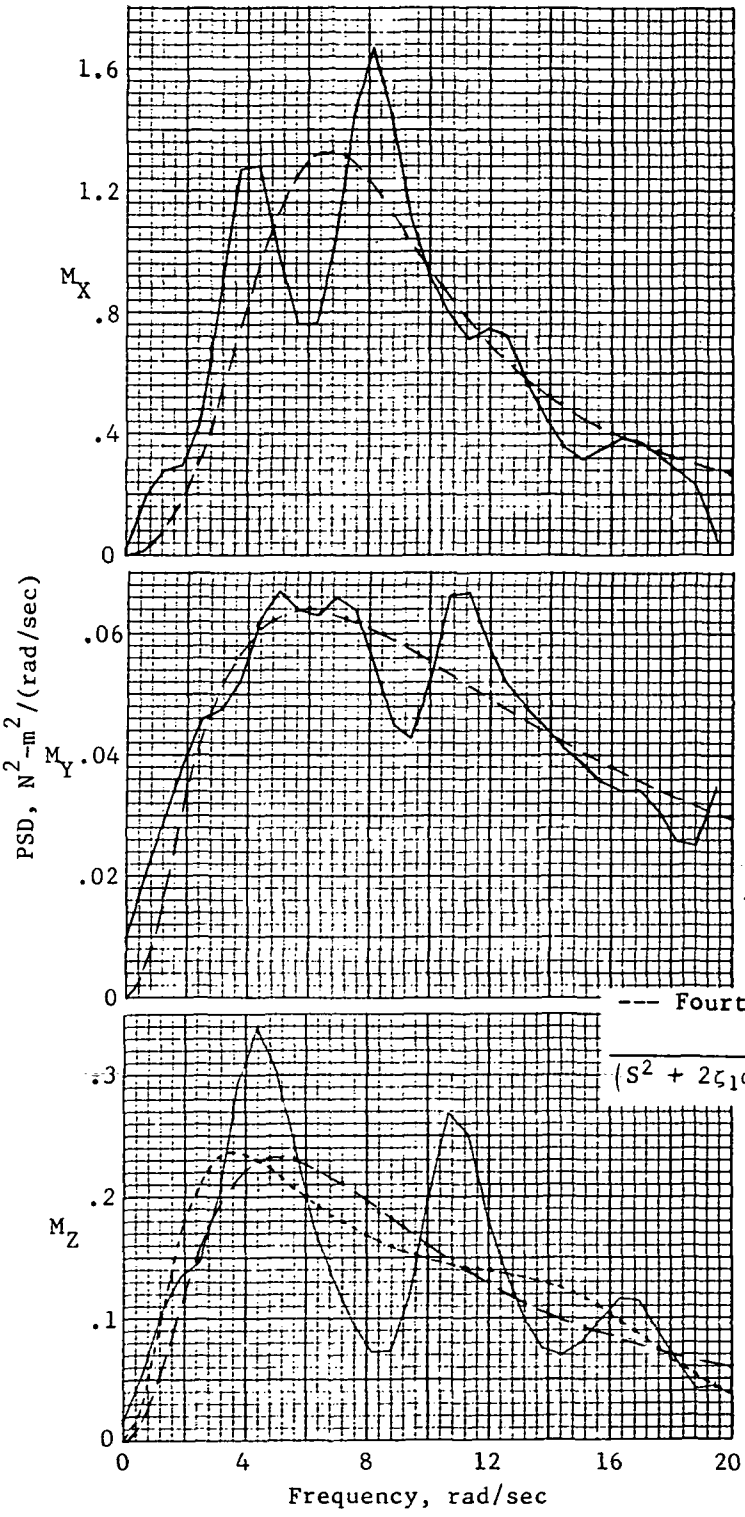

—— Experiment Data

– – Second Order

$$\frac{\tau S}{S^2 + 2\zeta\omega\ S + \omega^2}$$

	M_X	M_Y	M_Z
τ	10.11	4.24	5.35
ω	6.62	5.95	5.07
ζ	.66	1.41	1.09

--- Fourth Order

$$\frac{\tau S}{(S^2 + 2\zeta_1\omega_1\ S + \omega_1^2)(S^2 + 2\zeta_2\omega_2\ S + \omega_2^2)}$$

	M_Z
τ	966.47
ω_1	3.33
ω_2	17.02
ζ_1	1.06
ζ_2	.32

Figure A-24.- PSD of moment of arm flapping.

Comparisons among any of the three force components are not particularly significant since the peak PSD of F_Y is more than two orders of magnitude greater than F_X or F_Z.

The time history of F_Y shows two sequences of flapping arms, which as stated previously, are both quite regular. Both display two distinctively different patterns: the frequency of large positive force levels is about twice the frequency of large negative spikes. In addition, although the patterns of the two sequences are similar, upon closer scrutiny, the second set of flaps are closer together than the first set, indicating that the action was more rapid, and thus two new sets of frequencies appear. The corresponding PSD plot shows a large concentration of power throughout a fairly wide range of frequencies, and local maxima are indicated at 5, 8, 11, and 17 rad/sec. The same trend is present for the dominant moment component, that in the x-direction. Two very distinct peaks appear in the PSD plot of M_X with two secondary ones.

The PSD plot for M_X demonstrates something very noticeable about the theoretical PSD calculations; namely, they do not easily approximate large, separated maxima, but rather try to average the difference. For cases such as M_X and M_Z, both higher as well as lower order equations have difficulty in characterizing the actual PSD.

A.5.2 Crouch and push-off

A.5.2.1 Activity description

The second of the forceful exercises required the subject to place himself in a squatting position and then thrust himself upward while restrained to FMU 1. The in-flight instructions were:

Crouch and quickly straighten body (as in push-off); stabilize.

Perform five or six times (a total of 30 to 40 sec).

A.5.2.2 Time histories

Figures A-25 and A-26 present the force and moment profiles for crouch and straighten. Starting at 9 sec from the reference time, three squat-thrusts occurred, one every 5 sec. It is interesting to note that very large negative spikes occur in F_X in comparison to the positive values, while F_Z contains larger positive than negative levels. The same occurrence noted for F_X is also present in M_Y.

A.5.2.3 Statistics

Table A-18 identifies statistical data for two crouching exercises. The first crouching exercise was performed a little more vigorously, and it was described as "crouch and push-off"; the second was called "crouch and straighten." The description indicates that the first was intended to be more forceful. The difference is somewhat more dramatic (proportionally) in the x-direction than in the y-direction for force, but it is significant for both in the moment data.

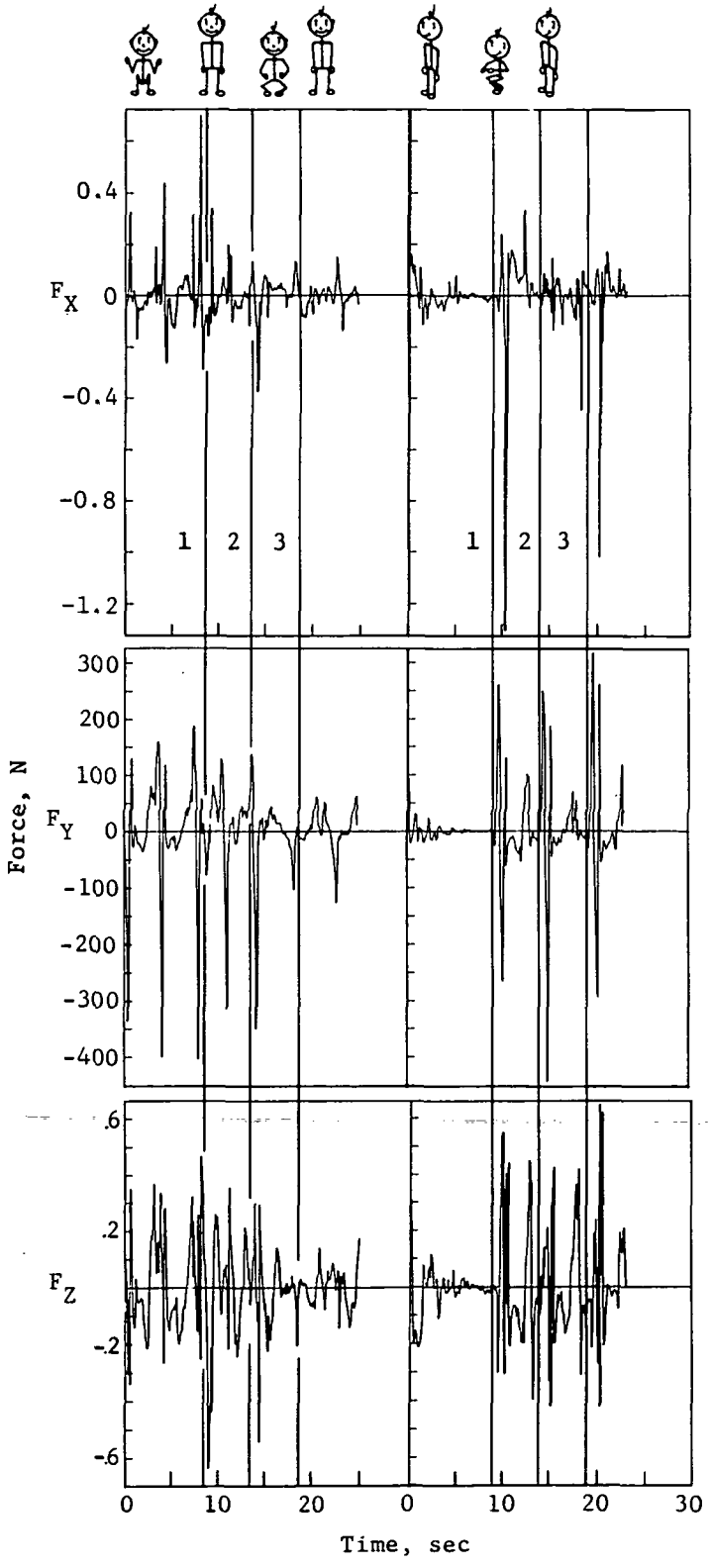

Reference time 1:
19757645., 3425.

Reference time 2:
19754872., 652.

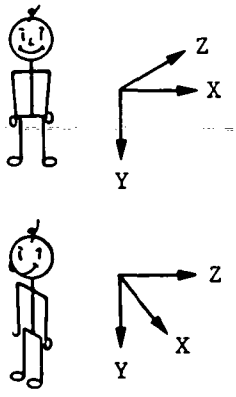

Figure A-25.- Force profile of crouch and push-off.

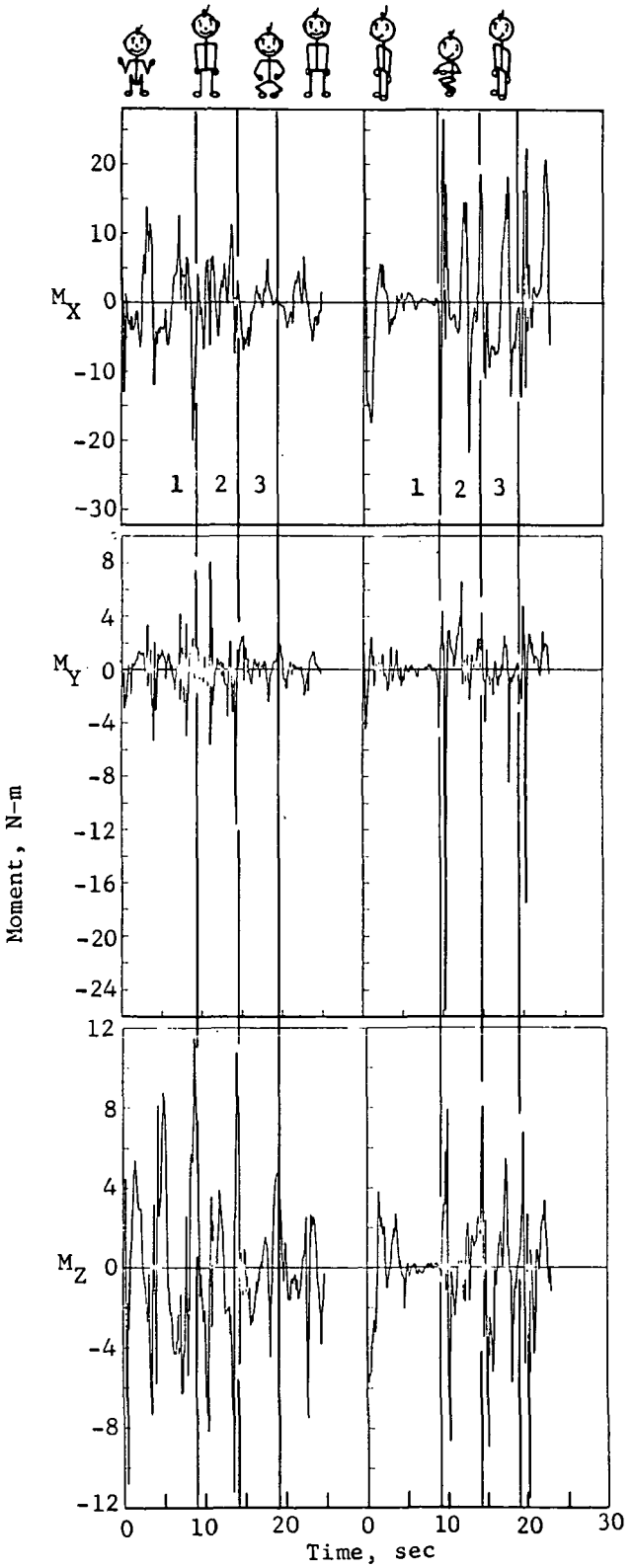

Reference time 1:
19757645., 3425.

Reference time 2:
19754872., 652.

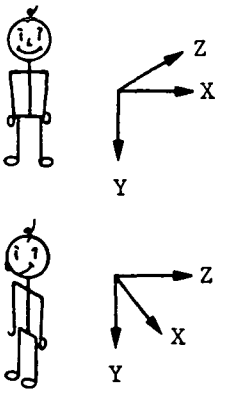

Figure A-26.- Moment profile of crouch and push-off.

APPENDIX A

TABLE A-18.- CROUCH AND STRAIGHTEN STATISTICS

Activity	Force, N				Moment, N-m			
	F_X	F_Y	F_Z	F_T	M_X	M_Y	M_Z	M_T
Range, maximum - minimum								
(1)	164.04	760.03	107.04	760.26	57.59	32.16	19.58	58.96
(2)	107.77	592.18	110.64	594.03	33.94	19.71	22.73	38.91
Maximum level								
(1)	130.47	443.52	64.71	443.58	30.94	25.54	11.50	31.34
(2)	70.14	403.65	63.84	405.07	20.07	11.65	11.50	22.91
Standard deviation								
(1)	18.46	94.45	19.90	98.28	9.27	3.48	2.73	10.27
(2)	11.90	101.20	18.45	103.53	5.83	2.11	4.31	7.55

A.5.2.4 Frequency content

The PSD plots of crouch and straighten force and moment, given in figures A-27 and A-28, are somewhat irregular on the whole because they contain several secondary peaks. These local maxima may well result from secondary movements which are quite likely to occur in a forceful thrusting motion, but they may also be caused by the fact that there are only two short time segments which describe this activity. In general, as table A-19 shows, the maximum PSD levels were attained at somewhat lower frequencies than the other forceful movement, arm flapping.

TABLE A-19.- CROUCH AND STRAIGHTEN FREQUENCY CHARACTERISTICS

Force	Maximum PSD, $N^2/(rad/sec)$	Frequency at maximum, rad/sec	rms, N
X	16.2	5.0	17.3
Y	600.0	6.2	92.9
Z	23.5	2.3	17.4

Moment	Maximum PSD, $N^2\text{-}m^2/(rad/sec)$	Frequency at maximum, rad/sec	rms, N-m
X	9.0	2.3	8.8
Y	.6	6.0	3.4
Z	.8	2.0	2.7

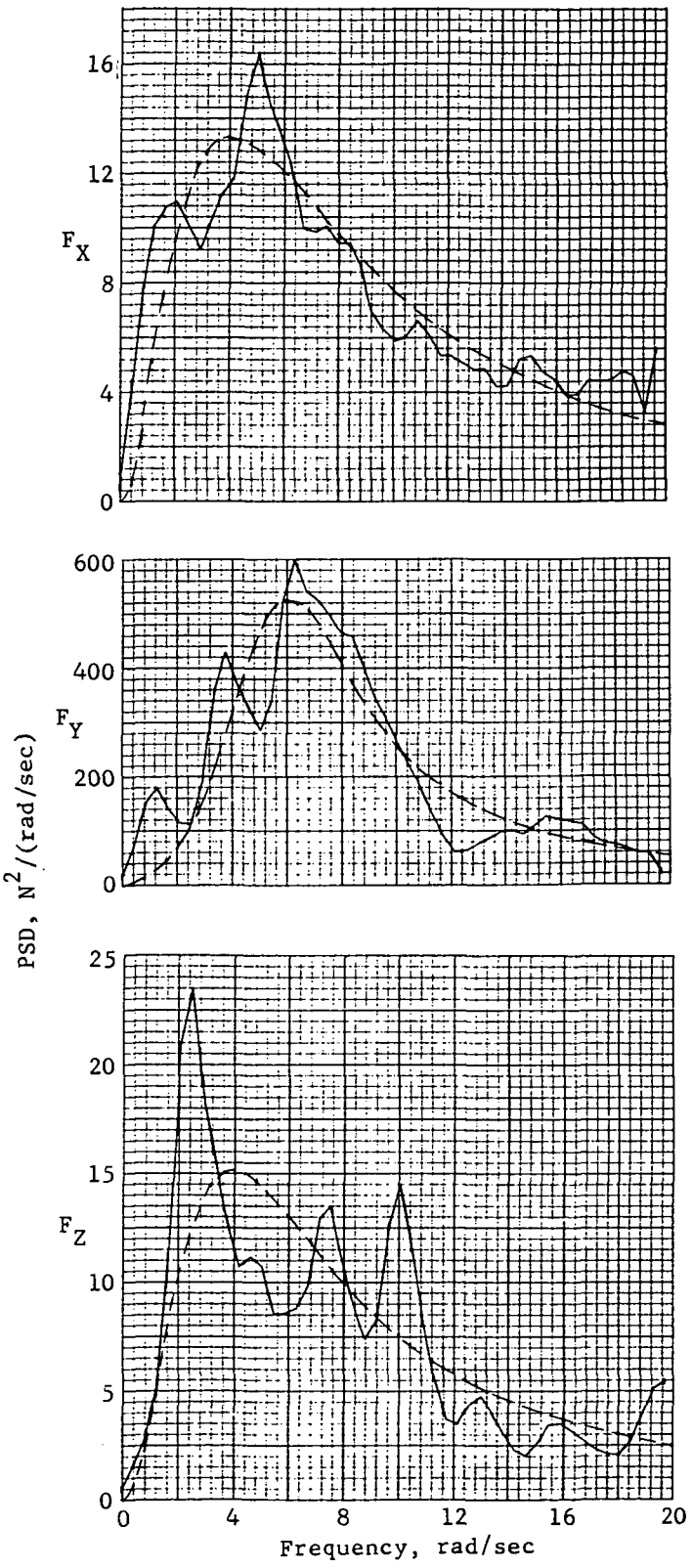

—— Experiment Data

— — Second Order

$$\frac{\tau S}{S^2 + 2\zeta\omega S + \omega^2}$$

	F_X	F_Y	F_Z
τ	36.05	144.80	32.77
ω	4.06	6.04	3.99
ζ	1.22	.52	1.06

Figure A-27.- PSD of force of crouch and push-off.

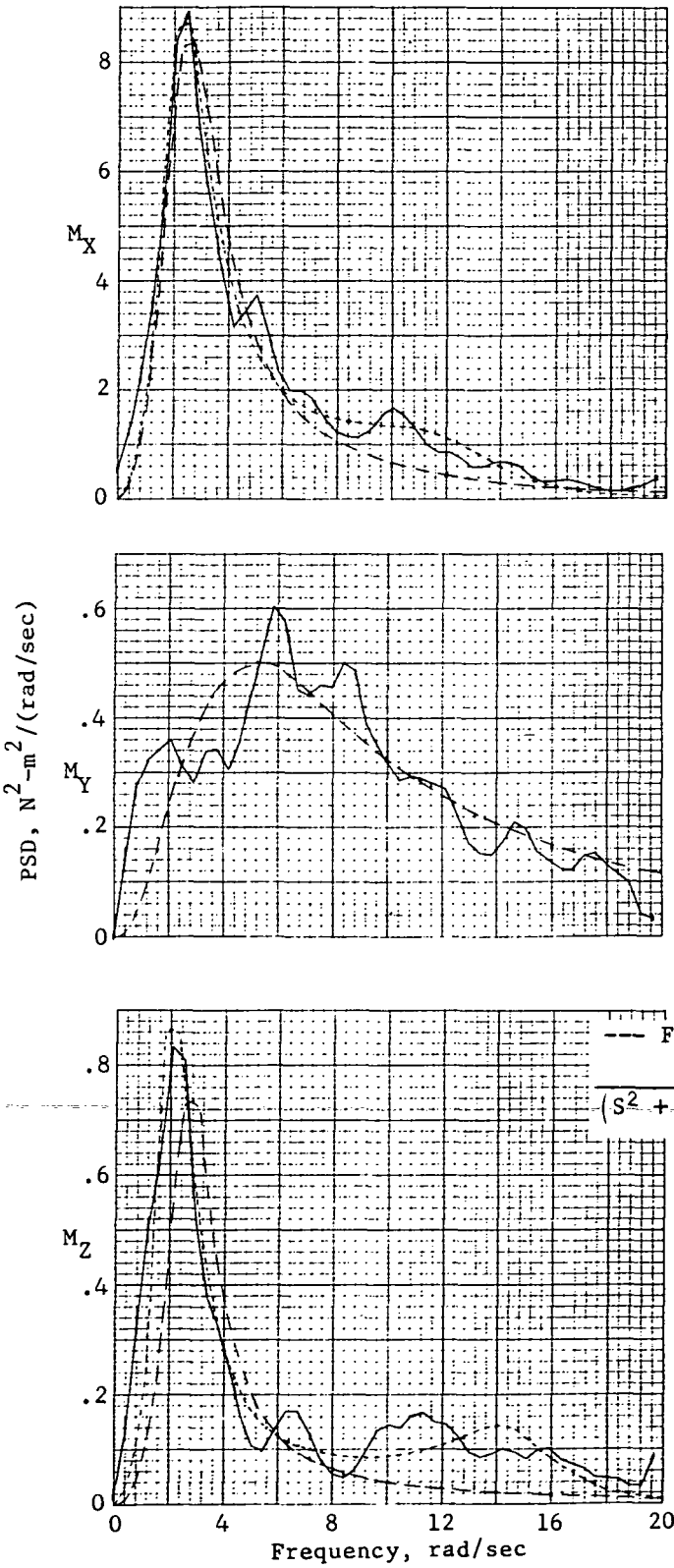

—— Experiment Data

– – Second Order

$$\frac{\tau S}{S^2 + 2\zeta\omega\, S + \omega^2}$$

	M_X	M_Y	M_Z
τ	7.90	7.15	1.89
ω	2.57	5.13	2.71
ζ	.53	.99	.40

--- Fourth Order

$$\frac{\tau S}{(S^2 + 2\zeta_1\omega_1 S + \omega_1^2)(S^2 + 2\zeta_2\omega_2 S + \omega_2^2)}$$

	M_X	M_Z
τ	10.88	378.71
ω_1	2.33	2.09
ω_2	12.87	14.95
ζ_1	.49	.44
ζ_2	.27	.17

Figure A-28.- PSD of moment of crouch and push-off.

A.5.3 Gross body exercise summary

Table A-20 is a composite of all tabulated data given in this section for gross body exercises. In general, comparison of the two types of forceful exercises indicates the same level of results. The maximum levels are of the same approximate order, and the standard deviations are close for force and moment for all three components and total values. Maximum PSD's are also similar, although crouch and push-off tends to have slightly higher values occurring at lower frequencies. In both cases, the dominant force component is y and the dominant moment is x.

A.6 Soaring

A.6.1 Activity description

Soaring is alternately known as wall push-off since the astronaut pushes himself from an FMU on one side of the Orbital Work Shop (OWS), soars, lands on the FMU on the opposite wall, stabilizes, and repeats the activity. The following excerpt from the Skylab experiments checklist describes the activity in detail.

Soaring exercises:

Release left foot from restraint and crouch for free soaring (use handhold to keep feet on FMU 1)

(a) Push off from FMU 1 (with feet), soar to FMU 2, and stabilize with hands only.

(b) Position feet on FMU 2, push off to FMU 1, and stabilize with hands only.

(c) Push off FMU 1 with hands, turn, and stabilize at FMU 2 with hands only.

(d) Push off FMU 2 with hands and return to FMU 1; stabilize with hands only.

Soaring is actually composed of four classes of activity: one man normal, one man forceful, two men normal, and two men forceful. In order to understand how the one- and two-man activities differ, figure 3-3 should be consulted. The primary subject soared between FMU's, as described; the second astronaut, however, chose a parallel but longer path across the center of the OWS. Thus, he never came in actual contact with either FMU.

A.6.2 Time histories

The data presented in the following profiles (figs. A-29 to A-36) are given for FMU 1 only, even though both FMU's were part of the exercise. Section A.1 describes the FMU 2 anomaly which resulted in inaccurate readings.

APPENDIX A

TABLE A-20.- SUMMARY OF DATA FOR GROSS BODY EXERCISES

Activity	Force, N				Moment, N-m			
	F_X	F_Y	F_Z	F_T	M_X	M_Y	M_Z	M_T
Range, maximum - minimum								
Arm flapping:								
(1)	99.23	567.11	139.79	569.34	30.12	21.96	16.68	32.84
(2)	108.10	595.57	111.34	598.07	45.82	18.20	21.66	45.85
(3)	58.57	395.73	125.37	407.84	12.43	12.16	15.66	19.32
Crouch and push-off	164.04	760.03	107.04	760.26	57.59	32.16	19.58	58.96
Crouch and straighten	107.77	592.18	110.64	594.03	33.94	19.71	22.73	38.91
Maximum level								
Arm flapping:								
(1)	54.43	360.04	81.81	360.13	19.60	11.42	8.91	19.70
(2)	65.43	366.31	56.74	366.32	29.34	11.53	13.24	29.37
(3)	39.43	256.36	87.87	264.69	7.10	7.32	8.36	10.52
Crouch and push-off	130.47	443.52	64.71	443.58	30.94	25.54	11.50	31.34
Crouch and straighten	70.14	403.65	63.84	405.07	20.07	11.65	11.50	22.91
Standard deviation								
Arm flapping:								
(1)	7.97	88.28	16.81	90.22	5.08	1.66	1.88	5.66
(2)	9.39	104.51	18.77	106.60	7.42	1.83	2.87	8.17
(3)	7.52	85.05	26.20	89.30	2.81	1.73	2.84	4.36
Crouch and push-off	18.46	94.45	19.90	98.28	9.27	3.48	2.73	10.27
Crouch and straighten	11.90	101.20	18.45	103.53	5.83	2.11	4.31	7.55
Maximum PSD, $unit^2/(rad/sec)$								
Arm flapping	1.30	520.00	32.00		1.70	0.07	0.34	
Crouch and push-off	16.20	600.00	23.50		9.00	.60	.80	
Frequency at maximum PSD, rad/sec								
Arm flapping	5.00	10.40	10.40		8.00	5 & 11	4.2	
Crouch and push-off	5.00	6.20	2.30		2.30	6.0	2.0	

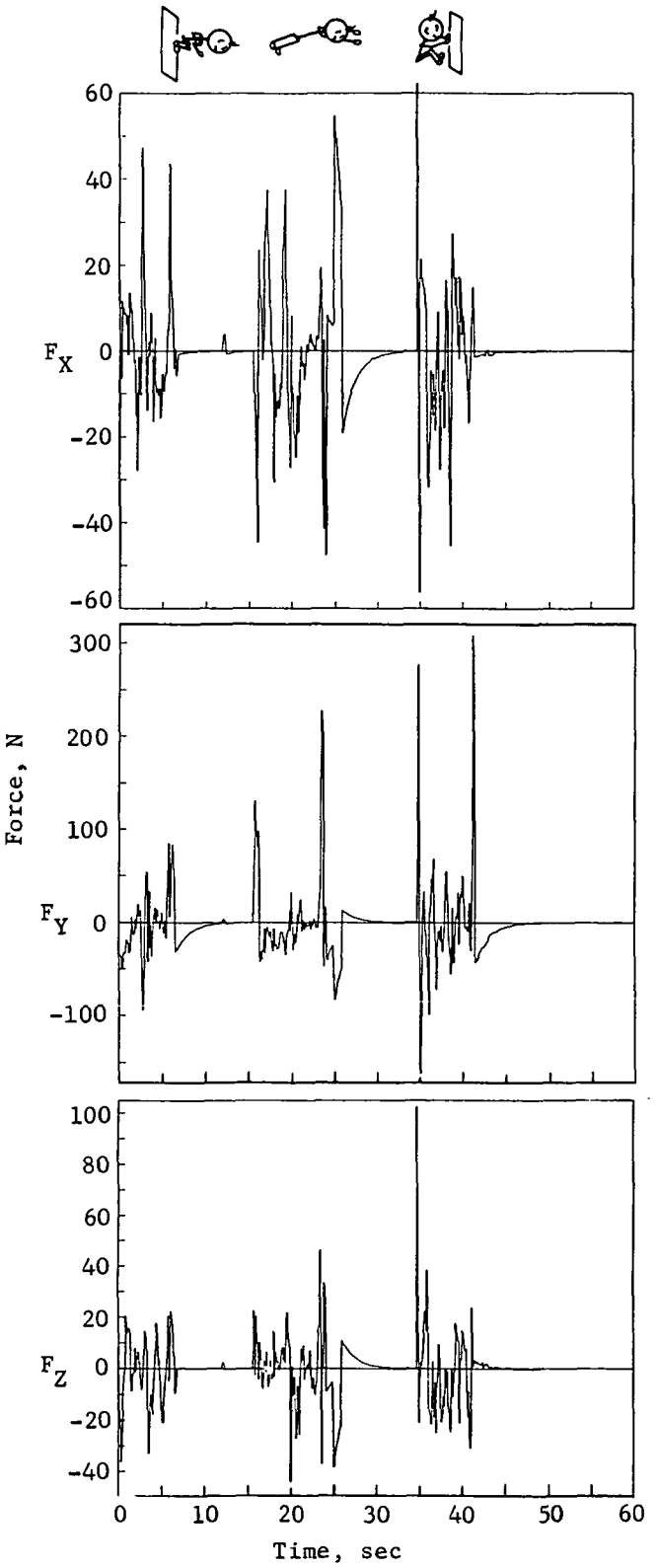

Reference time:
19755040., 820.

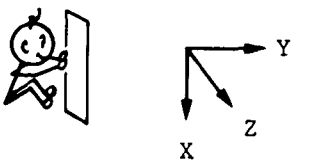

FMU 1
Landing

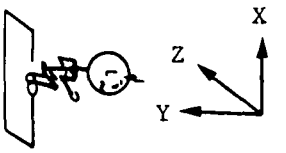

FMU 1
Push-off

Figure A-29.- Force profile of one-man normal soaring.

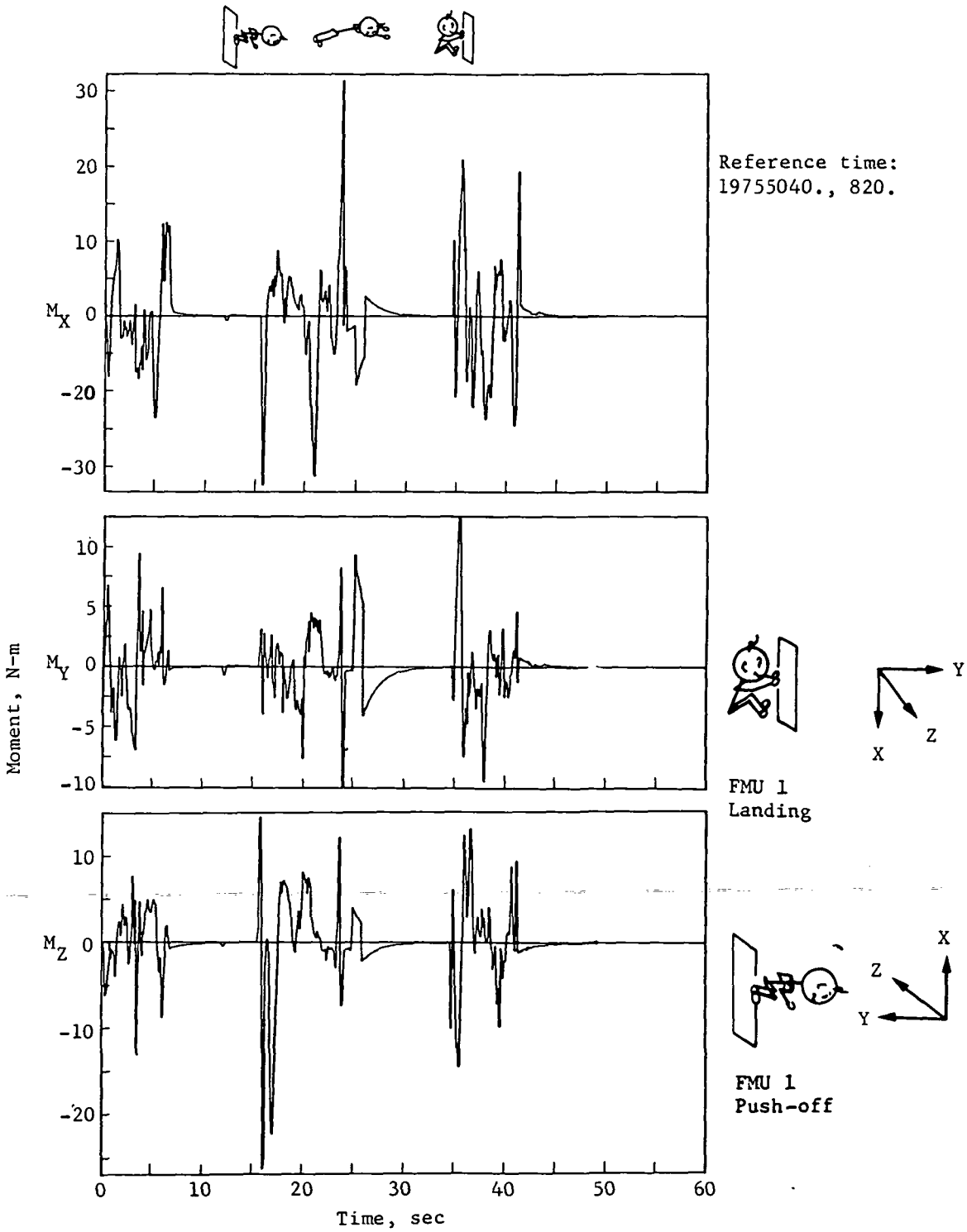

Figure A-30.- Moment profile of one-man normal soaring.

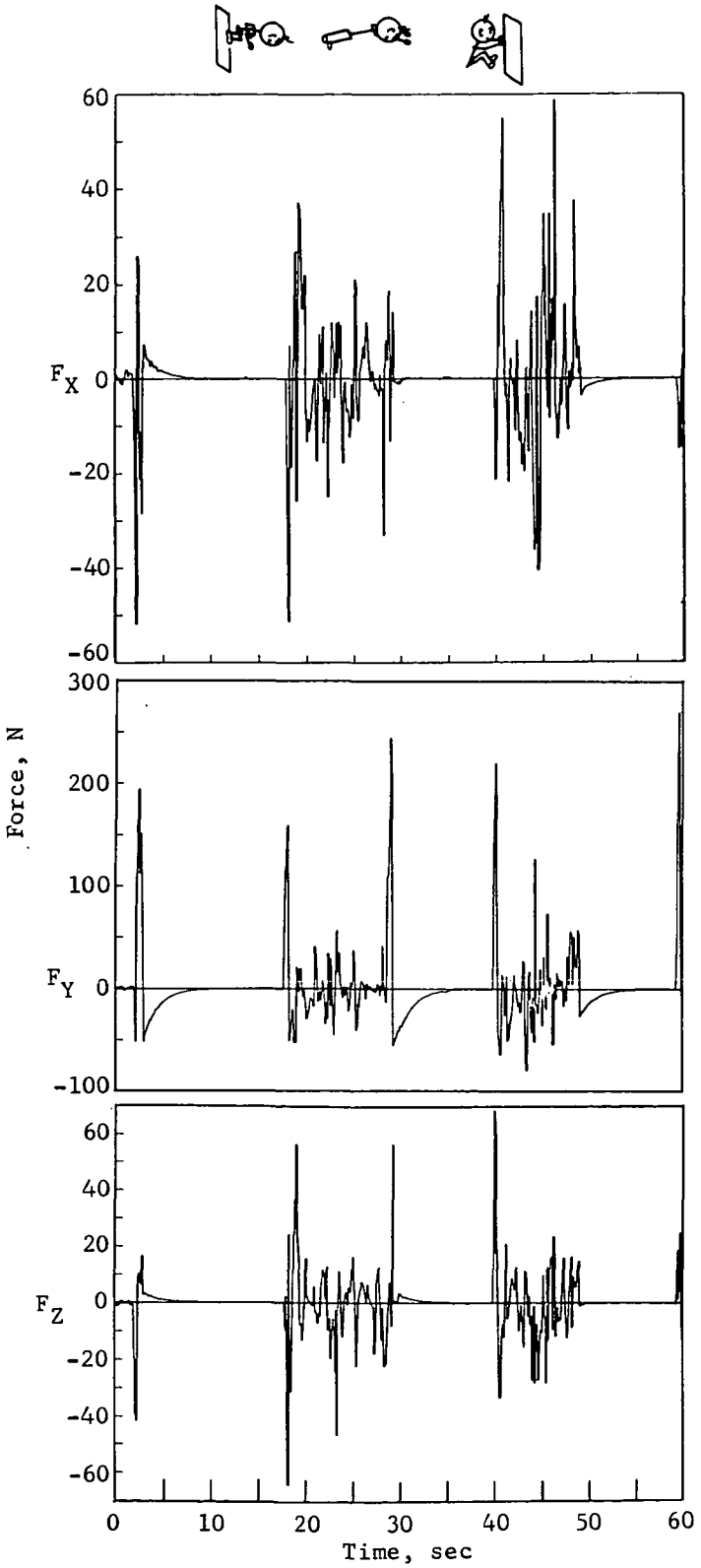

Reference time:
19754990., 770.

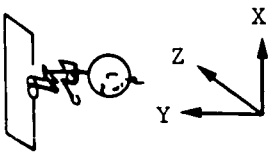

FMU 1
Push-off

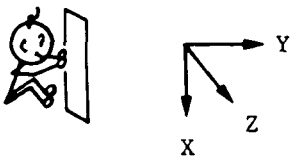

FMU 1
Landing

Figure A-31.- Force profile of one-man forceful soaring.

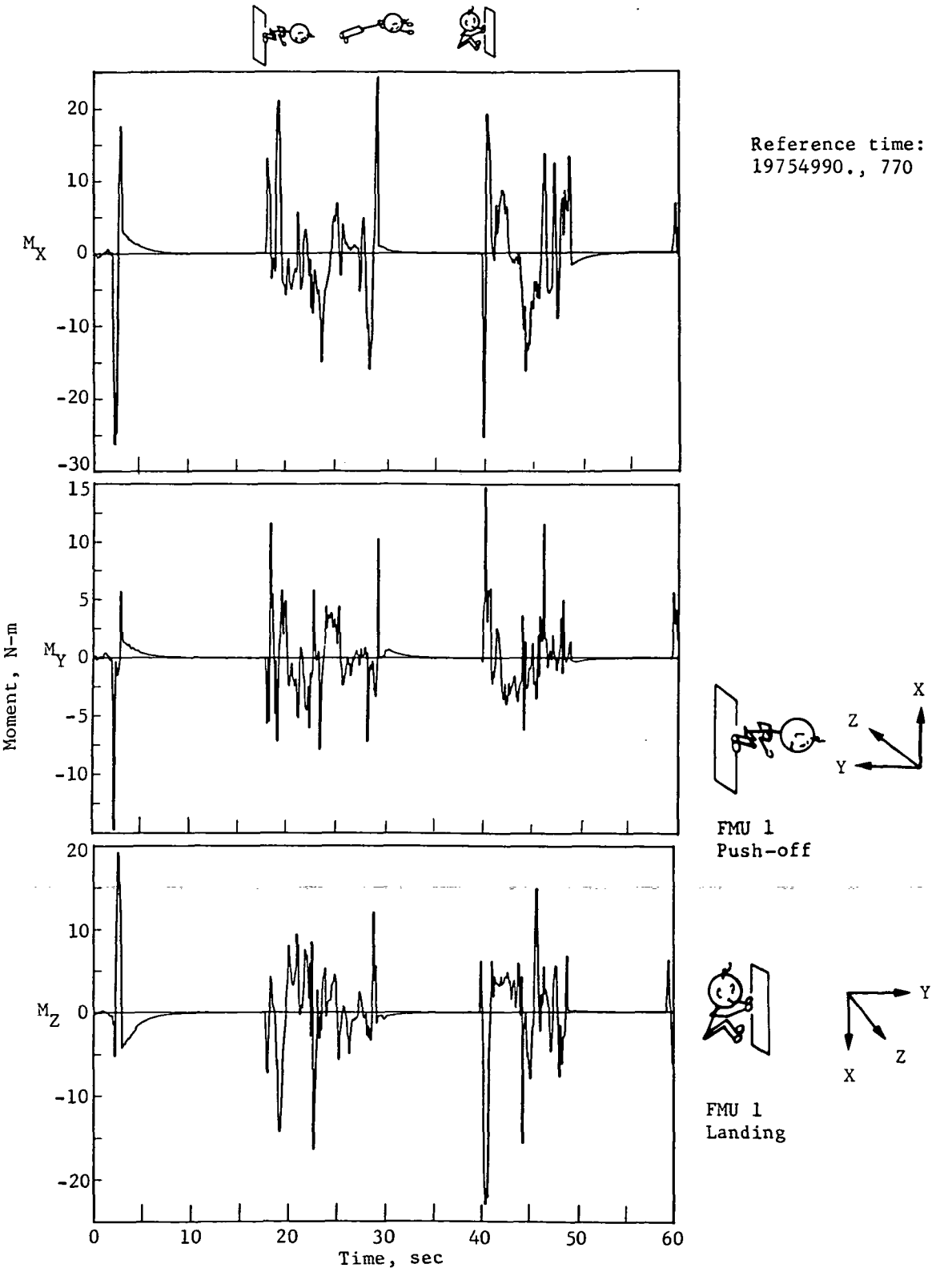

Figure A-32.- Moment profile of one-man forceful soaring.

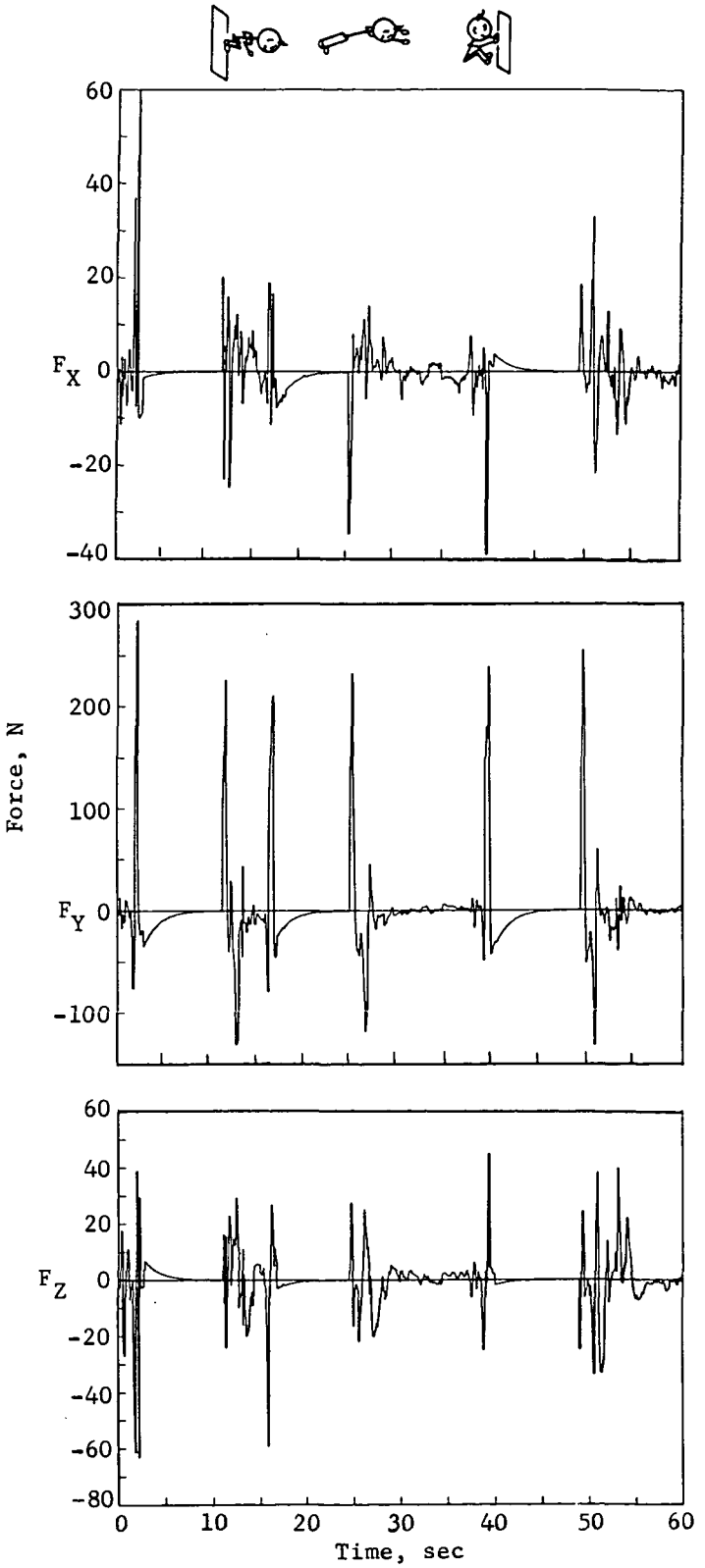

Reference time:
19757832., 3612.

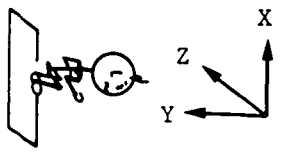

FMU 1
Push-off

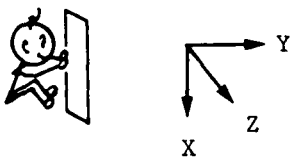

FMU 1
Landing

Figure A-33.- Force profile of two-man normal soaring.

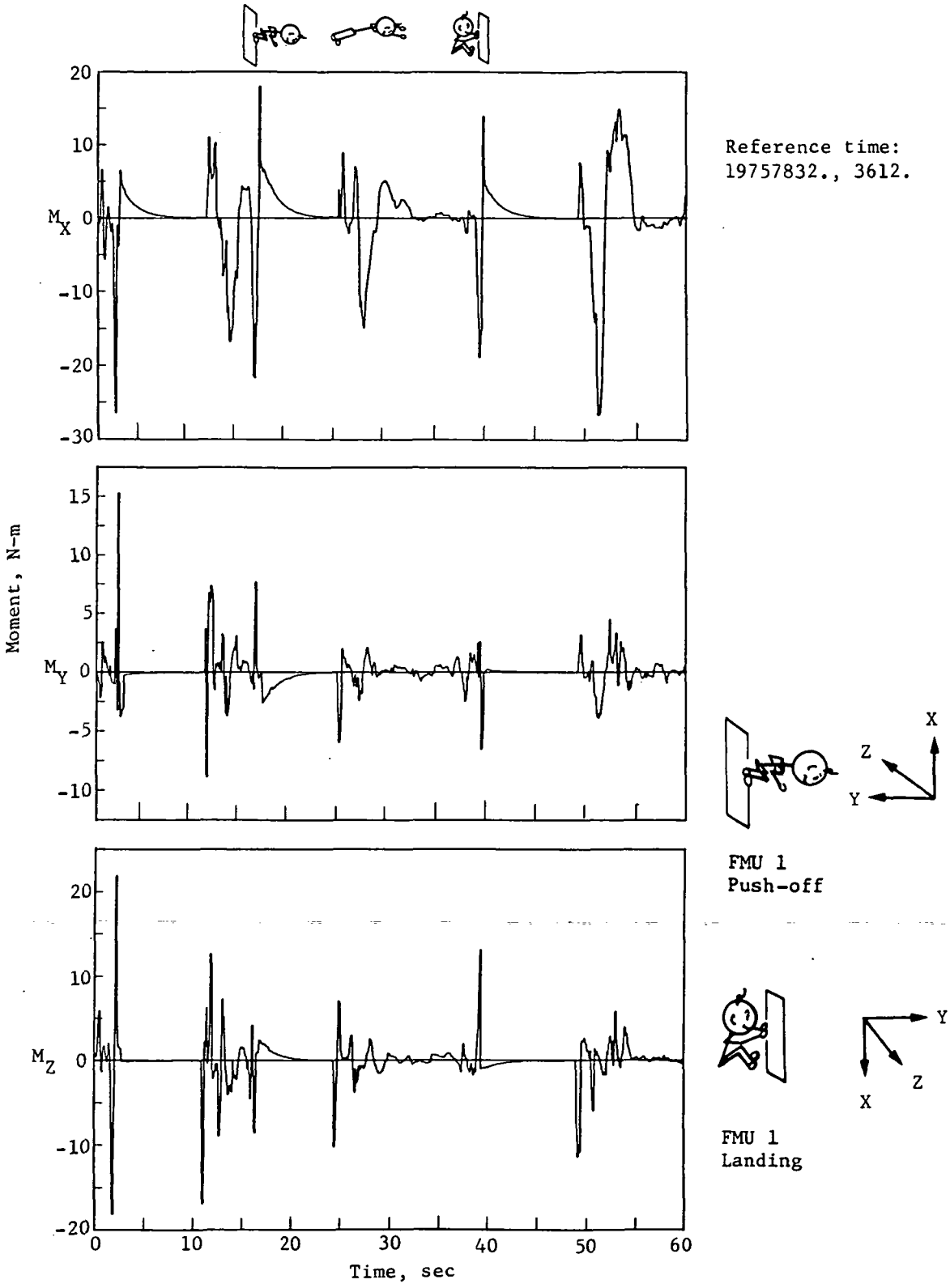

Figure A-34.- Moment profile of two-man normal soaring.

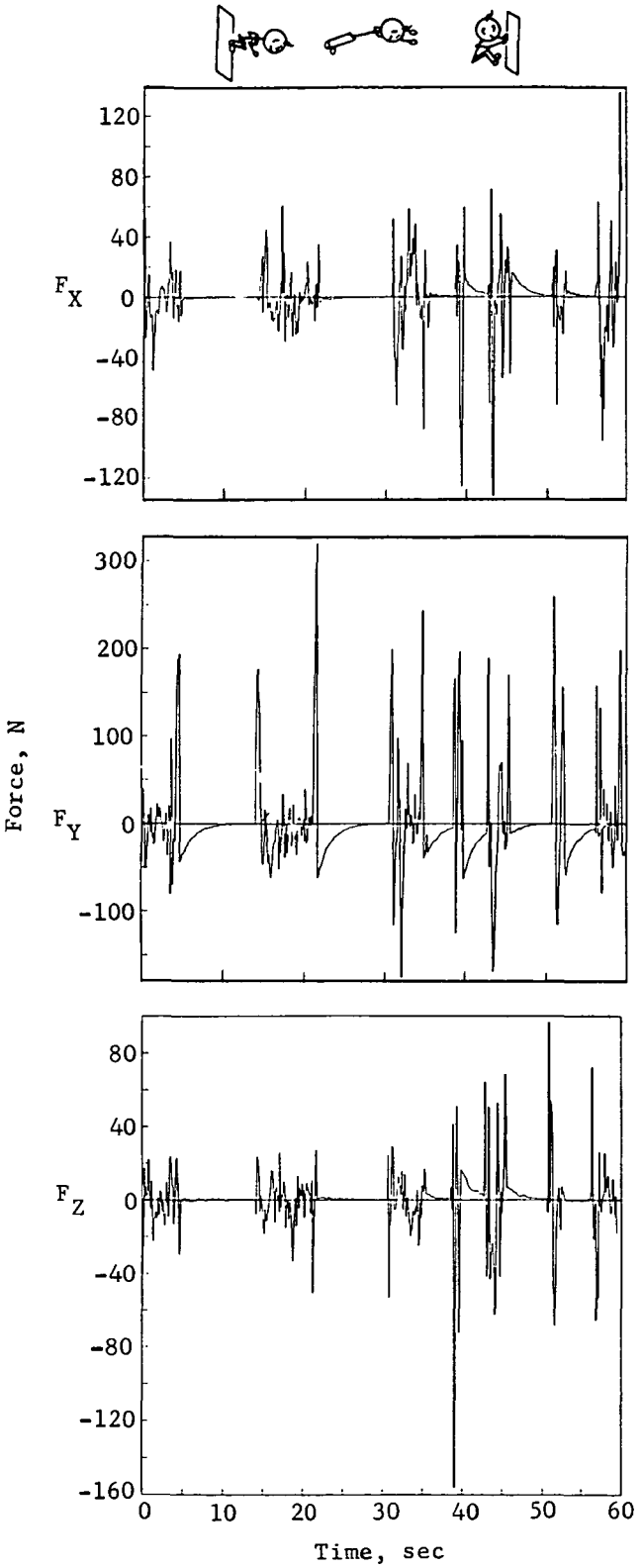

Reference time:
19755285., 1065.

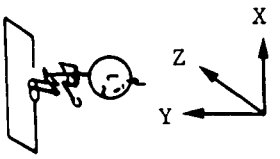

FMU 1
Push-off

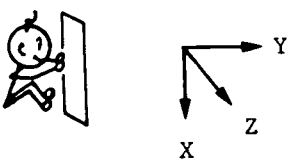

FMU 1
Landing

Figure A-35.- Force profile of two-man forceful soaring.

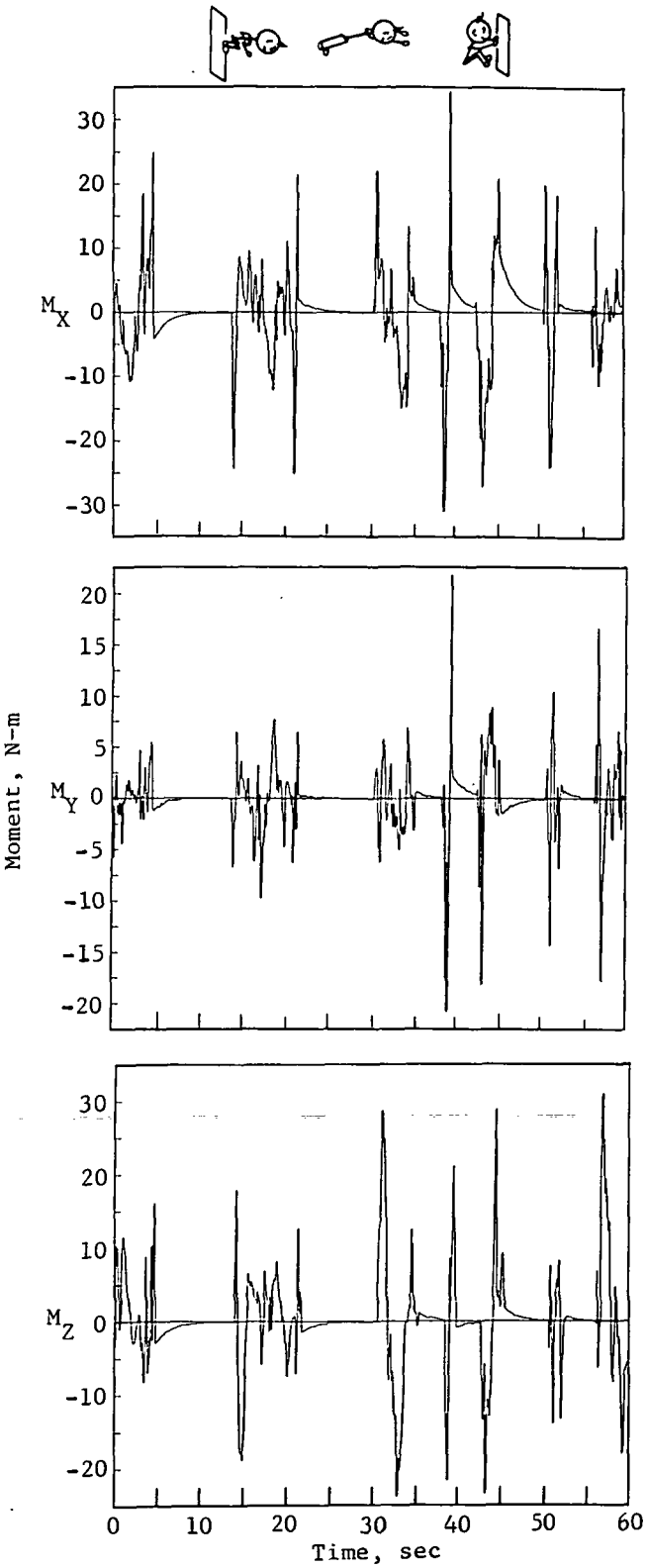

Reference time:
19755285., 1065.

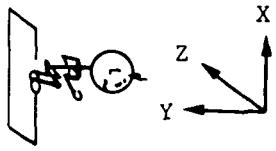

FMU 1
Push-off

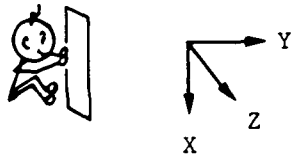

FMU 1
Landing

Figure A-36.- Moment profile of two-man forceful soaring.

The time histories are all characterized by a period of activity followed by a "gap." These gaps account for both the astronaut's soaring time and his time on the second FMU. The actual soarings last only a few seconds each.

The profiles in figures A-35 and A-36 for two men forcefully soaring show that the astronaut's apparent interpretation of "forceful" resulted in quickening the turnaround sequence; i.e., the somersault involved between landing and pushing off is more rapid. The first half of these plots resembles the other profiles, but the second half shows a definite increase in frequency and higher force and moment levels for most of the components.

A.6.3 Statistics

Table A-21 gives statistical data for the four types of soaring. Note that the tabulation of maximum levels shows a wide, varied, overlapping range among the four cases. There is no real pattern discernible to differentiate normal from forceful soaring or one-man from two-man soaring, other than the fact that "two-man forceful" can probably be identified as the worst soaring case.

A.6.4 Frequency content

Figures A-37 to A-44 show the PSD of the four force and moment soaring cases. Table A-22 describes the frequency content numerically.

There is a degree of similarity among the majority of the PSD curves, both of force and moment. This observation is supported by a study of table A-22 which shows a consistency of both peak values and the frequencies at which these peaks are found. All values for the case of two men soaring forcefully are higher than the other types of soaring, but the dominant components (F_Y and M_X) are larger for the two-man cases (both normal and forceful) than either of the one-man cases.

The PSD plots, for the most part, are smooth and regular. With the exception of F_X, two-man normal soaring, they are composed primarily of a single dominant frequency found in the lower range (2 to 3 rad/sec).

It is important to note that the PSD plots and data represent the composite of the three distinct actions that are collectively called "soaring." A PSD of only the push-offs or the landings is anticipated to have a higher peak. Thus, it is recommended that the filter parameters for the stochastic model not be used for soaring.

APPENDIX A

TABLE A-21.- SOARING STATISTICS

Activity	Force, N				Moment, N-m			
	F_X	F_Y	F_Z	F_T	M_X	M_Y	M_Z	M_T
Range, maximum - minimum								
One man:								
Normal								
(1)	86.61	388.41	211.04	420.69	52.48	19.59	39.09	59.96
(2)	15.24	223.13	47.84	237.04	31.50	8.36	7.57	31.87
(3)	146.57	471.76	150.48	473.74	53.91	28.73	42.23	62.41
Forceful								
(1)	110.72	324.08	132.68	331.15	50.51	29.56	42.22	56.97
(2)	106.51	541.57	98.31	547.17	51.24	19.67	33.25	58.66
Two men:								
Normal	99.27	417.57	108.12	423.25	44.76	24.21	40.17	58.92
Forceful								
(1)	268.18	496.41	253.21	501.95	65.41	43.26	74.13	81.56
(2)	82.01	466.83	107.90	475.17	54.96	22.17	43.62	57.95
Maximum level								
One man:								
Normal								
(1)	45.96	271.80	121.97	272.06	27.54	10.89	25.66	32.01
(2)	10.85	220.04	33.92	222.90	22.27	4.24	4.91	23.19
(3)	82.45	309.19	102.39	310.22	31.42	16.08	26.26	34.05
Forceful								
(1)	58.76	244.36	68.07	244.42	26.27	14.81	22.96	30.07
(2)	71.36	290.27	62.48	291.48	26.09	11.08	19.40	31.08
Two men:								
Normal	60.21	284.81	63.05	284.85	26.75	15.26	21.98	32.15
Forceful								
(1)	136.00	320.44	156.29	322.38	34.43	21.82	41.73	43.19
(2)	52.15	343.04	57.28	343.94	27.93	12.51	23.90	29.34
Standard deviation								
One man:								
Normal								
(1)	5.93	20.73	9.23	23.45	3.65	1.23	2.37	4.52
(2)	7.88	29.23	7.59	30.86	4.93	1.28	2.13	5.51
(3)	11.22	40.87	10.51	43.66	4.74	2.18	4.13	6.65
Forceful								
(1)	11.17	36.56	10.74	39.70	5.26	2.28	4.12	7.05
(2)	9.55	48.61	9.40	50.43	5.31	1.46	3.48	6.51
Two men:								
Normal	6.29	45.15	9.90	46.64	5.55	1.52	2.54	6.29
Forceful								
(1)	17.66	50.21	14.09	55.05	6.05	2.83	6.70	9.46
(2)	9.33	38.06	10.46	40.56	5.66	1.62	3.91	7.07

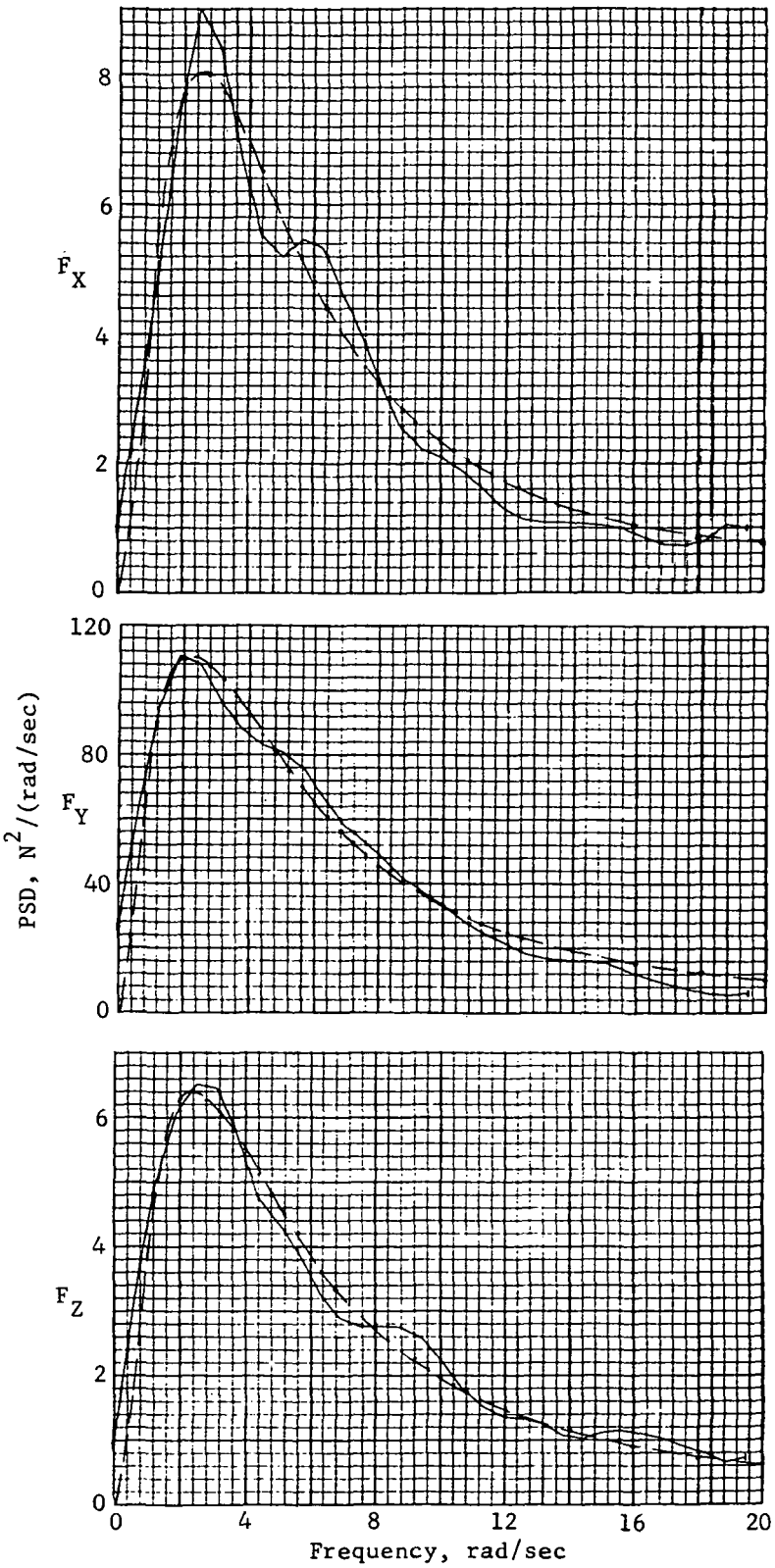

—— Experiment Data

– – Second Order

$$\frac{\tau S}{S^2 + 2\zeta\omega\, S + \omega^2}$$

	F_X	F_Y	F_Z
τ	16.91	65.22	15.92
ω	2.54	2.22	2.40
ζ	1.18	1.40	1.31

Figure A-37.- PSD of force of one-man normal soaring.

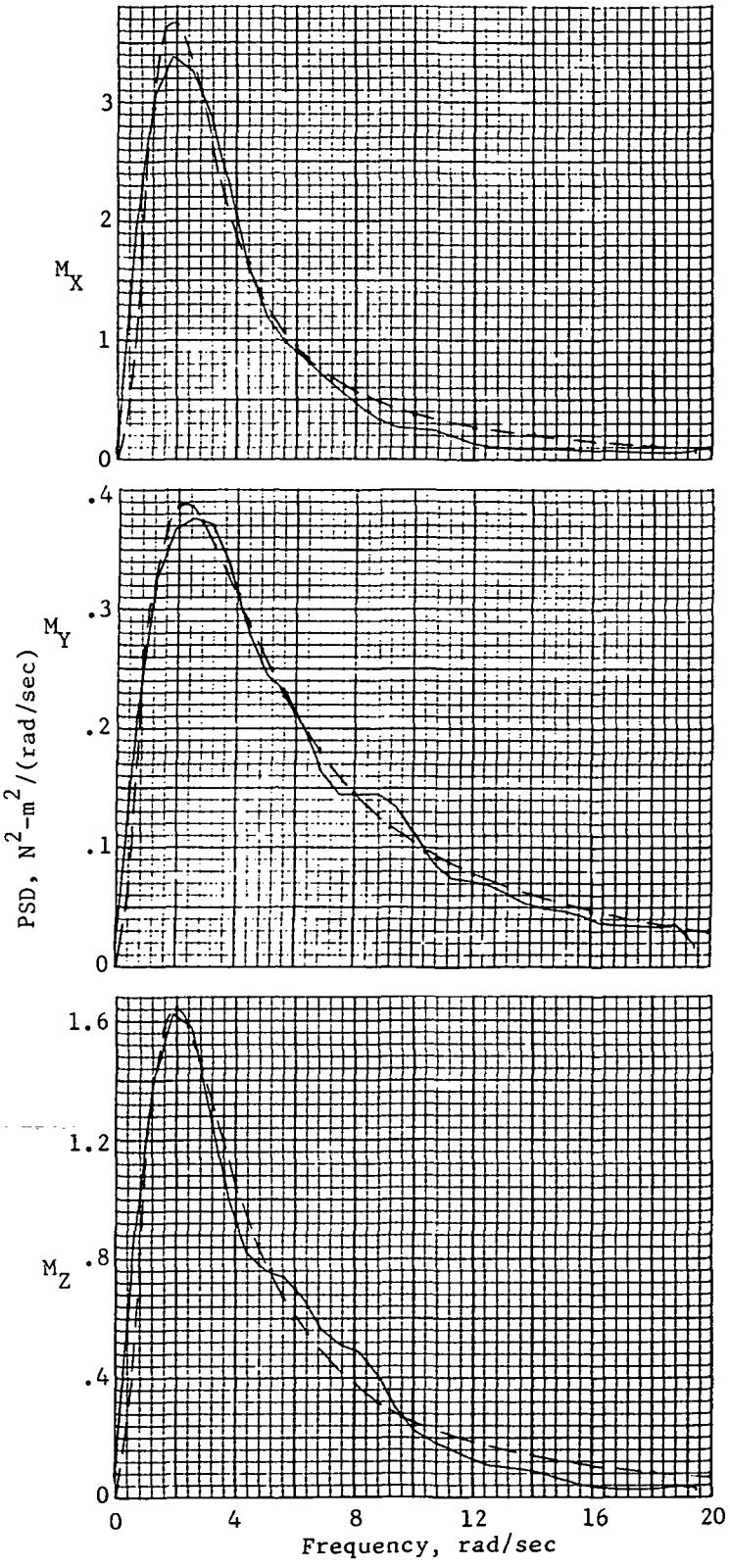

—— Experiment Data

– – Second Order

$$\frac{\tau S}{S^2 + 2\zeta\omega S + \omega^2}$$

	M_X	M_Y	M_Z
τ	6.17	3.57	5.29
ω	1.85	2.16	1.98
ζ	.86	1.33	1.04

Figure A-38.- PSD of moment of one-man normal soaring.

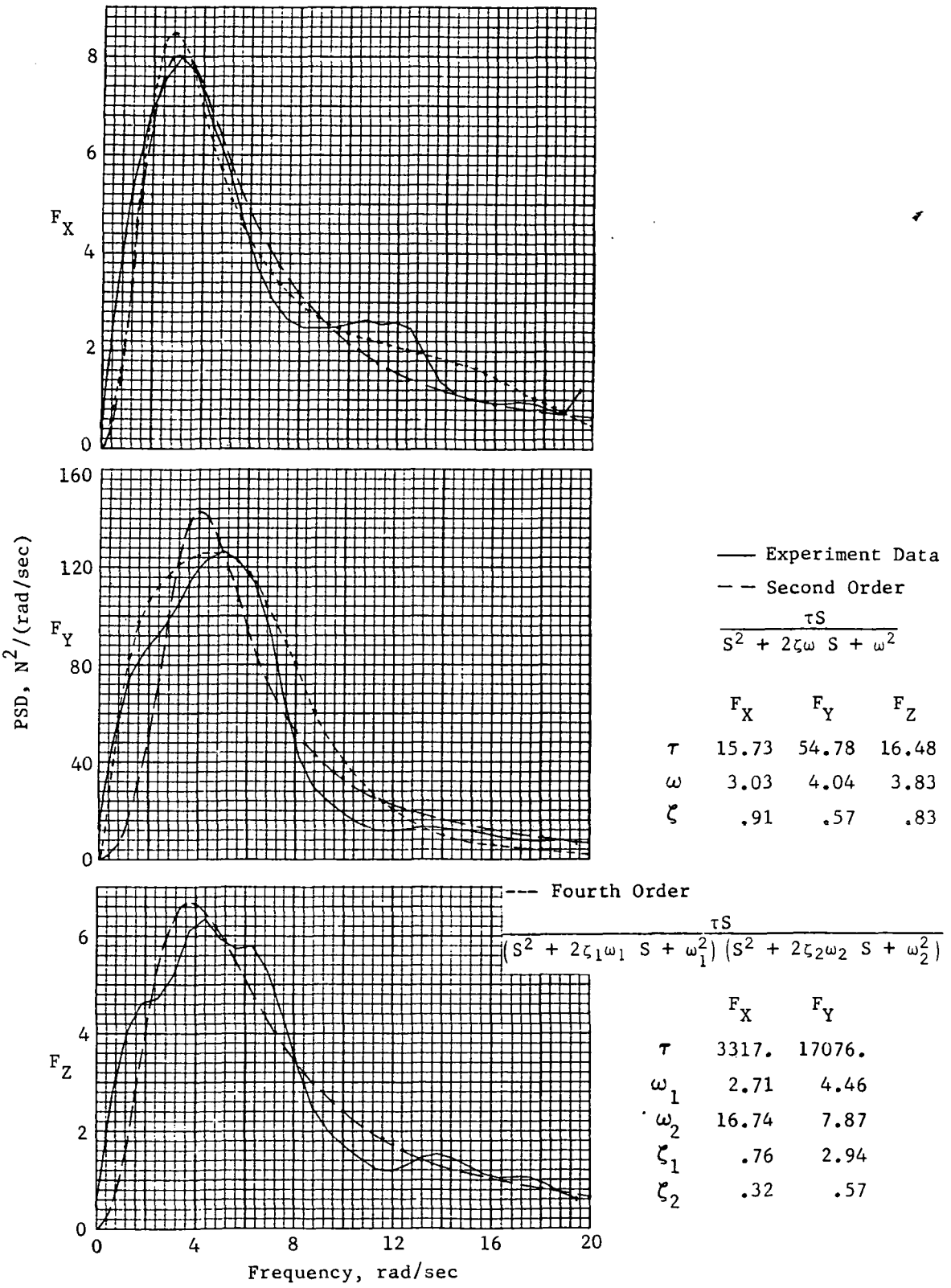

	F_X	F_Y	F_Z
τ	15.73	54.78	16.48
ω	3.03	4.04	3.83
ζ	.91	.57	.83

	F_X	F_Y
τ	3317.	17076.
ω_1	2.71	4.46
ω_2	16.74	7.87
ζ_1	.76	2.94
ζ_2	.32	.57

Figure A-39.- PSD of force of one-man forceful soaring.

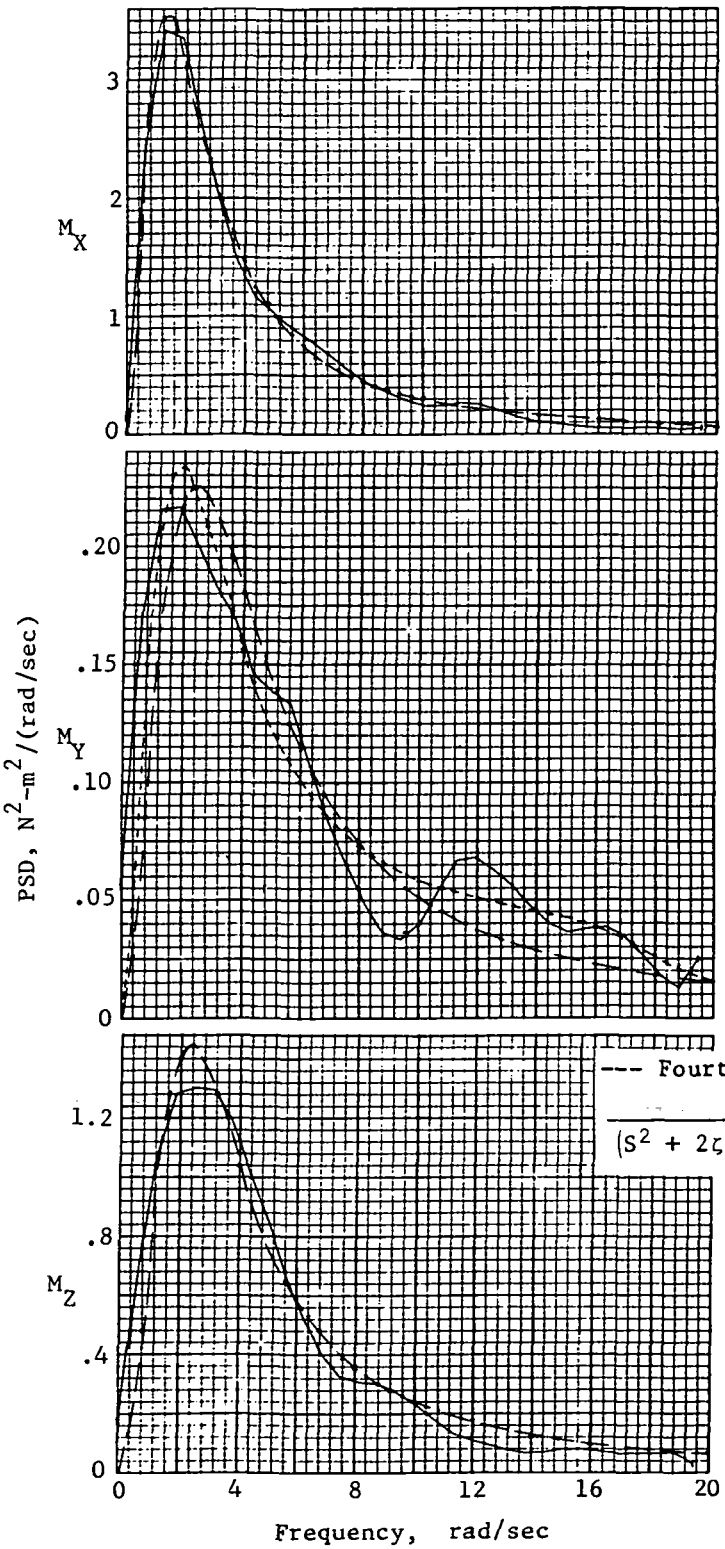

—— Experiment Data

– – Second Order

$$\frac{\tau S}{S^2 + 2\zeta\omega\, S + \omega^2}$$

	M_X	M_Y	M_Z
τ	5.57	2.42	5.07
ω	1.34	2.43	2.32
ζ	1.09	1.05	.91

--- Fourth Order

$$\frac{\tau S}{(S^2 + 2\zeta_1\omega_1\, S + \omega_1^2)(S^2 + 2\zeta_2\omega_2\, S + \omega_2^2)}$$

	M_Y
τ	619.00
ω_1	1.86
ω_2	17.72
ζ_1	1.10
ζ_2	.33

Figure A-40.- PSD of moment of one-man forceful soaring.

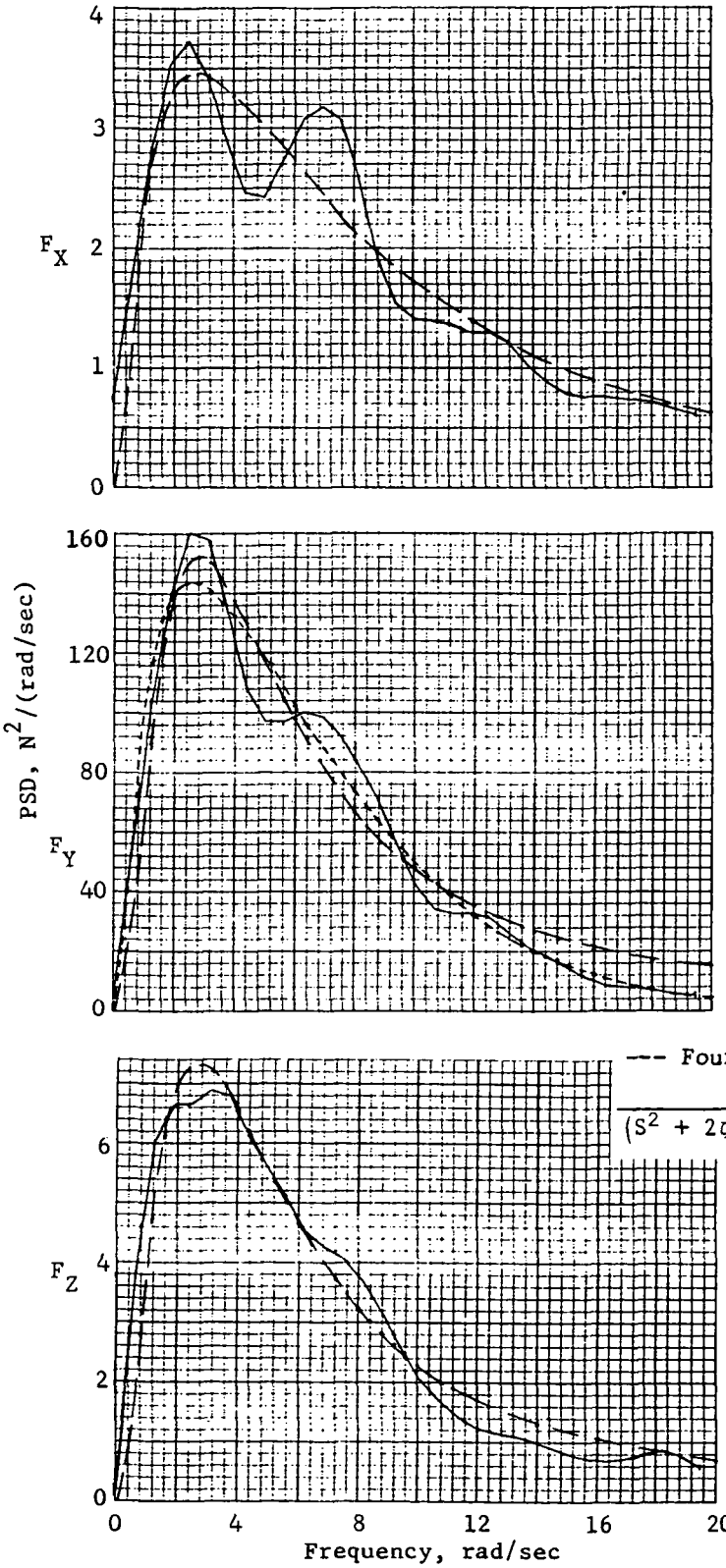

—— Experiment Data

– – Second Order

$$\frac{\tau S}{S^2 + 2\zeta\omega\, S + \omega^2}$$

	F_X	F_Y	F_Z
τ	17.00	76.95	17.02
ω	2.77	2.83	2.66
ζ	1.65	1.10	1.17

--- Fourth Order

$$\frac{\tau S}{(S^2 + 2\zeta_1\omega_1\, S + \omega_1^2)(S^2 + 2\zeta_2\omega_2\, S + \omega_2^2)}$$

	F_Y
τ	19027.
ω_1	2.53
ω_2	14.35
ζ_1	1.53
ζ_2	.67

Figure A-41.- PSD of force of two-man normal soaring.

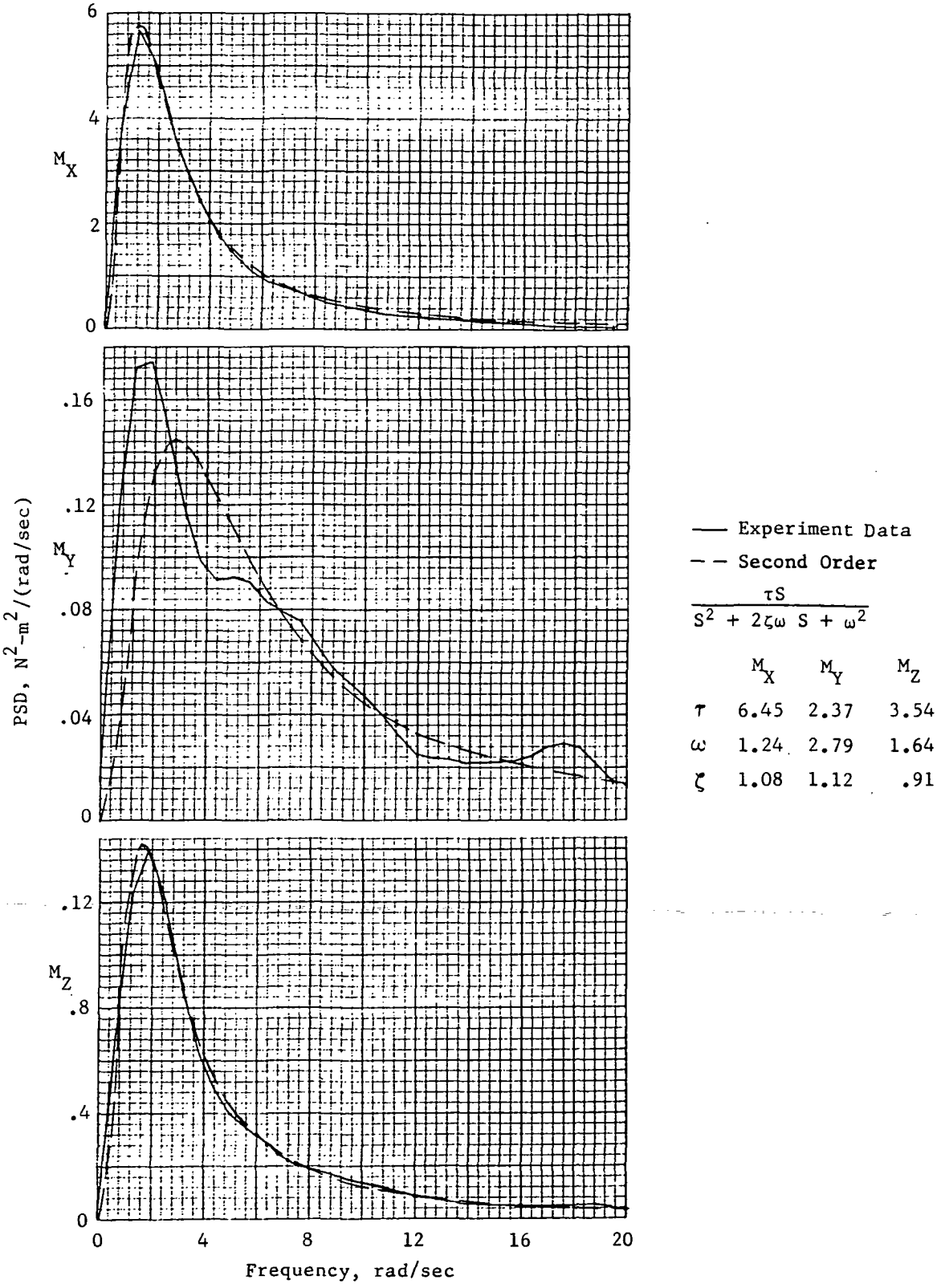

	M_X	M_Y	M_Z
τ	6.45	2.37	3.54
ω	1.24	2.79	1.64
ζ	1.08	1.12	.91

Figure A-42.- PSD of moment of two-man normal soaring.

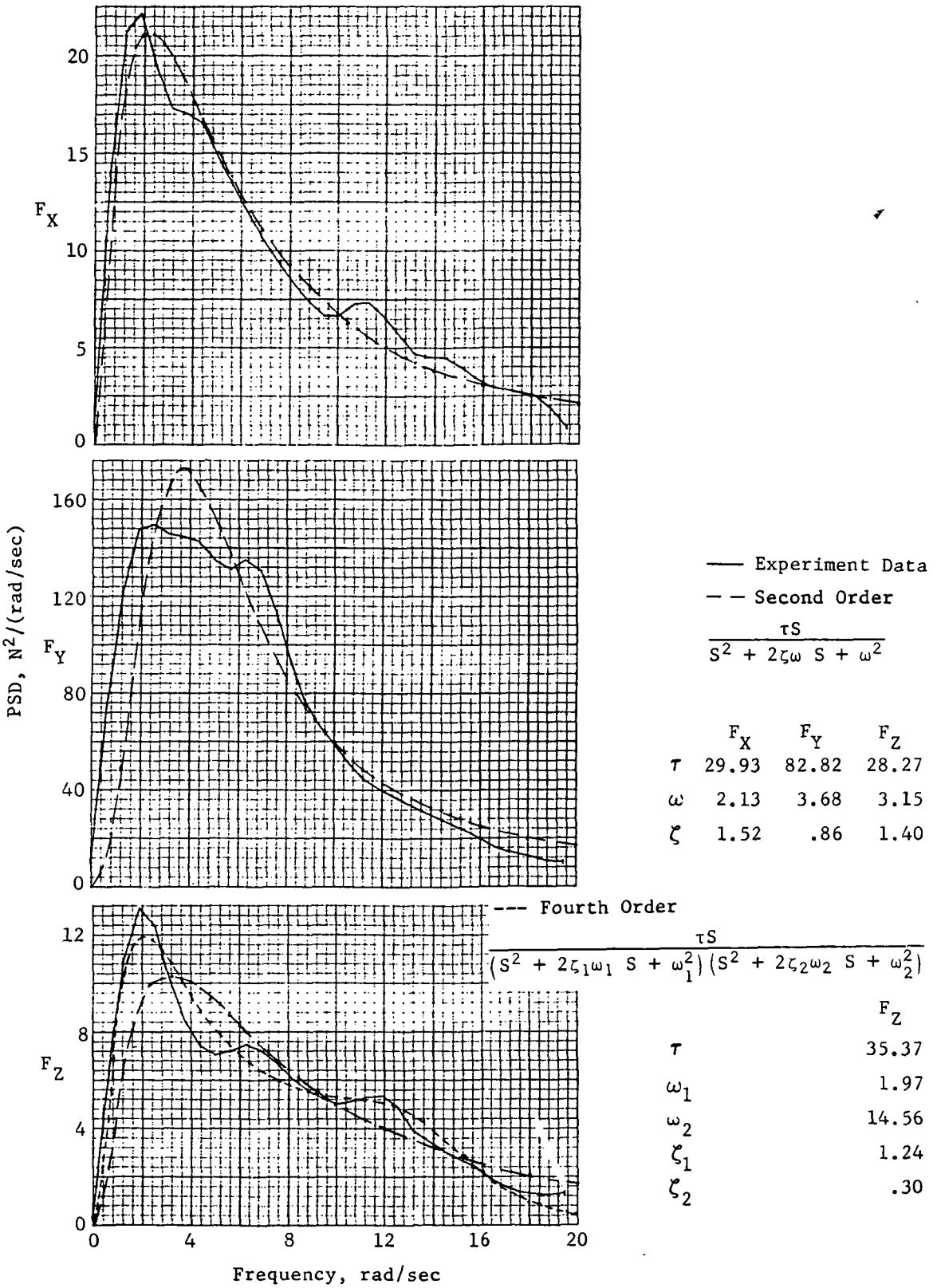

	F_X	F_Y	F_Z
τ	29.93	82.82	28.27
ω	2.13	3.68	3.15
ζ	1.52	.86	1.40

	F_Z
τ	35.37
ω_1	1.97
ω_2	14.56
ζ_1	1.24
ζ_2	.30

Figure A-43.- PSD of force of two-man forceful soaring.

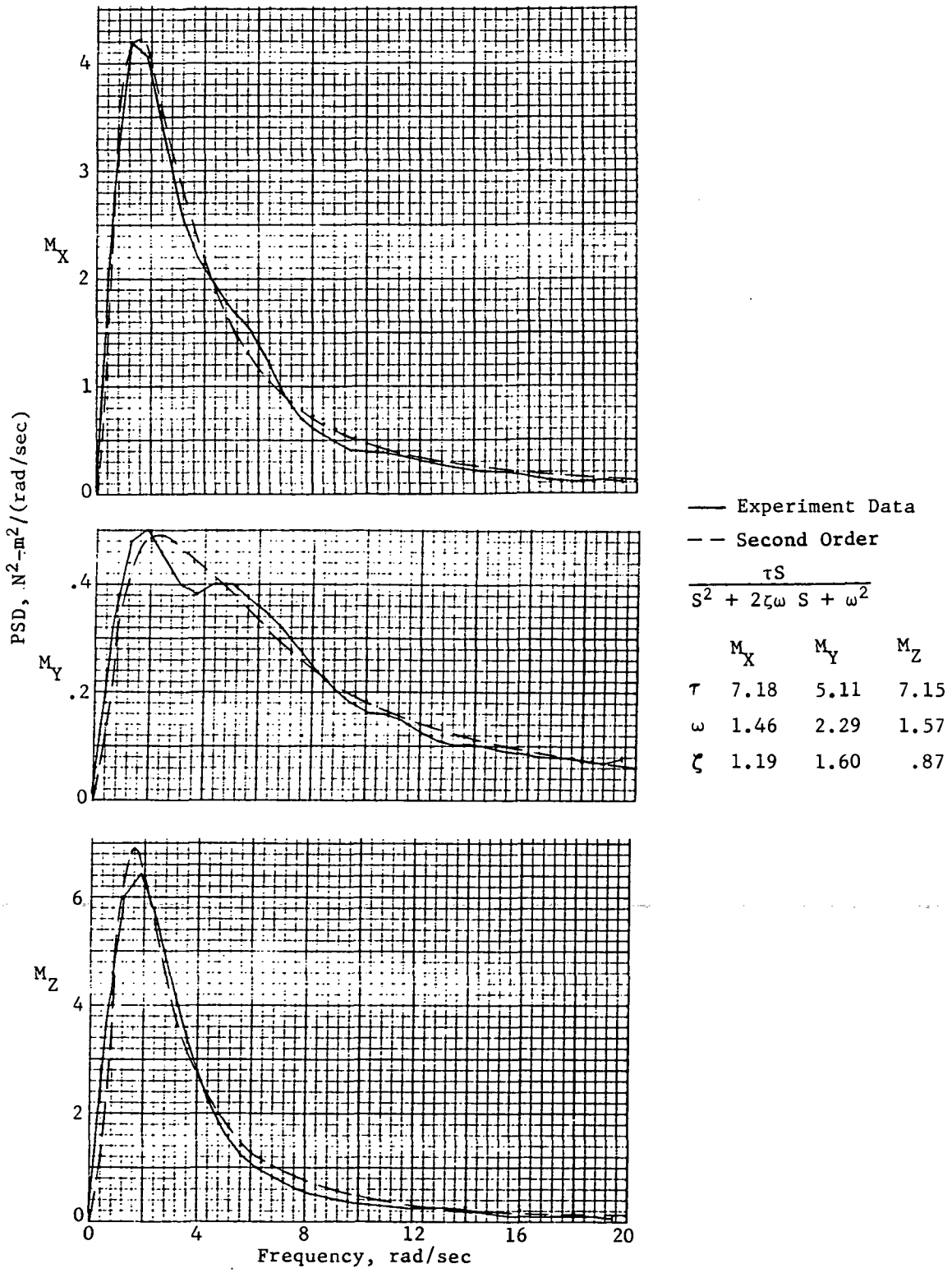

Figure A-44.- PSD of moment of two-man forceful soaring.

APPENDIX A

TABLE A-22.- SOARING FREQUENCY CHARACTERISTICS

Activity	Force, N			Moment, N-m		
	F_X	F_Y	F_Z	M_X	M_Y	M_Z
Maximum PSD, unit^2/(rad/sec)						
One man:						
Normal	9.0	110.0	6.5	3.4	0.38	1.6
Forceful	8.0	125.0	6.3	3.4	.22	1.5
Two men:						
Normal	3.7	160.0	6.8	5.7	.18	1.4
Forceful	22.0	150.0	13.0	4.2	.50	6.4
Frequency at maximum, rad/sec						
One man:						
Normal	2.5	2.0	2.5	2.0	2.5	2.0
Forceful	3.2	5.0	4.4	1.2	2.0	2.5
Two men:						
Normal	2.5	3.0	3.0	1.2	2.0	2.0
Forceful	2.0	2.4	2.0	1.2	2.0	2.0
rms, unit						
One man:						
Normal	11.1	41.8	10.2	5.7	2.4	4.3
Forceful	11.1	42.9	10.5	5.5	1.8	4.1
Two men:						
Normal	8.5	48.5	10.8	6.6	1.6	3.5
Forceful	18.8	53.5	14.7	6.4	3.0	7.2

A.6.5 Summary

There are two basic comparisons to be made about the soaring exercises: normal with forceful and one man with two.

It is difficult to reach any conclusion about the different levels of pushing off when only the data for one-man soaring are studied. Neither the statistical nor the frequency content information shows any noticeable difference between pushing off normally or forcefully. In fact, the normal results are sometimes larger. Thus, based on the single-man data, little can be inferred other than that "forceful" may not have truly been forceful. It cannot be stated that there was no difference between the two ways of pushing off, because the data for the two-man exercise do show the expected difference.

Correlation with the time histories shows an increase in the number of times the astronauts bounced between FMU's with some increase in applied forces and moments.

The comparison of the one- and two-astronaut cases is not straightforward because the secondary subject did not push off the FMU's; thus, his forces could not be recorded as directly as those of the primary subject. However, the activities of both astronauts account for the maximum values of all components of both force and moment, even though in some cases a value is greatest by only a small margin and in no instance is it larger by a factor of 2.

A.7 Swaying

A.7.1 Activity description

Swaying was an unscheduled activity which the subject performed spontaneously in between soaring activities while waiting for the other astronaut to change film in the cameras. For that reason, no formal description is available.

A.7.2 Time histories

The first 30 sec of the time histories given in figures A-45 and A-46 are recorded on film and show that the exercise consisted of swaying from side to side, forward and backward, light knee bends similar to a limbering motion, and arm movements. The remainder of the swaying time histories are part of a data gap and therefore cannot be described.

A.7.3 Statistics

Table A-23 presents the statistical data on swaying.

TABLE A-23.- SWAYING STATISTICS

Statistical results for -	Force, N				Moment, N-m			
	F_X	F_Y	F_Z	F_T	M_X	M_Y	M_Z	M_T
Range	99.79	228.93	194.46	267.37	81.71	24.18	66.75	82.23
Maximum level	53.90	122.32	122.53	144.29	44.16	12.37	34.08	44.45
Standard deviation	8.86	16.61	16.42	24.98	8.33	2.38	5.19	10.09

Swaying, more than any other exercise, used movement in all three axes. This is evident in studying the forces, both tabulated and plotted, and by noting the significance of the moments.

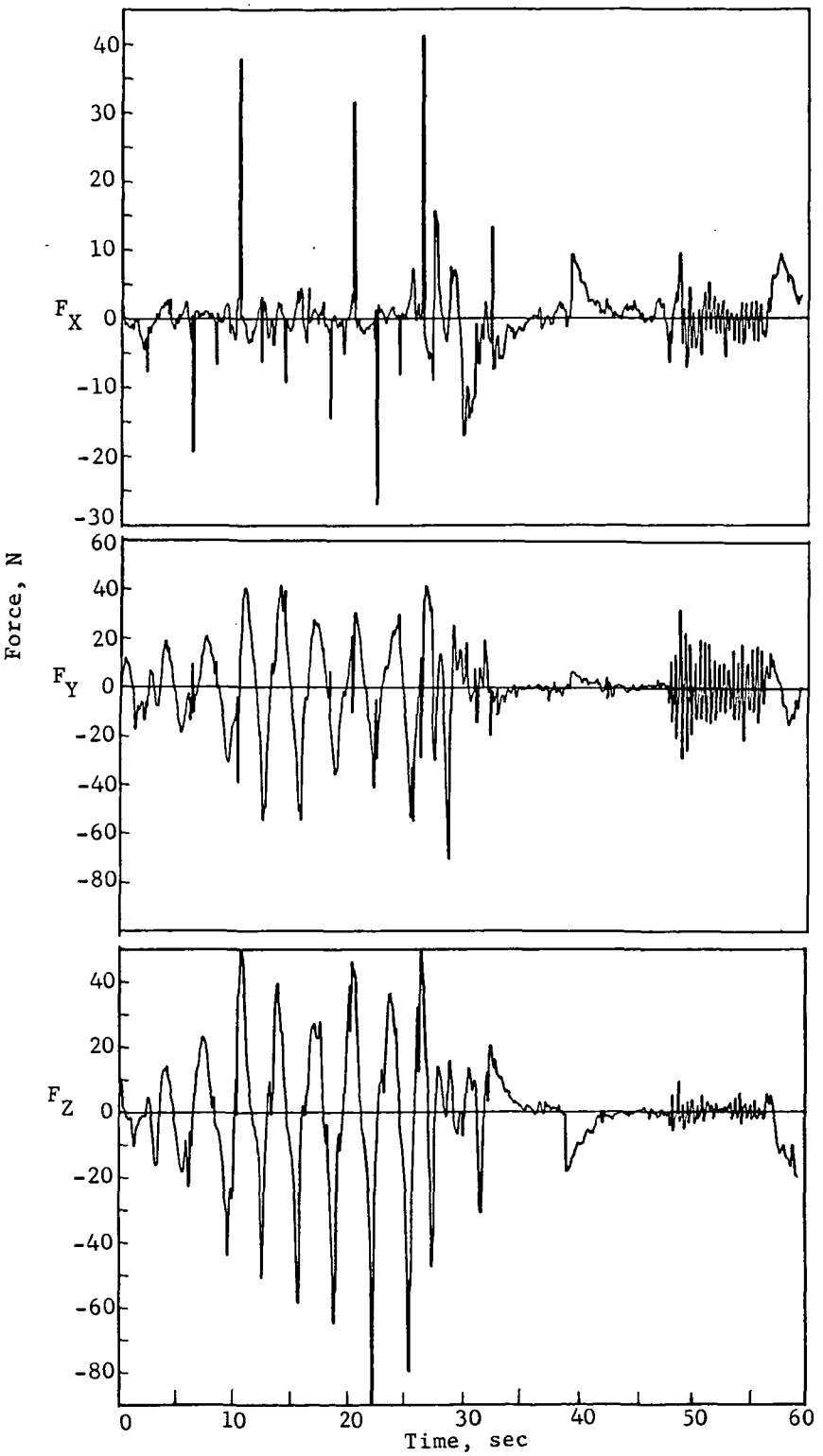

Reference time:
19756080., 1800.

Figure A-45.- Force profile of swaying.

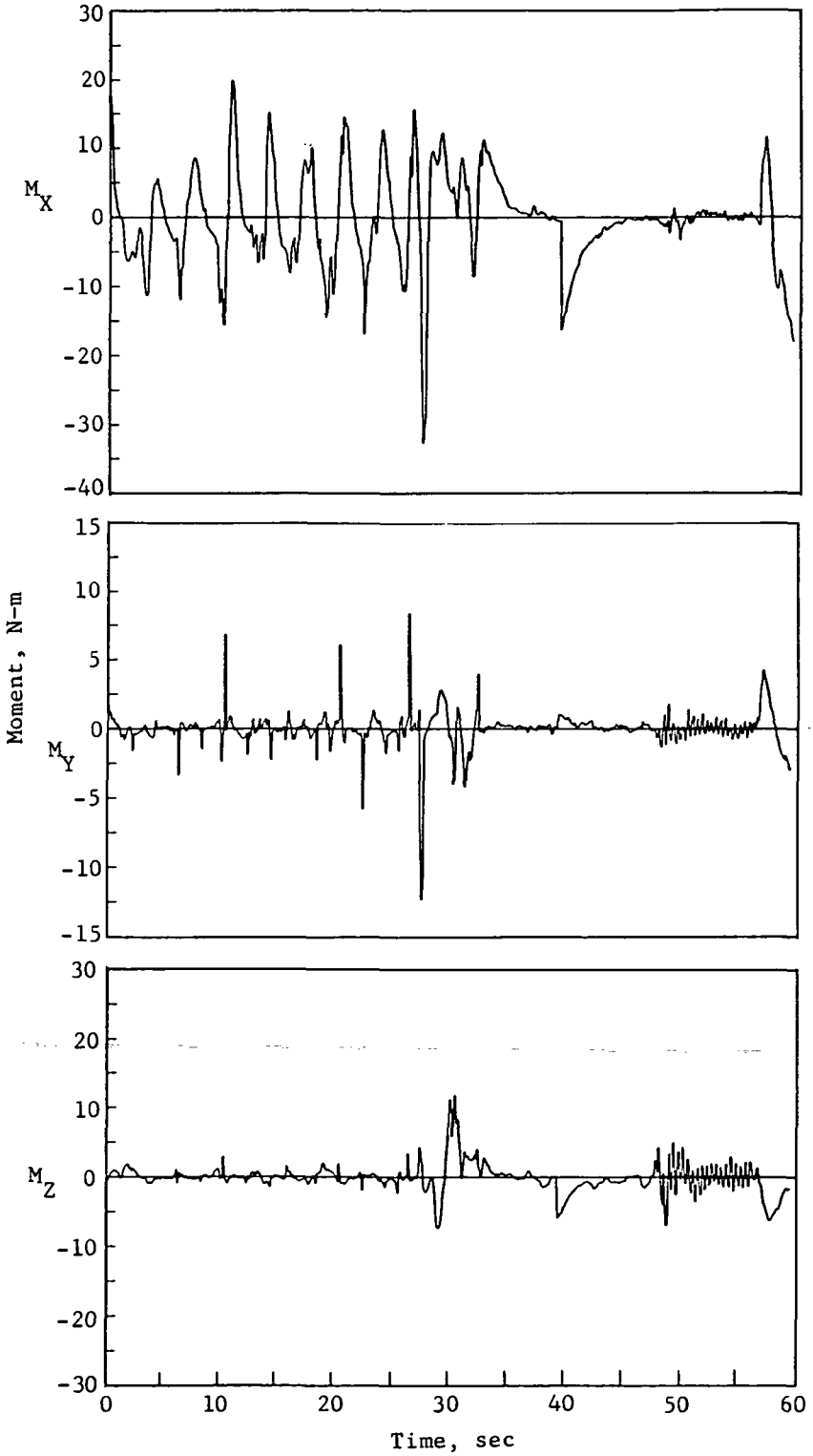

Reference time:
19756080., 1800.

Figure A-46.- Moment profile of swaying.

Both table A-23 and figure A-45 show that the force levels in the y- and z-directions are similar, and even the x-component has a relatively large magnitude. Concurrently, all the moments are large, but the x-component appears to dominate unlike the case in force.

Even though the forces of the individual components are not significant when compared with the other scheduled T-013 exercises, the x-moment of swaying turns out to be the largest torque produced by any exercise. Only the two-man forceful soaring activity produces moments anywhere near (within 10 N-m) this level.

A.7.4 Frequency content

Figures A-47 and A-48 display the PSD of swaying force and moment. Frequency content is described in table A-24.

TABLE A-24.- SWAYING FREQUENCY CHARACTERISTICS

Force	Maximum PSD, $N^2/(rad/sec)$	Frequency at maximum, rad/sec	rms, N
X	2.1	1.0	8.5
Y	52.0	2.0	16.0
Z	68.0	2.0	16.4

Moment	Maximum PSD, $N^2-m^2/(rad/sec)$	Frequency at maximum, rad/sec	rms, N-m
X	20.0	0.8	8.6
Y	1.5	.8	2.3
Z	9.2	1.0	5.2

The first thing immediately obvious from studying the PSD plots is that the power curves peak at low frequencies and then decrease rapidly. This seems indicative of a slow, steadily repeated movement.

The maximum levels attained for F_X and all moment components are larger than for any other T-013 activity, often significantly so, yet the corresponding comparison of rms values is not as dramatic. This restates the observation just drawn about the plots. The high power level, once achieved, is not sustained; within 2 or even 1 rad/sec of the maximum, the PSD is measured at a very low level, where other T-013 activities usually retain a higher degree of power.

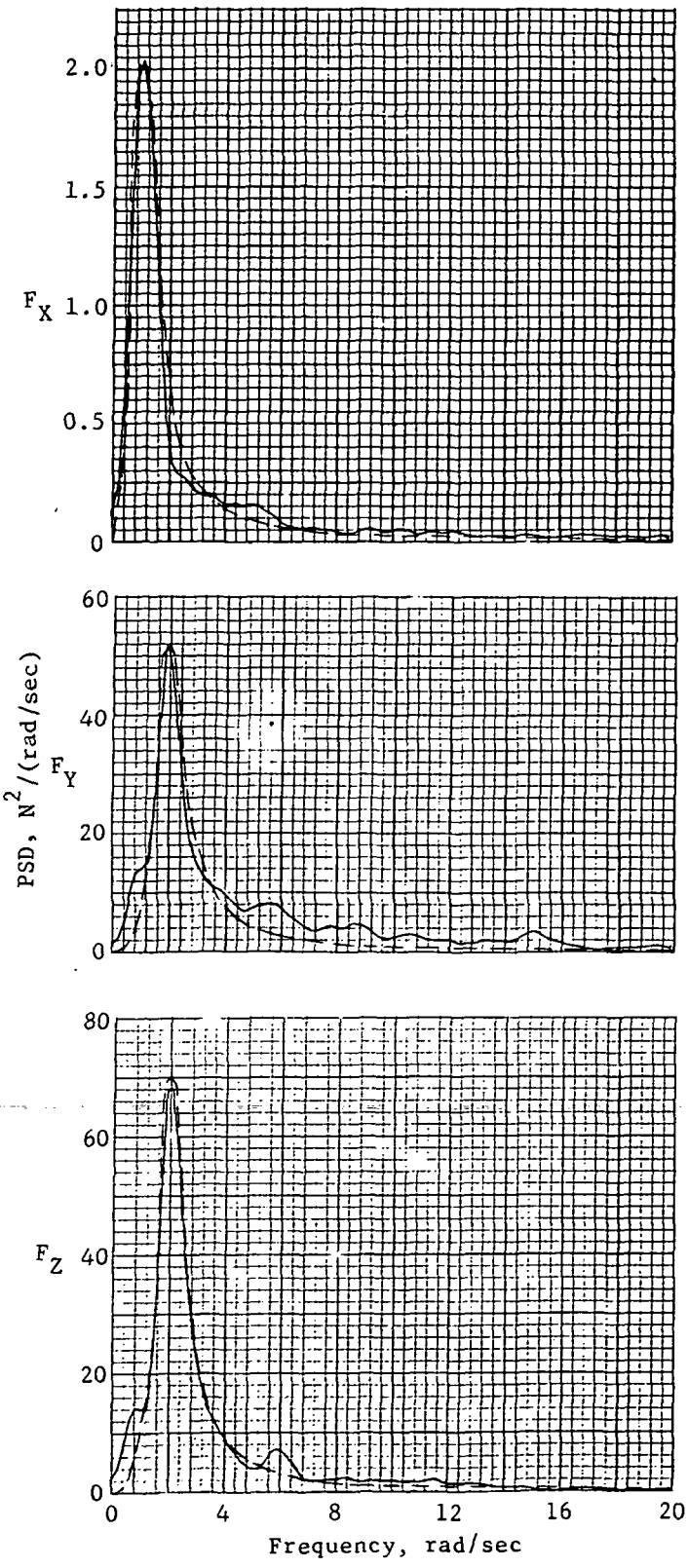

—— Experiment Data

– – Second Order

$$\frac{\tau S}{S^2 + 2\zeta\omega S + \omega^2}$$

	F_X	F_Y	F_Z
τ	4.43	8.76	9.40
ω	.98	2.02	2.03
ζ	.48	.31	.28

Figure A-47.- PSD of force of swaying.

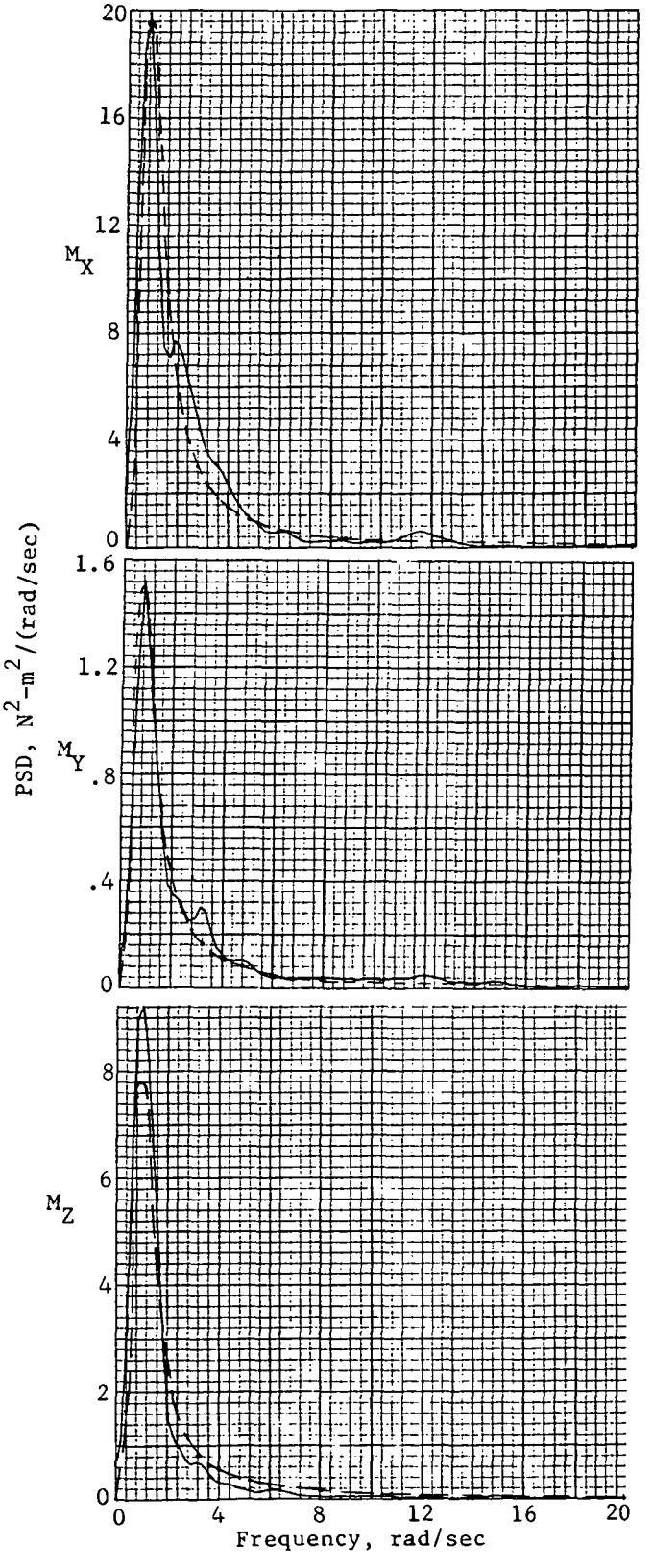

—— Experiment Data

– – Second Order

$$\frac{\tau S}{S^2 + 2\zeta\omega S + \omega^2}$$

	M_X	M_Y	M_Z
τ	4.80	1.29	2.79
ω	.87	.86	.98
ζ	.62	.61	.44

Figure A-48.- PSD of moment of swaying.

APPENDIX A

A.8 Summary

Drawing detailed conclusions from the tabularized results is difficult because of the different classifications to which possible comparisons belong. Furthermore, the size of the sample set varies significantly among the different activities, making any hard and fast conclusions difficult to reach because the number of data points affects statistical results fundamentally. Thus, instead of forcing numerous comparisons of doubtful origin, identification of trends within the activities is more useful.

The largest forces (400 to 440 N) occurred during the gross body exercises for the y-component; the restrained forceful thrust is responsible for the maximum. The corresponding standard deviation is also the maximum 1σ value of all the exercises. This supports the premise that this activity was the most forceful since the maximum level was approximately a 4.5σ occurrence, not a 10σ accident. The maximum torque was produced by the unscheduled swaying motion. This is not surprising since, unlike most of the other T-013 actions which were performed primarily in a single plane, swaying was a three-dimensional, revolving movement which caused a moment of 44 N-m.

Among the normal exercises, bowing accounts for the maximum force exerted in the y-direction, 230 N, while leg movements cause the maximum levels in the x- and z-components. The corresponding moment for bowing (the x-component) represents the largest torque among the normal exercises, but it is interesting to note that all other torques are close in value. Even the low force activity represented by console operations has relatively high moments. This case is verified by the corresponding standard deviations.

Tables A-25 to A-29 summarize statistical and frequency content for the T-013 activities. Tables A-30 to A-35 provide a record of filter parameter information.

APPENDIX A

TABLE A-25.- RANGE OF FORCES AND MOMENTS FOR T-013 ACTIVITIES

Activity	Force, N				Moment, N-m			
	F_X	F_Y	F_Z	F_T	M_X	M_Y	M_Z	M_T
Console operations . . .	57.36	57.41	26.97	75.77	30.19	12.13	24.37	31.06
Respiration exercises	94.07	325.39	70.39	330.09	23.28	17.26	33.74	37.15
Normal body exercises:								
Arm motion	35.89	270.31	99.69	280.64	18.34	18.22	13.07	21.69
Leg motion	159.29	166.96	112.73	188.38	18.18	15.39	23.02	27.78
Bowing	99.13	368.84	71.42	373.16	43.36	16.85	16.49	52.03
Gross body exercises:								
Arm flapping	108.10	595.57	139.79	598.07	45.82	21.96	21.66	45.85
Forceful thrust . . .	164.04	760.03	110.64	760.26	57.59	32.16	22.73	58.96
One-man soaring:								
Normal	146.57	471.76	211.04	473.74	53.91	28.73	42.23	62.41
Forceful	110.72	541.57	132.68	547.17	51.24	29.56	42.22	58.66
Two-man soaring:								
Normal	99.27	417.57	108.12	423.25	44.76	24.21	40.17	58.92
Forceful	268.18	496.41	253.21	501.95	65.41	43.26	74.13	81.56
Swaying	99.79	228.93	194.46	267.37	81.71	24.18	66.75	82.23

APPENDIX A

TABLE A-26.- FORCE AND MOMENT MAXIMA FOR T-013 ACTIVITIES

Activity	Force, N				Moment, N-m			
	F_X	F_Y	F_Z	F_T	M_X	M_Y	M_Z	M_T
Console operations . . .	33.55	32.29	13.50	41.95	15.35	7.06	13.58	16.10
Respiration exercises	56.63	212.69	39.83	216.29	12.68	10.74	18.63	19.22
Normal body exercises:								
Arm motion	25.81	149.30	53.48	157.01	11.12	10.50	8.40	11.20
Leg motion	102.54	109.56	58.92	125.54	9.39	8.16	15.07	18.05
Bowing	78.86	231.85	38.60	234.34	25.82	12.69	8.82	26.40
Gross body exercises:								
Arm flapping	65.43	395.73	125.37	407.84	29.34	12.16	15.66	29.37
Forceful thrust . . .	130.47	443.52	64.71	443.58	30.94	25.54	11.50	31.34
One-man soaring:								
Normal	82.45	309.19	121.97	310.22	31.42	16.08	26.26	34.05
Forceful	71.36	290.27	68.07	291.48	26.27	14.81	22.96	31.08
Two-man soaring:								
Normal	60.21	284.81	63.05	284.85	26.75	15.26	21.98	32.15
Forceful	136.00	343.04	156.29	343.94	34.43	21.82	41.73	43.19
Swaying	53.90	122.32	122.53	144.29	44.16	12.37	34.08	44.45

APPENDIX A

TABLE A-27.- FORCE AND MOMENT STANDARD DEVIATION FOR T-013 ACTIVITIES

Activity	Force, N				Moment, N-m			
	F_X	F_Y	F_Z	F_T	M_X	M_Y	M_Z	M_T
Console operations	3.93	4.13	3.28	6.57	3.40	0.99	2.30	4.22
Respiration exercises . . .	4.37	17.08	5.81	18.56	2.43	1.00	1.83	3.20
Normal body exercises:								
Arm motion	4.22	20.42	7.74	22.24	1.57	1.41	1.41	2.54
Leg motion	10.71	13.50	8.38	19.17	1.71	1.21	2.20	3.04
Bowing	9.08	63.47	11.98	65.22	7.46	1.65	2.69	8.10
Gross body exercises:								
Arm flapping	8.46	94.25	19.71	96.66	5.80	1.74	2.50	6.54
Forceful thrust	15.54	97.91	19.20	100.97	7.76	2.88	3.61	9.02
One-man soaring:								
Normal	10.50	35.77	9.98	37.31	4.82	1.89	3.76	5.47
Forceful	10.9	46.62	10.46	46.74	5.29	1.91	4.02	6.84
Two-man soaring:								
Normal	6.29	45.15	9.90	46.64	5.55	1.52	2.54	6.29
Forceful	15.97	47.44	13.27	51.78	5.96	2.58	6.12	8.92
Swaying	8.86	16.61	16.42	24.98	8.33	2.38	5.19	10.09

APPENDIX A

TABLE A-28.- FORCE AND MOMENT PSD MAXIMA FOR T-013 ACTIVITIES

Activity	PSD, $N^2/(rad/sec)$, for force -			PSD, $N^2-m^2/(rad/sec)$, for moment -		
	F_X	F_Y	F_Z	M_X	M_Y	M_Z
Console operations	2.5	1.0	1.7	2.6	0.15	1.20
Respiration exercises . . .	.35	8.0	.5	.8	.02	.15
Normal body exercises:						
Arm motion	.6	16.4	2.6	.29	.19	.11
Leg motion	20.0	17.5	8.0	.53	.15	.47
Bowing	3.8	490.0	12.4	10.00	.16	.50
Gross body exercises:						
Arm flapping	1.3	520.0	32.0	1.7	.07	.34
Crouch and push-off . . .	16.2	600.0	23.5	9.0	.60	.80
One-man soaring:						
Normal	9.0	110.0	6.5	3.4	.38	1.60
Forceful	8.0	125.0	6.3	3.4	.22	1.50
Two-man soaring:						
Normal	3.7	160.0	6.8	5.7	.18	1.40
Forceful	22.0	150.0	13.0	4.2	.50	6.40
Swaying	2.1	52.0	68.0	20.0	1.50	9.20

APPENDIX A

TABLE A-29.- FREQUENCIES AT PSD MAXIMA FOR T-013 ACTIVITIES

Activity	Frequency, rad/sec, for force -			Frequency, rad/sec, for moment -		
	F_X	F_Y	F_Z	M_X	M_Y	M_Z
Console operations	1.2	2.0	1.0	1.0	2.0	1.2
Respiration exercises . . .	2.0	5 and 12	1, 12, 15.5	1.0	2.5	1.7
Normal body exercises:						
Arm motion	2.5	10.0	10.0	1.0	4.4	2.0
Leg motion	5.8	8.8	5.8	2.5	3.2	8.8
Bowing	7.0	4.5	7.0	2.0	2.0	7.0
Gross body exercises:						
Arm flapping	5.0	10.3	10.3	8.0	5 and 11	4.2
Crouch and push-off . . .	5.0	6.2	2.3	2.3	6.0	2.0
One-man soaring:						
Normal	2.5	2.0	2.5	2.0	2.5	2.0
Forceful	3.2	5.0	4.4	1.2	2.0	2.5
Two-man soaring:						
Normal	2.5	3.0	3.0	1.2	2.0	2.0
Forceful	2.0	2.4	2.0	1.2	2.0	2.0
Swaying	1.0	2.0	2.0	.8	.8	1.0

APPENDIX A

TABLE A-30.- STOCHASTIC MODEL FILTER PARAMETERS, F_X

Activity	Second-order parameters			Fourth-order parameters				
	τ	ω	ζ	τ	ω_1	ω_2	ζ_1	ζ_2
Console operations	2.46	1.67	0.45					
Respiration exercises . . .	3.58	2.13	1.52	618.42	1.30	17.06	1.46	0.25
Normal body exercises:								
Arm motion	10.28	3.80	1.81					
Leg motion	21.47	5.33	.49	24.23	4.67	9.43	.85	.46
Bowing	17.23	4.23	1.15	8394.	4.61	27.54	.65	.15
Gross body exercises:								
Arm flapping	49.58	6.55	3.61					
Crouch and push-off . . .	36.05	4.06	1.22					
One-man soaring:								
Normal	16.91	2.54	1.18					
Forceful	15.73	3.03	.91	3317.	2.71	16.74	.76	.32
Two-man soaring:								
Normal	17.00	2.77	1.65					
Forceful	29.93	2.13	1.52					
Swaying	4.43	.98	.48					

APPENDIX A

TABLE A-31.- STOCHASTIC MODEL FILTER PARAMETERS, F_Y

Activity	Second-order parameters			Fourth-order parameters				
	τ	ω	ζ	τ	ω_1	ω_2	ζ_1	ζ_2
Console operations	12.29	3.80	1.81	10.40	2.25	14.68	1.06	0.31
Respiration exercises . . .	50.24	7.15	1.47	98.65	4.70	18.81	1.36	.37
Normal body exercises:								
Arm motion	52.47	9.36	.69	13082.	16.64	6.85	.38	1.06
Leg motion	25.28	7.54	.42	49.11	7.02	11.71	.81	.46
Bowing	67.32	4.34	.33	3123.	3.93	6.86	.47	.39
Gross body exercises:								
Arm flapping	128.10	10.37	.28	290.64	9.00	14.51	.47	.40
Crouch and push-off . . .	144.80	6.04	.52					
One-man soaring:								
Normal	65.22	2.22	1.40					
Forceful	54.78	4.04	.57	17076.	4.46	7.87	2.94	.57
Two-man soaring:								
Normal	76.95	2.83	1.10	19027.	2.53	14.35	1.53	.67
Forceful	82.82	3.68	.86					
Swaying	8.76	2.02	.31					

APPENDIX A

TABLE A-32.- STOCHASTIC MODEL FILTER PARAMETERS, F_Z

Activity	Second-order parameters			Fourth-order parameters				
	τ	ω	ζ	τ	ω_1	ω_2	ζ_1	ζ_2
Console operations	2.56	1.34	0.72					
Respiration exercises . . .	29.90	6.55	3.61					
Normal body exercises:								
Arm motion	19.82	9.51	.68	5282.	8.23	16.79	0.90	0.43
Leg motion	16.34	6.10	.49	27.21	4.87	10.68	1.13	.47
Bowing	17.96	5.96	.51	7846.	8.60	10.70	.57	1.70
Gross body exercises:								
Arm flapping	28.06	10.37	.28	63.56	9.50	14.70	.44	.39
Crouch and push-off . . .	32.77	3.99	1.06					
One-man soaring:								
Normal	15.92	2.40	1.31					
Forceful	16.48	3.83	.83					
Two-man soaring:								
Normal	17.02	2.66	1.17					
Forceful	28.27	3.15	1.40	35.37	1.97	14.56	1.24	.30
Swaying	9.40	2.03	.28					

APPENDIX A

TABLE A-33.- STOCHASTIC MODEL FILTER PARAMETERS, M_X

Activity	Second-order parameters			Fourth-order parameters				
	τ	ω	ζ	τ	ω_1	ω_2	ζ_1	ζ_2
Console operations	2.38	1.48	0.48					
Respiration exercises . . .	1.03	.93	.63	81.32	0.89	9.27	0.60	0.27
Normal body exercises:								
Arm motion	1.41	1.29	.97					
Leg motion	2.01	2.09	.64					
Bowing	6.06	1.58	.59					
Gross body exercises:								
Arm flapping	10.11	6.62	.66					
Crouch and push-off . . .	7.90	2.57	.53	10.88	2.33	12.87	.49	.27
One-man soaring:								
Normal	6.17	1.85	.86					
Forceful	5.57	1.34	1.09					
Two-man soaring:								
Normal	6.45	1.24	1.08					
Forceful	7.18	1.46	1.19					
Swaying	4.80	.87	.62					

APPENDIX A

TABLE A-34.- STOCHASTIC MODEL FILTER PARAMETERS, M_Y

Activity	Second-order parameters			Fourth-order parameters				
	τ	ω	ζ	τ	ω_1	ω_2	ζ_1	ζ_2
Console operations	0.78	2.21	0.46					
Respiration exercises . . .	.52	2.34	.87					
Normal body exercises:								
Arm motion	1.77	3.98	.54					
Leg motion	2.41	4.25	.76	591.25	3.75	11.48	1.73	0.67
Bowing	2.03	2.95	.85	855.60	2.40	22.37	.88	.27
Gross body exercises:								
Arm flapping	4.24	5.95	1.41					
Crouch and push-off . . .	7.15	5.13	.99					
One-man soaring:								
Normal	3.57	2.16	1.33					
Forceful	2.42	2.43	1.05	619.0	1.86	17.72	1.10	.33
Two-man soaring:								
Normal	2.37	2.79	1.12					
Forceful	5.11	2.29	1.60					
Swaying	1.29	.86	.61					

APPENDIX A

TABLE A-35.- STOCHASTIC MODEL FILTER PARAMETERS, M_Z

Activity	Second-order parameters			Fourth-order parameters				
	τ	ω	ζ	τ	ω_1	ω_2	ζ_1	ζ_2
Console operations	1.88	1.47	0.62					
Respiration exercises . . .	1.01	1.84	.84					
Normal body exercises:								
Arm motion	2.55	3.07	1.37	328.93	2.25	14.68	1.06	0.31
Leg motion	4.15	6.18	.49	727.28	4.87	10.68	1.13	.47
Bowing	3.68	3.95	.66	991.80	4.46	7.87	2.94	.57
Gross body exercises:								
Arm flapping	5.35	5.07	1.09	966.47	3.33	17.02	1.06	.32
Crouch and push-off . . .	1.89	2.71	.40	378.71	2.09	14.95	.44	.17
One-man soaring:								
Normal	5.29	1.98	1.04					
Forceful	5.07	2.32	.91					
Two-man soaring:								
Normal	3.54	1.64	.91					
Forceful	7.15	1.57	.87					
Swaying	2.79	.98	.44					

APPENDIX B

DOCUMENTATION OF MODELS

APPENDIX B

DOCUMENTATION OF MODELS

The two working models of crew motion disturbance documented here are the first-order and the stochastic models. These are the ones implemented in the applications chapter of this document. The anthropometric model is also given in this appendix in more detail than was presented in chapter 5.0. With the expenditure of additional time and effort, this model could become a very useful tool. The computer program of this model contains execution problems that made its implementation for this handbook impractical. However, if it were made efficiently operational and its results were validated, the anthropometric model could be a relatively easy and inexpensive way to obtain a quantity of data. For new activities, it would give better detailed results than a first-order model without the depth of analysis and investment in activity simulations that need to precede use of the stochastic model.

B.1 First-Order Model

The first-order model (developed for the soaring application as an example) is a simple time function that uses the identifiable peaks of a deterministic action to characterize the disturbance and sets low-level activity (noise) to zero. The appropriate x-, y-, and z-coordinates of force and moment are transformed from disturbances local to the FMU to a single torque about the vehicle's center of mass by incorporating the appropriate moment arms within equations derived from the particular vehicle geometry.

The applications chapter identifies a first-order model and an improved first-order model. The only significant difference between the two is the manner in which the peaks are described. While the first model uses a single midpoint value to define the particular force or moment, the second derived intermediate points in addition to the maximum by reading the information from the T-013 data tapes. Since this improvement requires detailed knowledge of the action, it is felt that any improvement in the quality of the results is not truly worth the effort required in developing the time function. All further discussion, then, relates only to the simpler version.

The z-coordinate vehicle torque is the one presented in the applications portion of this document because it incorporates F_Y, the dominant force, and R_X, the moment arm of largest magnitude. The model, pictured in figure B-1, was developed using the relationship expressed by

$$M_{ZV} = R_Y F_Z - R_X F_Y - M_X$$

APPENDIX B

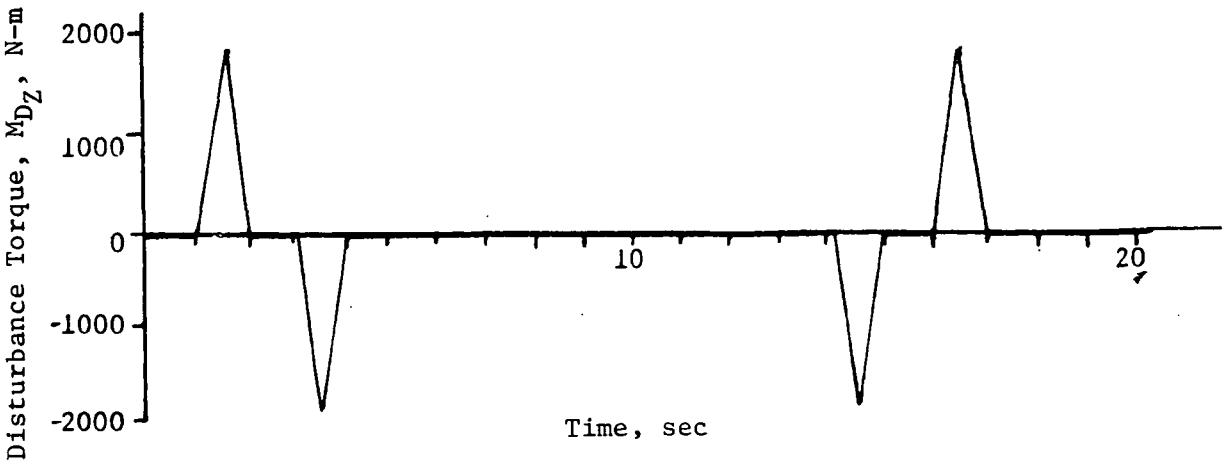

Figure B-1.- First-order model disturbance.

Figure B-2 is a sample of the original data taken from appendix A and is given to compare with figure B-1.

B.2 Stochastic Model

The stochastic model is a method of computing a crew motion disturbance that generates random noise and passes it through a shaping filter to give it the frequency characteristics of a specified action. White noise is theoretically the sum of all frequency components; its frequency spectrum is a straight line that is shaped by input filter parameters derived from the PSD of a particular activity. The output of the model is a disturbance in the time domain that can then be used as a driver for a control system simulation.

Chapter 5.0 in general, and specifically section 5.2.4, describes the model's limitations and the types of actions best suited to stochastic representation.

A thorough discussion describing the selection of the linear shaping filter structure and the synthesis procedure used to determine parameters of the filter is contained in reference 6. Briefly, the filter structure and parameters were chosen so the PSD of the output signal closely approximates the PSD of the crew motion being modeled.

The filter structure should be sufficiently complex to reproduce the prominent features of the PSD being approximated and yet not so complex as to exclude economical computer usage. Unimodal spectral densities are well approximated by a single quadratic in the denominator. The transfer function of such a filter is

$$H(s)_{1-2} = \frac{\tau s}{s^2 + 2\zeta\omega s + \omega^2}$$

where τ is gain, ω is frequency, and ζ is damping.

APPENDIX B

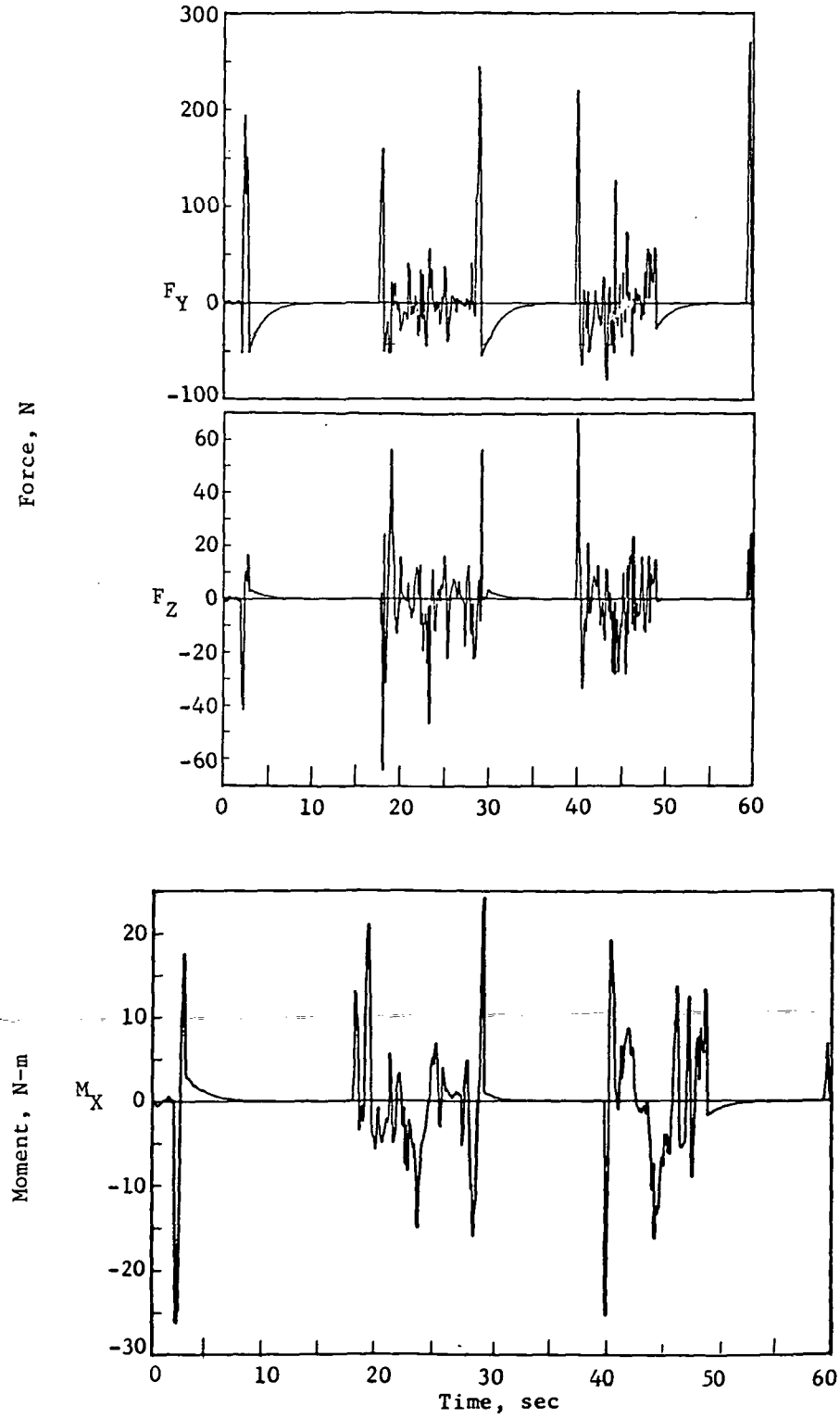

Figure B-2.- Actual T-013 soaring data.

APPENDIX B

To approximate a PSD curve containing two peaks requires a fourth-order polynomial in the denominator, and the transfer function is

$$H(s)_{1-4} = \frac{\tau s}{\left(s^2 + 2\zeta_1\omega_1 s + \omega_1^2\right)\left(s^2 + 2\zeta_2\omega_2 s + \omega_2^2\right)}$$

In actual practice, many of the original PSD curves contain more than one peak, but in most cases the single-filter form gives satisfactory results. In those instances where the fit can be improved by using the higher order filter, values for both sets of parameters are tabulated in appendix A.

The mechanization of the shaping filter, including preliminary gains and the white noise generation is shown in figure B-3. The implementation of the model is demonstrated by the following discussion of a sample listing (fig. B-4) of an actual input case used for Applications (section 6.1.5).

A preliminary note on figure B-4: the model is presented in a pseudo-Fortran language. The listing is actually an input to a Martin Marietta control system simulation program, MIMIC, which reads each line as either I/O control or executable code. MIMIC uses a digital computer to simulate the operations of an analog computer. The program uses a fourth-order Runge-Kutta integration routine. The input routine is flexible enough for the user to specify the type of operations he desires. Further information can be obtained through the Martin Marietta Data Center, Computer Utilization Report, JD 204, April 1968. The input to MIMIC so closely resembles Fortran that, for all executable statements, only an equal sign need be added to convert them to actual Fortran. The I/O statements are peculiar to MIMIC but easily understood. Input variables are identified at the beginning of the listing and are preceded by the word CON. Their values are found at the end of the listing and are identified by their order within the CON statements.

The listing contains comments which identify both the model and the control system simulation as much as possible. Because of the availability of comments and the fact that there is no looping or branching in the model logic, a flow chart is not included.

The actual implementation does not directly use the tabulated τ; instead, τ is used as a factor in the computation of the gains identified in figure B-3. The calculation is described in chapter 6.0, equation (6.14). It is equivalently (and more simply) expressed as

$$\Phi(0) = \frac{2\pi\tau_F^2\omega_1^2}{\omega_F^4}$$

where τ_F is tabulated parameter, ω_F is tabulated parameter, and ω_1 is model parameter. For the model implementation, calculation for PSD contains the dc component rather than starting at a zero origin; thus $\omega_1 = 1/1000$.

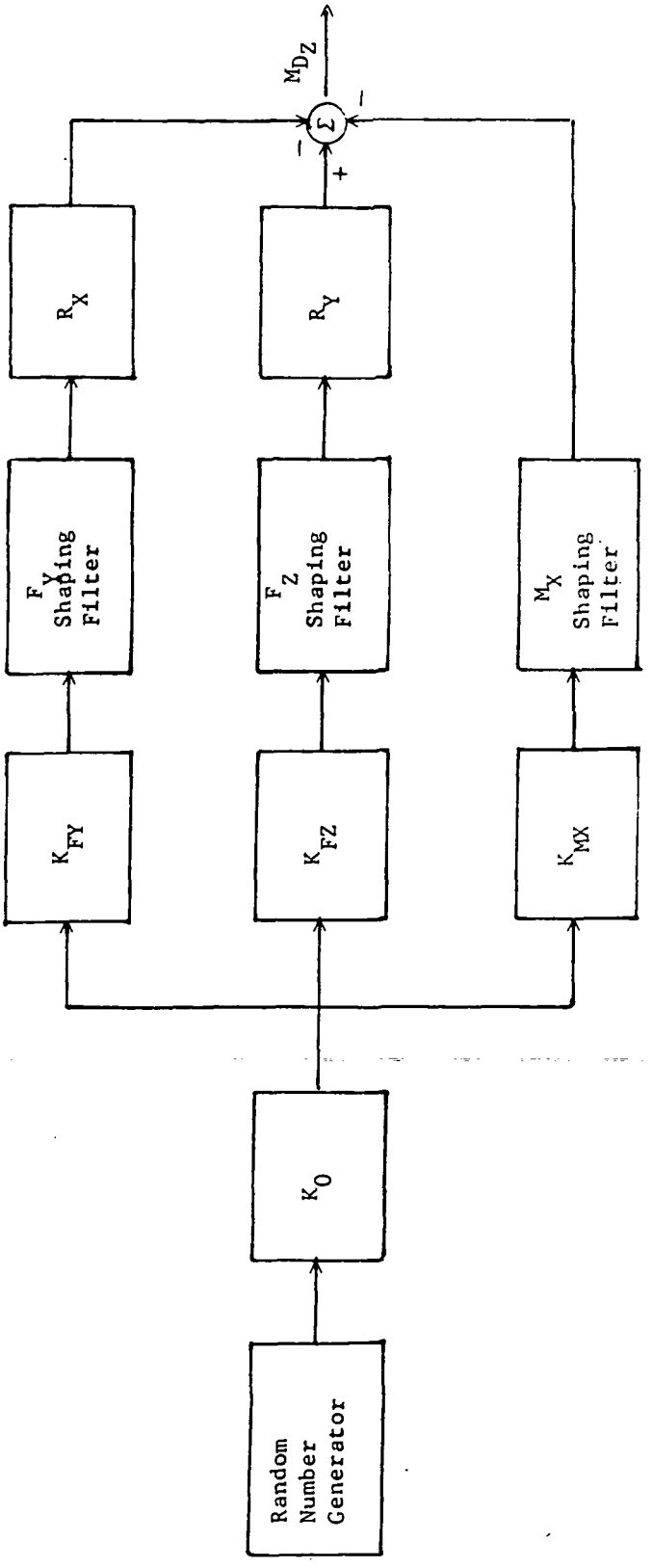

Uniform Distribution — Normal Distribution

Random Number K_0 = $\left[\frac{1}{\sigma^2 \Delta t}\right]^{\frac{1}{2}}$ or $\left[\frac{1}{\Delta t}\right]^{\frac{1}{2}}$

Gains K_{FY}, K_{FZ}, K_{MX} = $[\phi(0)]^{\frac{1}{2}}$ or $[\phi(0)]^{\frac{1}{2}}$

Figure B-3.- Stochastic model mechanization of disturbance torque.

APPENDIX B

```
*MIMIC          10
  SYSTEM RESPONSE TO CREW MOTION
                  CON(DT,TMAX,NPRINT,NPLOT)      Computing and printing intervals
                  CON(KR,KD,KA,1)                Gains and inertia
                  CON(KBP,KBR,ZETAB,OMEGAB)      Flexible body constants (N/A)
                  CON(KFY,TFY,ZFY,WFY,RX)        FY parameters
                  CON(KFZ,TFZ,ZFZ,WFZ,RY)        FZ parameters
                  CON(KMX,TMX,ZMX,WMX)           MX parameters
          DEL     DT/NPRINT
          NPRDT   NPRINT*DT
          NPLDT   NPLOT*DT
          DTMAX   DTMIN
          KI      1.0/I
          KN      SQR(3./DT)
          RDN     RNU(-1.0,1.0,0.1)              Random number generation
          RND     RDN*KN
          FYDD    WFY*WFY*(RND*KFY-FY)-2.*ZFY*WFY*FYD
          FYD     INT(FYDD,0.)                   FY shaping filter
          FY      INT(FYD,0.)
          FY1     FYD*TFY+FY
          FZDD    WFZ*WFZ*(RND*KFZ-FZ)-2.*ZFZ*WFZ*FZD
          FZD     INT(FZDD,0.)                   FZ shaping filter
          FZ      INT(FZD,0.)
          FZ1     FZD*TFZ+FZ
          MXDD    WMX*WMX*(RND*KMX-MX)-2.*ZMX*WMX*MXD
          MXD     INT(MXDD,0.)                   MX shaping filter
          MX      INT(MXD,0.)
          MX1     MXD*TMX+MX
          MD      RY*FZ1-RX*FY1-MX1              Disturbance torque (plotted)
          MC      KA*VE                          Correction torque
          ME      MC+MD                          Effective torque
          TDRB    KI*INT(ME,0.)                  Rigid body rate
          TRB     INT(TDRB,0.)                   Rigid body attitude
          Q       KBP*ME
          TFB     INT(TDFB,0.)
          TDFB    INT(TDDFB,0.)
          TPFB    Q-OMEGAB*OMEGAB*TFB            Flexible body characteristics
          TDDFB   TPFB-2.*ZETAB*OMEGAB*TDFB
          TD      TDRB+KBR*TDFB                  Total vehicle rate (plotted)
          THETA   TRB+TFB                        Total vehicle attitude (plotted)
          VD      (-1.0)*KD*THETA                Sensed vehicle attitude
          VR      KR*TD                          Error
          VE      VD-VR
          PRINT   QNT(T,NPRDT,DT)
          PRINTS  FSW(ABS(T-PRINT)-DEL,TRUE,TRUE,FALSE)
          PLOT    QNT(T,NPLDT,DT)                MIMIC output controls
          PLOTS   FSW(ABS(T-PLOT)-DEL,TRUE,TRUE,FALSE)
                  FIN(T,TMAX)
                  HDR(TIME,FY1,FZ1,MX1)
                  HDR(    ,MD,TDOT,THETA)
                  HDR
```

Figure B-4.- Stochastic model sample input listing, Skylab applications.

```
PRINTS          OUT(T,FY1,FZ1,MX1)
PRINTS          OUT( ,MD,TD,THETA)
PLOTS           PLO(FY1)
PLOTS           PLO(FZ1)                                    MIMIC outputs
PLOTS           PLO(MX1)
PLOTS           PLO(MD)
PLOTS           PLO(TD)
PLOTS           PLO(THETA)
                END
0.02        49.9        5.0         1.0                   Input variable values
965347.     85315.      1.0         6200000.
0.0         0.0         0.7         0.62832
 CONSOLE OPERATIONS                                        (Skylab)
0.0021373   1000.       1.81        3.80        -6.6294
0.0035746   1000.       0.72        1.34         1.9253
0.0027167   1000.       0.48        1.48
```

Figure B-4.- Concluded.

Table B-1 summarizes the input information required to operate the stochastic model.

TABLE B-1.- STOCHASTIC MODEL INPUT VARIABLES

Variable name	Symbol	Input value	Notes
Crew motion model parameters (a)			
KFY		0.00214	Preliminary gain, F_Y
TFY	$1/\omega_1$	1000.0	
ZFY	ζ_{FY}	1.81	Appendix A or table 7-1
WFY	ω_{FY}	3.80	Appendix A or table 7-1
RY			y-moment arm
Control system parameters			
KR		865347.	Rate gyro gain
KD		85315.	Displacement gyro gain
KA		1.0	Actuator gain
I		6200000.	Inertia
MIMIC controls			
DT		0.02	Computing interval
TMAX		49.9	End of time function
NPRINT		5.0	Printing increment
NPLOT		1.0	Plotting increment

[a]Symbols correspond to computer symbols in figure B-4.

APPENDIX B

B.3 Anthropometric Model

A discussion of an anthropometric model developed by the Langley Research Center during the late 1960's follows. The model exists as a Fortran program compatible with the CDC 6000 series, but, due to its large core requirements and some execution difficulties, it was not exercised for the purposes of this handbook. The purpose of this section is to familiarize the reader with the model's existence and describe the available input data recorded during experiment T-013. References are given for those who wish to implement the model or who are interested in the derivations of physical properties or dynamic equations.

B.3.1 Description of model

The analytic model of man is developed from earlier anthropometric research done by the U.S. Air Force. The model uses nine hinged, geometric solids to represent man's trunk and limbs and is capable of simulating most of man's motions. The torque relations corresponding to the model motions are incorporated in the rigid-body equations of motion for arbitrary spacecraft. Both the disturbance moments due to crew activity and the contribution of these moments to the spacecraft equations of motion are determined from the analytical model.

Figure B-5 illustrates the relation of the body segments. Segment 1 represents the torso and head, segments 2 and 3 the right and left upper arms, segments 4 and 5 the right and left lower arms and hands, segments 6 and 7 the right and left upper legs, and segments 8 and 9 the right and left lower legs and feet. The nine-segment model possesses possible limitations when used for crew motion disturbance analysis. No account is taken of wrist, ankle, or head motions, nor of bending of the spine. The hands and feet are relatively small masses when compared to other body segments, however, and would provide minimum disturbance effects if moved vigorously, whereas the head and spinal motions involve larger masses which could affect experimental data. The T-013 motion sequence was intended to be constrained where possible to movements of the nine principal segments only.

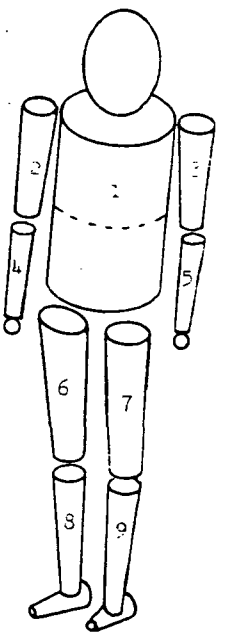

Figure B-5.- Anthropometric nine-segment model of man.

APPENDIX B

B.3.2 Description of data

Measurements of body limb motions of the astronaut were carried out for all the experiment activities. The limb angles were measured by the limb motion sensing system (LIMS), an external skeletal structure portrayed previously in figure 3-5. It was made up of pivots at 16 principal body rotation points, each pivot containing a linear potentiometer whose output is directly proportional to the magnitude of joint rotation. The LIMS provided a continuous measurement of body limb position relative to the torso as the subject performed the experiment movements. The structure was fabricated of aluminum and was designed to measure Euler angles (roll, pitch, and yaw sequence) at the shoulders and hips, a single pitch angle at the elbows and knees.

Time profiles of segment limb angles may be found in figures 17, 40, 43, 49, 51, and 53 of reference 2. The time histories of all LIMS data may be found on the same magnetic tape which contains the force and moment data.

B.3.3 References

The descriptions of how to obtain the data tape and how to read the data are given in reference 2, pages 61 to 67. Reference 1 details the development of the anthropometric model. References 1 and 2 both contain derivations of physical properties for the model of man and dynamic equations associated with motions of the anthropometric model.

REFERENCES

1. Conway, Bruce A. (appendix A by Charles T. Woolley; appendix B by Peter R. Kurzhals and Robert B. Reynolds): Development of Skylab Experiment T-013 Crew/Vehicle Disturbances. NASA TN D-6584, 1972.

2. Conway, Bruce A.; and Hendricks, T. C.: A Summary of the Skylab Crew/Vechile Disturbances Experiment T-013. NASA TN D-8128, 1976.

3. Hendricks, T. C.; and Johnson, C. H.: Stochastic Crew Motion Modeling. J. Spacecr. & Rockets, vol. 8, no. 2, Feb. 1971, pp. 150-154.

4. Brown, Robert Grover; and Nilsson, James William: Introduction to Linear Systems Analysis. John Wiley & Sons, Inc., c.1962.

5. Truxal, John G.: Automatic Feedback Control System Synthesis. McGraw-Hill Book Co., Inc., 1955.

6. Murrish, C. H.; and Smith, G. W.: Apollo Applications Program Crew Motion Experiment - Program Definition and Design Development. Contract NAS 1-7276, Martin Marietta Corp., Mar. 1968. (Available as NASA CR-66599.)

INDEX

INDEX

 183-184

1. Report No.	2. Government Accession No.	3. Recipient's Catalog No.
NASA RP-1025		

4. Title and Subtitle	5. Report Date
HANDBOOK ON ASTRONAUT CREW MOTION DISTURBANCES FOR CONTROL SYSTEM DESIGN	May 1979
	6. Performing Organization Code
7. Author(s)	8. Performing Organization Report No.
M. Conlon Kullas	L-12299
	10. Work Unit No. 506-19-13-02
9. Performing Organization Name and Address	11. Contract or Grant No.
NASA Langley Research Center Hampton, VA 23665	
	13. Type of Report and Period Covered
12. Sponsoring Agency Name and Address	Reference Publication
National Aeronautics and Space Administration Washington, DC 20546	14. Sponsoring Agency Code

15. Supplementary Notes

M. Conlon Kullas: Martin Marietta Aerospace, Denver, Colorado.
The preparation of this handbook was sponsored under Contract NASw-2982 with Martin Marietta Aerospace. The NASA Technical Monitor was Bruce Conway.

16. Abstract

This crew motion handbook summarizes the analyses and results pertinent to the characterization of the disturbances imparted to the Skylab vehicle by the T-013 crew motion experiments. It also provides guidelines to help control system designers assess anticipated crew motion disturbances during the design cycle of a new manned spacecraft control system. These guidelines, in conjunction with the T-013 characterizations just outlined, begin with the control system conceptual design and conclude with preliminary expectations for pointing performance as affected by crew motions. The handbook uses block diagrams to highlight the contents so that the reader can easily identify the information and data flow. These diagrams provide a handy cross reference of related topics.

17. Key Words (Suggested by Author(s))	18. Distribution Statement
Crew motion disturbance Attitude control system design Skylab	Unclassified - Unlimited Subject Category 18

19. Security Classif. (of this report)	20. Security Classif. (of this page)	21. No. of Pages	22. Price*
Unclassified	Unclassified	196	$9.00

* For sale by the National Technical Information Service, Springfield, Virginia 22161

NASA-Langley, 1979